Complexity and Entanglement in the AdS/CFT Correspondence

Dissertation zur Erlangung des
naturwissenschaftlichen Doktorgrades
der Julius-Maximilians-Universität Würzburg

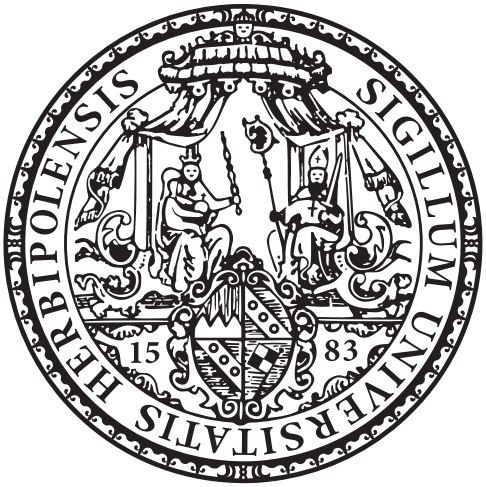

vorgelegt von

Nina Miekley

aus Oldenburg in Holstein

Würzburg, 2020

CC BY

Eingereicht am: 22.07.2019 .....
bei der Fakultät für Physik und Astronomie

1. Gutachter: Prof. Dr. Johanna Erdmenger ....
2. Gutachter: Prof. Dr. Björn Trauzettel .....
3. Gutachter: .....

der Dissertation

Vorsitzende(r): Prof. Dr. Giorgio Sangiovanni .....
1. Prüfer: Prof. Dr. Johanna Erdmenger ....
2. Prüfer: Prof. Dr. Björn Trauzettel .....
3. Prüfer: Prof. Dr. Raimund Ströhmer .....

im Promotionkolloquiums

Tag des Promotionskolloquiums: 30.10.2019 .....

Doktorurkunde ausgehändigt am: .....

Summary

The AdS/CFT correspondence is an explicit realization of the holographic principle. It describes a field theory living on the boundary of a volume by a gravitational theory living in the interior and vice-versa. With its origins in string theory, the correspondence incorporates an explicit relationship between the degrees of freedom of both theories: the AdS/CFT dictionary. One astonishing aspect of the AdS/CFT correspondence is the emergence of geometry from field theory.

On the gravity side, a natural way to probe the geometry is to study boundary-anchored extremal surfaces of different dimensionality. While there is no unified way to determine the field theory dual for such non-local quantities, the AdS/CFT dictionary contains entries for surfaces of certain dimensionality: it relates two-point functions to geodesics, the Wilson loop expectation value to two-dimensional surfaces and the entanglement entropy, i.e. a measure for entanglement between states in a region and in its complement, to co-dimension two surfaces in the bulk.

In this dissertation, we calculate these observables for gravity setups dual to thermal states in the field theory. The geometric dual is given by AdS Schwarzschild black holes in general dimensions. We find analytic results for minimal areas in this setup. One focus of our analysis is the high-temperature limit. The leading and subleading term in this limit have diverse interpretation for the different observables. For example, the subleading term of the entanglement entropy satisfies a c-theorem for renormalization flows and gives insights into the number of effective degrees of freedom.

The entanglement entropy emerged as the favorable way to probe the geometric dual. In addition to the extremal bulk surface, the holographic entanglement entropy associates a bulk region to the considered boundary region. The volume of this region is conjectured to be a measure of complexity, i.e. a measure of how difficult it is to obtain the corresponding field-theory state. Building on our aforementioned results for the entanglement entropy, we study this complexity for AdS Schwarzschild black

holes in general dimensions. In particular, we draw conclusions on how efficient holography encodes the field theory and compare these results to MERA tensor networks, a numerical tool to study quantum many-body systems.

Moreover, we holographically study the complexity of pure states. This sheds light on the notion of complexity in field theories. We calculate the complexity for a simple, calculable example: states obtained by conformal transformations of the vacuum state in AdS_3/CFT_2. In this lower-dimensional realization of AdS/CFT, the conformal group is infinite dimensional. We construct a continuous space of states with the same complexity as the vacuum state. Furthermore, we determine the change of complexity caused by small conformal transformation. The field-theory operator implementing this transformation is known and allows to compare the holographic results to field theory expectations.

Zusammenfassung

Die AdS/CFT Korrespondenz ist ein explizites Beispiel für das holographische Prinzip. Es beschreibt eine Feldtheorie auf dem Rand eines Volumens durch eine Theorie mit Gravitation im Inneren und vice-versa. Aus dem Ursprung in der Stringtheorie folgt ein expliziter Zusammenhang zwischen den Freiheitsgraden beider Theorien: das AdS/CFT Lexikon. Ein verblüffender Aspekt der AdS/CFT Korrespondenz ist die Entstehung der Geometrie aus der Feldtheorie.

Ein natürlicher Weg um die Geometrie auf der Gravitationsseite zu untersuchen sind extremale Flächen, die am Rand verankert sind. Es gibt keinen einheitlichen Weg um die duale Größe in der Feldtheorie für solche nichtlokalen Größen zu bestimmen, jedoch gibt es für Flächen bestimmer Dimension Einträge im AdS/CFT Lexikon: es bringt Zweipunktfunktionen mit Geodäten, Wilson loops mit zweidimensionalen Flächen und die Verschränkungsentropie, ein Maß für Verschränkung zwischen einer Region und ihrem Komplement, mit Flächen der Kodimension zwei in Verbindung.

In dieser Dissertation untersuchen wir diese Observablen für Geometrien dual zu thermischen Zuständen in der Feldtheorien. Die duale Geometrien sind AdS Schwarzschild schwarze Löcher in allgemeiner Raumzeitdimension. Wir erhalten analytische Ergebnisse. Ein Fokus liegt auf das Verhalten bei hoher Temperatur. Die in diesem Limit dominanten Terme haben vielfältige Interpretationen für die unterschiedlichen Observablen. Der Term zweiter Ordnung für die Verschränkungsentropie erfüllt zum Beispiel ein c-Theorem für Renormalizisierungsgruppen und gibt daher Aufschlüsse über die Anzahl der effektiven Freiheitsgrade.

Die Verschränkungsentropie stellt sich als erfolgreicher Weg heraus um die duale Geometrie zu untersuchen. Neben der extremalen Fläche bringt die holographische Verschränkungsentropie auch eine Raumregion zu der gegebenen Randregion in Verbindung. Das Volumen dieser Raumregion wird als Maß für die Komplexität, ein Maß für den Schwierigkeitsgrad den entsprechenden Zustand in der Feldtheorie

zu konstruieren, angesehen. Wir berechnen dieses Volumen für AdS Schwarzschild aufbauend auf unseren oben erwähnten Ergebnissen zu der Verschränkungsentropie. Wir ziehen Rückschlüsse wie effektiv Holographie die Feldtheorie beschreibt und vergleichen diese Ergebnisse zu MERA Tensornetzwerken, einer numerische Methode um Vielteilchensysteme zu beschreiben.

Anschließend betrachten wir die Komplexität von reinen Zuständen holographisch. Dies gibt Einblicke in das Konzept von Komplexität in Feldtheorien. Wir untersuchen die Komplexität für ein einfaches, berechenbares Beispiel: Zustände erzeugt von konformen Transformationen des Vakuumzustandes in AdS_3/CFT_2. Die konforme Gruppe hat unendlich viele Dimensionen in diesem niedrig dimensionalen Beispiel von AdS/CFT. Wir konstruieren ein kontinuierliches Raum von Zuständen mit gleicher Komplexität wie der Vakuumzustand. Außerdem bestimmen wir die Änderung der Komplexität für kleine konforme Transformationen. Der Operator in der Feldtheorie ist bekannt und erlaubt uns unsere Ergebnisse zu Feldtheorieerwartungen zu vergleichen.

Contents

List of Figures

List of Tables

Chapter 1

Introduction

In this year, we gained insights into two of physics' most striking phenomena. In April [1,2], the EHT[1] collaboration reported that they captured an image of a black hole for the first time. They used eight telescopes around the globe and observed the supermassive black hole in the galaxy M87 for several days in April 2017. This object has an enormous mass of 6.5 billion solar masses. Only three years prior, the LIGO[2] and Virgo collaborations announced the direct observation of gravitational waves [3,4]. The observed event GW150914 was caused by a merger of binary black holes into a black hole of 62 solar masses. This is a novel confirmation of Einstein's theory of general relativity.

Black hole physics is not the only currently exciting area of physics. In July of this year, scientists published the first picture of entanglement between two particles [5]. Entanglement is a crucial difference between classical and quantum systems. While it was first thought to be an unphysical behavior and tried to be explained away by hidden variables [6], it was shown that entanglement cannot be described by classical states [7]. Even more striking, it was discovered that any non-classical theory has to incorporate entanglement [8]. The image of entangled photons is a demonstration that the world is quantum in nature.

However, there is enormous trouble finding a quantum theory of gravity. The usual method of describing forces in the framework of quantum field theory is unsuccessful when applied to gravity and fundamentally different approaches are being developed. One of these approaches is string theory [9,10]. The fundamental objects of this theory are extended one-dimensional objects, so-called strings, and fields are vibrations of these. A metric and gauge bosons automatically emerge as massless

[1] Event Horizon Telescope

[2] Laser Interferometer Gravitational-Wave Observatory

excitations, which establishes string theory as a candidate to describe all forces of nature. One development of string theory is the AdS/CFT correspondence [11–13], which is a correspondence between gravitational theories and quantum field theories. The striking feature of this duality is that these field theories live in one spacetime dimension less then the gravitational theories.

Clues on how this is possible arise from studies of black holes in classical gravity. Black holes cause contradiction with thermodynamics: if a matter system with entropy falls into a black hole, the only object which remains is a black hole and naively the entropy would be lost. For black holes to be consistent with the laws of thermodynamics, they necessarily have an entropy, the so called *Bekenstein–Hawking entropy* [14, 15]. Inspired by Hawking's area theorem that the area of the horizon always increases [16] and the analogy to the second law of thermodynamics

$$\mathrm{d}S_{\mathrm{Matter}} \geq 0 \qquad \longleftrightarrow \qquad \mathrm{dArea}_{\mathrm{Horizon}} \geq 0,$$

Bekenstein conjectured the black hole entropy as

$$S_{\mathrm{BH}} = \frac{k_B c^3}{4 G_N \hbar} \cdot \mathrm{Area}_{\mathrm{Horizon}}.$$

Furthermore, he postulated that throwing matter into a black hole transforms conventional entropy into horizon area. This resulted in the formulation of the *generalized second law* [17, 18], which demands that not the thermodynamical entropy, but the total entropy

$$\begin{aligned} S &= S_{\mathrm{Matter}} + S_{\mathrm{BH}}, \\ \mathrm{d}S &\geq 0 \end{aligned}$$

always increases. As a consequence, black holes satisfy laws analogous to the laws of thermodynamics [19].

Black holes are extreme objects. However, the Bekenstein-Hawking entropy has tremendous consequences for any matter: if the entropy of a matter system becomes too large, a black hole is formed. Therefore, the entropy is bounded by

$$S_{\mathrm{Matter}} \leq \frac{2\pi k_B}{\hbar c} E R,$$

where E is the energy of the system and R the characteristic size of the system[3]. This is the so called *Bekenstein entropy bound* [20]. A weaker form of the entropy bound is the *spherical entropy bound* [21, 22]

$$S_{\text{Matter}} \leq \frac{k_B c^3}{4G_N \hbar} \cdot \text{Area}_{\text{Boundary}},$$

where the entropy is bounded by the area of a sphere which can enclose the system. In thermodynamics, entropy is an extensive quantity and scales with the volume. Therefore, gravity places strict constraint on the entropy and on the degrees of freedom contained in a volume.

This sparked the idea of the *holographic principle*[4]: it claims that in a theory with gravity the information contained in a volume of space can be encoded on the boundary surface, on which the information scales extensively as familiar from thermodynamics. The gravitational theory has to emerge from the information on the boundary surface.

The AdS/CFT correspondence is an explicit realization of the holographic principle. By considering a particular low-energy limit in string theory, Maldacena conjectured that a gravitational theory in Anti-de Sitter space is dual to a conformal field theory living on the boundary [11]. The best examined case is the duality between type IIB supergravity on $\text{AdS}_5 \times S^5$, which reduces to a theory on AdS_5 by dimensional reduction, and $\mathcal{N} = 4$ supersymmetric Yang-Mills theory on its boundary.

One fundamental question is how the geometry emerges from the field theory. An interesting setup to study is the two sided AdS-Schwarzschild black hole [24]. This geometry has two exterior regions with disconnected boundaries, on which field theory states live. Both sides are connected by the interior of the black hole, i.e. by a wormhole as shown in Figure 1.1. The dual field theory state is the thermofield double state, an entangled state of the form

$$|\text{TFD}\rangle = \frac{1}{\sqrt{Z}} \sum_n e^{-\beta E_n/2} |n\rangle_{\text{L}} \otimes |n\rangle_{\text{R}},$$

where $|n\rangle_{\text{L/R}}$ describe the energy eigenstates on left and right boundary respectively.

[3]This applies for weakly gravitating systems in asymptotically flat space. The entropy bound in this form is difficult to rephrase in a covariant form.

[4]See [23] for a review.

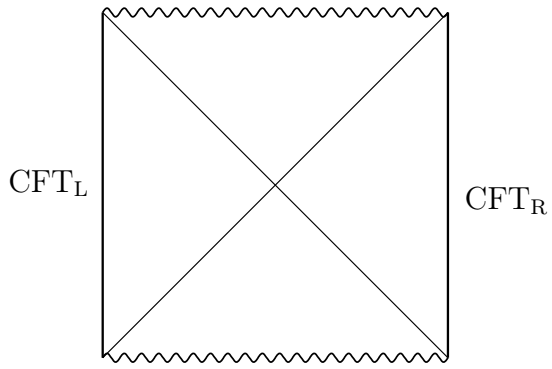

Figure 1.1: Two-Sided Black Hole in AdS.
The two CFTs live on the vertical boundary. The horizontal wavy lines are the singularities and the diagonal lines are the black hole horizon.

This state is pure, but reducing it to only one boundary results in a mixed thermal state

$$\rho_\mathrm{R} = \frac{1}{Z}\sum_n e^{-\beta E_n/2}|n\rangle_\mathrm{R}\langle n|_\mathrm{R}, \qquad \rho_\mathrm{L} = \frac{1}{Z}\sum_n e^{-\beta E_n/2}|n\rangle_\mathrm{L}\langle n|_\mathrm{L}.$$

Therefore, while the boundaries are spacelike separated, they are entangled. The measure to quantify the entanglement between left and right boundary is the *entanglement entropy*

$$S_{EE} = -\operatorname{Tr}_R \rho_\mathrm{R} \ln \rho_\mathrm{R}.$$

The entanglement entropy between the two boundaries reduces to the thermal entropy of the reduced state. The AdS/CFT correspondence maps this entropy to the entropy of the black hole.

The notion of entanglement entropy applies to arbitrary regions. Motivated by the Bekenstein entropy bound, the holographic entanglement entropy for a state reduced to a region A is proportional to the bulk surface γ homologous to the boundary region [25, 26], i.e.

$$S_{EE}(A) = \frac{k_B c^3}{4G_N\hbar} \cdot \min_{\partial\gamma=\partial A} \mathrm{Area}(\gamma).$$

Therefore, the geometry is related to the entanglement structure of the field theory. To stretch the importance of entanglement, it was shown that known quantum information properties of the entanglement entropy have consequences for the gravitational theory. For example, the change of entanglement entropy under small per-

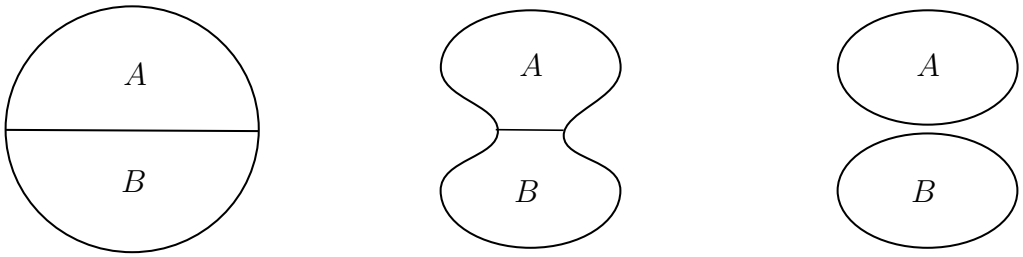

Figure 1.2: Removing Entanglement between two Regions.

turbations is described by *entanglement thermodynamics*, which relates the change of entanglement entropy to the change of energy

$$T_E \, \delta S_{EE} = \delta E$$

via a entanglement temperature T_E, which does not depend on the perturbation. It is shown that entanglement thermodynamics implies the linearized Einstein equations around AdS on the gravity side [27–29]. Furthermore, properties such as subadditivity and strong subadditivity imply energy conditions for the gravitational theory. Therefore, fundamental properties of the gravitational theory arise from quantum information properties of entanglement.

The importance of entanglement for the emergence of gravity and spacetime was further developed by van Raamsdonk [30, 31]. He considers a state with a holographic dual and removes entanglement between two regions A and B. This reduces the entangled state to a product state, for which the mutual information

$$\mathcal{I}(A:B) = S(A) + S(B) - S(A \cup B) \tag{1.1}$$

vanishes. The mutual information places an upper bound on the connected correlation functions

$$\mathcal{I}(A:B) \geq \frac{1}{2|\mathcal{O}_A|^2|\mathcal{O}_B|^2}(\langle \mathcal{O}_A \mathcal{O}_B \rangle)^2$$

for any operator on A and B. For some operators, there is a geometric way to calculate these correlation functions: the correlation function between two points is related to the length $\mathcal{L}$ of the connecting bulk geodesic

$$\langle \mathcal{O}_A \mathcal{O}_B \rangle = \exp\left(-\Delta \cdot \mathcal{L}\right), \tag{1.2}$$

where Δ is the scaling dimension of the operator. Therefore, reducing the entangle-

ment between two regions corresponds to pulling these regions apart (i.e. $\mathcal{L} \to \infty$) and pinching them off from each other. A disentangled product state corresponds to two disconnected spacetimes. This is shown in Figure 1.2. Therefore, the role of entanglement is significant in holography: it is the glue which holds everything together.

While entanglement entropy is difficult to calculate in field theories, calculating the extremal area is a feasible task in classical gravity. In Chapter 3, I calculate the entanglement entropy in a highly symmetry setup: strip regions in field theory states dual to AdS Schwarzschild black holes in general dimension. Since the extremal surfaces are anchored on only one boundary, they do not probe the interior of the black hole, but reach arbitrary close to the horizon. Furthermore, I calculate additional field theory observables dual to extremal surfaces on the gravity side: the two-point correlation function which is dual to geodesics and the Wilson loop expectation value which is dual to two-dimensional surfaces. While all of these non-local observables probe the bulk, it is known that the entanglement entropy is highly effective as it probes deepest into the bulk and therefore closest to the horizon. I am able to derive analytic results for the entanglement and the other observables in this setup.

While the low-temperature behavior of these observables can be treated perturbatively, the high-temperature behavior is highly non-trivial as it depends on the entire spacetime geometry. The qualitative behavior of the extremal surfaces in this limit is known: the horizon creates an effective potential which pushes the extremal surfaces away. The surfaces in this limit approach a rectangle consisting of to pieces connecting the horizon with the boundary and a vertical piece along the horizon. This approximation captures the leading order behavior correctly. In particular, this results in an extensive behavior for the entanglement entropy due to the thermal entropy and an exponential decay of the two-point function due to a thermally induced mass. My analytic results show that the subleading term deviates from this approximation.

For the entanglement entropy, this subleading term is proportional to the area of the entangling surface, i.e. the boundary of the considered region, and a so-called area term [32–34]. For renormalization flows, the area term is larger at the UV fixed point than at the IR fixed point [35, 36]. Therefore, the area term satisfies a c-theorem [37][5]. This assigns the interpretation of the number of effective degrees

[5]It satisfies a weak c-theorem, since the area term does not have to decrease monotonically

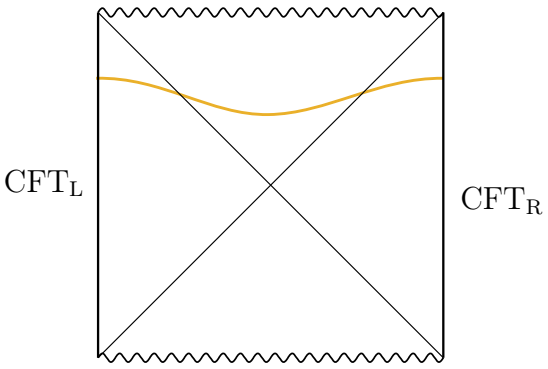

Figure 1.3: Extremal Slice in Two-Sided Black Hole.

of freedom to the area term. My results show an interesting behavior for the entanglement entropy. While the area term is negative for CFT dimension $d \leq 6$, it is positive for higher-dimensional theories. From the field theory perspective, we expect that turning on a temperature decreases the number of effective degrees of freedom: fields obtain a thermally induced mass and can be integrated out at high-temperature. This is reflected in the negativity of the area term for small spacetime dimension. However, my results show that this is not the case for large spacetime dimensions: the area term is positive for $d \geq 7$. This is also reflected in the behavior of the entanglement negativity, a measure for entanglement in mixed states which is related to the entanglement entropy in holography. For this observable, the area term shows increased entanglement in the high-temperature limit, where the field theory is supposed to behave classically. This gives us insights into the dual field theory: asymptotically AdS geometries are expected to be dual to states in superconformal field theories. However, these theories only exists for spacetime dimensions $d < 7$. Furthermore, for larger dimensions there are also no string theory models, which would provide us with well-defined map between two theories. Our results show that the IR fixed points of the dual field theories are not described by d dimensional CFT for $d \geq 7$.

When studying the two-sided AdS black hole, Susskind [38–42] noticed that while the entanglement entropy does not allow to probe deep into the interior of the black hole, there is a construction on the gravity side which does: extremal hypersurfaces anchored on the boundary as shown in Figure 1.3. These define a 'nice'[6], unique time slicing even if the spacetime is not static and there is no unique way do extend

when going into the IR.

[6]The slices avoid singularities and regions of high curvature.

a boundary time slice into the bulk. This construction associates the volume of the hypersurface to the state living on the boundary equal-time slice. The late time behavior of the volume for the two-sided black hole motivates the *complexity=volume proposal*: the volume is conjectured to be dual to the *complexity*, a measure of how difficult it is to construct a state using unitary operators. The complexity depends implicitly on the reference state $|\mathcal{R}\rangle$ from which we start and on the gate set μ_i used to construct the unitary operator

$$|\psi\rangle = U\,|\mathcal{R}\rangle\,, \tag{1.3a}$$

$$U \approx \mu_1 \dots \mu_{\mathcal{C}}. \tag{1.3b}$$

While this concept arises naturally from theoretical computer science and (quantum) computers, there is no well-defined notion of field theory complexity.

In particular, holographic complexity can easily be applied to subregions: the volume reduces to the volume inside the Ryu-Takayanagi surface. This is even of interest without considering it to be a dual to a field theory complexity: the holographic entanglement entropy automatically associates a bulk region to a boundary region. Measuring the size of this region therefore loosely speaking gives a measure on how efficient the field theory is encoded in the dual geometry. Based on the aforementioned studies on entanglement entropy, I study this subregion complexity in AdS Schwarzschild. Using a similar treatment as before, I derive analytic results for the volume in Chapter 4.

The subregion complexity shows an interesting behavior in this setup: while it is extensive at high-temperatures, the leading order correction at small temperatures is negative. Therefore, for strips with a width smaller than a certain critical value, temperature reduces the subregion complexity. However, there is a transition at ℓ_{crit} and for larger strips the temperature increases the complexity of the reduced state. Qualitatively speaking, the near-boundary region reduces the subregion complexity for small strips and contribution arising from the horizon increase the subregion complexity for large strips.

We compare these results to predictions from tensor networks [43–46], a numerical tool to study states in quantum many-body theory. A special kind of tensor networks, the so-called multi-scale entanglement renormalization ansatz (MERA), shares many structural features of the AdS/CFT correspondence. In particular, an additional dimension emerges from the entanglement structure of the state. Furthermore, entanglement entropy is measured analogously to the holographic Ryu-

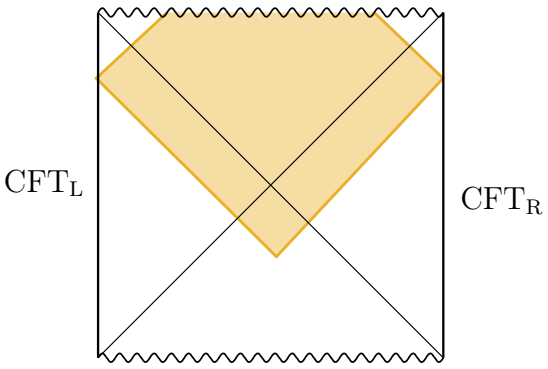

Figure 1.4: Wheeler-DeWitt patch for Two-Sided Black Hole.

Takayanagi formula. There is a model describing thermal states, however it might not be optimized, i.e. it is more complex then necessary. We use this MERA model and calculate the subregion complexity in the analogous gravity model: vacuum AdS with a hard wall. Also in this geometry the subregion complexity exhibits an interesting transition: while at low-temperatures the subregion complexity is identical to the vacuum complexity, we have an increased complexity at high temperature. Our results show that the subregion complexity in this setup is always larger than AdS Schwarzschild. This tells us that AdS/CFT encodes thermal states more efficiently then tensor networks.

The considered reduced states are mixed, which makes the definition of a proper definition of complexity a delicate topic. States obtained by applying unitary operators to a pure reference state as shown in (1.3a) are pure. For mixed states, the definition of complexity has to be extended. However, even the complexity for pure states is not well-defined in field theory and an active area of research. It is not clear whether holographic complexity=volume proposal corresponds to a well-defined field theory prescription, if it does to which one and what implicit choices are involved. Furthermore, there are competing proposals for a holographic dual of the complexity, most notably the *complexity=action proposal* [47, 48] which relates the complexity to the gravitational action evaluated on a spacetime region known as Wheeler-DeWitt patch, see Figure 1.4. Therefore, it is of particular interest to study holographic complexity, put constraints on possible dual field theory notions and determine differences between the different proposals.

In Chapter 5, I present my approach in doing this by studying complexity in relationship with conformal transformations in AdS$_3$/CFT$_2$. In this lower-dimension example of an AdS/CFT correspondence, the conformal group is local and infinite dimensional. This allows to construct various states by applying conformal

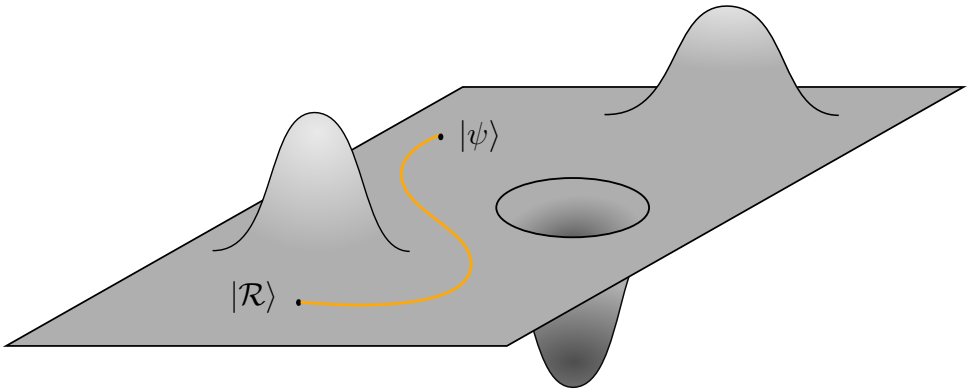

Figure 1.5: Curved Space of States.

transformations to the vacuum state. These transformations exist for any CFT. Complexity can be interpreted as a distance measure between state and reference state. The result is a induced geometry on the space of states as shown in Figure 1.5. We construct conformal transformations, which have the same complexity as the vacuum state. Furthermore, we calculate the change of complexity for small conformal transformations perturbatively. Our results show that the change of complexity for a small conformal transformation is always non-negative. Consequently, the vacuum state locally minimizes complexity. Moreover, it is known how the energy momentum tensor of the field theory transforms under such a transformation, which allows to construct the corresponding operator. Therefore, the complexity of this operator can also be studied in field theory proposals for complexity and is an upper bound for the complexity of the resulting state. Our results comply with field theory predictions, whereas the competing complexity=action proposal yields contradictions [49]. Furthermore, a field theory calculation using a method inspired by holography verifies our results [50].

This dissertation is based on my research under the supervision of Prof. Dr. Johanna Erdmenger first at the Max Planck Institute for Physics in Munich and later at the Julius-Maximilians-Universität in Würzburg. Chapter 3 presents my work published in [P1]. The results presented in Chapter 4 are a continuation of this project and are soon going to be published in [P2]. Furthermore, Chapter 5 presents results from a project done in collaboration with M. Flory and published in [P3].

Chapter 2

Foundations

The $\mathrm{AdS}_{d+1}/\mathrm{CFT}_d$ correspondence is a duality between a conformal field theory (CFT) in d spacetime dimensions and a gravitational theory in Anti-de Sitter (AdS) space in $d+1$ spacetime dimensions. The theory on the field theory side is a gauge theory and the correspondence is therefore an example of a gauge/gravity duality. Furthermore, AdS/CFT is an explicit realization of the holographic principle: the dual gauge theory lives on the boundary of the AdS space. The correspondence and its dictionary, i.e. its one-to-one mapping between field theory and gravity quantities, arise from string theory.

This chapter reviews the basic ingredients of AdS/CFT, its origins in string theory and insights into the holographic principle learned from it. The outline is as follows. To understand what the duality is about, we first take a look at the theories on both sides. In particular, Section 2.1 reviews Anti-de Sitter space and Section 2.2 conformal field theory. Therefore, these section review the theories on both sides of the duality. Afterwards, Section 2.3 takes a short look at string theory, with special emphasis on supergravity and branes. With these ingredients on hand, Section 2.4 sketches the derivation of the duality for $\mathrm{AdS}_5/\mathrm{CFT}_4$, i.e. for a four-dimensional field theory, and reviews the general AdS/CFT correspondence. More information can be found in the standard literature for CFTs (e.g. [51]), for string theory (e.g. [9, 10]) and in the standard reviews of AdS/CFT (see [52–55]). Afterwards, Section 2.5 takes a more general look at holography and discusses what AdS/CFT can teach us about holography.

2.1 Gravity and Anti-de Sitter Space

The dynamics of gravity is determined from the Einstein-Hilbert action

$$S_{EH}[g] = \frac{1}{16\pi G_N} \int \mathrm{d}^D x \sqrt{-\det g} \cdot (R - 2\Lambda), \tag{2.1}$$

where G_N is the gravitational constant in D dimensions and Λ is the cosmological constant[1]. R is the scalar curvature[2]. The associated equation of motions for the metric g are the vacuum Einstein equations

$$R_{MN} - \frac{1}{2} R \cdot g_{MN} + \Lambda \cdot g_{MN} = 0, \tag{2.2}$$

where the spacetime indices M, N run over $0, \ldots, D-1$. Equivalently, the equation of motion can be written as

$$R_{MN} = \frac{2\Lambda}{D-2} \cdot g_{MN}. \tag{2.3}$$

In case we have matter coupled to gravity, the matter action S_{matter} depends of the metric. Einstein equations are then sourced by the energy momentum tensor T, i.e. the right-hand side of Equation (2.2) changes to

$$8\pi G_N T_{MN} = -\frac{16\pi G_N}{\sqrt{\det g}} \cdot \frac{\delta S_{\text{matter}}}{\delta g^{MN}}. \tag{2.4}$$

Anti-de Sitter (AdS) space is a solution to the vacuum Einstein Equation (2.2) for negative cosmological constant $\Lambda < 0$. More specifically, it is the maximally symmetric solution[3]. The AdS metric in Poincaré coordinates is

$$\mathrm{d}s^2 = \frac{L^2}{z^2} \left(\mathrm{d}z^2 + \eta_{\nu\mu} \mathrm{d}x^\nu \mathrm{d}x^\mu \right) = \frac{L^2}{z^2} \left(\mathrm{d}z^2 - \mathrm{d}t^2 + \mathrm{d}\vec{x}^2 \right), \tag{2.5}$$

[1] We consider the metric with mostly positive signature.

[2] The scalar curvature is the trace of the Ricci curvature tensor, i.e. it can be written as

$$R = g^{MN} (\Gamma^P{}_{MN,P} - \Gamma^P{}_{MP,N} + \Gamma^Q{}_{MN} \Gamma^P{}_{PQ} - \Gamma^Q{}_{MP} \Gamma^P{}_{NQ}),$$
$$\Gamma^M{}_{NP} = \tfrac{1}{2} g^{MQ} (g_{QP,N} + g_{QN,P} - g_{NP,Q}).$$

[3] In gravity, symmetries are expressed as diffeomorphisms which preserve the metric. A maximally symmetric spacetime has the maximal number of independent metric preserving diffeomorphisms.

where η is the $(D-1)$-dimensional Minkowski metric. This geometry has a conformally flat[4] boundary at $z = 0$. In spacetimes with boundaries, boundary terms have to be added to the action to keep the variational principle well defined. These boundary terms do not influence the equation of motions. The appropriate boundary term for a timelike boundary is the Gibbons-Hawking-York boundary term. For the AdS case, this yields

$$S_{\mathrm{GHY}} = \frac{1}{8\pi} \int_{\partial AdS} \mathrm{d}^{D-1}x \sqrt{-\det h} \cdot K, \tag{2.6}$$

where h is the induced metric on the boundary and K is its extrinsic curvature.

Instead of considering pure AdS, one can also consider geometries which are only asymptotically AdS. One example is to consider a black hole solution such as the AdS Schwarzschild black hole

$$\mathrm{d}s^2 = \left(\frac{L}{z}\right)^2 \left(-b(z)\mathrm{d}t^2 + \mathrm{d}\vec{x}^2 + b(z)^{-1}\mathrm{d}z^2\right), \tag{2.7a}$$

$$b(z) = 1 - \left(\frac{z}{z_h}\right)^{D-1}. \tag{2.7b}$$

Due to the blackening factor $b(z)$, this spacetime has a horizon at radial position z_h. To make black holes consistent with thermodynamics, black holes have to have an entropy. In particular, the AdS Schwarzschild black hole has an entropy

$$\begin{aligned} S &= \frac{1}{4G_N}\mathrm{Area(Horizon)}, \\ &= \frac{1}{4G_N}\left(\frac{L}{z_h}\right)^{D-2} \mathrm{Vol}(\mathbb{R}^{D-2}) \end{aligned} \tag{2.8}$$

and an associated temperature

$$T = \frac{D-1}{4\pi z_h}. \tag{2.9}$$

[4]For completeness, let us mention that there also exist AdS solutions with spherical and hyperbolic boundary.

2.2 Field Theory and Symmetries

Field theory in flat space is invariant under translations and Lorentz transformations. These transformations form the Poincaré group $ISO(d-,1)$, where d is the spacetime dimension of the field theory group. This symmetry group can be further extended. To maintain causality of the theory, these transformations should not change whether two points are spacelike, timelike or lightlike separated. The condition can be written as

$$x^\mu \to f^\mu(x), \tag{2.10a}$$

$$g_{\mu\nu}(x) \to e^{2\sigma(x)} g_{\mu\nu}(x) \tag{2.10b}$$

for a finite transformation $f(x)$. Therefore, the transformation rescales the metric by a positive factor. Transformations of these type are called conformal transformations and form the conformal group $SO(d,2)$. A theory which is invariant under these conformal transformations does not have a preferred length-scale. In particular, it is massless and all coupling constants are dimensionless. Furthermore, this symmetry can be broken by quantum corrections. In particular, all beta-functions have to vanish for quantum field theory invariant under this symmetry.

For an infinite transformation, this yields

$$x^\mu \to x^\mu + \epsilon^\mu(x), \tag{2.11a}$$

$$g_{\mu\nu}(x) \to (1 + 2\sigma(x)) \cdot g_{\mu\nu}(x) \tag{2.11b}$$

For flat space, i.e. the metric is the flat Minkowski metric $g_{\mu\nu} = \eta_{\mu\nu}$, this is satisfied for diffeomorphisms ϵ which satisfy the conformal killing equation

$$\partial_\mu \epsilon_\nu + \partial_\nu \epsilon_\mu = 2\sigma(x)\eta_{\mu\nu}. \tag{2.12}$$

In two dimensions, this conformal killing equation reduces to the Cauchy-Riemann differential equation and the conformal group becomes infinite dimensional. Therefore, we first focus on spacetime dimension larger than two and look at the special case afterwards.

Table 2.1: Infinitesimal Conformal Transformations.

$\epsilon^\mu(x)$		Number	Generator
$\parallel$			
a^μ	Translations	d	P^μ
$+$			
$w^{[\mu\nu]}x_\nu$	Lorentz Transformations	$\frac{1}{2}d(d-1)$	$J^{\mu\nu}$
$+$			
λx^μ	Dilatation	1	D
$+$			
$b^\mu x^2 - 2b_\nu x^\nu x^\mu$	Special conformal transformations	d	K^μ

2.2.1 Conformal Field Theory for Higher Dimensions

For $d > 2$, there is a finite number of transformations satisfying the conformal killing equations: additionally to translations and Lorentz transformations, these are dilatations and special conformal transformations. These are shown in Table 2.1 with their corresponding generator. From Equation (2.12), the change of the metric is determined by

$$\sigma(x) = \frac{1}{d}\,\partial \cdot \epsilon = \lambda - 2(b \cdot x).$$

Dilatations correspond to a rescaling of the coordinates. The effect of the special conformal transformation is more subtle since it is non-linear. The transformation for a finite special conformal transformation is

$$x^\mu \to \frac{x^\mu + b^\mu x^2}{1 + 2b \cdot x + b^2 x^2}\,. \tag{2.13}$$

It can be directly seen that this maps the $(d-1)$-sphere at infinity to a point b^μ/b^2 and the point $-b^\mu/b^2$ to infinity. Furthermore, lines are mapped the circles and vice versa.

Conformal transformations rescale the metric by a positive factor. In particular, the action in a conformal theory is invariant under a rescaling of the metric. For the energy momentum tensor

$$\langle T_{\mu\nu} \rangle = -\frac{2}{\sqrt{-\det g}} \frac{\delta S}{\delta g^{\mu\nu}}, \tag{2.14}$$

this implies that its trace vanishes

$$\langle T^{\mu}_{\mu} \rangle \propto \delta_{\sigma} S = \frac{\delta S}{\delta g^{\mu\nu}} g^{\mu\nu} = 0. \tag{2.15}$$

However, this is only true for the classical theory. In a quantum theory, the action contains counter terms, which in general to not respect these symmetries and cause anomalies. It can be shown that a conformal anomaly, i.e. $\langle T^{\mu}_{\mu} \rangle \neq 0$, can only appear in even spacetime dimensions.

The generators presented in Table 2.1 form an algebra. This conformal algebra is an extension of the Poincaré algebra

$$[J_{\mu\nu}, P_{\rho}] = i \left(\eta_{\mu\rho} P_{\nu} - \eta_{\nu\rho} P_{\mu} \right), \; [P_{\mu}, P_{\nu}] = 0, \tag{2.16a}$$

$$[J_{\mu\nu}, J_{\rho\sigma}] = i \left(\eta_{\mu\rho} J_{\nu\sigma} - \eta_{\mu\sigma} J_{\nu\rho} - \eta_{\nu\rho} J_{\mu\sigma} + \eta_{\nu\sigma} J_{\mu\rho} \right). \tag{2.16b}$$

The additional non-vanishing commutation relations are

$$[D, K_{\mu}] = -i K_{\mu}, \qquad [D, P_{\mu}] = i P_{\mu}, \tag{2.17a}$$

$$[K_{\mu}, L_{\nu\rho}] = i(\eta_{\mu\nu} K_{\rho} - \eta_{\mu\rho} K_{\nu}), \qquad [K_{\mu}, P_{\nu}] = 2i(\eta_{\mu\nu} D - L_{\mu\nu}). \tag{2.17b}$$

It can be shown that this is the Lorentz algebra in one dimension more, i.e. in dimension $(d+1)$. Therefore, the conformal group and its algebra are denoted as $SO(d,2)$ and $so(d,2)$ respectively.

Different representations of the group are labeled by their eigenvalue $-i\Delta$ with respect to the generator of scale transformations D. Δ is called the scaling dimension. As can be seen from Equation (2.17a), the scaling dimension can be raised by P_{μ} and lowered by K_{μ}.

An operator of scaling dimension Δ transforms as

$$x \to x' = \lambda x, \tag{2.18a}$$

$$\phi(x) \to \phi'(x') = \lambda^{\Delta} \phi(\lambda x). \tag{2.18b}$$

The two-point function for two operators is highly constrained by the conformal symmetry. In particular, it has to vanish for operators of different scaling dimension and is

$$\langle \mathcal{O}(x) \mathcal{O}(y) \rangle \propto \frac{1}{|x-y|^{2\Delta}}. \tag{2.19}$$

for two operators of the same scaling dimension Δ.

2.2.2 Conformal Field Theory for two Dimensions

What is different in two dimensions? To discuss this, let us go to Euclidean signature, i.e. we use $x^0 = -ix^2$. The conformal Killing Equation (2.12) reduces to

$$\partial_2\epsilon^1 = -\partial_1\epsilon^2, \qquad \partial_2\epsilon^2 = \partial_1\epsilon^1,$$

which is the Cauchy-Riemann differential equation. We can define complex coordinates[5] $z = x^2 + ix^1$.In these coordinates, a conformal transformation has the form

$$z \to z + \epsilon. \tag{2.22}$$

The constrain put on ϵ is that it only depends on z, i.e. it is holomorphic. Analogously, $\bar{\epsilon}$ is anti-holomorphic. Therefore, the symmetry group in two-dimensions is infinite-dimensional with an infinite number of generators

$$l_n = -z^{n+1}\frac{\partial}{\partial z}, \qquad \bar{l}_n = -\bar{z}^{n+1}\frac{\partial}{\partial \bar{z}}, \qquad n \in \mathbb{Z}.$$

The corresponding algebra is build buy two copies of the Witt algebra

$$[l_n, l_m] = (m-n)l_{m+n}, \qquad [\bar{l}_n, \bar{l}_m] = (m-n)\bar{l}_{m+n}, \qquad [l_n, \bar{l}_m] = 0.$$

However, these commutation relations are only valid for the classical theory and receive quantum corrections. The resulting algebra is the direct sum of two copies of the Virasoro algebra

$$[l_n, l_m] = (m-n)l_{m+n} + \frac{c}{12}m(m^2-1)\delta_{m+n,0}, \tag{2.23a}$$

$$[\bar{l}_n, \bar{l}_m] = (m-n)\bar{l}_{m+n} + \frac{c}{12}m(m^2-1)\delta_{m+n,0}, \tag{2.23b}$$

$$[l_n, \bar{l}_m] = 0, \tag{2.23c}$$

where c is the central charge and commutes with all generators. Therefore, The Virasoro algebra is a central extension of the Witt algebra and it can be shown to be unique. The central charge is related to the conformal anomaly, which in two

[5] Going back to Euclidean signature, we obtain independent variables $z = ix^+$, $\bar{z} = ix^-$, where $x^\pm = t \pm x$ are the light-cone coordinates of the field theory.

dimensions is

$$\langle T^{\mu}_{\mu} \rangle = \frac{c}{24\pi} R,$$

where R is the Ricci scalar. The value of c depends on the specific theory considered.

A subset of these generators, to be concrete the three generators $\{l_{-1}, l_0, l_1\}$ and their complex conjugate ones, form a subalgebra whose commutation relations do not contain the central charge. These six generators correspond to $D, K^{\mu}, P^{\mu}, J^{01}$ and generate so-called global conformal transformations[6]. The remaining generators generate local conformal transformations and have no equivalent in higher dimensions.

2.2.3 Supersymmetry

In the previous section, we discussed how we can extend the Poincaré group to the conformal group. The additional generators are bosonic. Another way to extend the Poincaré group is to use fermionic generators Q^i_{α}, where $i = 1, \ldots, \mathcal{N}$ labels the different generators added and α is the spinor index.

Dirac fermions are introduced by first defining Gamma matrices, i.e. matrices which satisfy the Clifford algebra

$$\{\gamma^M, \gamma^N\} = -2\eta^{MN}.$$

It can be shown that these matrices have dimension $2^n \times 2^n$, where n is given by $D = 2n$ for even and $D = 2n + 1$ in odd spacetime dimension. In even spacetime dimension, we can define an additional Gamma matrix

$$\gamma^{D+1} = i^{D/2-1} \gamma^0 \cdots \gamma^D \text{ with } (\gamma^{D+1})^2 = 1, \ \{\gamma^{D+1}, \gamma^M\} = 0.$$

It can be shown that $S^{MN} = \frac{1}{4}[\gamma^M, \gamma^N]$ satisfy the Lorentz algebra (2.16b). Therefore, they define a different representation of the Lorentz group. The objects transforming in this representations are spinors with n components, i.e. they have $2n$ real degrees of freedom. However, these representations are not in general irreducible. For example, left- and right-handed Weyl fermions are fermions with eigenvalue $+1$ and -1 with respect to $\bar{\gamma}$ respectively. Another possibility is to consider Majorana

[6] $l_0 + \bar{l}_0$ generate dilatations, $i(l_0 - \bar{l}_0)$ rotations, l_{-1}, $\bar{l}_{-1}$ translations and l_1, $\bar{l}_1$ special conformal transformations.

Table 2.2: Number of Spinor Degrees of Freedoms.

$D = 4$	:	8 real components	$\longrightarrow$	Majorana or Weyl fermions with 4 real components
$D = 10$	:	64 real components	$\longrightarrow$	Majorana-Weyl fermions with 16 real components

fermions, which are fermions which are their own charge conjugate

$$\psi^* = \mathcal{C}\psi, \text{ with } \gamma_M^* = \mp\mathcal{C}\gamma_M\mathcal{C}^{-1}. \tag{2.24}$$

These are defined for dimension $D = 0, 1, 2, 3, 4 \mod 8$ and reduce the number of degrees of freedom by two. Furthermore, in dimension $D = 2 \mod 8$ it is possible to construct Majorana-Weyl spinors. Table 2.2 shows how this reduces the number of degrees of freedom for $D = 4$ and $D = 10$ as an example.

In the following, let us focus on $D = 4$. For notation, we switch from from Latin indices to Greek ones. A convenient choice for the Gamma matrices is

$$\gamma^\mu = \begin{pmatrix} 0 & \sigma^\mu \\ \bar{\sigma}^\mu & 0 \end{pmatrix} \text{ with } \sigma^\mu = (-\mathbb{1}, \vec{\sigma}),\ \bar{\sigma}^\mu = (-\mathbb{1}, -\vec{\sigma}),$$

where $\vec{\sigma}$ are the Pauli matrices. With this choice, the fifth Gamma matrix is

$$\bar{\gamma} = \begin{pmatrix} \mathbb{1} & 0 \\ 0 & -\mathbb{1} \end{pmatrix} \tag{2.25}$$

and a four component Dirac spinor splits into two-component Weyl spinors as

$$\Psi = \begin{pmatrix} \Psi_L \\ \Psi_R \end{pmatrix} = \begin{pmatrix} \psi_\alpha \\ \bar{\psi}_{\dot{\alpha}} \end{pmatrix}. \tag{2.26}$$

Left- and right-handed spinor transform in different representations of the Lorentz group, as can be seen from

$$S^{\mu\nu} = \begin{pmatrix} \sigma^{\mu\nu} & 0 \\ 0 & \bar{\sigma}^{\mu\nu} \end{pmatrix}, \tag{2.27a}$$

$$\sigma^{\mu\nu} = \frac{i}{4}\left(\sigma^\mu\bar{\sigma}^\nu - \sigma^\nu\bar{\sigma}^\mu\right), \tag{2.27b}$$

$$\bar{\sigma}^{\mu\nu} = \frac{i}{4}\left(\bar{\sigma}^\mu\sigma^\nu - \bar{\sigma}^\nu\sigma^\mu\right). \tag{2.27c}$$

The way the fermionic supercharges Q^i extend the Poincaré algebra is highly constrained by symmetry. In particular, we have

$$\left[J^{\mu\nu}, Q^i_\alpha\right] = -(\sigma^{\mu\nu})_\alpha{}^\beta Q^i_\beta, \tag{2.28a}$$

$$\left[J^{\mu\nu}, \bar{Q}^i_{\dot\alpha}\right] = -\epsilon_{\dot\alpha\dot\beta}(\bar\sigma^{\mu\nu})^{\dot\beta}{}_{\dot\alpha}\bar{Q}^i_{\dot\beta}, \tag{2.28b}$$

$$\left\{Q^i_\alpha, \bar{Q}^j_{\dot\beta}\right\} = 2\delta^{ij}(\sigma^\mu)_{\alpha\dot\beta}P_\mu. \tag{2.28c}$$

This is the most general supersymmetry algebra. The theory has a $SU(\mathcal{N})_R$ symmetry with respect to special unitary transformations acting on i, j. P^2 is a Casimir operator of the algebra, i.e. representations can be labeled by their eigenvalue with respect to it.

In particular, we are interested in massless representations, i.e. $P^2 = 0$. We may consider $P^\mu = (E, 0, 0, E)$. With this choice, the supersymmetry algebra simplifies, in particular

$$\left\{Q^i_\alpha, \bar{Q}^j_{\dot\beta}\right\} = 4E\delta^{ij}\begin{pmatrix} 1 & 0 \\ 0 & 0 \end{pmatrix}_{\alpha\dot\beta} P_\mu.$$

This implies that acting with Q^i_2 on physical states results in zero and does not create a new state. Furthermore, we can define creation and annihilation operators proportional to Q^i_1 and $\bar{Q}^i_{\dot 1}$ respectively. The little group, i.e. the subgroup of the Poincaré group leaving this choice invariant is J_{12}. We can label the states in this representation with their eigenvalue to respect to J_{12}. This eigenvalue is called the helicity λ. These supersymmetry generators raise or increase the helicity

$$\left[Q^i_1, J_{12}\right] = \frac{1}{2}Q^i_1, \qquad \left[\bar{Q}^i_{\dot 1}, J_{12}\right] = -\frac{1}{2}\bar{Q}^i_{\dot 1}. \tag{2.29}$$

Therefore, they create a fermionic state from a bosonic one and vice-versa. Consequently, a supersymmetric theory has the same number of bosonic and fermionic degrees of freedom.

We can construct the massless multiplet by starting with a state of maximal helicity $|\lambda\rangle$ and acting with $\bar{Q}^i$ on it to obtain all possible states of lower helicity. Each of these supercharges can be applied at most one time since $\left(\bar{Q}^i\right)^2 = 0$. To have a representation invariant under CPT conjugation, one also has to add the states with negative helicity. Table 2.3 shows different multiplets. Supersymmetry with $\mathcal{N} = 4$ is special, since it has the maximal number of supersymmetries to obtain a multiplet without gravity. Furthermore, the representation is automatically CPT

Table 2.3: Massless Supersymmetric Multiplets in $D = 4$.

λ			$\mathcal{N}=1$	$\mathcal{N}=2$	$\mathcal{N}=4$
1	vector boson	A^μ	•		•
$\frac{1}{2}$	Weyl spinor	ψ	•	•	• • • •
0	scalar field	ϕ		• •	• • • • • •
$-\frac{1}{2}$	Weyl spinor	$\bar{\psi}$	•	•	• • • •
-1	vector boson	A^μ	•		•

invariant. Let us focus in this highly symmetric theory in the following.

2.2.4 $\mathcal{N} = 4$ Supersymmetric Yang-Mills Theory in $D = 4$

The above discussed multiplet for $\mathcal{N} = 4$ is described by the following fields, which transform in different representations in the $SU(4)_R$ symmetry group:

- a gauge field A_μ transforming as a singlet,
- four Weyl fermions λ^a transforming in the fundamental representation,
- six real scalars ϕ^i transforming in the two-index anti-symmetric representation.

It is possible to construct a supersymmetric Yang-Mills theory, i.e. a gauge theory where all these fields transform in the adjoint representation of $SU(N)$. The CP-invariant Lagrangian for this theory is[7][8]

$$\begin{aligned}\mathcal{L} = \mathrm{Tr}\Bigg[& -\frac{1}{2g_{YM}^2} F_{\mu\nu}F^{\mu\nu} + \frac{\theta}{16\pi^2} F_{\mu\nu}\tilde{F}^{\mu\nu} - i\lambda^a \bar{\sigma}^\mu D_\mu \lambda_a - D_\mu \phi^i D^\mu \phi^i \\ & + g_{YM} C_i^{ab} \lambda_a [\phi^i, \lambda_b] + \bar{C}_{iab} \lambda^a [\phi^i, \bar{\lambda}^b] + \frac{g_{YM}^2}{2} [\phi^i, \phi^j]^2 \Bigg]. \end{aligned} \tag{2.30}$$

The Yang-Mills coupling g_{YM} is dimensionless, which results in the theory being scale invariant on a classical level. Interestingly, quantization does not break the scale invariance. Therefore, the beta function vanishes and the theory does not have a preferred length-scale.

[7] C_i^{ab} are Clebsch-Gordan coefficients.

[8] Used conventions: $F_{\mu\nu} = \partial_\mu A_\nu - \partial_\nu A_\mu + i[A_\mu, A_\nu]$, $D_\mu \cdot = \partial_\mu + i[A_\mu, \cdot\,]$

2.3 String Theory

The fundamental objects of string theory are strings, i.e. two-dimensional objects embedded into a D-dimensional target spacetime. Table 2.4 shows how the description of a relativistic point particle can be generalized to a string. In the following, we first review the quantization of strings. Afterwards, I take a closer look at two concepts important for the AdS/CFT duality: the low-energy limit known as supergravity and Dp-branes, which are non-perturbative objects arising from open strings.

Table 2.4: Transition from Point-Particle to String.

point-particle	$\longrightarrow$	**string**
world-line $X^M(\tau)$		world-sheet $X^M(\tau,\sigma)$
mass m		tension $T = \dfrac{1}{2\pi l_s^2}$
$S = -m\int \mathrm{d}\tau\, \sqrt{-\partial_\tau X^M \partial_\tau X_M}$		$S = -T\int \mathrm{d}\tau\, \mathrm{d}\sigma\, \sqrt{-\det(\partial_\alpha X^M \partial_\beta X_M)}$

The action arising from the analogue to the relativistic point-particle is the Nambu-Goto action

$$S_{NG} = -T\int \mathrm{d}\tau\, \mathrm{d}\sigma\, \sqrt{-\det(\partial_\alpha X^M \partial_\beta X^N \eta_{MN})}, \tag{2.31}$$

where the metric η is the metric of the target spacetime, which in the following will be the Minkowski metric. X^M is the target space embedding of the string and $\sigma^\alpha = \{\tau, \sigma\}$ are the worldsheet coordinates[9]. T is the tension of the string $T = (2\pi l_s^2)^{-1}$ and l_s is the string length $l_s^2 = \alpha'$.

For quantization, it is more convenient to work with the classically equivalent Polyakov action[10]

$$S_P = -\frac{T}{2}\int_\Sigma \mathrm{d}\tau\, \mathrm{d}\sigma\, \partial_\alpha X \cdot \partial_\beta X\ \eta^{\alpha\beta}, \tag{2.32a}$$

[9] The conventions used in this thesis are summarized in Section A.3.

[10] The dot implies contraction with the D-dimensional Minkowski metric.

with the additional constraint[11]

$$T_{\alpha\beta} = \partial_\alpha X \cdot \partial_\beta X - \frac{1}{2}\eta_{\alpha\beta}\eta^{\gamma\delta}\partial_\gamma X \cdot \partial_\delta X. \tag{2.32b}$$

$\eta_{\alpha\beta}$ is the two-dimensional Minkowski metric.

Convenient coordinates are light-cone coordinates for the worldsheet coordinates, i.e. $\sigma^\pm = \tau \pm \sigma$. In these coordinates, the equations of motions arising from the Polyakov action (2.32a) are

$$\partial_+\partial_- X^M = 0. \tag{2.33}$$

This allows to split the excitations into left- and right-moving ones

$$X^M(\tau,\sigma) = X^M_{(L)}(\sigma^+) + X^M_{(R)}(\sigma^-). \tag{2.34}$$

The equation of motion allows the following mode expansion

$$X^M_{(L)}(\sigma^+) = \frac{x_0^M}{2} + \frac{l_s}{\sqrt{2}}\tilde{\alpha}_0^M\sigma^+ + i\frac{l_s}{\sqrt{2}}\sum_{\substack{n\in\mathbb{Z}\\ n\neq 0}}\frac{\tilde{\alpha}_n^M}{n}\exp\bigl(-in\sigma^+\bigr), \tag{2.35a}$$

$$X^M_{(R)}(\sigma^-) = \frac{x_0^M}{2} + \frac{l_s}{\sqrt{2}}\alpha_0^M\sigma^- + i\frac{l_s}{\sqrt{2}}\sum_{\substack{n\in\mathbb{Z}\\ n\neq 0}}\frac{\alpha_n^M}{n}\exp\bigl(-in\sigma^-\bigr). \tag{2.35b}$$

Since X^M have to be real, the coefficients have to satisfy $\alpha^M_{-n} = (\alpha^M_n)^*$, $\tilde{\alpha}^M_{-n} = (\tilde{\alpha}^M_n)^*$. Using canonical quantization for X^M and their conjugate momenta, the coefficients α_n and $\tilde{\alpha}_n$ are proportional to ladder operators of an harmonic oscillator

$$[\alpha_m^M, \alpha_n^N] = m\eta^{MN}\delta_{m+n,0}, \tag{2.36a}$$

$$[\tilde{\alpha}_m^M, \tilde{\alpha}_n^N] = m\eta^{MN}\delta_{m+n,0}. \tag{2.36b}$$

There is one subtlety: to make the variational principle well defined, bound-

[11] Exactly speaking, the Nambu-Goto action is equivalent to

$$S_P = -\frac{T}{2}\int_\Sigma \mathrm{d}\tau\,\mathrm{d}\sigma\,\sqrt{-h}h^{\alpha\beta}\partial_\alpha X^M\partial_\beta X^N\eta_{MN}.$$

This action contains an auxiliary, non-dynamical field h, which has the interpretation of a worldsheet metric. It is gauged in Equation (2.32a) and its equation of motion remains as constraint.

ary terms have to vanish. The Polyakov action Equation (2.32a) gives rise to the boundary term

$$\left[\partial_\sigma X^M \delta X_M\right]_0^{\sigma_{\max}} \tag{2.37}$$

The trivial case for this term to vanish is to consider a closed string, i.e. the embedding is periodic $\sigma \sim \sigma + 2\pi$ and we have $\alpha_0 = \tilde{\alpha}_0$. The other case are open strings, where we have $\sigma \in [0, \sigma_{\max}]$[12]. There are two possibilities for the boundary terms to vanish at the endpoints $\sigma_0 \in \{0, \sigma_{\max}\}$:

- ***N**eumann boundary condition:* $\partial_\sigma X^M(\tau, \sigma_0) = 0$,
  These boundary condition ensures that there is no momentum flow at the endpoint.

- ***D**irichlet boundary condition:* $\partial_\tau X^M(\tau, \sigma_0) = 0$.
  This boundary condition fixes the endpoint of the string.

By choosing the boundary conditions on both ends independently, NN, DD, ND and DN boundary conditions are possible[13].

Additionally to the equations of motions, we have to impose the constraint Equation (2.32b): the vanishing of the stress-energy tensor. In the coordinates $\sigma^\pm$, these are

$$\begin{aligned} T_{++} &= \partial_+ X \cdot \partial_+ X & T_{--} &= \partial_- X \cdot \partial_- X, \\ &= l_s^2 \sum_{m=\mathbb{Z}} \tilde{L}_m e^{-im\sigma^+}, & &= l_s^2 \sum_{m=\mathbb{Z}} L_m e^{-im\sigma^-}. \end{aligned} \tag{2.38}$$

In a classical theory, these modes have to vanish. However, things are more subtle for a quantum theory: these modes become operators. The conditions for physical states $|\phi\rangle$ are

$$\tilde{L}_m |\phi\rangle = L_m |\phi\rangle = 0, \tag{2.39a}$$

$$(\tilde{L}_0 - a)|\phi\rangle = (L_0 - a)\,|\phi\rangle = 0, \tag{2.39b}$$

[12] It is possible to keep the mode-expansion (2.35b) the same for all boundary conditions by choosing $\sigma_{\max}$ appropriately.

[13] Imposing Dirichlet or Neumann boundary conditions at $\sigma = 0$ results in $\alpha_n = \tilde{\alpha}_n$ and $\alpha_n = -\tilde{\alpha}_n$ respectively. Imposing the same boundary condition at $\sigma_{\max}$ is achieved automatically by $\sigma_{\max} = \pi$, whereas imposing the opposite boundary condition is achieved by $\sigma_{\max} = \pi/2$.

where a is a constant arising from normal ordering. For the modes $\tilde{L}_0$, L_0, one obtains

$$\tilde{L}_0 = \frac{1}{2}\tilde{\alpha}_0 \cdot \tilde{\alpha}_0 + \tilde{N} \ , \qquad L_0 = \frac{1}{2}\alpha_0 \cdot \alpha_0 + N, \tag{2.39c}$$

$$\tilde{N} = \sum_{n\in\mathbb{N}} \tilde{\alpha}_{-n} \cdot \tilde{\alpha}_n, \qquad N = \sum_{n\in\mathbb{N}} \alpha_{-n} \cdot \alpha_n, \tag{2.39d}$$

where N and $\tilde{N}$ are number operator. It can be shown that $N = \tilde{N}$ for all boundary conditions, which is called level-matching.

The mass of the string can be derived from $P^2 = -M^2$ where P is the canonical momentum. This yields

$$M^2 = \frac{1}{l_s^2}(N - a) \cdot \begin{cases} 1 & \text{open string with NN boundary conditions,} \\ 4 & \text{closed string.} \end{cases} \tag{2.40}$$

To evaluate the mass, a has to be determined. One has to be careful to avoid over-counting: the commutation relations Equation (2.36) show that there are negative norm states in the theory, which have to be removed by gauge fixing. Considering this yields

$$a = \frac{1}{2}(D-2)\sum_{n=1}^{\infty} n = -\frac{D-2}{24}, \tag{2.41}$$

where D is the dimension of the target spacetime.

For open strings, the excitation of lowest mass is a vector boson $\alpha_1^i|0,\vec{k}\rangle$ and transforms under $SO(D-2)$. To avoid anomalies of the Lorentz symmetry, these states have to be massless. Therefore, we have the restriction $a = 1$, forcing the dimension of the target space to be $D = 26$. The zero-mass excitation of the closed string is $\alpha_1^i\tilde{\alpha}_1^j|0,\vec{k}\rangle$, i.e. a rank-two tensor which can be decomposed into a symmetric traceless tensor, an antisymmetric tensor and a scalar.

This emphasizes why string theory is a candidate for unifying gauge theory and gravity: the lowest excitations of open strings describe gauge bosons, whereas the lowest excitations of closed strings contain a symmetric rank-2 tensor which describes a graviton.

The previous discussion only considers bosonic strings. A straight forward way to achieve fermionic degrees of freedom is to impose worldsheet supersymmetry. Every bosonic field X^M obtains a fermionic superpartner $\Psi^M = \begin{pmatrix}\psi_-^M & \psi_+^M\end{pmatrix}^T$. The

action receives the additional contribution[14]

$$\begin{aligned} S_f &= \frac{1}{4\pi l_s^2} \int d^2\sigma \bar{\Psi}^M \rho^\alpha \partial_\alpha \Psi_M, \\ &= \frac{-i}{2\pi l_s^2} \int d^2\sigma \left(\bar{\psi}_+ \partial_- \psi_+ + \bar{\psi}_- \partial_+ \psi_- \right). \end{aligned} \tag{2.42}$$

The quantization and the calculation of the spectrum is then analogous to bosonic string theory. The equation of motion for the fermions allows to split the result in terms of left- and right-moving excitations

$$\psi_+ = \frac{1}{\sqrt{2}} \sum_n d_n \exp(-in\sigma_+), \qquad \psi_- = \frac{1}{\sqrt{2}} \sum_n \tilde{d}_n \exp(-in\sigma_-). \tag{2.43}$$

These Grassmann-valued coefficients satisfy anti-commutation relations

$$\{d_m^M, d_n^N\} = \eta^{NM} \delta_{m+n,0}. \tag{2.44}$$

To keep the variational principle well-defined, the boundary term

$$[\psi_+ \delta\psi_+ - \psi_- \delta\psi_-]_0^{\sigma_{\max}} = 0 \tag{2.45}$$

has to vanish for open strings. This yields the boundary conditions

- *at* $\sigma = 0$*:* $\psi_+(\tau, 0) = \psi_-(\tau, 0)$,
- ***R****amond boundary condition:* $\psi_+(\tau, \pi) = \psi_-(\tau, \pi)$,
- ***N****eveu* ***S****chwarz boundary condition:* $\psi_+(\tau, \pi) = -\psi_-(\tau, \pi)$.

The NS boundary conditions describes bosons, whereas the R sector contains fermions. For closed strings, the left- and right-moving excitations can be either periodic (R) or antiperiodic (NS). This can be chosen for both type of excitations independently, resulting in four different boundary conditions labeled as R-R, NS-NS, R-NS and NS-R[15].

[14] Used conventions:

$$\rho^0 = \begin{pmatrix} 0 & -1 \\ 1 & 0 \end{pmatrix}, \ \rho^1 = \begin{pmatrix} 0 & 1 \\ 1 & 0 \end{pmatrix}, \ \Psi = \begin{pmatrix} \psi_- \\ \psi_+ \end{pmatrix}$$

[15] These boundary conditions for both types of strings are named the same because they have the same effect: NS boundary conditions cause $n + \frac{1}{2} \in \mathbb{Z}$, wheres R boundary conditions cause

Repeating the same procedure as in the bosonic case, the same mass formula as in equation (2.40) is obtained where know the number operator N is

$$N = \sum_{n=1}^{\infty} \alpha_{-n} \cdot \alpha_n + \sum_{n=1}^{\infty} d_{-n} \cdot d_n n \tag{2.46}$$

and a is changed. For superstrings, Lorentz invariance now requires spacetime dimension $D = 10$, resulting in

$$a = \begin{cases} \frac{1}{2} & \text{NS}, \\ 0 & \text{R}. \end{cases} \tag{2.47}$$

There are problems with the spectrum. It contains tachyons. Furthermore, consistency requires spacetime supersymmetry, resulting in an equal number of fermionic and bosonic degrees of freedom for each mass. This is obtained by truncating the spectrum. For the Neveu-Schwarz sector, only states with odd fermion number $\sum_{n>0} d_{-n} d_n$ are considered to avoid the tachyon. For the Ramon sector, one can choose to consider either states with even or with odd fermion number. We will go with the first choice. The resulting massless spectrum for open strings consists of

- a gauge boson: $d^M_{-1/2}|0\rangle_{NS}$,
- its superpartner, the gaugino: $|0\rangle_R$.

For the closed string spectrum, one can pick left- and right-movers from these states, resulting in the combinations

- $d^M_{-1/2}|0\rangle_{NS} \otimes d^N_{-1/2}|0\rangle_{NS}$
- $|0\rangle_R \otimes |0\rangle_R$
- $|0\rangle_R \otimes d^N_{-1/2}|0\rangle_{NS},\ d^M_{-1/2}|0\rangle_{NS} \otimes |0\rangle_R$

These states split into irreducible representations as shown in Table 2.5.

In string theory, one can either consider a theory with only closed strings or a theory with open and closed strings.

$n \in \mathbb{Z}$. Therefore, the Ramond sector contains d_0 modes, whose anti-commutation relations are the Clifford algebra and who hence create fermionic degrees of freedom, while the Neveu-Schwarz sector only contains bosons.

Table 2.5: Particle Content of Massless Closed IIB String Theory.

Sector	Field	Particle
NS-NS	ϕ	scalar (dilaton)
	$B_{(2)}$	antisymmetric two-form gauge field (Kalb-Ramond field)
	g_{MN}	metric (graviton)
R-R	$C_{(n)},\ n \in \{0, 2\}$	n-form gauge field
	$C_{(4)}$	self-dual 4-form gauge field
NS-R	$\lambda_I,\ I \in \{1, 2\}$	spin 1/2 dilatinos
	$\Psi_I^M,\ I \in \{1, 2\}$	spin 3/2 gravitinos with same chirality

2.3.1 Supergravity

The only length-scale of string theory (in Minkowskian background) is the string length l_s. Therefore, the low energy limit of the theory corresponds to $E \cdot l_s$ small and can be considered by taking $l_s \to 0$. In this limit, all modes except the zero-mass modes become infinitely heavy (see Equation (2.40)) and can be integrated out. Only the massless modes shown in Table 2.5 survive. Furthermore, the strings become pointlike. This results in being able to describe the theory by an effective theory living in the ten-dimensional target space. As discussed above, the theory has (spacetime) supersymmetry and contains gravity. The effective low-energy action is the so-called supergravity (SUGRA) action. It is a theory where supersymmetry is promoted to a gauge theory. The resulting gauge fields are the gravitinos Ψ_I^M. Since two supersymmetric transformations result in a translation, gauging supersymmetry automatically produces diffeomorphism invariance and consequently gravity.

The bosonic action of type IIB supergravity is

$$\begin{aligned} S_{IIB} =& \frac{1}{2\tilde{\kappa}_{10}^2}\left[\int \mathrm{d}^{10}X\sqrt{-g}\left(e^{-2\phi}(R + 4\partial_M\phi\partial^M\phi - \frac{1}{2}|H_{(3)}|^2)\right.\right. \\ & \left.\left. -\frac{1}{2}|F_{(1)}|^2 - \frac{1}{2}|\tilde{F}_{(3)}|^2 - \frac{1}{4}|\tilde{F}_{(5)}|^2\right) + \frac{1}{2}\int C_{(4)} \wedge H_{(3)} \wedge F_{(3)}\right]. \end{aligned} \tag{2.48}$$

The field-strength tensors in this action are $F_{(p)} = dC_{(p-1)}$ and $H_{(3)} = dB_{(2)}$, as well as

$$\begin{aligned} \tilde{F}_{(3)} &= F_{(3)} - C_{(0)}H_{(3)}, \\ \tilde{F}_{(5)} &= F_{(5)} - \frac{1}{2}C_{(2)} \wedge H_{(3)} + \frac{1}{2}B_{(2)} \wedge F_{(3)}. \end{aligned}$$

This action correctly produces the equation of motions for the massless spectrum of closed type IIB string theory. However, the action does not automatically incorporate the self-duality constraint on the five-form. Instead, it has to be imposed separately. The complete action also contains the fermionic terms. We will not present them here. Later on, we consider classical solutions of this action, for which fermionic fields vanish.

To conclude this section, the gravitational constant can be expressed in terms of the string length

$$2\tilde{\kappa}_{10}^2 = (2\pi)^7 l_s^8. \tag{2.49}$$

Furthermore, one can expand the dilaton around its classical solution ϕ_0, which is related to the string coupling g_s

$$g_s = e^{\phi_0}. \tag{2.50}$$

Identifying the Einstein-Hilbert term of the action yields for the 10-dimensional Newton constant G_{10}

$$2\tilde{\kappa}_{10}^2 e^{2\phi_0} = 2\kappa_{10}^2 = 16\pi G_{10}. \tag{2.51}$$

2.3.2 D-branes

For open strings, there are two type of boundary conditions: Neumann boundary condition and Dirichlet boundary condition. The physical interpretation of Dirichlet boundary conditions is that the endpoint is fixed. This breaks translational invariance and momentum is no longer conserved. The reason is that there is momentum flow at the endpoints. Consequently, these strings have to end on physical objects which can absorb this momentum flow. For a string with Neumann boundary conditions for $(p+1)$ spacetime directions and Dirichlet boundary conditions for the remaining spatial directions, this physical object is a $(p+1)$ dimensional surface called Dp-brane. These objects are stable if they couple to one of the gauge fields of the theory and have a conserved charge. In type IIB string theory, we have n-form gauge fields with $n = 0, 2, 4$[16]. Therefore, the theory allows for stable Dp branes with odd p.

These Dp branes are not rigid objects, but in fact dynamical [56]. The massless

[16]These couple electrically to D$(n-1)$ branes and magnetically to D$(7-n)$ branes.

spectrum contains a worldvolume gauge field A_μ from the open-strings excitations and $9-p$ massless scalar fields, which arise as goldstone modes from broken translational symmetry and describe transverse excitations of the brane. The interaction between these fields and the NS-NS sector of the closed strings is described by the Dirac-Born Infeld (DBI) action[17]

$$S_{\text{DBI}} = -\tau_p \int \mathrm{d}^{p+1}\xi \, e^{-\phi} \sqrt{-\det\left(g_{\mu\nu} + B_{\mu\nu} + 2\pi\alpha' F_{\mu\nu}\right)}. \tag{2.52}$$

The indices $\mu,\ \nu = 0,\ \ldots\ p$ are for the coordinates parallel to the branes and $g_{\mu\nu}, B_{\mu\nu}$ are the pull-back of the metric and the Kalb-Ramond field respectively. The coupling between R-R sector and the brane-fields is described by a Chern-Simons term S_{CS} and yields to the brane being charged. If only the metric is fluctuating, the DBI-action reduces to

$$B = F = 0, \phi = \ln g_s : \qquad S_{\text{DBI}} = -\frac{\tau_p}{g_s} \int \mathrm{d}^{p+1}\xi \, \sqrt{-\det g_{\mu\nu}}. \tag{2.53}$$

This is the higher-dimensional generalization of the Nambu-Goto action (2.31) (see also Table 2.4). The tension of the brane is determined by examining a closed string colliding with the brane and matching this process to the analog open string process (see [56]), yielding

$$\tau_p = (2\pi)^{-p} \cdot l_s^{-(p+1)}. \tag{2.54}$$

If we in contrast focus on the field-strength F in flat space, we obtain

$$B = 0,\ g = \eta,\ \alpha \ll 1 : \qquad S_{\text{DBI}} = const. - \frac{\tau_p (2\pi\alpha')^2}{4 g_s} \int \mathrm{d}^{p+1}\xi \, F_{\mu\nu} F^{\mu\nu}. \tag{2.55}$$

This is the Yang-Mills action with coupling constant

$$g_{YM}^2 = (2\pi)^{p-2} {l_s}^{p-3} g_s. \tag{2.56}$$

The DBI action can therefore be understood as non-linear generalization of the Yang-Mills action.

Instead of considering a single Dp-brane, one can also consider a stack of N

[17] For a small field strength, the DBI action reduces to Yang-Mills action in flat spacetimes. Consequently, it can be understood as a non-linear generalization of Yang-Mills theory. The corresponding coupling is $g_{YM}^2 = (2\pi)^{p-2} g_s l_s^{p-3}$.

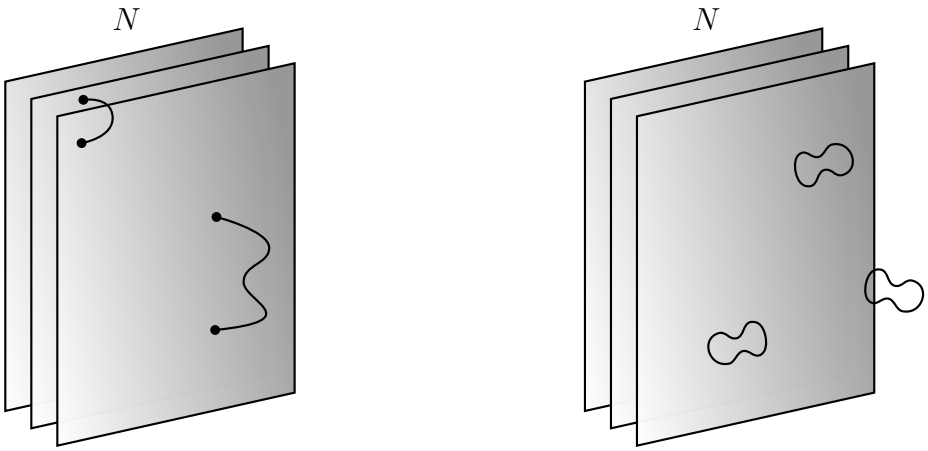

(a) Open String Perspective

(b) Closed String Perspective

Figure 2.1: Dp-Branes

coinciding Dp branes. This promotes the fields to $N \times N$ matrices, where the indices label the branes the open strings ends on. In particular, the gauge field A_μ becomes a $U(N)$ gauge field. All open strings states transform in the adjoint representation of this gauge group. The DBI-action now involves taking the trace

$$S_{\text{DBI}} = -\tau_p \int \mathrm{d}^{p+1}\xi \, e^{-\phi} \, \mathrm{Tr} \sqrt{-\det\left(g_{\alpha\beta} + B_{\alpha\beta} + 2\pi\alpha' F_{\alpha\beta}\right)}. \tag{2.57}$$

From Equation (2.53), we see that the tension of Dp-branes is given by τ_p/g_s. Therefore, these branes are non-perturbative objects. Therefore, they are treated as rigid objects and strings as perturbations. For this picture to work, the coupling between open and closed strings has to be small, i.e. $g_s N \ll 1$.

Interestingly, it was shown in [57] that Dp-branes are equivalent to massive $(p+1)$-dimensional surfaces in closed string theory. In the low-energy limit, these p-branes are solitonic solutions of SUGRA. The ansatz for the metric preserving the $\mathbb{R}^{p+1} \times SO(p,1) \times SO(9-p)$ symmetry is

$$\mathrm{d}s^2 = H_p(r)^{-1/2} \eta_{\mu\nu} \mathrm{d}x^\mu \mathrm{d}x^\nu + H_p(r)^{1/2} \mathrm{d}y^i \mathrm{d}y^i, \tag{2.58a}$$

where x^μ are the coordinates parallel to the surface and y^i are the transverse directions. The function H_p only depends on the distance from the surface $r = \sqrt{\sum_i (y^i)^2}$. The only other non-vanishing SUGRA fields are the dilaton and the gauge field under

which couples to the brane

$$e^{\phi} = g_s H_p(r)^{(3-p)/4}, \tag{2.58b}$$

$$C_{(p+1)} = \left(H_p(r)^{-1} - 1\right) \mathrm{d}x^0 \wedge \mathrm{d}x^1 \wedge \cdots \wedge \mathrm{d}x^p. \tag{2.58c}$$

This solves the SUGRA equations for motions if

$$\begin{aligned} \Box H_p(r) &= 0, \\ H_p(r) &= 1 + \left(\frac{L_p}{r}\right)^{7-p}, \end{aligned} \tag{2.59}$$

where L_p is an integration constant at this point. To ensure that the SUGRA descriptions can be applied, L_p should be large.

To understand what these objects are, two limits are interesting:

- Asymptotically (i.e. for $r \to \infty$), the metric reduces to flat Minkowski space.
- In contrast, the metric diverges as we approach the surface, i.e. $r \to 0$. The spacetime has a $(p+1)$-dimensional singularity at $r = 0$.

These p-branes are therefore higher-dimensional generalizations of black holes.

Therefore, there are two perspective of Dp-branes are shown in Figure 2.1: in the open strings picture, they are dynamical objects where strings can end and which effectively give rise to a non-abelian gauge theory. In the closed string picture, they are massive objects which curve the space around them and correspond to higher-dimensional generalizations of black holes. How are these two perspectives related? In both perspectives, these objects are charged under the p-form gauge field. Matching the charge yields

$$L_p^{7-p} = (4\pi)^{(5-p)/2} \Gamma\left(\frac{7-p}{2}\right) g_s N \alpha'^{(7-p)/2}, \tag{2.60}$$

where N is the number of considered branes[18].

[18] Therefore, the limit L_p large corresponds to $g_s N \gg 1$. This implies that these two perspectives only work in opposite limits.

2.4 The AdS/CFT Correspondence

There are several realizations of AdS/CFT arising from considering branes in string theory. In the following, we first review the most prominent example: the duality between a four-dimensional CFT and AdS space in five dimensions (i.e. $\mathrm{AdS}_5/\mathrm{CFT}_4$) as conjectured by Maldacena [11]. Afterwards, we take a look at the general AdS/CFT correspondence and review aspects relevant for it. This also introduces the conventions used in the remaining chapters.

2.4.1 Derivation of $\mathrm{AdS}_5/\mathrm{CFT}_4$

In 1997, Maldacena considered the low-energy limit of D3-branes [11]. As discussed in Section 2.3.2, these objects are described by two perspectives: as surfaces where open strings end (open string perspective) or as heavy objects, which deform the space around them and form a black hole (closed string perspective).

Open string perspective

In the open-string perspective, the action splits into three parts:

$$S = S_{\text{bulk}} + S_{\text{brane}} + S_{\text{int}}, \tag{2.61}$$

where S_{bulk} describes the closed string sector, S_{brane} describes the open string sector and S_{int} captures the interactions between both sectors. In the low energy limit, S_{bulk} reduces to the type IIB SUGRA action. The bosonic part of the remaining terms arises from the DBI action S_{DBI} and the Chern-Simons term. For a stack of N D3 branes, the DBI action (see (2.57)) is

$$S_{\text{DBI}} = -\tau_p \int \mathrm{d}^{p+1}\xi \, e^{-\phi} \, \mathrm{Tr} \sqrt{-\det\left(g_{\mu\nu} + 2\pi\alpha' F_{\mu\nu}\right)}, \tag{2.62}$$

where B is set to zero for simplicity. The Greek indices μ, ν label the $(p+1)$ directions parallel to the brane, ξ are the coordinates parameterizing the brane and $g_{\mu\nu}$ is the pull-back of the metric. The DBI action describes the interaction of the metric and the dilaton field with the bosonic fields living on the brane: the $SU(N)$ gauge field A^μ with the associated field strength $F_{\mu\nu}$ and six Goldstone modes X^i

for the broken translational invariance in six directions[19].

As discussed previously, the DBI action reduces to the Yang-Mills action for small α', see Equation (2.55). The corresponding Yang-Mills coupling is (see Equation (2.56))

$$2\pi g_s = g_{YM}^2. \tag{2.63}$$

Considering also the remaining terms contributing to S_{brane} yields for the Lagrangian describing the open string excitations

$$\begin{aligned}\mathcal{L}_{\text{brane}} = \text{Tr}\Bigg[&-\frac{1}{2g_{YM}^2}F_{\mu\nu}F^{\mu\nu} + \frac{\theta}{16\pi^2}F_{\mu\nu}\tilde{F}^{\mu\nu} - i\lambda^a\bar{\sigma}^\mu D_\mu\lambda_a - D_\mu X^i D^\mu X^i \\ &+ g_{YM}C_i^{ab}\lambda_a[X^i,\lambda_b] + C_{iab}\lambda^a[X^i,\lambda^b] + \frac{g_{YM}^2}{2}[X^i,X^j]^2\Bigg],\end{aligned} \tag{2.64}$$

where $F_{\mu\nu}$ is the field strength tensor of A^μ and C_i^{ab} are Clebsch-Gordan coefficients[20].

The only parameter of the Lagrangian is the dimensionless coupling constant g_{YM}. Therefore, the theory is conformal on the classical level. A special feature of this theory is that it also has conformal invariance as a quantum theory. This implies that the beta function for the coupling vanishes. Furthermore, this is a theory with $\mathcal{N} = 4$ supersymmetry in $d = 4$ dimensions. This corresponds to 8 supercharges. They arise since we started with a supersymmetric theory in $D = 10$, which has 16 supercharges. However, half of the supersymmetries are broken due to the brane. The fields on the brane arrange in a $\mathcal{N} = 4$ gauge multiplet in four dimensions. This theory is $\mathcal{N} = 4$ supersymmetric Yang-Mills (SYM) theory on $\mathbb{R}^{3,1}$.

The remaining part of the action is S_{int}. When taking the small α limit, one has to be careful with normalizing all fields appropriately. If done correctly, the interaction term vanishes. Therefore, the closed and the open string modes decouple and we obtain

$$\mathcal{N} = 4 \text{ SYM theory on } \mathbb{R}^{3,1} + \text{type IIB SUGRA on } \mathbb{R}^{9,1}.$$

[19] In the DBI action above, these are hidden in the pull-back.

[20] Used conventions: $F_{\mu\nu} = \partial_\mu A_\nu - \partial_\nu A_\mu + i[A_\mu, A_\nu]$, $D_\mu\cdot = \partial_\mu + i[A_\mu, \cdot\,]$, $\bar{\sigma}^\mu = \left(-\mathbb{1}_2, -\sigma^i\right)$

Closed string perspective

For 3-branes, the corresponding soliton-like solution of SUGRA has the metric

$$\mathrm{d}s^2 = H(r)^{-1/2}\eta_{\mu\nu}\mathrm{d}x^\mu \mathrm{d}x^\nu + H(r)^{1/2}\mathrm{d}y^i\mathrm{d}y^i, \tag{2.65a}$$

$$H(r) = 1 + \left(\frac{L}{r}\right)^4. \tag{2.65b}$$

x^μ are the coordinates parallel to the brane and y^i the transverse ones. A special feature of the $p = 3$ case is that dilaton field is constant

$$e^\phi = g_s = const, \tag{2.66}$$

corresponding to a vanishing beta function for the coupling. The function $H(r)$ appearing in the metric contains an integration constant L, which is related to the number of branes

$$L^4 = 4\pi g_s N l_s^4. \tag{2.67}$$

In the flat-space limit $r \to \infty$, the geometry reduces to flat Minkowski space. In the opposite limit $r \to 0$, one obtains

$$\mathrm{d}s^2 \approx \left(\frac{L}{r}\right)^{-2}\eta_{\mu\nu}\mathrm{d}x^\mu\mathrm{d}x^\nu + \left(\frac{L}{r}\right)^2\mathrm{d}r^2 + L^2\mathrm{d}\Omega_5^2,$$

where we wrote $\mathrm{d}y^2 = \mathrm{d}r^2 + \mathrm{d}\Omega_5$. Therefore, the transverse S^5 has a constant size. Combining these two limits, the geometry is shown in Figure 2.2.

When taking the low-energy limit in a theory with gravity, one has to specify with respect to which observer one is measuring the energy. The dual field theory lives at $r = \infty$, hence the low-energy limit has to be taken there. Considering the energy E_r measured at radial position r, the energy for an observer at infinity is

$$E_\infty = H(r)^{-1/4}E_r. \tag{2.68}$$

Therefore, there are two types of low-energy excitations: massless bulk excitations with $E_r = 0$ and near horizon excitations located at $r/L \to 0$ with finite energy

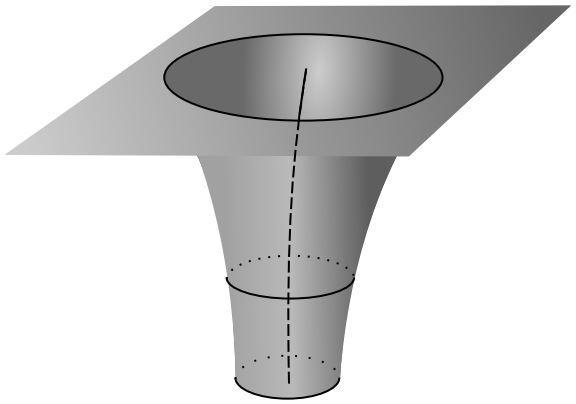

Figure 2.2: p-brane in SUGRA.
The six transverse directions are shown. The position of the brane is represented by the dashed line.

E_r[21]. In this limit, the metric reduces to the AdS metric[22] times a five-sphere of constant size. The metric can be written as

$$\mathrm{d}s^2_{\mathrm{AdS}_5\times S^5} = \left(\frac{L}{z}\right)^2 \left(\eta_{\mu\nu}\mathrm{d}x^\mu \mathrm{d}x^\nu + \mathrm{d}z^2\right) + L^2 \mathrm{d}\Omega_5^2, \tag{2.69}$$

where we used the coordinate transformation $z = L^2/r$. The cross-section between these different excitations goes to zero and the bulk excitations decouple from the near horizon excitations. Therefore, we obtain

$$\text{type IIB SUGRA on } \mathrm{AdS}_5 \times S^5 + \text{type IIB SUGRA on } \mathbb{R}^{9,1}$$

in the closed string perspective.

[21] This limit has to be taken carefully. One has to fix $l_s E_r$ to obtain arbitrary excitations in the $r \to 0$ region. The energy measured at infinity is the field theory energy $E_\infty \sim \frac{r}{l_s^2} \cdot l_s E_r$, which also has to be kept fixed. This is achieved by the coordinate transformation $\hat{r} = r/l_s^2$. $\hat{r}$ is kept constant while l_s is taken to infinity. This yields an additional factors of l_s in front of the metric, which cancels with factors of l_s in front of the action.

[22] See the review in Section 2.1

Combining both perspectives

Combining these two perspectives, one notices that both sides contain type IIB SUGRA on $\mathbb{R}^{9,1}$, which does not couple to the other sector. Therefore, the remaining two sectors have to be correspond to each other. This yields

$$\mathcal{N} = 4 \; SU(N_c) \text{ SYM theory on } \mathbb{R}^{3,1} \longleftrightarrow \text{type IIB SUGRA on } \mathrm{AdS}_5 \times S^5.$$

Maldacena used the argument above and conjectured that both sides are equivalent for arbitrary coupling [11]. The parameter of the field theory are the Yang-Mills coupling g_{YM} and the rank of the gauge group N, which can be combined to the 't Hooft coupling $\lambda = g_{YM}^2 N$. It is related to the string theory quantities by

$$\lambda = \frac{1}{2}\left(\frac{L}{l_s}\right)^4, \tag{2.70}$$

where L is the radius of the AdS space and l_s is the string length. The field theory is only well-understood in the perturbative regime, i.e. $\lambda \ll 1$, whereas SUGRA is only well-understood for weak gravity, i.e. $\lambda \gg 1$. This empathizes the power of the duality: one can work with a weakly curved gravitational theory to understand a strongly coupled field theory or one can work with a weakly coupled field theory to understand a strongly curved gravitational theory.

Both sides of the correspondence are highly symmetric theories. Focusing on the bosonic symmetries, the CFT has the conformal symmetry $SO(4,2)$ and the $SU(4)_R$ R-symmetry from rotating the supercharges. These correspond to the symmetries of AdS_5 and S^5 respectively.

2.4.2 General Correspondence and Field-Operator-Map

The limits used to derive the $\mathrm{AdS}_5/\mathrm{CFT}_4$ correspondence are the large N and large λ limit. The duality in its strongest form is far more general: it conjectures that $\mathcal{N} = 4$ $SU(N)$ Super Yang-Mills theory with arbitrary N and coupling is dual to type IIB string theory on $\mathrm{AdS}_5 \times S^5$. This statement is then weakened by performing the limits mentioned above. The three forms of the correspondence obtained in this way are presented in Table 2.6.

Besides $\mathrm{AdS}_5/\mathrm{CFT}_4$, similar dualities for different dimensions can be derived by considering other brane-setups[23]. Formulating the correspondence in a general way,

[23] For example, $\mathrm{AdS}_3/\mathrm{CFT}_2$, $\mathrm{AdS}_4/\mathrm{CFT}_3$ and $\mathrm{AdS}_7/\mathrm{CFT}_6$ can be derived this way [58–60].

Table 2.6: Different Forms of the AdS/CFT Correspondence.

Strongest	general $\mathcal{N}=4$ SYM theory	Quantum string theory on $AdS_5 \times S^5$
	$\downarrow$ 't Hooft limit $N\to\infty,\ \lambda=const.$	$\downarrow$ $g_s \to 0,\ l_s/L = const.$
Strong	Large N $\mathcal{N}=4$ SYM theory	Classical string theory on $AdS_5 \times S^5$
	$\downarrow$ strong coupling limit $\lambda\to\infty$	$\downarrow$ point-particle limit $_s\to\infty$
Weak	Strongly coupled large N $\mathcal{N}=4$ SYM theory	Classical SUGRA on $AdS_5 \times S^5$

one considers

$$\mathrm{CFT}_d \qquad \longleftrightarrow \qquad \text{massless theory on } \mathrm{AdS}_{d+1} \times K,$$

where K is a compact space. Using Kaluza-Klein reduction, the theory on the gravity side can be written as a massive theory on AdS_{d+1}, i.e. the statement is

$$\mathrm{CFT}_d \qquad \longleftrightarrow \qquad \text{massive theory on } \mathrm{AdS}_{d+1},$$

where the mass-spectrum depends on the compact space. The gravitational theory has three length-scales: the string-length l_s, the AdS radius L and the Planck length determined by the gravitational constant $G_N^{(d+1)}$. The field theory is parameterized by an effective coupling λ and the central charge c, which is proportional to the number of fields and for a $SU(N)$ gauge theory therefore proportional to N^2. Qualitatively, both sides are related by

$$c \propto \frac{L^{d-1}}{G_N^{(d+1)}} \tag{2.71a}$$

$$\lambda \propto \left(\frac{L}{l_s}\right)^{\gamma} \tag{2.71b}$$

with positive γ. This is known as *AdS/CFT dictionary*. The action on the gravity side is of the form

$$S = \frac{1}{16\pi G_N^{(d+1)}} \int \mathrm{d}^d x \, \sqrt{-\det g} \left(R + \frac{d(d-1)}{L^2} + \text{matter terms} \right), \tag{2.72}$$

where the second term arises from the cosmological constant $\Lambda = -\frac{d(d-1)}{2L^2}$. The $(d+1)$-dimensional Newton constant $G_N^{(d+1)}$ is related to the string length as $G_N^{(d+1)} \propto$

l_s^{d-1}.

The AdS metric has the scale invariance of the conformal theory. A rescaling of the CFT coordinates $x^\mu \to \lambda x^\mu$ leaves the metric invariant if the radial coordinate is rescaled appropriately, i.e. $z \to \lambda z$. This has an interesting interpretation when associating high energies with short distances and vice-versa. The radial coordinate z can be interpreted as an energy scale with $z \to 0$ corresponding to the UV and $z \to \infty$ to the IR. In particular, a UV cutoff in the field theory corresponds to a cutoff at $z = \epsilon \ll 1$.

How exactly does it work to reduce the theory on AdS$d+1 \times K$ to an effective theory on AdS$d+1$? Since we consider a product space, the d'Alembert operator reduces to

$$\Box_{\mathrm{AdS}_{d+1}\times K} = \Box_{\mathrm{AdS}_{d+1}} + \Box_K.$$

Therefore, we can compactify the compact space K using Kaluza-Klein reduction. The ansatz is assume

$$\phi(z, x, y) = \phi(z, x) \cdot Y(y),$$

where Y is an eigenfunction of the d'Alembert operator on K. Therefore, the equations of motion reduce to

$$\Box_{\mathrm{AdS}_{d+1}} \phi(z, x) = m^2 \phi(z, x),$$

where the mass m is determined by the eigenvalue of Y. Therefore, SUGRA of massless fields ϕ on $\mathrm{AdS}_{d+1} \times K$ can be understood as a theory with massive fields ϕ_l on AdS_{d+1}. For a sphere $K = S^{D-d-1}$, the fields can be decomposed into spherical harmonics, e.g. for a scalar field ϕ

$$\phi(z, x, y) = \sum_l \phi_l(z, x) Y_l(y), \quad \text{with} \quad \Box_K Y_l(y) = -\frac{1}{L^2} l(l + D - d - 2) Y_l(y), \tag{2.73}$$

where y are the coordinates of K. Therefore, the exact form of the compact space determines the possible eigenvalues of $\Box_K$ and consequently the mass spectrum.

The mapping between degrees of freedom on both sides can be understood by

considering the near boundary expansion of the equation of motions

$$\Box_{\mathrm{AdS}_{d+1}}\phi(z,x) = \frac{1}{L^2}\left(z^2\partial z - (d-1)z\partial_z + z^2\eta^{\mu\nu}\partial_\mu\partial_\nu\right)\phi(z,x), \tag{2.74a}$$

$$\approx \frac{1}{L^2}\left(z^2\partial z - (d-1)z\partial_z\right)\phi(z,x), \tag{2.74b}$$

$$= m^2\phi(z,x) \tag{2.74c}$$

The asymptotic solution has the form

$$\phi(z,x) \approx \phi_{(0)}(x)\cdot z^{\Delta_-} + \phi_{(+)}(x)\cdot z^{\Delta_+} \tag{2.75}$$

where the powers $\Delta_\pm$ depend on the mass m of the scalar field

$$\Delta_\pm = \frac{d}{2} \pm \sqrt{\frac{d^2}{4} + m^2L^2}. \tag{2.76}$$

Therefore, the differential equation (2.74) has two solutions: a normalizable one proportional to z^{Δ_+} and a non-normalizable one proportional to z^{Δ_-} [61][24].

Dimensional analysis helps to understand what the normalizable and the non-normalizable solution correspond to on the field theory side. A scaling transformation can be performed on the gravity side by considering $x^\mu \to \lambda x^\mu$, $z \to \lambda z$. Looking at the solution Equation (2.75) and the scaling behavior of $\phi_{(0)}(x)$, $\phi_{(+)}(x)$, one can identify $\phi_{(+)}(x)$ with the expectation value of an operator of conformal dimension $\Delta = \Delta_+$ and $\phi_{(0)}(x)$ with its source. This identification is known as field-operator map, which for scalar operators states

$$\begin{aligned} \mathcal{O}_\Delta \quad &\longleftrightarrow \quad \phi(z,x), \\ \Delta \quad &\longleftrightarrow \quad m^2 = \Delta(\Delta - d). \end{aligned}$$

For field of different spin, the relation between mass and scaling dimension Δ is changed, but the fundamental statement is the same: there is a one-to-one map between operators of a certain scaling dimension Δ and fields of a certain mass m.

In [12, 13], the partition function on both sides of the correspondence are identi-

[24]The action evaluated for a normalizable solution is finite, whereas the action evaluated for a non-normalizable solution is infinite. The non-normalizable solution exists independent of the signature of the spacetime. In contrast, the differential equation (2.74) only allows for a normalizable solution in Lorentzian signature.

fied. For classical SUGRA this implies

$$Z_{CFT}[\phi_0(x)] = Z_{\text{IIB}}[\phi(z,x)]\Big|_{\lim\limits_{z\to 0}\phi(z,x)z^{-\Delta_-}=\phi_0(x)}, \tag{2.77a}$$

$$\left\langle \exp\left(\int \phi_0 \mathcal{O}\right)\right\rangle_{CFT} = \exp\left(iS_{\text{SUGRA}}(\phi)\right)\Big|_{\lim\limits_{z\to 0}\phi(z,x)z^{-\Delta_-}=\phi_0(x)}, \tag{2.77b}$$

where the sources ϕ_0 and the fields ϕ are related as discussed above. This relation is called GKP-Witten relation after the authors of the aforementioned papers. While the saddle-point approximation in the second line is only valid for the weak form of the duality, the identification of the generation functionals in the first line applies also to the strong form. This relation allows to calculate correlation functions by considering derivatives with respect to the sources.

There are two approaches to obtain a duality of the form

$$\text{CFT}_d \qquad \longleftrightarrow \qquad \text{massive theory on AdS}_{d+1}.$$

In the top-down approach the duality is derived by starting with an explicit string theory setup and compactifying the compact space K. These models have an explicit mapping between field theory parameters and string theory parameters. Furthermore, the explicit theories on both sides are known. In contrast, it is also possible to follow a bottom-up approach by modeling the gravitational theory corresponding to the properties of the CFT. In this approach, the relation between parameters on both sides has to be read of from observables.

2.4.3 Special Aspects of $\text{AdS}_3/\text{CFT}_2$

Section 2.4.1 reviews the near-horizon limit to obtain $\text{AdS}_5/\text{CFT}_4$ from the low-energy limit of D3 branes. The same procedure can be applied to other brane setups resulting in other examples of $\text{AdS}_{d+1}/\text{CFT}_d$. In particular, Maldacena [11] published cases resulting in $\text{AdS}_3/\text{CFT}_2$ already in his first paper conjecturing the AdS/CFT correspondence.

Symmetries of the metric are formulated in terms of Killing vector, i.e. infinitesimal diffeomorphisms which leave the metric invariant. The number of Killing vectors is finite. However, one can also consider asymptotic symmetries. Therefore, we consider diffeomorphism which leave the boundary behavior of the metric to be

asymptotically AdS, as was done in [62, 63]. For a metric

$$\mathrm{d}s^2 = g_{MN}\mathrm{d}x^M\mathrm{d}x^N \tag{2.78}$$

with $x^M = (t, x, z)$ to be considered asymptotically AdS, the required boundary behavior is

$$g_{\mu\nu} = \frac{L^2}{z^2}\eta_{\mu\nu} + \mathcal{O}(z^0), \qquad g_{z\mu} = \mathcal{O}(z), \qquad g_{zz} = \frac{L^2}{z^2}\eta_{\mu\nu} + \mathcal{O}(z^0). \tag{2.79}$$

If we consider now an infinitesimal diffeomorphism of the form $x^M \to x^M + \xi^M$ which leaves this asymptotic form invariant, the solutions are of the form

$$\xi^+ = \sigma g_+(x^+) + \frac{1}{2}\sigma g_-''(x^-)z^2 + \mathcal{O}(z^4) \tag{2.80a}$$

$$\xi^- = \sigma g_-(x^-) + \frac{1}{2}\sigma g_+''(x^+)z^2 + \mathcal{O}(z^4) \tag{2.80b}$$

$$\xi^z = -\sigma\frac{z}{2}\left(g_+{}'(x^+) + g_-{}''(x^-)\right) + \mathcal{O}(z^3), \tag{2.80c}$$

where $g_\pm$ are arbitrary functions and σ is a small expansion parameter. On the boundary, the diffeomorphisms reduce to $x^\pm \to x^\pm + g_\pm(x^\pm)$, i.e. the asymptotic symmetry reduces to the local conformal symmetry on the boundary. The algebra for the generators may be derived using Hamiltonian analysis on the gravity side, see [62]. This results in two copies of the Virasoro algebra with central charge

$$c = \frac{3L}{2G_N}. \tag{2.81}$$

Therefore, it was already discovered before AdS/CFT that the asymptotic symmetry of AdS_3 agrees with the conformal symmetry in CFT_2. Furthermore, the mapping between central charge c and AdS-radius L is universal.

What happens if we do not consider the vacuum state of the CFT, i.e. $T^{\mu\nu} = 0$, but a state with

$$8\pi G_N T_{++} = \frac{1}{4}\,L(x^+), \tag{2.82a}$$

$$8\pi G_N T_{--} = \frac{1}{4}\,\bar{L}(x^-)? \tag{2.82b}$$

The energy momentum tensor on the boundary is dual to the metric on the gravity side. This however only fixes the asymptotic behavior of the metric, see Equation (2.75). To determine the whole metric, one has to solve the Einstein equations

for the metric order by order in z^2. This expansion is not guaranteed to converge in general. For AdS_3 however, it was shown in [64] that this expansion yields

$$ds^2 = \frac{1}{z^2}\left(dz^2 - dx^+dx^-\right) - \frac{z^2}{16}dx^+dx^- + \frac{1}{4}\left(L(x^+)(dx^+)^2 + L(x^-)(dx^-)^2\right).$$

This metric is singularity at the horizon at radial position

$$z_0 = \frac{2}{\left(L(x^+)\bar{L}(x^-)\right)^{1/4}}$$

The coordinates used in Equation (2.83) only cover the outside region and not the interior.

2.5 Holography and Quantum Information

This chapter takes a look at quantum information and its importance in holography.

2.5.1 Quantum Information and Entanglement

This short review of quantum information is based on [65, 66].

One crucial ingredient when considering quantum systems is entanglement. It is no longer enough to understand each part of the system, but one also has to understand the entanglement between different parts [6, 67, 68]. This has interesting effects: subsystems can no longer described independently from each other.

More formally, let us consider a bipartite system $\mathcal{H} = \mathcal{H}_A \otimes \mathcal{H}_B$. The composite state is described by a density matrix ρ. The entropy of the state is given by the von Neumann entropy

$$S(\rho) = -\operatorname{Tr}\rho\ln\rho. \tag{2.83}$$

It can be understood as the missing information about the state. In particular, it is non-negative and only vanishes for pure states,

$$S(\rho) \geq 0 \quad \text{with} \quad S(\rho) = 0 \iff \rho = |\phi\rangle\langle\phi|, \text{ i.e. } \rho \text{ is a pure state.} \tag{2.84}$$

The subsystems are described by reduced density matrices

$$\rho_A = \operatorname{Tr}_B \rho, \qquad \rho_B = \operatorname{Tr}_A \rho, \tag{2.85}$$

where we integrate out the degrees of freedom living in the complement. Let us turn to the difference between classical states and quantum states. Classical pure states are of the form

$$|\psi\rangle = |\psi_A\rangle \otimes |\psi_B\rangle \quad \text{with} \quad |\psi_{A,B}\rangle \in \mathcal{H}_{A,B}, \tag{2.86a}$$

$$\rho = |\psi\rangle \langle\psi|. \tag{2.86b}$$

For these states, the reduced states of the pure state

$$\rho_A = |\psi_A\rangle \langle\psi_A|, \qquad \rho_B = |\psi_B\rangle \langle\psi_B|$$

are also pure. Mixed classical states are of the form

$$\rho = \sum_i p_i |\psi_i\rangle \langle\psi_i|. \tag{2.87}$$

gg lIn contrast, a quantum state can be any normalized states in the Hilbert state $\mathcal{H}_A \otimes \mathcal{H}_B$. Therefore, quantum states are of the form

$$|\psi\rangle = \sum_i a_i |\psi_i\rangle \text{ with } \langle\psi|\psi\rangle = 1. \tag{2.88}$$

Any pure state in $\mathcal{H}$ can be written as

$$|\psi\rangle = \sum_i c_i |e_i\rangle \otimes |f_i\rangle, \tag{2.89}$$

where $|e_i\rangle$ and $|f_i\rangle$ are appropriately chosen orthonormal bases of $\mathcal{H}_A$ and $\mathcal{H}_B$ respectively. This decomposition is called Schmidt decomposition. For these states, the reduced states are

$$\rho_A = \sum_i |c_i|^2 |e_i\rangle\langle e_i|, \qquad \rho_B = \sum_i |c_i|^2 |f_i\rangle\langle f_i|$$

and are in general mixed. This mixture is caused by entanglement between A and B. It shows that complete knowledge of the state $|\rho\rangle$ does not imply complete knowledge of the reduced states $|\rho\rangle_A$ and $|\rho\rangle_B$ and vice-versa.

How can this entanglement be quantified? First, we consider pure states. As we discussed above, entanglement creates missing information about the reduced states even with full knowledge of the state. This missing information can be quantified using the entropy of the reduced state. This entropy is called the entanglement

entropy

$$S_{EE}(\rho_A) = -\operatorname{Tr}_A \rho_A \ln \rho_A. \tag{2.90}$$

If we consider a pure state $|\rho\rangle$, the entanglement entropies for both subsystems agree, which can be seen from the Schmidt decomposition (2.89). However, the problem is more subtle for mixed states. For these, the entanglement entropy also receives contributions from classical correlations. How can we see whether a mixed states is entangled? A mixed state without entanglement between A and B can be written as

$$\rho = \sum_i p_i \rho_A^i \otimes \rho_B^i. \tag{2.91}$$

Such states are called separable. These states can be created by so called Local Operations and Classical Communication (LOCC), which allows operators which only act on one subsystem as well as classical communication between both subsystems. Unfortunately, there is no definite answer on what is a good measure for entanglement for mixed states. Necessary conditions on such a measure $E(\rho)$ are the following:

- They are positive, i.e. $E(\rho) \geq 0 \ \forall \rho \in \mathcal{H}$.
- They only vanish for separable states.
- They do not increase under LOCC, as these transformations do not create entanglement.

Any function E satisfying these conditions is called an entanglement monotone. For an entanglement monotone to be a measure of entanglement, it has to reduce to the entanglement entropy for any pure state.

There are many different proposals for measures of entanglement. One computable measure is the entanglement negativity [69]. It is based on the Pere's criterion [70] for separable states, which considers the eigenvalues of the partial transpose ρ^{T_A} of the density matrix. The partial transpose is defined as

$$\langle f_j| \otimes \langle e_i| \ \rho^{T_A} \ |e_k\rangle \otimes |f_l\rangle = \langle f_j| \otimes \langle e_k| \ \rho \ |e_i\rangle \otimes |f_l\rangle. \tag{2.92}$$

While the eigenvalues of the density matrix ρ are positive, the eigenvalues of ρ^{T_A} can become negative. The Pere's criterion states that ρ^{T_A} has no negative eigenvalues if the state is separable. These can be measured by the trace norm of the partial

transpose

$$||\rho^{T_A}|| = \operatorname{Tr}\sqrt{(\rho^{T_A})^\dagger \rho^{T_A}} = \sum_i |\lambda_i|,$$

$$||\rho^{T_A}|| - 1 = 2 \sum_{i,\ \lambda_i<0} |\lambda_i|,$$

where λ_i are the eigenvalues of ρ^{T_A}. The second line follows from $\operatorname{Tr}\rho^{T_A} = \operatorname{Tr}\rho = 1$. It is however more convenient to consider

$$\varepsilon(A) = \ln ||\rho^{T_A}||, \tag{2.93}$$

which is called entanglement negativity. While the entanglement negativity is an entanglement monotone, it is strictly speaking not an entanglement measure since it does not reduce to the entanglement entropy for all pure states.

Let us empathize that there exist numerous other entanglement measures. We focus on the entanglement negativity because it is calculable and, as we later see, has a holographic dual.

2.5.2 Holographic Entanglement Entropy

When considering entanglement in AdS/CFT, one considers the entanglement in a field theory. Here, the Hilbert space can be written as a tensor product

$$\mathcal{H} = \bigotimes_{\vec{x}\in\mathbb{R}^{d-1}} \mathcal{H}_{\vec{x}}.$$

Therefore, it is natural to split the system into parts by considering a region A and split the Hilbert space into degrees of freedom living on A and degrees of freedom living on the complement A_c [25]

$$\mathcal{H} = \mathcal{H}_A \otimes \mathcal{H}_{A_c}.$$

The surface splitting this regions is called entangling surface ∂A. This decomposition is shown in Figure 2.3. We can now restrict our attention to the degrees of freedom

[25] Splitting degrees of freedom in this way is problematic in gauge theories. There is no gauge-invariant way to perform this decomposition.

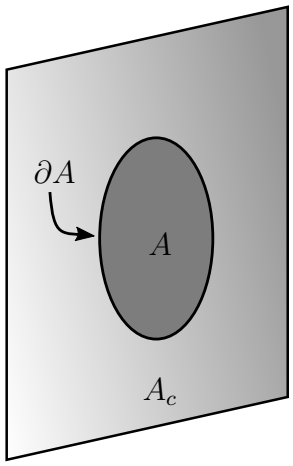

Figure 2.3: Decomposition of Space into Region A and Complement A_c.

living in A by considering the reduced density matrix

$$\rho_A = \mathrm{Tr}_{A_c}\, \rho. \tag{2.94}$$

This reduces density matrix has an intuitive physical interpretation: it describes the state for an observer in A without access to the complement. In this interpretation, the entanglement entropy measures the missing information for an observer in A, who has no access to the complement A_c.

The entanglement entropy gives insights into the entanglement structure of the state. Therefore, it is an interesting observable to study. In particular, it can be used as an order parameter for quantum phase transition. Calculating the entanglement entropy requires knowledge of the eigenvalues of the reduced density matrix. For systems with a finite number of freedoms, this is often a feasible problem. However, in quantum field theories we have an infinite number of freedoms the problem becomes drastically more complex, even for free field theories. The exception from this are two-dimensional CFTs, where the problem can be rephrased into evaluating the partition function on an n-sheeted Riemann surface [71–73] and reduces to evaluating two-point correlation functions of particular twist fields. There do not exist numerous results for higher-dimensional field theories, making it particularly interesting to study the entanglement holographically.

In [25, 26], a dual for static time-independent states was conjectured, which was later generalized to time-dependent setups [74]. An extensive review of these holographic proposals can be found in [75]. Let us follow an heuristic argument to derive the holographic entanglement entropy. In this discussion, we restrict ourselves to time-independent setups. They have the special feature that the timelike killing

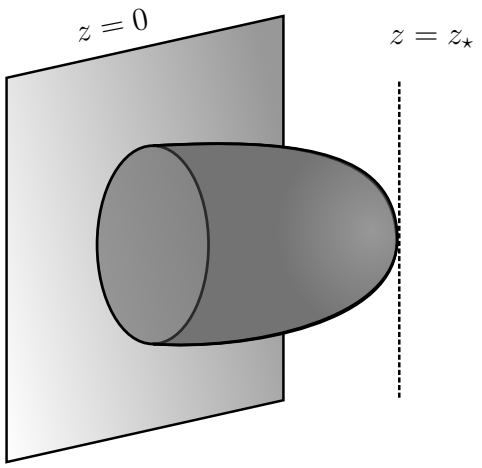

Figure 2.4: Bulk Surface anchored on Entangling Surface.

vector uniquely extends the boundary time-slicing into the bulk. Therefore, we can restrict ourselves to considering a constant bulk time-slice. Let us return to the setup shown in Figure 2.3. We consider a reduced state ρ_A, i.e. the state for an observer who only has access to A. This state should be dual to the gravitational theory in an attached region of space. The entanglement entropy is the entropy of this reduced state, i.e. it measures the number of degrees of freedom. The duality is a one-to-one map, i.e. this number of degrees of freedom has to agree with the number of degrees of freedom living in the dual bulk region. However, this number is bounded in a theory with gravity: the Bekenstein entropy bound tells us that it is bounded by area of the surrounding surface. This construction is shown in Figure 2.4. To obtain the strictest bound, one selects the region with the minimal boundary area. It was conjectured in [25, 26] that this bound is saturated, i.e. the entanglement entropy can be calculated via[26]

$$S_{EE}(B) = \frac{\mathcal{A}}{4G_N^{d+1}}, \tag{2.95a}$$

$$\mathcal{A} = \min_{\gamma_A | \partial\gamma_A = \partial A} \text{Area}(\gamma_B). \tag{2.95b}$$

This considers only surfaces γ_A which are homologous to A, i.e. which can be smoothly retracted to the boundary region A. This proposal for the holographic

[26] [74] generalizes this to time-dependent states. For these, one has to minimize over extremal co-dimension two surfaces.

entanglement entropy relates the entanglement entropy to the area of the minimal co-dimension one surface anchored on the entangling surface ∂A. One further motivation for this conjecture was that it correctly reproduces field-theory calculations for $d = 2$. An explicit proof for spherical regions in CFTs was later found in [76]. For a more general setup, it was proven in [77][27].

Let us briefly discuss how this works. Our surfaces γ_A can be parameterized by $(d-2)$ coordinates w. The embedding is $x_m(w)$. The surface area is

$$\mathcal{A} = \int \mathrm{d}^{d-1} w \sqrt{\gamma}, \tag{2.96a}$$

$$\gamma_{\alpha\beta} = g_{\mu\nu} \partial_\alpha x^\mu_m \partial_\beta x^\nu_m, \tag{2.96b}$$

where γ is the induced metric on the surface. Therefore, finding the minimal surface reduces to solving the variational problem with respect to the embedding x_m. The boundary conditions are given by anchoring the surface on ∂A.

Already before the proofs of the conjecture, there was already confidence in its validity since it satisfied several properties of the entanglement entropy[28]. Two prominent inequalities for the entanglement entropy are the subadditivity and strong subadditivity. They arise when considering a region A split into two or three regions A_i respectively and state

$$S_{EE}(A) \leq S_{EE}(A_1) + S_{EE}(A_2), \tag{2.97a}$$

$$S_{EE}(A) + S_{EE}(A_2) \leq S_{EE}(A_1 + A_2) + S_{EE}(A_2 + A_3). \tag{2.97b}$$

Holographically, these inequalities can be proven geometrically: by cutting and gluing the different surfaces on the right-hand side yields non-minimal surfaces anchored on the regions on the left-hand side [81, 82]. Interestingly, the holographic entanglement entropy satisfies an infinite set of inequalities, which are not necessarily satisfied by the field theory entanglement entropy [83]. They carve out the so called holographic entropy cone in the space of entropies, i.e. a subset of entropy combinations allowing a holographic dual.

Further supporting evidence is the agreement with the UV-behavior of the entanglement entropy. Due to UV-correlations across the entangling surface, the entanglement entropy is UV divergent, which requires to introduce a UV cutoff $\epsilon \ll 1$.

[27] See [78] for the covariant proof.

[28] More properties are discussed in [79, 80].

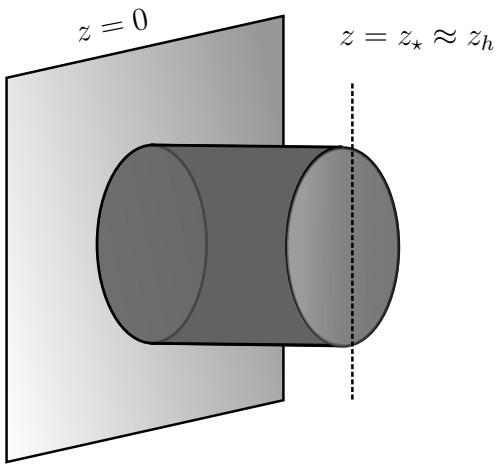

Figure 2.5: Bulk Surface for Finite Temperature.

The divergent term scales with the area of the entangling surface ∂A. On the bulk side, this is reproduced by introducing a bulk cutoff. The AdS metric diverges at the boundary, yielding the correct area term. For conformal theories, there is no length-scale. Therefore, the UV-divergent term is $S_{EE} \sim \text{Area}(\partial A)/\epsilon^{d-2}$. Furthermore, let us have a look at finite temperature states in CFTs, i.e. states dual to AdS Schwarzschild black holes. The radial component of the metric diverges at the horizon. This results in a repulsive for the minimal surface. For a large boundary region A, the minimal surface can be approximated by a part falling straight into the bulk and a part along the horizon as shown in Figure 2.5. In this limit, the leading contribution to the entanglement entropy is the thermal entropy of A, which is obtained by the part of the surface along the horizon.

As discussed previously, the entanglement entropy is only a measure for entanglement for a pure state. Therefore, it in particular does not apply to thermal states. One measure suggested for CFT states at finite temperature is the entanglement negativity [84–88]. A holographic dual for the entanglement negativity is proposed in [89, 90]. Starting from the result for a two-dimensional CFT reduces to

$$\varepsilon(A) = \frac{3}{2}\left(S_{EE}(A) - S^{th}(A)\right) + f\left(e^{-2\pi\ell T}\right), \tag{2.98}$$

where f is a non-universal function which depends on the particle content. In general, f is non-vanishing and the entanglement negativity is more than just a

combination of entropies[29]. Fortunately, this non-universal contribution is subleading in the large central charge limit considered in AdS/CFT and can be neglected. Therefore, the entanglement negativity for a two-dimensional field theory

$$\varepsilon(A) = \frac{3}{2}\left(S_{EE}(A) - S^{th}(A)\right). \tag{2.99}$$

The authors of [89, 90] conjecture that this result is as it is also valid for strip entangling regions in higher dimensions. The entanglement negativity may also be expressed in terms of the mutual information, which is defined as

$$\mathcal{I}(A:B) = S_{EE}(A) + S_{EE}(B) - S_{EE}(A \cup B). \tag{2.100}$$

The complement for a strip can be split into two parts as shown in Figure 2.6. Using this, the holographic entanglement negativity can be expressed as

$$\varepsilon(A) = \frac{3}{4}\left(\mathcal{I}(A:B_1) + \mathcal{I}(A:B_2)\right) = \frac{3}{2}\mathcal{I}(A:B_i) \text{ for } i = 1, 2. \tag{2.101}$$

The mutual information is an upper bound on the correlations between two regions. The connected correlation function for two observables $\mathcal{O}_A$, $\mathcal{O}_B$ acting on A and B respectively is bounded by [91, 92]

$$\mathcal{I}(A:B) \geq \frac{1}{2|\mathcal{O}_A|^2|\mathcal{O}_B|^2}(\langle \mathcal{O}_A \mathcal{O}_B \rangle)^2.$$

Holographically, the mutual information between two regions can vanish. However, one has to keep in mind that the Ryu-Takayanagi proposal works applies to classical gravity, i.e. it only captures the leading N contribution. Considering quantum effects on the gravity side, one obtains subleading terms in N which result in a positive mutual information [93][30].

Let us empathize that this proposal for the entanglement negativity is a purely holographic proposal. In general, the entanglement negativity is not simply given in terms of mutual information or entanglement entropies. In particular, we saw

[29] This non-universal part arises from four-point functions in the theory and depends on the detailed field content of the CFT.

[30] In quantum information, it can be shown that $\mathcal{I} = 0$ only happens for product states $\rho_{A\cup B} = \rho_A \otimes \rho_B$. If these states have a holographic duals, they are disconnected. One way to see this is to consider correlation functions of operators with large scaling dimension in the geodesic approximation, where the bulk-distance have to become infinite when the mutual information goes to zero, see Section 3.1.1.

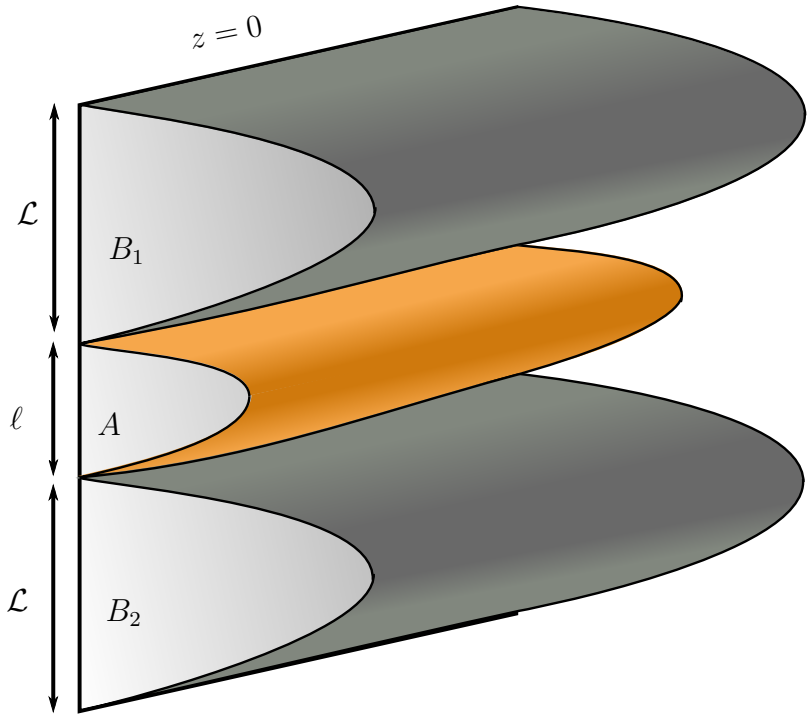

Figure 2.6: Construction for Entanglement Negativity.
Consider a strip A with width ℓ. The complement can be split into two strips B_1 and B_2 with width $\mathcal{L} \to \infty$. The mutual information $\mathcal{I}(A, B_i)$ is calculated holographically using minimal surfaces.

that in two-dimensional CFTs the entanglement negativity contains a non-universal term [84–86]. Such a term depends on the detail field content. Therefore, such a term could not depend solely on the geometric of the gravity dual. Fortunately, this term is subleading in the large central charge limit, which is exactly the limit we consider in AdS/CFT.

2.5.3 Complexity

The success of the holographic entanglement entropy sparked the interest in considering holography from a quantum information point of view [38,41,94]. In particular, it was noted that not everything is captured by the entanglement entropy. When considering a reduced density matrix ρ_A, the entanglement entropy

$$S_{EE} = -\operatorname{Tr} \rho_A \ln \rho_A = -\sum \lambda_i \ln \lambda_i$$

only depends on its eigenvalues λ_i. Therefore, also other quantum information measures are of interest.

One interesting measure is the notion of *complexity*, which measures how difficult it is to construct a state. To define such a measure, we first have to fix some implicit assumptions. The first one is the state we are starting from: the *reference state* $|\mathcal{R}\rangle$. To this we apply unitary operators to construct the desired state. Therefore, we can write our state as

$$|\psi\rangle = U\,|\mathcal{R}\rangle\,. \tag{2.102}$$

Furthermore, one has to assign a notion of difficulty to operators. This is done by considering a *gate-set* $\{\mu_i\}$ of universal gates and counting how many of these we need to construct an operator. This cannot be achieved exactly, but in a certain *error tolerance* ε. Therefore, the complexity $\mathcal{C}$ of an operator is the minimal number of gates in the circuit constructing it

$$U \approx \mu_1 \dots \mu_{\mathcal{C}}.$$

After assigning this notion of difficulty to an operator, it is straight-forward to define a notion of difficulty for states: the *complexity of a state* is defined as the minimal number of gates to construct it from the reference state

$$|\Psi\rangle \approx \mu_1 \dots \mu_{\mathcal{C}}|\mathcal{R}\rangle.$$

Equivalently speaking, it is the minimal complexity of operators U satisfying (2.102).

Nielsen formulated the problem in a different way [95–97]. Instead of applying discrete gates step by step, the unitary operator is implemented continuously

$$\frac{\mathrm{d}U(s)}{\mathrm{d}s} = -iH(s)U(s),$$

where s parameterizes the path in the space of unitaries which begins at $U(0) = \mathbb{1}$ and ends at $U(1) = U$. This removes the necessity of an error tolerance. Assigning a difficulty to the infinitesimal steps is done by imposing a Finsler geometry on the tangent space where $H(s)$ lives. For this, a cost function $F(H)$ with the following properties is assigned:

- It is subadditiv: $F(H_1 + H_2) \leq F(H_1) + F(H_2)$.
- It is positive homogeneous: $F(\lambda H) = \lambda H$ for $\lambda \geq 0$.
- It is positive definite.

Therefore, the length of the path $U(s)$ is

$$\int_0^1 \mathrm{d}s F[U].$$

In this framework, finding the optimal circuit reduces to finding the optimal geodesic. Therefore, the complexity of an operator U is

$$\mathcal{C} = \min_{\substack{U(0)=\mathbb{1}, \\ U(1)=U}} \int_0^1 \mathrm{d}s \; F[U] \tag{2.103}$$

While complexity is a natural measures for quantum computers and discrete qubits, the field theory definition is not that straight forward. The group of unitary operators in this case is infinite dimensional. Furthermore, it is not know what cost functions and reference state are appropriate.

What does this has to do with holography? Susskind studied extremal volume slices to probe inside the black hole. He found that their volume change linearly for late times in the two-sided AdS black holes, This linear increase in time is known for complexity, which provoked Susskind to conjecture that volume of the extremal slice is proportional to the circuit complexity [40, 42, 98]

$$\mathcal{C} = \frac{\mathcal{V}}{G_N L}, \tag{2.104}$$

where G_N is the Newton constant and L the AdS radius[31]. $\mathcal{V}$ is the maximal volume of a spacelike slice anchored on the boundary time slice. The proposal is known as *complexity = volume* proposal. The reasoning behind using extremal spatial slices is that for spacetimes without timelike killing vector, there is no unique way to extend the boundary equal time-slice into the bulk. Considering maximal volume grands a unique covariant way to do this.

For completeness, let us mention that there is also a competing proposal: it relates the complexity to the gravitational action evaluated on the Wheeler-DeWitt

[31] For the cases we consider, the length-scale in the denominator will be the AdS radius. However, that is not the case in general.

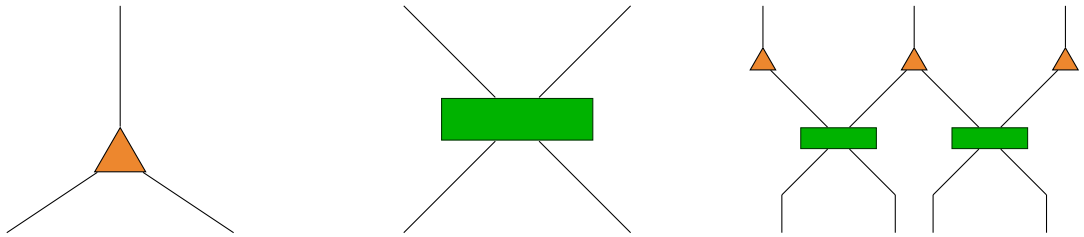

(a) Isometries. **(b)** Disentanglers. **(c)** Combination.

Figure 2.7: Building Blocks of Tensor Networks. Isometries implement coarse graining by mapping two spins to one effective one. To correctly coarse-grain all short-range correlations, one has to apply disentangler on neighboring spins which go into different isometries.

patch [47, 48]

$$\mathcal{C} = \frac{I}{\pi\hbar}, \tag{2.105}$$

This is known ad *complexity=actions* proposal. At first, this expression was not well defined since it requires additional boundary terms to be added to the action, but the form of these boundary was is known by now [99]. Both holographic proposals are only conjectures: it is not known whether they really correspond to circuit complexity as known from quantum information. Even if they do, the corresponding cost function and reference state are unknown. In this thesis, we focus at the volume proposal for the holographic complexity. As discussed in the next section, this is analogous to the notion of complexity in tensor networks.

2.5.4 Tensor Networks

As discussed in Section 2.5.3, there are various open question about the realization of field theory complexity. There is the question of finding an appropriate set of gates, an appropriate cost function and an appropriate reference state. Furthermore, considering complexity for mixed states and particular for reduced states is not well defined.

Therefore, let us approach complexity from a different perspective: tensor networks [43–46]. Tensor networks are a method in many-body physics to approximate quantum states. They allow efficient computational treatment and a pictorial representation of states in terms of a quantum circuit. We focus on a special type of tensor network: multi-scale renormalization ansatz (MERA). Considering a discrete

lattice width n lattice points, a quantum state is of the form

$$|T\rangle = \sum_{\mu_1,\ldots,\mu_n} T_{\mu_1,\ldots,\mu_n} |\mu_1\rangle \otimes \cdots \otimes |\mu_n\rangle. \tag{2.106}$$

The basis of the Hilbert space at the kth point is written as $|\mu_k\rangle$ with $\mu_k = 1, \ldots, \dim(\mathcal{H}_k)$. The idea is to start with this UV state and coarse-grain the tensor. This coarse graining operation is implemented by *isometries*. The lattice points are grouped in blocks of size two on which the isometries act to describe them by one effective degree of freedom, see Figure 2.7a. The idea is to start with a lattice of size n and apply a layer of isometries. This reduces the number of points by a factor of two. This is done repeatedly until one ends with one point. The full UV state then is encoded in the used isometries. This results in a tree-like structure as shown in Figure 2.8a. However, a tensor network like this does not appropriately simplify the state, as it does not remove all short range correlations. This makes describing the quantum state in terms of the isometries inefficient. The reason is short-range entanglement between different blocks. It has to be removed by acting with *disentanglers* on neighboring points which are not contained in the same coarse graining block, see Figure 2.7b and Figure 2.7c. For simplicity, the disentanglers are not drawn explicitly in the following.

The tensor network approach has similarities with AdS/CFT. One starts with a field theory state and constructs a structure in an additional direction. In both pictures, this additional direction has the interpretation of an energy scale. It is shown that MERA can be understood as a discrete version of AdS/CFT and reproduces the pure AdS geometry [100, 101]. The layer number in MERA is related to the radial coordinate in AdS by

$$u \propto \log\left(\frac{z}{\epsilon}\right).$$

The approach to obtain MERA for a continuous system is called continuous MERA (cMERA). It can be used for more general setups as AdS/CFT to obtain a geometric dual, see [102]. Entanglement entropy in tensor networks is determined by the minimal cut-surface. This is the discrete analogue of the Ryu-Takayanagi surface. The area of the surface is replaced by the number of lines one has to cut.

Such a tensor network can be interpreted as a circuit constructing the vacuum wave-function. For this, ancillary spins are added to promote the isometries to unitaries. Therefore, the network is the circuit constructing the vacuum state from

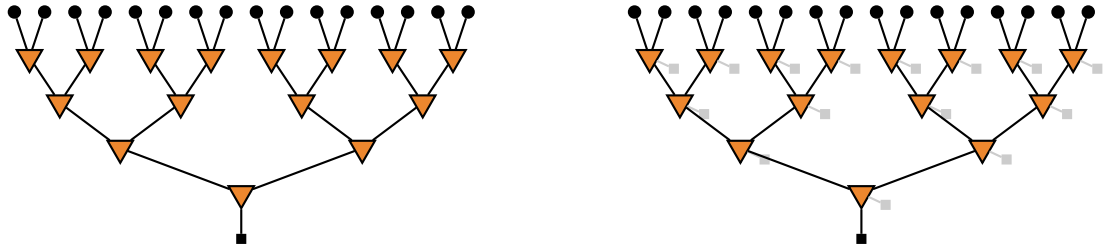

(a) TN with Isometries. **(b)** TN as Constructive Circuit.

Figure 2.8: Tensor Network.

an unentangled reference state, This gives tensor network an intuitive notion of complexity: they represent a circuit synthesizing the wave function from a simple (i.e. unentangled) reference state. The complexity of the circuit is measured by the minimal number of tensors required. Therefore, every network gives an upper bound on the complexity of the state. An optimized circuit then should reproduce the complexity of the state. Therefore, MERA does us also give some intuition about subregion complexity. The minimal-cut surface used to determine the entanglement entropy splits the circuit into two parts. The subregion complexity measures the complexity of the part connected to the subregion.

Connecting this to field theory, a quantum state is constructed using the Euclidean path integral. For the vacuum state, this is shown in Figure 2.9a. Optimizing this circuit yields MERA as shown in [103]. This approach can also be applied to finite temperature state. For finite temperature, the Euclidean time-direction is finite and we have two open boundaries. Using MERA to optimize this circuit starting from both boundaries results in two MERA networks being 'glued together' by bridge tensors. In particular, the tensor layers in the UV are identical to the vacuum tensor network. The bridge tensor entangle both sides and are responsible for the thermal spectrum of the state. There is diverse discussion on the exact form of these bridge tensors [100, 101, 104, 105], but it is not important to gain qualitative intuition. This network can be understood as the MERA network dual to a spatial slice of the two-sided AdS Schwarzschild black hole. The bridge corresponds to the horizon. The intuition is that the bridge layers growth over time, see Figure 2.10a. This corresponds to the linear growth of the wormhole over time.

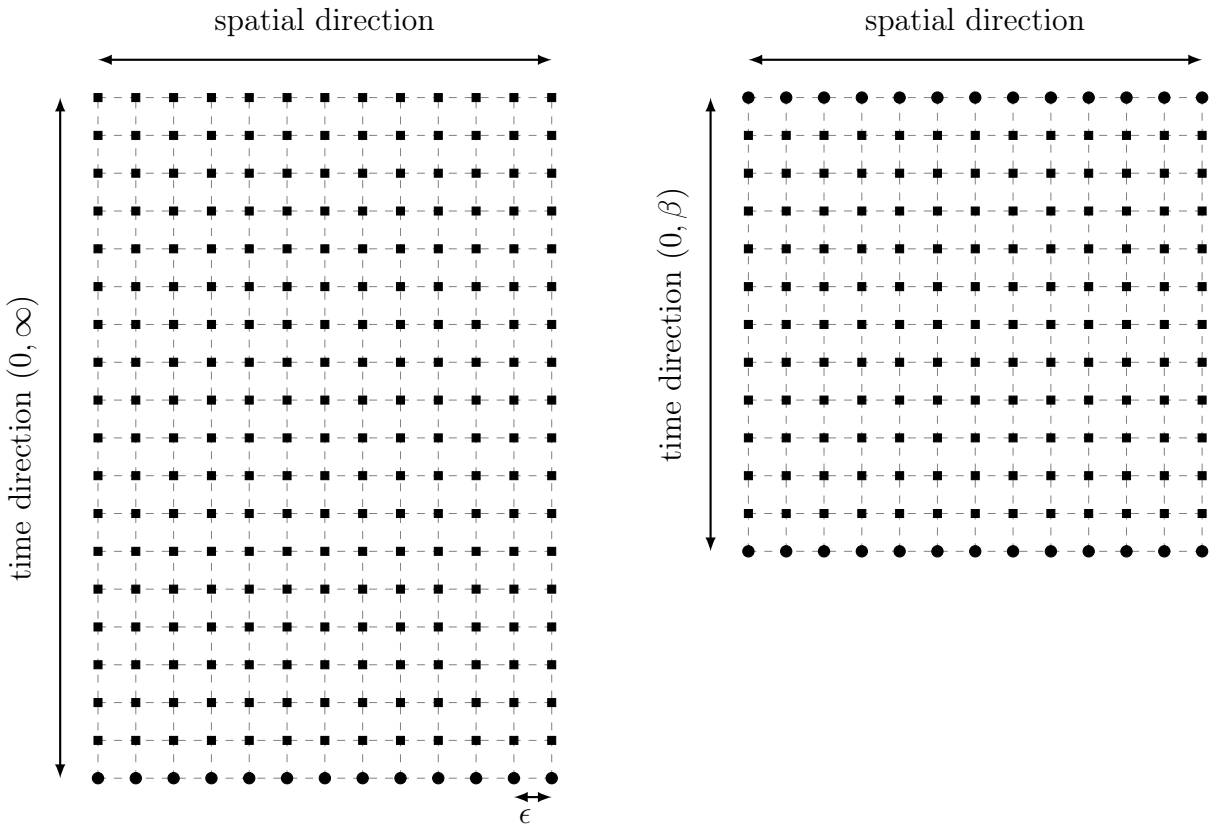

(a) Vacuum State. **(b)** Thermofield Double State.

Figure 2.9: Discretized Path-Integral.
The round dots represent the open indices. The rectangular ones the fixed-point tensors.

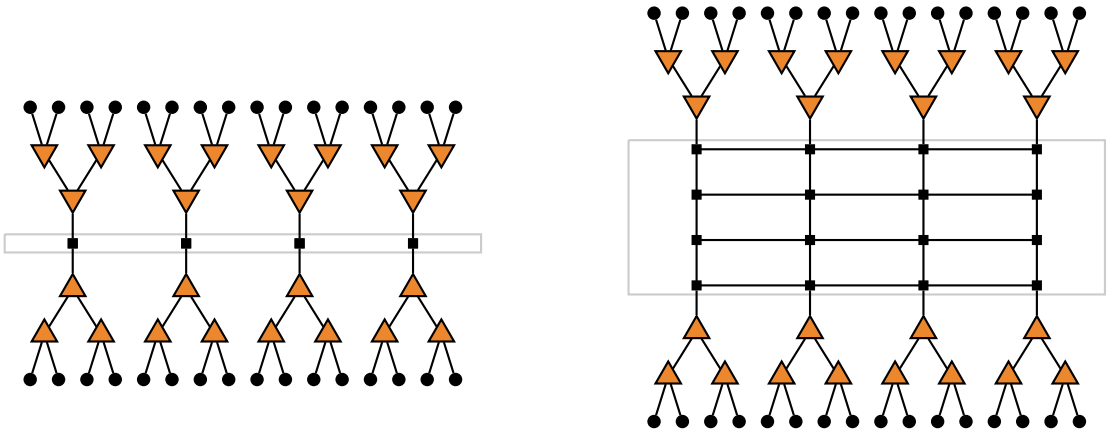

(a) Growing Bridge Layer.

Figure 2.10: MERA Network for a Thermal State.

Chapter 3

Non-Local Observables at finite Temperature

One approach to study the emergent geometry and make contact with field theory observables is using the field-operator-map (see Equation (2.75) and Equation (2.76)) and study the operator dual to the metric, which is the stress energy tensor of the CFT. The expectation value of the field theory stress energy tensor determines the asymptotic behavior of the dual geometry. This is the most intuitive approach from the field theory perspective: expectation values are natural observables in the field theory and the GKP-Witten relation (2.77) allows for an explicit mapping to gravity quantities. In this work, I follow a different approach motivated from a quantity that is natural to consider on the gravity side: extremal surfaces anchored on the boundary. These assign a unique minimal[1] area to given boundary conditions in the CFT in a covariant manner. These extremal surfaces probe the geometry of the gravitational dual along their support. The derivation of the dual field theory quantities does not follow systematically from the partition functions for these non-local objects. We already get to know one observable corresponding to minimal surfaces: in Section 2.5.2 we saw that the holographic dual of the entanglement entropy is a co-dimension one surface in a constant time-slice. This is not the only entry of the AdS/CFT dictionary referring to extremal surfaces. A second example is the Wilson loop expectation value. This gauge-invariant observable is associated with the phase factor arising for a probe quark which is parallel transported along a closed loop. Holographically, the Wilson loop expectation value is related to the minimal area of dimension two surfaces anchored on the closed loop [106]. A third observable related to extremal surfaces is the two-point correlation function

[1] There are potentially several extremal surfaces, but the minimal area of these is unique.

Table 3.1: AdS/CFT Dictionary for non-local Observables.

two-point function	$\longleftrightarrow$	one-dimensional minimal surface, i.e. a geodesic
Wilson loop	$\longleftrightarrow$	two-dimensional minimal surface
Entanglement entropy	$\longleftrightarrow$	$(d-1)$-dimensional surface

for operators in the limit of large scaling dimension. Holography relates them to the length of the bulk geodesic connecting both boundary points [107]. These three observables are so-called *non-local observables*[2].

In this work, I study these observables in AdS Schwarzschild geometries in general dimension. These black hole geometries correspond to finite temperature states of the dual field theory. In Section 3.1 the additional non-local observables are reviewed: the two-point correlation function and the Wilson loop. Since there is no constructive way to obtain the field theory dual of non-local objects such as these minimal surfaces, the origins of these entries to the holographic dictionary are diverse. Afterwards, Section 3.2 discusses the considered geometric setup. In particular, the problem is phrased in a general fashion: I consider minimal surfaces anchored on a strip on the boundary. The dimension of these surfaces is arbitrary and the restriction to the cases relevant for the non-local observables is done later. I derive closed, analytic expressions for the width of the strip and the area of the attached minimal surface for arbitrary surface dimension. In Section 3.3, I use the aforementioned results to obtain results for the non-local observables.

3.1 Non-Local Observables in AdS/CFT

In this section, we review the new non-local observables considered here, i.e. the two-point correlation function and the Wilson loop expectation value. The third observable, the entanglement entropy, is already introduced in Section 2.5.1 and its holographic dual is presented in Section 2.5.2. These observables all correspond to boundary-anchored minimal surfaces of different dimension on the gravity side. Table 3.1 shows the relationship between observables and dimension.

[2]There has to be some caution using the terms 'observable' and 'non-local' here. The entanglement entropy is not an observable in the sense of a linear operator acting on states. Furthermore, the two-point correlation is bi-local, but since it also correspond to extremal surfaces holographically, it is often considered as non-local in this context.

3.1.1 Two-Point Function

The first observable is the two-point correlation function

$$\langle \mathcal{O}(x)\mathcal{O}(y)\rangle$$

for an operator $\mathcal{O}$[3]. Correlation functions give insights into how different points in space are correlated. This can be seen by understanding the two-point correlation function as the overlap of two states: the state obtained by acting with $\mathcal{O}(x)$ on the vacuum state and the state obtained by acting with $\mathcal{O}(y)$ on the vacuum state.

Holography relates the generating functional of the correlation functions to the classical gravity action Equation (2.77). This relates the two-point correlation function for an operator $\mathcal{O}$ to the correlation function of the dual field φ. The exact prescription is [108]

$$\langle \mathcal{O}(t,\vec{x})\mathcal{O}(t',\vec{y})\rangle = \lim_{\epsilon\to 0} \epsilon^{-2\Delta}\langle \varphi(b_x(\epsilon))\varphi(b_y(\epsilon))\rangle, \tag{3.1}$$

where the bulk-points $b_x(\epsilon)$ and $b_y(\epsilon)$ approach the boundary points $(t,\vec{x})$ and $(t',\vec{y})$ respectively in the limit $\epsilon \to 0$ (see also [108]). For a general operator $\mathcal{O}$ one therefore has to calculate the two-point correlation function on the gravity side. As conjectured in [107], the two-point correlation function can also be obtained by evaluating the path integral

$$\langle \varphi(\mathbf{x})\varphi(\mathbf{y})\rangle = \int \mathcal{D}\mathcal{P}\ \exp\left(i\Delta\cdot\frac{\mathcal{L}(\mathcal{P})}{L}\right), \tag{3.2}$$

where $\mathbf{x},\mathbf{y}$ are bulk-points and the integral is over all paths $\mathcal{P}$ connecting these points[4]. $\mathcal{L}$ is the proper length of the path in the given geometry. Here, the conventions are in a way that spacelike geodesics have positive imaginary length. This alternative expression for the two-point correlation function is obtained by demanding that it is a Green's function to the equation of motion and solving this dif-

[3]What we consider here is the connected two-point correlation function $\langle \mathcal{O}(x)\mathcal{O}(y)\rangle_{\text{conn.}}$. It is obtained from the ordinary one via

$$\langle \mathcal{O}(x)\mathcal{O}(y)\rangle_{\text{conn.}} = \langle \mathcal{O}(x)\mathcal{O}(y)\rangle - \langle \mathcal{O}(x)\rangle\langle \mathcal{O}(y)\rangle.$$

The appropriate generating functional is the effective action. In AdS/CFT, the GKP-Witten relation tells us that the effective action of the field theory is given by the classical gravity action.

[4]The path-integral measure is not specified as this expression is only used in the saddle-point approximation.

ferential equation in the WKB approximation, i.e. in the semi-classical limit [109]. Furthermore, if one considers an operator with large scaling dimension Δ, we can approximate the path-integral by evaluating the integrand at the saddle-point, i.e. we only have to find the minimal path connecting $\mathbf{x}$ and $\mathbf{y}$. In this limit, the two-point correlation function of the field φ reduces to

$$\langle\varphi(\mathbf{x})\varphi(\mathbf{y})\rangle = \exp\left(-\Delta\cdot\frac{\mathcal{A}}{L}\right), \tag{3.3}$$

where $\mathcal{A}$ is the length of the connecting geodesic. Combining these expressions yields

$$\langle\mathcal{O}(t,\vec{x})\mathcal{O}(t,\vec{y})\rangle = \lim_{\epsilon\to 0}\epsilon^{-2\Delta}\exp\left(-\Delta\cdot\frac{\mathcal{A}(\epsilon)}{L}\right) \tag{3.4}$$

for the CFT two-point correlation function.

Hence, the two-point correlation function for an operator $\mathcal{O}$ with large scaling dimension Δ is related to the length of the bulk-geodesic connection the two boundary points.

3.1.2 Wilson Loop

The second observable considered in this work is the Wilson loop expectation value (see [110] for a review). The theories we consider in AdS/CFT are gauge theories, therefore we in particular have a gauge field A^μ and a gauge symmetry. For the fields transforming in the fundamental representation of this symmetry, there is a well-defined notion of parallel transport along a path $\mathcal{C}$

$$W(\mathcal{C}) = \mathcal{P}\exp\int_{\mathcal{C}}\mathrm{d}x^\mu A_\mu, \tag{3.5}$$

where $\mathcal{P}$ is the path-ordering operator. This acts on fields Ψ in the fundamental representation of the gauge group, i.e. which source the gauge field. A field $\Psi(x)$ being parallel transported from x to y transforms as a field at y,

$$\begin{aligned}\Psi(x)&\to U(x)\Psi(x),\\ W(\mathcal{C})\Psi(x)&\to U(y)W(\mathcal{C})\Psi(x).\end{aligned}$$

Therefore, the phase factor $W(\mathcal{C})$ transforms in the adjoint representation for a closed loop $\mathcal{C}$. A gauge-invariant observable is obtained by considering the trace of

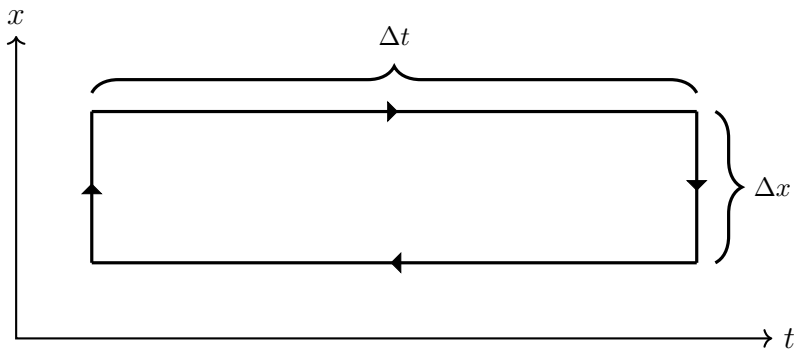

Figure 3.1: Rectangular Wilson loop corresponding to a Quark-Antiquark Pair.

this expression, i.e.

$$\mathcal{W}(\mathcal{C}) = \frac{1}{N} \operatorname{Tr} \left(\mathcal{P} \exp \oint_{\mathcal{C}} \mathrm{d}x^{\mu} A_{\mu} \right). \tag{3.6}$$

Therefore, this Wilson loop expectation value is proportional to the phase factor associated to the parallel transport of a particle in the fundamental representation (e.g. a quark) along a closed path. The particle is a probe particle and does not backreact on the gauge-field, i.e. it is assumed to have infinite mass.

The Wilson loop expectation value can be used an order parameter e.g. for confinement. Of particular interest for this is to consider a path describing a quark-antiquark pair. The corresponding path is shown in Figure 3.1: a rectangle with width Δx in one spatial direction and width $\Delta t \to \infty$ in the time direction. This corresponds to a quark-antiquark pair of constant distance Δx being created at $t = -\infty$ and being annihilated at $t = \infty$. Using this configuration, the quark-antiquark potential for a probe quarks in distance Δx is

$$V_{q\bar{q}} = - \lim_{\Delta t \to \infty} \frac{\ln \langle \mathcal{W} \rangle}{\Delta t}. \tag{3.7}$$

The behavior for large separation, i.e. for large Δx, determines whether the potential is confining or not. In a non-confining theory, the potential converges as

$$\lim_{\Delta x \to \infty} V_{q\bar{q}} \propto \Delta x^0 + \text{ subleading terms}\,.$$

In contrast, a confining theory has a potential grows with separation Δx as

$$\lim_{\Delta x \to \infty} V_{q\bar{q}} \propto \Delta x^a \qquad \text{with} \qquad a \geq 1\,.$$

Let us consider examples if this. For a confining theory with a constant force between quark and anti-quark, the potential is linear in the distance, i.e.

$$V_{q\bar{q}} \sim \sigma \Delta x,$$

where Δx is the tension. This tension introduces a length-scale. In contrast, a scale invariant theory only allows

$$V_{q\bar{q}} = \frac{\alpha}{\Delta x},$$

where α is a dimensionless constant. In four dimensions, this is the Coulomb potential.

In AdS/CFT, the relevant Wilson loops are the supersymmetric version of Equation (3.6). For these, also the compact space comes into play. How can we calculate Wilson loops expectation values holographically? To consider Wilson loops, one has to introduce probe quarks. However, the standard fields considered in AdS/CFT arise from a stack of branes deep in the bulk. Therefore, all of the field theory fields arise from open strings between these branes and transform in the adjoint representation of the gauge group. To obtain fundamental degrees of freedom, one has to have a different brane where strings can end as shown in Figure 3.2. The fundamental degrees of freedom arise from strings with one end on the stack of branes and one end on the probe brane. The distance between the stack of branes and the additional brane is related to the quark mass. If we consider probe quarks, i.e. infinitely heavy quarks, the distance is infinite and the probe brane is at the boundary. The action of these strings is given by the Nambu-Goto action

$$\begin{aligned} S_{NG} &= \frac{1}{2\pi\alpha'} \int \mathrm{d}\tau \mathrm{d}\sigma \sqrt{|\det g_{\mu\nu} \partial_\chi x^\mu \partial_\beta x^\nu|}, \\ &= \frac{1}{2\pi\alpha'} \mathcal{A}, \end{aligned} \tag{3.8}$$

and consequently proportional to the volume spanned by these branes. As shown in [106], the holographic dual of the Wilson loop expectation value is

$$\langle \mathcal{W}(\mathcal{C}) \rangle = \exp\left(-S_{NG}\right). \tag{3.9}$$

Of particular interest is to consider the rectangular temporal Wilson loop corresponding to a quark-antiquark pair. Using the holographic proposal, the potential

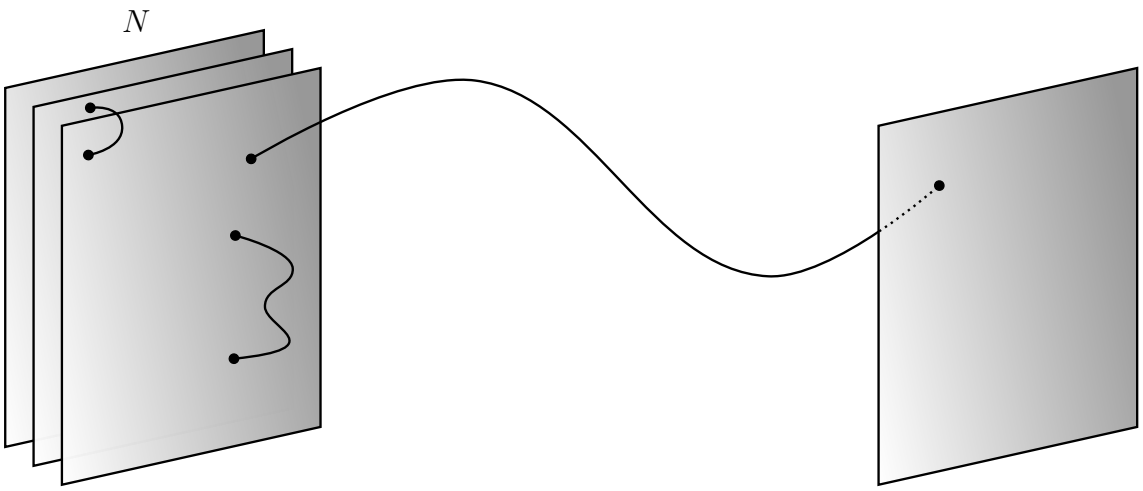

Figure 3.2: Flavor Branes in AdS/CFT.

is

$$V_{q\bar{q}} = -\lim_{\Delta t\to\infty} \frac{\ln\langle \mathcal{W}\rangle}{\Delta t} = -\lim_{\Delta t\to\infty} \frac{S_{NG}}{\Delta t}\,. \tag{3.10}$$

The result is UV-divergent, i.e. it diverges as we take the bulk cutoff ϵ to zero. This divergent term is due to the infinite mass of the quark. After deducing the mass terms from the potential [111], the renormalized quark-antiquark potential is

$$\begin{aligned} V_{q\bar{q}} &= \frac{S_{NG}}{\tilde{\ell}} - \frac{L^2}{\pi\alpha'\epsilon}, \\ &= \frac{\mathcal{A}}{2\pi\alpha'\tilde{\ell}} - \frac{L^2}{\pi\alpha'\epsilon} \end{aligned} \tag{3.11}$$

where $\mathcal{A}$ is the minimal area of the attached two-dimensional surface.

3.2 Results for extremal surfaces at finite temperature

I derive the minimal area of boundary anchored extremal surfaces in this section. Since the non-local observables reviewed in the previous section are dual to minimal surfaces of different dimension, this allows a combined treatment of all three of them. First, I follow the usual method to determine extremal surfaces in geometry. The results are integral expressions. These can be expressed as power series, as was done for minimal surfaces of specific dimensionality already in [112]. Using this

groundwork, I write these power series as generalized hypergeometric functions and find closed, analytic expressions.

We consider a CFT state in d dimensions at finite temperature. The geometric dual is described by planar AdS Schwarzschild [113, 114] with a horizon at radial position z_h (see Equation (2.7))

$$\mathrm{d}s^2 = \left(\frac{L}{z}\right)^2 \left(-b(z)\mathrm{d}t^2 + \mathrm{d}\vec{x}^2 + b(z)^{-1}\mathrm{d}z^2\right), \tag{3.12a}$$

$$b(z) = 1 - \left(\frac{z}{z_h}\right)^d. \tag{3.12b}$$

The temperature of the dual field theory is

$$T = \frac{d}{4\pi z_h} \tag{3.13}$$

and density of the thermal entropy is

$$s = \frac{1}{4G_N}\left(\frac{L}{z_h}\right)^{d-1} = \frac{L^{d-1}}{4G_N}\left(\frac{4\pi}{d}\right)^{d-1} \cdot T^{d-1}. \tag{3.14}$$

Furthermore, the energy density is

$$\langle T_{tt}\rangle = \frac{(d-1)L^{d-1}}{16\pi G {z_h}^d}, \tag{3.15}$$

which follows from the asymptotic falloff of the metric [115].

As reviewed in the previous section, the AdS/CFT dictionary relates the two-point correlation function, the Wilson loop expectation value and the entanglement entropy to one-, two- and $(d-1)$-dimensional surfaces on the gravity side respectively. For the entanglement entropy, the considered surfaces are extremal surfaces are anchored on an equal time slice. The metric of AdS Schwarzschild is static, which allows to restrict the attention to a constant time slice and calculate the minimal surface. Motivated by this, my work focuses on non-local observables dual to minimal surfaces in this constant time-slice, as these can be calculated using a similar procedure as for the entanglement entropy. Therefore, we consider the two-point correlation function for two spacelike separated points and the spatial Wilson loop expectation value.

After having specified the gravity dual we consider, I still have to specify how the minimal surfaces are anchored on the boundary. For the two-point correlation

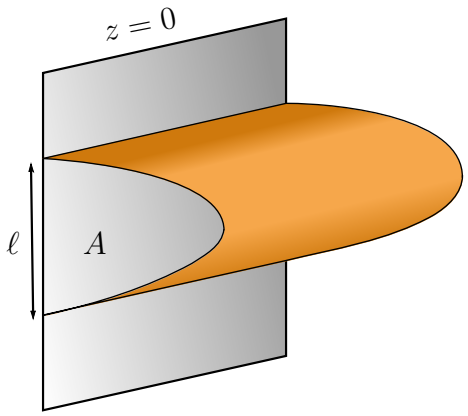

Figure 3.3: Boundary Region and associated Bulk Surface.
The strip has the width ℓ in direction x^1 and length $\tilde{\ell} \gg \ell$ in the directions x^i with $i = 2, \ldots, n$. The remaining directions (i.e. x^j with $j = n+1, \ldots, d-1$) are not shown.

function this is trivial: it depends on two-points, i.e. the boundary of a line. The Wilson loop expectation value depends on the closed path (i.e. the boundary of a closed two-dimensional surface) considered, whereas the entanglement entropy on the entangling surface (or equivalently on the entanglement region). In this work, I consider a strip on the boundary. The width in one spatial direction, which is without loss of generality $x^1 = x$ in the following, is ℓ. The length $\tilde{\ell}$ in the remaining spatial directions is much larger. Figure 3.3 shows this configuration. The advantage of this setup that the metric is independent of the spatial coordinates. The transverse directions only yield the transverse volume as an overall factor. The whole problem can be phrased as finding geodesics in a conformally equivalent metric, as discussed in [116, 117]. Furthermore, the metric does not depend on the coordinate x, which results in a conserved quantity along the geodesic.

To summarize, I consider the two-point correlation function for two points of distance ℓ, the Wilson loop expectation value for a rectangular path and the entanglement entropy for a spatial region bounded by two parallel hyperplanes of distance ℓ. In the considered limit $\ell \ll \tilde{\ell}$, the length of the strip appears as an factor of $\tilde{\ell}$ or $\tilde{\ell}^{d-2}$ for Wilson loop and entanglement entropy respectively.

Qualitative aspects of extremal surfaces anchored on strip geometries are studied in [118]. In particular, it is shown that for fixed spacetime dimension d, higher-dimensional surfaces reach deeper into the bulk. This implies that the holographic entanglement entropy is the non-local observable probing deepest into the bulk. Furthermore, these extremal surfaces cannot cross the horizon, but can reach arbitrarily close. This happens because the horizon acts as a potential wall pushing the

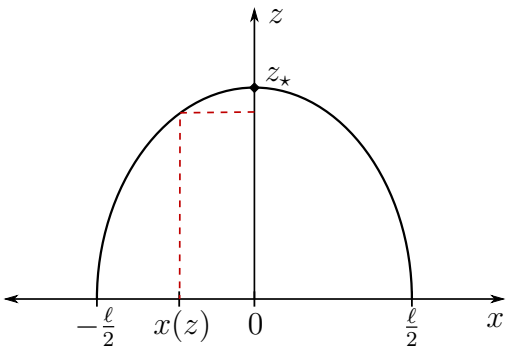

Figure 3.4: Minimal Bulk Surface.
The strip has the width ℓ in the spatial direction x. The $(n-1)$ remaining spatial directions are not shown, since the shape of the surface is independent of these coordinates.

minimal surfaces away. Therefore, the radial position of the turning point of the minimal surface lies in the range

$$0 \leq z_\star < z_h.$$

In the following, I present my results for the area of a minimal surface of general dimension. It is obtained in a closed form involving generalized hypergeometric functions. While the results do not simplify further, various well-known properties of these functions (such as known derivatives, indefinite integrals and transformations) make properties of the result easier accessible. I use one of these properties to examine the high-temperature/large-width limit closer and derive a closed form for the leading subleading contribution. Since this term depends on the whole bulk metric, it can not be derived from a simple approximation as is possible for the leading contribution.

3.2.1 General Formulation of Problem

In this section, I derive the minimal area of bulk surfaces attached to strips on the boundary of $(d+1)$-dimensional AdS Schwarzschild. Figure 3.3 shows the boundary region: a strip with width ℓ and infinite extend in the $(n-1)$ transverse direction. For a geodesic, i.e. the case $n = 1$, some subtleties related to logarithmic divergences arise.

The embedding of the bulk minimal surface is shown in Figure 3.4. The transverse directions are not shown, since the surface is translational invariant in these directions. Consequently, the only relevant spatial direction is $x^1 = x$. Following

standard procedure, the minimal surface is parameterized by the radial direction z and the $(n-1)$ transverse direction. The integration in these transverse directions yield an overall factor of $\tilde{\ell}^{n-1}$. The turning point of the minimal surface is at radial position $z_\star$. The area of the surface can therefore be written as a one-dimensional integral

$$\mathcal{A} = 2L^n \tilde{\ell}^{n-1} \int_\epsilon^{z_\star} \mathrm{d}z \; z^{-n} \sqrt{\frac{1}{b(z)} + x'(z)^2}, \tag{3.16}$$

where $x(z)$ is the embedding of the surface. The factor of two arises because we obtain the same length for the left ($x' > 0, x < 0$) and the right ($x' < 0, x > 0$) branch. As empathized by [116, 117], the minimal surfaces can be treated as geodesics in an auxiliary spacetime

$$\mathrm{d}s^2 = \left(\frac{L}{z}\right)^{2n} \left(\frac{1}{b(z)}\mathrm{d}z^2 + \mathrm{d}x^2\right).$$

At this point, the advantage of considering a strip emerges: the metric is independent of the spatial coordinates. This implies that along the minimal surface, the quantity

$$\frac{x'(t)}{z^n} \frac{1}{\sqrt{\frac{1}{b(z)} + x'(z)^2}} = \pm \frac{1}{{z_\star}^n} \tag{3.17}$$

is conserved. The sign is for the left and the right branch respectively. This conserved quantity is expressed in terms of the radial position of the turning point by considering the limit $z \to 0$. Therefore, the extremal embedding is determined by the differential equation

$$x'(t) = \pm \left(\frac{z}{z_\star}\right)^n \frac{1}{\sqrt{b(z)}} \frac{1}{\sqrt{1 - (z/z_\star)^{2n}}}. \tag{3.18}$$

The sign depends on whether the left or the right branch of the surface is considered. This is equivalent to

$$\left(\frac{\partial z}{\partial x}\right)^2 = b(z) \left(\left(\frac{z_\star}{z}\right)^d - 1\right) = -V_{\text{eff}}$$

with the effective potential V_{eff}. This helps to understand why these extremal sur-

faces cannot cross the horizon, as discussed in [118]: assuming that the turning point of the minimal surface is inside the horizon at radial position $z_\star > z_h$, there is a range $z_h < z < z_\star$ where the potential becomes positive and there exists no solution to this differential equation. Therefore, extremal surfaces cannot cross the horizon and we have $z_\star < z_h$. The whole spacetime outside the horizon is accessible, i.e. we can reach arbitrary close to the horizon with minimal surfaces.

Since we are not interested in the explicit embedding, this differential equation does not have to be solved explicitly. Instead, it can be used to obtain an integral expression for the minimal Area $\mathcal{A}$. The resulting expression for the minimal area is

$$\mathcal{A} = 2L^n \tilde{\ell}^{n-1} \int_\epsilon^{z_\star} \mathrm{d}z \;\; z^{-n} \frac{1}{\sqrt{1-(z/z_h)^d}} \frac{1}{\sqrt{1-(z/z_\star)^{2n}}}. \tag{3.19a}$$

This expresses the minimal area in terms of the turning point $z_\star$. The relevant field theory parameter is the width of the strip ℓ. It can be expressed as

$$\ell = 2\int_0^{z_\star} \mathrm{d}z \; |x'(z)| = 2\int_0^{z_\star} \mathrm{d}z \;\; \left(\frac{z}{z_\star}\right)^n \frac{1}{\sqrt{1-(z/z_h)^d}} \frac{1}{\sqrt{1-(z/z_\star)^{2n}}}. \tag{3.19b}$$

The difficulty integrating these expressions arises from the appearing square roots[5]. This expression shows that higher-dimensional surfaces reach deeper into the bulk: increasing n while keeping the turning point $z_\star$ fixed increases the denominator and hence decreases the integrand and the width[6]. Therefore, the same turning point corresponds to a smaller width for a higher-dimensional surface.

These integrals can be written as power series as derived by [112]. First, both square roots are expressed as power series as follows from their representation as

[5] A closer analysis shows that these terms are of the form

$$\sqrt{1-\sigma}^{-1}, \; \sigma \leq 1$$

These can be expressed as hypergeometric functions ${}_1F_0\left(1/2;;\sigma\right)$ (see Equation (B.12a)) and may be expressed as a power series in σ.

[6] This can be seen by writing the integral as

$$\ell = 2\int_0^{z_\star} \mathrm{d}z \;\; \frac{1}{\sqrt{1-(z/z_h)^d}} \frac{1}{\sqrt{(z_\star/z)^{2n}-1}}.$$

hypergeometric functions, see (B.1a) in the appendix. These power series are absolutely convergent and it is possible to exchange summation and integration. After simplification, the area can be written as power series[7]

$$\mathcal{A} = \frac{2L^n}{n-1}\frac{\tilde{\ell}^{n-1}}{\epsilon^{n-1}} + \frac{\sqrt{\pi}L^n}{n}\frac{\tilde{\ell}^{n-1}}{{z_\star}^{n-1}}\sum_{m=0}^{\infty}\frac{1}{m!}\left(\frac{1}{2}\right)_m\left(\frac{z_\star}{z_h}\right)^{md}\frac{\Gamma\left(\frac{md-n+1}{2n}\right)}{\Gamma\left(\frac{md+1}{2n}\right)} \tag{3.20a}$$

for $n \neq 1$ and as

$$\mathcal{A} = 2L\ln\left(\frac{2z_\star}{\epsilon}\right) + \sqrt{\pi}L\sum_{m=1}^{\infty}\frac{1}{m!}\left(\frac{1}{2}\right)_m\left(\frac{z_\star}{z_h}\right)^{md}\frac{\Gamma\left(\frac{md}{2}\right)}{\Gamma\left(\frac{md+1}{2}\right)} \tag{3.20b}$$

for $n = 1$ The analogous procedure can be applied to the width of the strip, resulting in

$$\ell = \frac{z_\star\sqrt{\pi}}{n}\sum_{m=0}^{\infty}\frac{1}{m!}\left(\frac{1}{2}\right)_m\left(\frac{z_\star}{z_h}\right)^{md}\frac{\Gamma\left(\frac{1}{2n}\left(md+n+1\right)\right)}{\Gamma\left(\frac{1}{2n}\left(md+2n+1\right)\right)}. \tag{3.20c}$$

A review of hypergeometric functions and Pochhammer functions $(a)_p$ can be found in Section B.1 of the appendix. The results in [112] focused on the cases $n = 1, 2, d-2$, which my calculation generalizes to general n, i.e. general dimension of the extremal surface.

How can these power series be simplified? In a generalized hypergeometric function or rather their power series representation, the ratio of consecutive coefficients c_m and c_{m+1} have a certain form: they have to be a rational function of m, i.e.

$$\frac{c_{m+1}}{c_m} = u \cdot \frac{P(-m)}{Q(-m)}\frac{1}{m},$$

where P and Q are polynomial functions. As discussed in Equation (B.4), the roots of P and Q correspond to numerator and denominator parameter of the resulting hypergeometric function respectively and u is the argument of the hypergeometric function. It is directly obvious that the coefficients of the power series derived in (3.20) do not have correct form. The problem lies in the denominator $2n$ appearing in the Gamma functions. However, the ratio between the coefficients c_m and c_{m+2n} has the correct form for generalized hypergeometric functions. Therefore, I am able

[7]The result is in terms of a double sum. One of the sums simplifies to a hypergeometric function at unit argument[8]. This hypergeometric function is finite at unit argument and simplifies in terms of Gamma functions, see Equation (B.7).

to construct generalized hypergeometric functions from the power series derived in (3.20) by reordering them. This is allowed because these series are absolutely convergent for $z_\star < z_h$. The reordering is done by redefining the index of summation

$$m = \Delta m + 2n \cdot \delta m, \qquad \delta m = 0, \ldots, \infty, \qquad \Delta m = 0, \ldots, 2n-1.$$

δm is the quotient with respect to $2n$ and Δm is the remainder. Using this, I split the series into $(2n)$ series which in the following are expressed as hypergeometric functions. Δm labels the different series, whereas δm becomes the new index of summation. However, it is not always necessary to split the original series into $(2n)$ ones. If the greatest common denominator between $2n$ and d is larger than one, less hypergeometric series are required to express the result. Incorporating possible simplifications, the redefinition of the index of summation reads

$$m = \Delta m + \frac{2n}{\chi}\delta m, \qquad \chi = \gcd(2n, d) \in \mathbb{N}, \tag{3.21a}$$

$$\delta m = 0, \ldots, \infty, \qquad \Delta m = 0, \ldots, \frac{2n}{\chi} - 1. \tag{3.21b}$$

This performs the replacement

$$\sum_{m=0}^{\infty}(\cdots) \longrightarrow \sum_{\Delta m=0}^{\frac{2n}{\chi}-1}\left[\sum_{\delta m=0}^{\infty}(\cdots)\right].$$

Since all of these sums are absolutely convergent in the argument range considered, this reordering is allowed and does not change the result.

For the area, the coefficients of the series are

$$\hat{c}_{\delta m} = c_m\big|_{\Delta m + \frac{2n}{\chi}\delta m} \qquad \text{with } c_m = \frac{1}{m!}\left(\frac{1}{2}\right)_m \left(\frac{z_\star}{z_h}\right)^{md} \frac{\Gamma\left(\frac{md-n+1}{2n}\right)}{\Gamma\left(\frac{md+1}{2n}\right)}.$$

The ratio we are interested in is

$$\begin{aligned}\frac{\hat{c}_{\delta m+1}}{\hat{c}_{\delta m}} = \left(\frac{z_\star}{z_h}\right)^{\frac{2nd}{\chi}\delta m} &\frac{\Gamma\left(\frac{1}{2} + \Delta m + \frac{2n}{\chi}\delta m + \frac{2n}{\chi}\right)}{\Gamma\left(\frac{1}{2} + \Delta m + \frac{2n}{\chi}\delta m\right)} \frac{\Gamma\left(1 + \Delta m + \frac{2n}{\chi}\delta m\right)}{\Gamma\left(1 + \Delta m + \frac{2n}{\chi}\delta m + \frac{2n}{\chi}\right)} \\ &\times \frac{\Gamma\left(\frac{\Delta md-n+1}{2n} + \frac{d}{\chi}(\delta m+1)\right)}{\Gamma\left(\frac{\Delta md-n+1}{2n} + \frac{d}{\chi}\delta m\right)} \frac{\Gamma\left(\frac{\Delta md+1}{2n} + \frac{d}{\chi}\delta m\right)}{\Gamma\left(\frac{\Delta md+1}{2n} + \frac{d}{\chi}(\delta m+1)\right)}.\end{aligned} \tag{3.22}$$

χ is the greatest common denominator of d and $2n$, hence both $2n/\chi$ and d/χ are integer numbers. As we see, the trick of summing over δm instead of m results in these the arguments of the numerator and denominator Gamma functions differing by integer values. Consequently, the Gamma function can be rewritten as products

$$\frac{\hat{c}_{\delta m+1}}{\hat{c}_{\delta m}} = \left(\frac{z_\star}{z_h}\right)^{\frac{2nd}{\chi}\delta m} \prod_{j=0}^{2n/\chi-1} \left(\frac{(\frac{1}{2}+\Delta m+\frac{2n}{\chi}\delta m+j)}{(1+\Delta m+\frac{2n}{\chi}\delta m+j)}\right) \prod_{k=0}^{d/\chi-1} \left(\frac{\frac{\Delta md-n+1}{2n}+\frac{d}{\chi}\delta m+k}{\frac{\Delta md+1}{2n}+\frac{d}{\chi}\delta m+k}\right).$$

Therefore, the ratio has the desired form

$$\frac{\hat{c}_{\delta m+1}}{\hat{c}_{\delta m}} = \left(\frac{z_\star}{z_h}\right)^{\frac{2nd}{\chi}\delta m} \prod_{j=0}^{2n/\chi-1} \left(\frac{\delta m+b_{j+\frac{1}{2}}}{\delta m+b_{j+1}}\right) \prod_{k=0}^{d/\chi-1} \left(\frac{\delta m+a_{k-\frac{1}{2}}}{\delta m+a_k}\right), \tag{3.23}$$

where the parameters are

$$a_i = \frac{\chi}{2nd}\left(\Delta md+1+2ni\right), \qquad b_j = \frac{\chi}{2n}\left(\Delta m+j\right). \tag{3.24}$$

Furthermore, hypergeometric functions are normalized such that $\hat{c}_0 = 1$. Careful analysis of the coefficients therefore yields

$$\begin{aligned}\mathcal{A} = \frac{2L^n}{n-1}\left(\frac{\tilde{\ell}}{\epsilon}\right)^{n-1} + \frac{\sqrt{\pi}L^n}{n}\frac{\tilde{\ell}^{n-1}}{{z_\star}^{n-1}} \sum_{\Delta m=0}^{\frac{2n}{\chi}-1} \frac{1}{\Delta m!}\left(\frac{1}{2}\right)_{\Delta m}\left(\frac{z_\star}{z_h}\right)^{\Delta md} \frac{\Gamma\left(\frac{d}{\chi}a_{-1/2}\right)}{\Gamma\left(\frac{d}{\chi}a_0\right)} \\ \times \ {}_{\frac{2n+d}{\chi}+1}F_{\frac{2n+d}{\chi}}\left(\left.\begin{matrix}1, a_{-\frac{1}{2}}, \ldots, a_{\frac{d}{\chi}-\frac{3}{2}}, b_{\frac{1}{2}}, \ldots, b_{\frac{2n}{\chi}-\frac{1}{2}} \\ a_0, \ldots, a_{\frac{d}{\chi}-1}, b_1, \ldots, b_{\frac{2n}{\chi}}\end{matrix}\right| \left(\frac{z_\star}{z_h}\right)^{\frac{2nd}{\chi}}\right)\end{aligned} \tag{3.25}$$

for the area of the surface.

Following the same procedure, the coefficients for the width are

$$\hat{c}_{\delta m} = c_m\big|_{\Delta m+\frac{2n}{\chi}\delta m} \qquad \text{with } c_m = \frac{1}{m!}\left(\frac{1}{2}\right)_m\left(\frac{z_\star}{z_h}\right)^{md}\frac{\Gamma\left(\frac{md+n+1}{2n}\right)}{\Gamma\left(\frac{md+2n+1}{2n}\right)}.$$

The difference to the analog calculation for the area is the shift in the argument of the Gamma functions. This results in

$$\frac{\hat{c}_{\delta m+1}}{\hat{c}_{\delta m}} = \left(\frac{z_\star}{z_h}\right)^{\frac{2nd}{\chi}\delta m} \prod_{j=0}^{2n/\chi-1} \left(\frac{\delta m+b_{j+\frac{1}{2}}}{\delta m+b_{j+1}}\right) \prod_{k=0}^{d/\chi-1} \left(\frac{\delta m+a_{k+\frac{1}{2}}}{\delta m+a_{k+1}}\right). \tag{3.26}$$

Consequently, the width of the strip can be expressed as

$$\ell = \frac{\sqrt{\pi} z_\star}{n} \sum_{\Delta m=0}^{\frac{2n}{\chi}-1} \frac{1}{\Delta m!} \left(\frac{1}{2}\right)_{\Delta m} \left(\frac{z_\star}{z_h}\right)^{\Delta m d} \frac{\Gamma\left(\frac{d}{\chi} a_{1/2}\right)}{\Gamma\left(\frac{d}{\chi} a_1\right)}$$
$$\times \ {}_{\frac{2n+d}{\chi}+1}F_{\frac{2n+d}{\chi}} \left(\begin{matrix} 1, a_{\frac{1}{2}}, \ldots, a_{\frac{d}{\chi}-\frac{1}{2}}, b_{\frac{1}{2}}, \ldots, b_{\frac{2n}{\chi}-\frac{1}{2}} \\ a_1, \ldots, a_{\frac{d}{\chi}}, b_1, \ldots, b_{\frac{2n}{\chi}} \end{matrix} \middle| \left(\frac{z_\star}{z_h}\right)^{\frac{2nd}{\chi}} \right). \tag{3.27}$$

for the minimal area of the surface. Therefore, the results can be written in term of $2n/\chi$ hypergeometric functions.

As mentioned above, the case $n = 1$ requires some subtlety when calculating the area. The power series result in Equation (3.20a) applies for $m \neq 0$ and only the $m = 0$ term has to be modified by using the correct logarithmic term. Therefore, the construction above remains valid for part of the result if Δm is shifted. Combining this with the correct treatment of the lowest order term yields

$$\mathcal{A} = 2L \ln\left(\frac{2z_\star}{\epsilon}\right) + \sqrt{\pi} L \sum_{\Delta m=1}^{\frac{2}{\chi}} \frac{1}{\Delta m!} \left(\frac{1}{2}\right)_{\Delta m} \left(\frac{z_\star}{z_h}\right)^{\Delta m d} \frac{\Gamma\left(\frac{d}{\chi} a_{-1/2}\right)}{\Gamma\left(\frac{d}{\chi} a_0\right)} \tag{3.28}$$
$$\times \ {}_{\frac{2+d}{\chi}+1}F_{\frac{2+d}{\chi}} \left(\begin{matrix} 1, a_{-\frac{1}{2}}, \ldots, a_{\frac{d}{\chi}-\frac{3}{2}}, b_{\frac{1}{2}}, \ldots, b_{\frac{2}{\chi}-\frac{1}{2}} \\ a_0, \ldots, a_{\frac{d}{\chi}-1}, b_1, \ldots, b_{\frac{2}{\chi}} \end{matrix} \middle| \left(\frac{z_\star}{z_h}\right)^{\frac{2d}{\chi}} \right), \qquad n = 1.$$

3.2.2 Low-Temperature/Small-Strip Limit

The above discussed calculations started with the result as power series in the dimensionless parameter $(z_\star/z_h)$ in (3.20), as was discussed in [112]. I generalize this discussion to general values for n. Therefore, a low-temperature/small-strip expansion can be directly derived from (3.20). First, the width ℓ is

$$\ell = \frac{z_\star \sqrt{\pi}}{n} \frac{\Gamma\left(\frac{n+1}{2n}\right)}{\Gamma\left(\frac{2n+1}{2n}\right)} \left(1 + \frac{\Gamma\left(\frac{d+n+1}{2n}\right)}{2\Gamma\left(\frac{d+2n+1}{2n}\right)} \frac{\Gamma\left(\frac{2n+1}{2n}\right)}{\Gamma\left(\frac{n+1}{2n}\right)} \left(\frac{z_\star}{z_h}\right)^d + \mathcal{O}\left(\frac{z_\star}{z_h}\right)^{2d}\right), \tag{3.29}$$

which allows to express the turning point as

$$z_\star = \frac{n\ell}{\sqrt{\pi}} \frac{\Gamma\left(\frac{2n+1}{2n}\right)}{\Gamma\left(\frac{n+1}{2n}\right)} \left(1 - \frac{\Gamma\left(\frac{d+n+1}{2n}\right)}{2\Gamma\left(\frac{d+2n+1}{2n}\right)} \frac{\Gamma\left(\frac{2n+1}{2n}\right)}{\Gamma\left(\frac{n+1}{2n}\right)} \left(\frac{n\ell}{\sqrt{\pi} z_h}\right)^d + \mathcal{O}\left(\frac{z_\star}{z_h}\right)^{2d}\right). \tag{3.30}$$

The behavior of the area reduces to

$$\mathcal{A} = \frac{2L^n}{n-1}\frac{\tilde{\ell}^{n-1}}{\epsilon^{n-1}} + \frac{\sqrt{\pi}L^n}{n}\frac{\tilde{\ell}^{n-1}}{{z_\star}^{n-1}}\left(\frac{\Gamma\left(\frac{-n+1}{2n}\right)}{\Gamma\left(\frac{1}{2n}\right)} + \frac{1}{2}\left(\frac{z_\star}{z_h}\right)^d \frac{\Gamma\left(\frac{d-n+1}{2n}\right)}{\Gamma\left(\frac{d+1}{2n}\right)} + \dots\right). \tag{3.31}$$

Since the turning point can be expressed in terms of the width ℓ, also the area $\mathcal{A}$ can be expressed in terms of it. Keep in mind that the width is the quantity of interest in the field theory, whereas there is no physical meaning attached to the turning point $z_\star$. Combining the correction of the turning point with the leading order change of $\mathcal{A}$ yields

$$\begin{aligned}\mathcal{A} \approx \frac{2L^n}{n-1}\left(\frac{\tilde{\ell}}{\epsilon}\right)^{n-1} - \frac{L^n}{n-1}\left(\frac{2\sqrt{\pi}\Gamma\left(\frac{n+1}{2n}\right)}{\Gamma\left(\frac{1}{2n}\right)}\right)^n \cdot \left(\frac{\tilde{\ell}}{\ell}\right)^{n-1} \\ + \frac{2L^n\sqrt{\pi}\Gamma\left(\frac{d-n+1}{2n}\right)}{(d+1)\Gamma\left(\frac{d+1}{2n}\right)}\left(\frac{2\sqrt{\pi}\Gamma\left(\frac{n+1}{2n}\right)}{\Gamma\left(\frac{1}{2n}\right)}\right)^{n-1-d} \cdot \frac{\ell^{d+1-n}\tilde{\ell}^{n-1}}{{z_h}^d} + \mathcal{O}(T\cdot\ell)^{1-n+2d}.\end{aligned} \tag{3.32}$$

The terms in first line are the result for zero-temperature. The term in the second line yields a positive leading-order change. We postpone the discussion of the physical interpretation of this term to a later point.

For the geodesic, one has to start with the power series result in 3.20b, which results in

$$\mathcal{A} = 2L\ln\left(\frac{2z_\star}{\epsilon}\right) + \frac{\sqrt{\pi}L}{2}\left(\frac{z_\star}{z_h}\right)^d \frac{\Gamma\left(\frac{d}{2}\right)}{\Gamma\left(\frac{d+1}{2}\right)} + \mathcal{O}\left(\frac{z_\star}{z_h}\right)^{2d}. \tag{3.33}$$

In particular, only the $\mathcal{O}(T\cdot\ell)^0$ term differs from the $n > 1$ result. It can also be obtained by taking the limit $n \to 1$ of (3.31) under consideration of

$$\frac{1}{n-1}x^{n-1} \longrightarrow \log x.$$

This yields

$$\mathcal{A} \approx 2L\ln\left(\frac{\ell}{\epsilon}\right) + \frac{2L\sqrt{\pi}\Gamma\left(\frac{d}{2}\right)}{(d+1)\Gamma\left(\frac{d+1}{2}\right)}\cdot\left(\frac{\ell}{2z_h}\right)^d + \mathcal{O}(T\cdot\ell)^{2d} \tag{3.34}$$

for the low-temperature/small-width limit of the area.

3.2.3 High-Temperature/Large-Strip Limit

It is interesting to examine the high-temperature/large-width limit more closely. In this limit, the arguments of the hypergeometric functions approach unity. To understand how the hypergeometric functions behave in this limit, the difference between the sum of the denominator parameter and the sum of numerator parameter is relevant. Both for the area and the width, this difference vanishes, result in a logarithmic behavior of the hypergeometric functions, see Equation (B.8) in the appendix. Therefore, the high-temperature/large-strip limit is

$$\mathcal{A}, \ell \propto \ln\left(1 - \frac{z_\star}{z_h}\right) \tag{3.35}$$

and the minimal area becomes proportional to the width in this limit.

The reason is that the minimal surface reaches far into the bulk and wraps along the horizon as shown in Figure 3.5. This already shows the structure of the result we can expect. The leading-order term of the area is proportional to the width of the strip and arises from the horizontal piece along the horizon. Additional, the vertical pieces yield a constant contribution as subleading term. The leading-order term is already derived correctly from this approximation and only depends on the geometry at the horizon. Following this approximation, the area of this piecewise-smooth surface is

$$\begin{aligned}\mathcal{A}_{\text{disc.}} &= \tilde{\ell}^{n-1} \int_{-\ell/2}^{\ell/2} \mathrm{d}x \left(\frac{L}{z_h}\right)^n + 2\tilde{\ell}^{n-1} \int_{\epsilon}^{z_h} \mathrm{d}z \left(\frac{L}{z}\right)^n \sqrt{b(z)}^{-1}, \\ &= L^n \frac{\tilde{\ell}^{n-1}\ell}{{z_h}^n} + \begin{cases} L^n \left(\frac{2}{n-1}\left(\frac{\tilde{\ell}}{\epsilon}\right)^{n-1} + \frac{2\sqrt{\pi}}{d}\frac{\Gamma\left(\frac{1-n}{d}\right)}{\Gamma\left(\frac{1}{2}+\frac{1-n}{d}\right)}\left(\frac{\tilde{\ell}}{z_h}\right)^{n-1}\right), & n > 1, \\ 2L\left(-\ln\left(\frac{\epsilon}{z_h}\right) + \frac{2}{d}\ln 2\right), & n = 1. \end{cases}\end{aligned} \tag{3.36}$$

The authors of [112] derived an expression for the subleading term in terms of a power series for the considered observables, i.e. for $n = 1, 2, d-1$. I generalize their calculation to general dimension n, which yields

$$\begin{aligned}\mathcal{A} = &\frac{2L^n}{n-1}\frac{\tilde{\ell}^{n-1}}{\epsilon^{n-1}} + \frac{L^n\tilde{\ell}^{n-1}\ell}{{z_\star}^n} \\ &+ \frac{\sqrt{\pi}L^n}{2n}\frac{\tilde{\ell}^{n-1}}{{z_\star}^{n-1}} \sum_{m=0}^{\infty} \frac{1}{m!}\left(\frac{1}{2}\right)_m \left(\frac{z_\star}{z_h}\right)^{md} \frac{\Gamma\left(\frac{md-n+1}{2n}\right)}{\Gamma\left(\frac{md+1+2n}{2n}\right)}\end{aligned} \tag{3.37a}$$

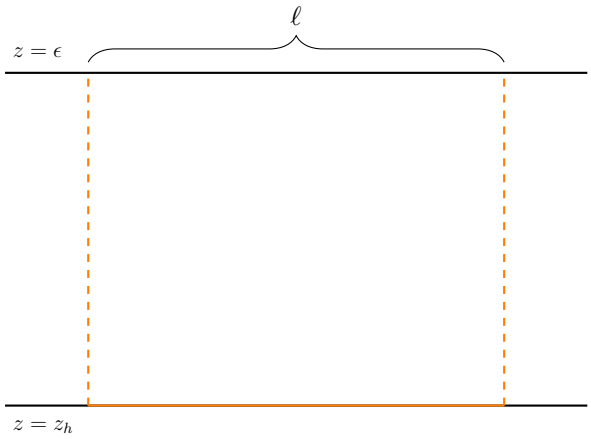

Figure 3.5: Rectangular Approximation of the Minimal Surface.

for $n > 1$. For the geodesic with $n = 1$ the result is

$$\mathcal{A} = 2L \ln\left(\frac{2z_\star}{\epsilon}\right) + \frac{L\ell}{z_\star} - 2L + \frac{\sqrt{\pi}L}{2} \sum_{m=1}^{\infty} \frac{1}{m!} \left(\frac{1}{2}\right)_m \left(\frac{z_\star}{z_h}\right)^{md} \frac{\Gamma\left(\frac{md}{2}\right)}{\Gamma\left(\frac{md+3}{2}\right)}. \tag{3.37b}$$

The subleading term depends on the whole bulk geometry and is not captured correctly by the naive approximation analyzed above.

The same method to construct hypergeometric functions may be applied to the power series in Equation (3.37). More intuitively, I derive them using the so called contiguous relations of hypergeometric functions, see Equation (B.11) in the appendix. The relevant property is that only two parameters appearing in the hypergeometric functions in the result for the minimal area differ by integer values from parameters for the width. The relevant parameters in (3.25) and (3.27) are

$$a_{-\frac{1}{2}} = a_{\frac{d}{\chi}-\frac{1}{2}} - 1, \qquad\qquad a_0 = a_{\frac{d}{\chi}} - 1,$$

where the parameter on the left-hand side applies to the area and the one on the right-hand side to the width. This allows to express part of the minimal area in terms of the width

$$\mathcal{A} = \frac{2L^n}{n-1}\left(\frac{\tilde{\ell}}{\epsilon}\right)^{n-1} + \frac{L^n \tilde{\ell}^{n-1}}{{z_\star}^n}\ell + \frac{\sqrt{\pi}L^n}{2n}\frac{\tilde{\ell}^{n-1}}{{z_\star}^{n-1}} \sum_{\Delta m=0}^{\frac{2n}{\chi}-1} \frac{1}{\Delta m!}\left(\frac{1}{2}\right)_{\Delta m}\left(\frac{z_\star}{z_h}\right)^{\Delta m d} \frac{\Gamma\left(\frac{d}{\chi}a_{-1/2}\right)}{\Gamma\left(\frac{d}{\chi}a_1\right)}$$
$$\times \ {}_{\frac{2n+d}{\chi}+1}F_{\frac{2n+d}{\chi}}\left(\begin{matrix} 1, a_{-\frac{1}{2}}, \ldots, a_{\frac{d}{\chi}-\frac{3}{2}}, b_{\frac{1}{2}}, \ldots, b_{\frac{2n}{\chi}-\frac{1}{2}} \\ a_1, \ldots, a_{\frac{d}{\chi}}, b_1, \ldots, b_{\frac{2n}{\chi}} \end{matrix} \middle| \left(\frac{z_\star}{z_h}\right)^{\frac{2nd}{\chi}}\right). \tag{3.38}$$

While the last term has the same structure as before, there is one important difference: one parameter is shifted. Due to this shift, these hypergeometric functions converge at unit argument, which allows for an asymptotic expansion.

As seen from the asymptotic behavior of the width (3.35), the radial position of the turning point is identical to the radial position of the horizon up to exponentially decaying corrections in the large ℓ limit. Therefore, the leading terms are

$$\mathcal{A} = \frac{2L^n}{n-1}\left(\frac{\tilde{\ell}}{\epsilon}\right)^{n-1} + \frac{L^n}{{z_h}^n}\tilde{\ell}^{n-1}\ell + \frac{\sqrt{\pi}L^n}{2n}\frac{\tilde{\ell}^{n-1}}{{z_h}^{n-1}}\sum_{\Delta m=0}^{\frac{2n}{\chi}-1}\frac{1}{\Delta m!}\left(\frac{1}{2}\right)_{\Delta m}\frac{\Gamma\left(\frac{d}{\chi}a_{1/2}\right)}{\Gamma\left(\frac{d}{\chi}a_1\right)}$$
$$\times\ {}_{\frac{2n+d}{\chi}+1}F_{\frac{2n+d}{\chi}}\left(\left.\begin{matrix}1, a_{-\frac{1}{2}}, \ldots, a_{\frac{d}{\chi}-\frac{3}{2}}, b_{\frac{1}{2}}, \ldots, b_{\frac{2n}{\chi}-\frac{1}{2}} \\ a_1, \ldots, a_{\frac{d}{\chi}}, b_1, \ldots, b_{\frac{2n}{\chi}}\end{matrix}\right| 1\right) + \ldots \tag{3.39}$$

The dots represent subleading contributions. We discussed above, that the leading order correction at low temperature is positive. In contrast, the sign of the first sub-leading term at high temperature is ambiguous as the parameter $a_{-\frac{1}{2}}$ can be negative. Therefore, this has to be studied case-by-case.

The case $n = 1$ is similar. The rewritten result for the area is

$$\mathcal{A} = 2L\ln\left(\frac{2z_\star}{\epsilon}\right) + \frac{L}{z_\star}\ell - 2L + \frac{\sqrt{\pi}L}{2}\sum_{\Delta m=1}^{\frac{2}{\chi}}\frac{1}{\Delta m!}\left(\frac{1}{2}\right)_{\Delta m}\left(\frac{z_\star}{z_h}\right)^{\Delta m d}\frac{\Gamma\left(\frac{d}{\chi}a_{-1/2}\right)}{\Gamma\left(\frac{d}{\chi}a_1\right)}$$
$$\times\ {}_{\frac{2+d}{\chi}+1}F_{\frac{2+d}{\chi}}\left(\left.\begin{matrix}1, a_{-\frac{1}{2}}, \ldots, a_{\frac{d}{\chi}-\frac{3}{2}}, b_{\frac{1}{2}}, \ldots, b_{\frac{2}{\chi}-\frac{1}{2}} \\ a_1, \ldots, a_{\frac{d}{\chi}}, b_1, \ldots, b_{\frac{2}{\chi}}\end{matrix}\right| \left(\frac{z_\star}{z_h}\right)^{\frac{2d}{\chi}}\right). \tag{3.40}$$

Therefore, the high-temperature/large-width behavior is described by

$$\mathcal{A} = 2L\ln\left(\frac{2z_h}{\epsilon}\right) + \frac{L}{z_h}\ell - 2L + \frac{\sqrt{\pi}L}{2}\sum_{\Delta m=1}^{\frac{2}{\chi}}\frac{1}{\Delta m!}\left(\frac{1}{2}\right)_{\Delta m}\frac{\Gamma\left(\frac{d}{\chi}a_{-1/2}\right)}{\Gamma\left(\frac{d}{\chi}a_1\right)}$$
$$\times\ {}_{\frac{2+d}{\chi}+1}F_{\frac{2+d}{\chi}}\left(\left.\begin{matrix}1, a_{-\frac{1}{2}}, \ldots, a_{\frac{d}{\chi}-\frac{3}{2}}, b_{\frac{1}{2}}, \ldots, b_{\frac{2}{\chi}-\frac{1}{2}} \\ a_1, \ldots, a_{\frac{d}{\chi}}, b_1, \ldots, b_{\frac{2}{\chi}}\end{matrix}\right| 1\right) + \ldots. \tag{3.41}$$

In this case, the subleading term is always positive. The reason is that the parameter $a_{-1/2}$ is always positive for the considered values of Δm.

To summarize, my results allow to derive the high-temperature/large-width limit.

In particular, it yields a closed form for the subleading term, which differs from the naive approximation in (3.36).

3.2.4 Result in terms of Meijer G-Functions

In the last section, I presented the result in terms of hypergeometric functions (c.f. (3.25) and (3.27)). Comparing these to Meijer G-functions (B.15) yields

$$\ell = \frac{2\pi z_h}{\sqrt{2nd}}\, G^{\frac{2n}{\chi},\frac{d}{\chi}}_{\frac{2n+d}{\chi},\frac{2n+d}{\chi}}\left(\begin{matrix}\hat{a}_{1/2},\dots,\hat{a}_{d/\chi-1/2},\hat{b}_{1/2},\dots,\hat{b}_{2n/\chi-1/2}\\ \hat{b}_0,\dots,\hat{b}_{2n/\chi-1},\hat{a}_0,\dots,\hat{a}_{d/\chi-1}\end{matrix}\,\middle|\, \left(\frac{z_\star}{z_h}\right)^{\frac{2nd}{\chi}}\right) \tag{3.42a}$$

for the width of the strip. Analogously, the minimal area can be written as

$$\begin{aligned}\mathcal{A} = \frac{2L^n}{n-1}\left(\frac{\tilde{\ell}}{\epsilon}\right)^{n-1} + \frac{2\pi L^n}{\sqrt{2nd}}\frac{\tilde{\ell}^{n-1}z_h}{{z_\star}^n} \\ \times\; G^{\frac{2n}{\chi},\frac{d}{\chi}}_{\frac{2n+d}{\chi},\frac{2n+d}{\chi}}\left(\begin{matrix}\hat{a}_{3/2},\dots,\hat{a}_{d/\chi+1/2},\hat{b}_{1/2},\dots,\hat{b}_{2n/\chi-1/2}\\ \hat{b}_0,\dots,\hat{b}_{2n/\chi-1},\hat{a}_1,\dots,\hat{a}_{d/\chi}\end{matrix}\,\middle|\, \left(\frac{z_\star}{z_h}\right)^{\frac{2nd}{\chi}}\right).\end{aligned} \tag{3.42b}$$

The new parameters are

$$\hat{a}_i = \frac{\chi}{d}i, \qquad\qquad \hat{b}_j = \frac{\chi}{2n}\left(j+\frac{1}{d}\right). \tag{3.43a}$$

The convergence criterion for Meijer G-functions (B.16) shows that both expressions diverge in the limit $z_\star \to z_h$, which matches our earlier observation.

Furthermore, the properties of Meijer G-functions can also be used to derive the alternative expression which simplifies the limit $z_\star \to z_h$. The analog expression to the contiguous relations for hypergeometric functions are recurrence relations (B.17) for Meijer G-functions. These allow to write the area as

$$\begin{aligned}\mathcal{A} = \frac{2L^n}{n-1}\left(\frac{\tilde{\ell}}{\epsilon}\right)^{n-1} + \frac{\tilde{\ell}^{n-1}\ell L^n}{{z_\star}^n} + \frac{\chi\pi L^n}{\sqrt{2nd^3}}\frac{\tilde{\ell}^{n-1}z_h}{{z_\star}^n} \\ \times\; G^{\frac{2n}{\chi},\frac{d}{\chi}}_{\frac{2n+d}{\chi},\frac{2n+d}{\chi}}\left(\begin{matrix}\hat{a}_{3/2},\dots,\hat{a}_{d/\chi+1/2},\hat{b}_{1/2},\dots,\hat{b}_{2n/\chi-1/2}\\ \hat{b}_0,\dots,\hat{b}_{2n/\chi-1},\hat{a}_0,\dots,\hat{a}_{d/\chi-1}\end{matrix}\,\middle|\, \left(\frac{z_\star}{z_h}\right)^{\frac{2nd}{\chi}}\right).\end{aligned} \tag{3.44}$$

Expressing the result in terms of Meijer G-functions is in particular useful when generalizing the construction of hypergeometric functions from power series expressions. The whole procedure presented above depends on being allowed to reorder

the original power series. Therefore, it has to be absolutely converging. In our case, that was given for $z_\star < z_h$. However, for general problems of this type that is not always possible. If the series is no absolutely convergent, reordering changes the result. The Meijer G-function is the analytic continuation for the hypergeometric functions. Therefore, these Meijer G-functions are a powerful tool to tackle far more general integral expressions. First one solves the problem in terms of hypergeometric functions for arguments where reordering is allowed. If the result is expressed in terms of a Meijer G-function, this result as the analytic continuation also applies to arguments where the result in hypergeometric functions does not apply. In some case, there is an alternative expression in terms of hypergeometric functions applying for these parameters.

3.3 Results for non-local observables at finite temperature $\mathrm{AdS}_{d+1}/\mathrm{CFT}_d$

After deriving the general result for minimal surfaces anchored on strips on the boundary, it is now evaluated for a one-dimensional surface corresponding to the two-point correlation function, a two-dimensional surface corresponding to the three-point function and the $(d-1)$-dimensional surface corresponding to the entanglement entropy.

3.3.1 Results for the Two-Point Function

As reviewed, the two-point function of an operator $\mathcal{O}$ of large scaling dimension Δ is holographically dual to a bulk geodesic. Following Equation (3.4), the field theory two-point function is given by

$$\langle \mathcal{O}(t,\vec{x})\mathcal{O}(t,\vec{y})\rangle = \lim_{\epsilon\to 0} \epsilon^{-2\Delta} \exp\left(-\Delta \cdot \frac{\mathcal{A}(\epsilon)}{L}\right), \tag{3.45}$$

where Δ is the scaling dimension and $\mathcal{A}$ the length of the geodesic. The UV-divergent term of the length is completely removed and the result hence UV finite. Furthermore, by length is divided by the AdS radius L which thereby drops out. Therefore, the holographic results are of zeroth order of both the central charge c and the 't Hooft coupling λ. We are applying AdS/CFT to the large c, large λ limit and only determine the leading term. Subleading corrections to the observables require to consider quantum gravity and stringy corrections respectively.

My results for the length of the geodesic (i.e. the case $n = 1$) are derived in (3.27) and (3.28). For the two sets of parameters, we can write out one set explicitly. The remaining appearing parameters are related to[9]

$$a_i = \frac{1}{2d}\left(\Delta m d + 1 + 2i\right). \tag{3.46}$$

For the area of the geodesic, i.e. the geodesic length, the result is

$$\begin{aligned}\mathcal{A} = 2L\ln\left(\frac{2z_\star}{\epsilon}\right) &+ \frac{L}{2}\frac{\sqrt{\pi}\Gamma\left(\frac{d}{2}\right)}{\Gamma\left(\frac{d+1}{2}\right)}\left(\frac{z_\star}{z_h}\right)^d {}_{d+2}F_{d+1}\left(\left.\begin{matrix}\frac{3}{4},\frac{5}{4},a_{-\frac{1}{2}},\dots,a_{d-\frac{3}{2}}\\ \frac{3}{2},a_0,\dots,a_{d-1}\end{matrix}\right|\left(\frac{z_\star}{z_h}\right)^{2d}\right)\Bigg|_{\Delta m=1}\\ &+ \frac{3L}{8}\frac{\sqrt{\pi}\Gamma\left(d\right)}{\Gamma\left(\frac{2d+1}{2}\right)}\left(\frac{z_\star}{z_h}\right)^{2d} {}_{d+3}F_{d+2}\left(\left.\begin{matrix}1,\frac{5}{4},\frac{7}{4},a_{-\frac{1}{2}},\dots,a_{d-\frac{3}{2}}\\ \frac{3}{2},2,a_0,\dots,a_{d-1}\end{matrix}\right|\left(\frac{z_\star}{z_h}\right)^{2d}\right)\Bigg|_{\Delta m=2}.\end{aligned} \tag{3.47a}$$

In even spacetime dimension d, the two hypergeometric functions simplify to

$$\mathcal{A} = \cdots + \frac{L}{2}\frac{\sqrt{\pi}\Gamma\left(\frac{d}{2}\right)}{\Gamma\left(\frac{d+1}{2}\right)}\left(\frac{z_\star}{z_h}\right)^d {}_{\frac{d}{2}+2}F_{\frac{d}{2}+1}\left(\left.\begin{matrix}\frac{3}{2},1,2a_{-\frac{1}{2}},\dots,2a_{\frac{d}{2}-\frac{3}{2}}\\ 2,2a_0,\dots,a_{\frac{d}{2}-1}\end{matrix}\right|\left(\frac{z_\star}{z_h}\right)^{d}\right)\Bigg|_{\Delta m=1}. \tag{3.47b}$$

The width in terms of the turning point is

$$\begin{aligned}\ell = \frac{\sqrt{\pi}z_\star}{2}\frac{\Gamma\left(\frac{d+2}{2}\right)}{\Gamma\left(\frac{d+3}{2}\right)}&\left(\frac{z_\star}{z_h}\right)^d {}_{d+2}F_{d+1}\left(\left.\begin{matrix}a_{\frac{1}{2}},\dots,a_{d-\frac{1}{2}},\frac{3}{4},\frac{5}{4}\\ a_1,\dots,a_d,\frac{3}{2}\end{matrix}\right|\left(\frac{z_\star}{z_h}\right)^{2d}\right)\Bigg|_{\Delta m=1}\\ &+ 2z_\star\ {}_{d+2}F_{d+1}\left(\left.\begin{matrix}a_{\frac{1}{2}},\dots,a_{d-\frac{1}{2}},\frac{1}{4},\frac{3}{4}\\ a_1,\dots,a_d,\frac{1}{2}\end{matrix}\right|\left(\frac{z_\star}{z_h}\right)^{2d}\right)\Bigg|_{\Delta m=0}.\end{aligned} \tag{3.48a}$$

This can be further simplified for even spacetime dimension d to[10]

$$\ell = 2z_\star\ {}_{\frac{d}{2}+1}F_{\frac{d}{2}}\left(\left.\begin{matrix}2a_{\frac{1}{2}},\dots,2a_{\frac{d-1}{2}},\frac{1}{2}\\ 2a_1,\dots,2a_{\frac{d}{2}}\end{matrix}\right|\left(\frac{z_\star}{z_h}\right)^{d}\right)\Bigg|_{\Delta m=0}. \tag{3.48b}$$

As can be seen, some hypergeometric functions have one numerator and one denom-

[9] For better readability, we removed the factor χ in the definition of the parameter.

[10] I incorporated this simplification in the general calculation with the greatest common devisor χ. This can also be derived from properties of hypergeometric functions.

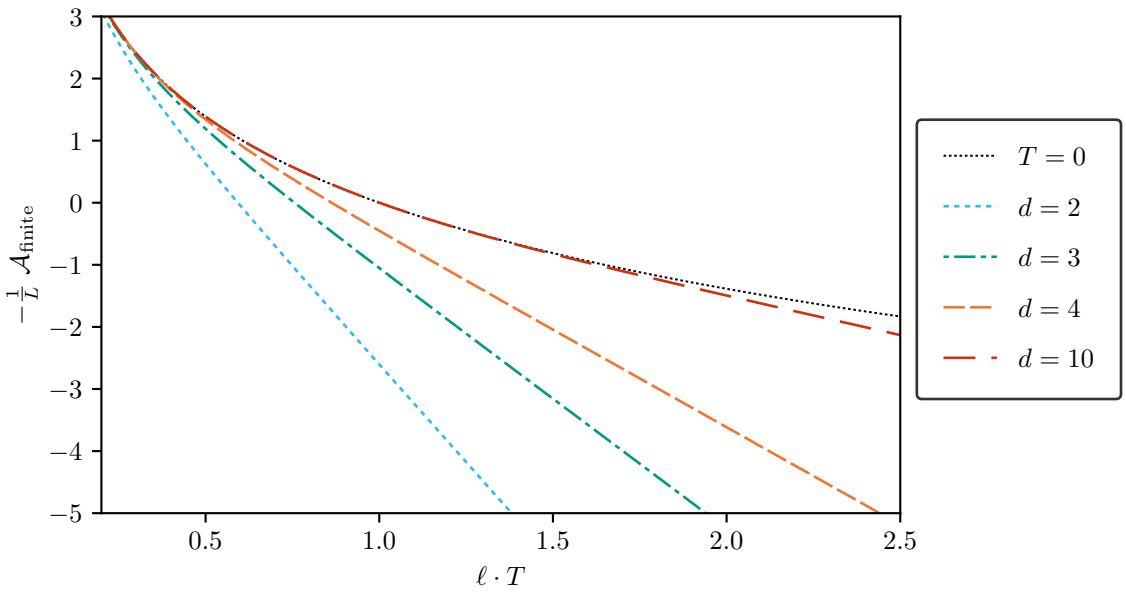

Figure 3.6: Result for two-point Function at Finite Temperature.

inator parameter less than the ones describing the area, while the one appearing in the general result all had the same number of parameter. The reason behind this is that in some cases the unit numerator parameter is identical to a denominator parameter and cancels out.

The finite part of the geodesic length is shown in Figure 3.6 It is obtained by removing the $\log \epsilon \cdot T$ term. Keep in mind that z_h does not have a field theory interpretation on its own and only the temperature $T = d/4\pi z_h$ is relevant. The dashed line in the plot represent the zero temperature result

$$\mathcal{A}_{\text{finite}}|_{T=0} = 2L \ln\left(\frac{\ell}{\epsilon}\right),$$

which is independent of the spacetime dimension considered. It corresponds to the power-law behavior of the correlation function

$$\langle \mathcal{O}(t,\vec{x})\mathcal{O}(t,\vec{y})\rangle = \ell^{-2\Delta}.$$

Let us focus on the low- and high-temperature limits. Considering the low-temperature/small strip limit, my results in (3.48) and (3.47) easily reproduce the known behavior in this limit known from the result in terms of a power series (3.20).

The hypergeometric functions behave as

$$ {}_pF_q\left(\begin{matrix}\dots\\ \dots\end{matrix}\middle| u\right) = 1 + \mathcal{O}(u), $$

Therefore, in this limit my results simplify to the low-temperature expansion discussed in [112]

$$ \langle \mathcal{O}(t,\vec{x})\mathcal{O}(t,\vec{y})\rangle = \ell^{-2\Delta}\left[1 - \frac{\Delta\sqrt{\pi}\Gamma\left(\frac{d}{2}\right)}{4\Gamma\left(\frac{d+3}{2}\right)}\cdot\left(\frac{2\pi T\cdot\ell}{d}\right)^d + \mathcal{O}\left(\ell\cdot T\right)^{2d}\right]. \tag{3.49} $$

The strong feature of my result is that it also captures the high-temperature/large strip limit. As discussed in [112], the geodesic length in this limit takes the form

$$ \mathcal{A} \approx -LA_d - 2L\ln\left(\epsilon\cdot T\right) + \frac{L\ell}{z_h}. \tag{3.50} $$

For the two-point function, this implies

$$ \langle \mathcal{O}(t,x)\mathcal{O}(t,y)\rangle \approx T^{2\Delta}\exp(\Delta\cdot A_d)\exp\left(-4\pi\Delta\cdot T|x-y|/d\right). \tag{3.51} $$

My result yields a closed analytic expression for A_d. The high-temperature limit corresponds to $z_\star \to z_h$. The hypergeometric functions appearing in (3.47) all diverge logarithmically. However, this consideration only yields the well-known leading behavior. It is not possible to perform a Taylor expansion around $z_\star = z_h$. Taking derivatives of hypergeometric functions yields

$$ \frac{\mathrm{d}^n}{\mathrm{d}u^n}\,{}_{p+1}F_p\left(\begin{matrix}a_1,\dots,a_{p+1}\\ b_1,\dots,b_q\end{matrix}\middle| u\right) = {}_{p+1}F_p\left(\begin{matrix}a_1+n,\dots,a_{p+1}+n\\ b_1+n,\dots,b_p+n\end{matrix}\middle| u\right) $$

Since this increased the difference

$$ \Psi = \sum b_i - \sum a_i \to \Psi - n $$

and hypergeometric functions diverge as $(1-u)^\Psi$, taking derivatives worsens the divergence. Therefore, it is a non-trivial problem to perform a systematic high-temperature expansion to high orders. In particular, the geodesic length also receives exponentially decaying corrections, see [112]. For the subleading term however, it is useful to consider the alternative result for the geodesic length I derived in (3.40).

It yields

$$\begin{aligned}\mathcal{A} = 2L\ln\left(\frac{2z_\star}{\epsilon}\right) &+ \frac{L}{2}\frac{\sqrt{\pi}\Gamma\left(\frac{d}{2}\right)}{\Gamma\left(\frac{d+1}{2}\right)}\left(\frac{z_\star}{z_h}\right)^d {}_{d+2}F_{d+1}\left(\left.\begin{matrix}\frac{3}{4},\frac{5}{4},a_{-\frac{1}{2}},\ldots,a_{d-\frac{3}{2}}\\ \frac{3}{2},a_0,\ldots,a_{d-1}\end{matrix}\right|\left(\frac{z_\star}{z_h}\right)^{2d}\right)\Bigg|_{\Delta m=1}\\ &+ \frac{3L}{8}\frac{\sqrt{\pi}\Gamma\left(d\right)}{\Gamma\left(\frac{2d+1}{2}\right)}\left(\frac{z_\star}{z_h}\right)^{2d} {}_{d+3}F_{d+2}\left(\left.\begin{matrix}1,\frac{5}{4},\frac{7}{4},a_{-\frac{1}{2}},\ldots,a_{d-\frac{3}{2}}\\ \frac{3}{2},2,a_0,\ldots,a_{d-1}\end{matrix}\right|\left(\frac{z_\star}{z_h}\right)^{2d}\right)\Bigg|_{\Delta m=2}\\ &+ \frac{L\ell}{z_h}\end{aligned} \tag{3.52a}$$

for general spacetime dimension and simplifies to

$$\begin{aligned}\mathcal{A} = 2L\ln\left(\frac{2z_\star}{\epsilon}\right) &+ \frac{L}{2}\frac{\sqrt{\pi}\Gamma\left(\frac{d}{2}\right)}{\Gamma\left(\frac{d+1}{2}\right)}\left(\frac{z_\star}{z_h}\right)^d {}_{\frac{d}{2}+2}F_{\frac{d}{2}+1}\left(\left.\begin{matrix}\frac{3}{2},1,2a_{-\frac{1}{2}},\ldots,2a_{\frac{d}{2}-\frac{3}{2}}\\ 2,2a_0,\ldots,a_{\frac{d}{2}-1}\end{matrix}\right|\left(\frac{z_\star}{z_h}\right)^{d}\right)\Bigg|_{\Delta m=1}\\ &+ \frac{L\ell}{z_h}.\end{aligned} \tag{3.52b}$$

in even spacetime dimension. In principle, this has the same form as in (3.47) with an additional extensive term. There is one crucial difference: one denominator parameter is shifted by $+1$. Therefore, Ψ is no longer zero, which was the reason for the logarithmic divergence previously. It is now larger than zero and the hypergeometric functions converge for a finite value as $z_\star \to z_h$. This allows to evaluate the subleading term of $\mathcal{A}$ explicitely. Since the width ℓ diverges logarithmically in this limit, correction to the turning point $z_\star$ decay exponentially fast. The subleading term A_d therefore reduces to

$$\begin{aligned}A_d = 2 - 2\log\left(\frac{d}{2\pi}\right) &- \frac{\sqrt{\pi}\Gamma\left(\frac{d}{2}\right)}{4\Gamma\left(\frac{d}{2}+\frac{3}{2}\right)} {}_{d+2}F_{d+1}\left(\left.\begin{matrix}\frac{3}{4},\frac{5}{4},a_{-\frac{1}{2}},\ldots,a_{d-\frac{3}{2}}\\ \frac{3}{2},a_0,\ldots,a_{d-1}\end{matrix}\right|1\right)\Bigg|_{\Delta m=1}\\ &- \frac{3\sqrt{\pi}\Gamma\left(d\right)}{16\Gamma\left(d+\frac{3}{2}\right)} {}_{d+3}F_{d+2}\left(\left.\begin{matrix}1,\frac{5}{4},\frac{7}{4},a_{-\frac{1}{2}},\ldots,a_{d-\frac{3}{2}}\\ \frac{3}{2},2,a_1,\ldots,a_d\end{matrix}\right|1\right)\Bigg|_{\Delta m=2}.\end{aligned} \tag{3.53}$$

For even spacetime dimension d, this simplifies to

$$A_d = 2 - 2\log\left(\frac{d}{2\pi}\right) - \frac{\sqrt{\pi}}{4}\frac{\Gamma\left(\frac{d}{2}\right)}{\Gamma\left(\frac{d}{2}+\frac{3}{2}\right)} {}_{\frac{d}{2}+2}F_{\frac{d}{2}+1}\left(\left.\begin{matrix}\frac{3}{2},1,2a_{-\frac{1}{2}},\ldots,2a_{\frac{d}{2}-\frac{3}{2}}\\ 2,2a_1,\ldots,2a_{\frac{d}{2}}\end{matrix}\right|1\right)\Bigg|_{\Delta m=1}. \tag{3.54}$$

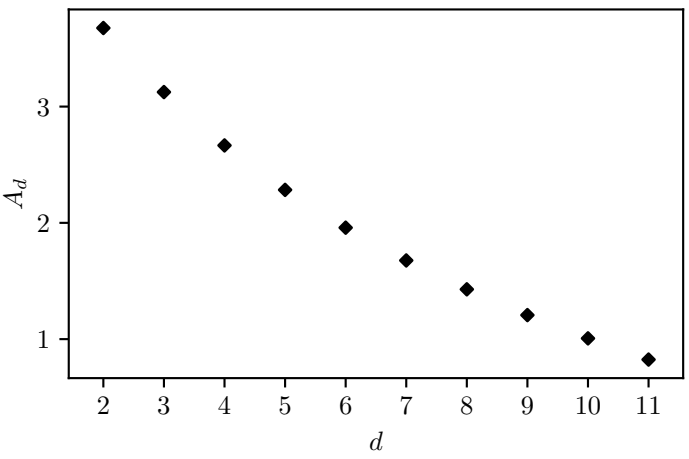

d	A_d
2	3.6758
3	3.1248
4	2.6659
5	2.2836
6	1.9585
7	1.6767
8	1.4284
9	1.2067
10	1.0065
11	0.8242

Figure 3.7 & Table 3.2: Subleading Term for two-point Function at High-Temperature.

These expressions can be evaluated using computer algebra systems. The values for A_d for $d = 2, \ldots, 11$ are presented in Figure 3.7 and Table 3.2.

3.3.2 Comparison to the AdS_3/CFT_2 Two-Point Function

For two-dimensional CFTs, a closed expression for the two-point function is known both from CFT considerations and from holographic calculations. Therefore, my general result derived above simplifies to this expressions. Evaluation the distance Equation (3.48b) for $d = 2$ yields

$$\ell = |\vec{x} - \vec{y}| = 2z_\star \, {}_2F_1\left(\left.\begin{matrix}1, \frac{1}{2} \\ \frac{3}{2}\end{matrix}\right| \left(\frac{z_\star}{z_h}\right)^2\right). \tag{3.55}$$

Therefore, the hypergeometric functions only has three parameter. This hypergeometric function can be expressed as areatangens hyperbolicus (see Equation (B.12b) in the appendix)

$$|\vec{x} - \vec{y}| = 2z_h \, \operatorname{artanh}\left(\frac{z_\star}{z_h}\right). \tag{3.56}$$

In contrast to the general result, we are able to express the turning point as a function of the distance

$$z_\star = z_h \tanh\left(\frac{|\vec{x} - \vec{y}|}{2z_h}\right). \tag{3.57}$$

Similarly, the expression for the geodesic length (3.47b) simplifies to

$$\mathcal{A} = 2L \ln\left(\frac{2z_\star}{\epsilon}\right) + L\left(\frac{z_\star}{z_h}\right)^2 {}_2F_1\left(\begin{matrix}1,1\\2\end{matrix}\middle|\left(\frac{z_\star}{z_h}\right)^2\right). \tag{3.58}$$

As for the distance, the hypergeometric function can be expressed in terms of a known function, in this case the logarithm (B.12c). Therefore, the geodesic length simplifies to

$$\mathcal{A} = 2L \ln\left(\frac{2z_\star}{\epsilon}\right) - L \ln\left(1 - \left(\frac{z_\star}{z_h}\right)^2\right). \tag{3.59}$$

Combining these two simplifications allows to express the geodesic length in the (field theory) distance

$$\mathcal{A} = 2L \ln\left(\frac{\beta}{\pi\epsilon} \sinh\left(\frac{|\vec{x}-\vec{y}|\pi}{\beta}\right)\right). \tag{3.60}$$

Using this result to evaluate the two-point function holographically yields

$$\begin{aligned}\langle \mathcal{O}(t,\vec{x})\mathcal{O}(t,\vec{y})\rangle &= \lim_{\epsilon\to 0} \epsilon^{-2\Delta} \exp\left(-\Delta \cdot \frac{\mathcal{A}}{L}\right), \\ &= \left(\frac{\beta}{\pi}\sinh\left(\frac{\pi|\vec{x}-\vec{y}|}{\beta}\right)\right)^{-2\Delta},\end{aligned} \tag{3.61}$$

where $\beta = T^{-1}$. This results also applies for the holographic entanglement entropy in in two dimensions. Therefore, this shows how my general result in Equation (3.48) and Equation (3.47) simplifies to the known closed form expression [25, 26].

3.3.3 Results for Wilson Loop

Let us turn to Wilson loops. They correspond holographically to two-dimensional surfaces in the bulk. My result applies to spatial Wilson loops. However, the temporal Wilson loop is the one related to the quark-antiquark potential and interesting for confinement[11]. Considering the quark-antiquark potential can be achieved by a double-Wick rotation: this transforms the AdS Schwarzschild into the AdS-Soliton

[11] Similarly to the temporal Wilson loop, the spatial Wilson loop expectation value is an order parameter for confinement. At finite temperature, a better order parameter is the temporal Wilson-Polyakov loop: a loop with constant spatial coordinate, which is closed in the imaginary time direction $\left[0, \frac{1}{T}\right]$.

solution [119–121]

$$\mathrm{d}s^2 = \left(\frac{L}{z}\right)^2 \left(-\mathrm{d}t^2 + b(z)\mathrm{d}y^2 + \sum_{i=1}^{d-2} \mathrm{d}x_i^2 + b(z)^{-1}\mathrm{d}z^2\right), \tag{3.62a}$$

$$b(z) = 1 - (z\Lambda)^d. \tag{3.62b}$$

The dual CFT lives on $\mathbb{R}^{1,d-1} \times S^1$, i.e. one spacetime direction is compact. The size of the compact direction is $4\pi\Lambda/d$, where Λ plays the rule of the QCD scale. The geometry ends smoothly at radial position $z = \Lambda^{-1}$. In particular, the theory is confining [122]. In the IR, the compact direction can be integrated out and most fields acquire a mass of order Λ. The resulting effective theory is a $(d-1)$-dimensional pure gauge theory. The interpretation of the results in this setting is in particular helpful for the Wilson loop: my results derived for the spatial Wilson loop apply to the temporal Wilson loop in this geometry. The quark-antiquark potential (3.11) is related by the area by

$$V_q = \frac{\mathcal{A}}{2\pi\alpha'\tilde{\ell}} - \frac{L^2}{\pi l_s^2 \epsilon}.$$

The UV-term is subtracted to remove the (infinite) mass of the quark-antiquark pair.

Let us turn to my result for the Wilson loop, i.e. for the case $n = 2$. As discussed during the calculation, the result simplifies for certain spacetime dimensions. For the Wilson loop, this happens for spacetime divisible by two and even more for spacetime dimension divisible by four. I define χ as the greatest common divisor between d and 4

$$\chi = \begin{cases} 4 & \text{for } d \text{ divisible by four,} \\ 2 & \text{for } d \text{ even,} \\ 1 & \text{else} \end{cases} \tag{3.63}$$

to incorporate these simplifications in the result. The parameters of the hypergeometric functions (see Equation (3.24) for the general result) are in this case

$$a_i = \frac{\chi}{4d}\left(\Delta m d + 1 + 4i\right), \tag{3.64a}$$

$$b_j = \frac{\chi}{4}\left(\Delta m + j\right). \tag{3.64b}$$

Evaluating my result in Equation (3.25) for $n = 2$ results into

$$V_q = \frac{\sqrt{\pi}L^2}{4\pi l_s^2}\frac{1}{z_\star}\sum_{\Delta m=0}^{\frac{4}{\chi}-1}\frac{1}{\Delta m!}\left(\frac{1}{2}\right)_{\Delta m}\left(\frac{z_\star}{z_h}\right)^{\Delta m d}\frac{\Gamma\left(\frac{d}{\chi}a_{-1/2}\right)}{\Gamma\left(\frac{d}{\chi}a_0\right)} \\ \times \ {}_{\frac{4+d}{\chi}+1}F_{\frac{4+d}{\chi}}\left(\begin{matrix}1, a_{-\frac{1}{2}}, \ldots, a_{\frac{d}{\chi}-\frac{3}{2}}, b_{\frac{1}{2}}, \ldots, b_{\frac{4}{\chi}-\frac{1}{2}} \\ a_0, \ldots, a_{\frac{d}{\chi}-1}, b_1, \ldots, b_{\frac{4}{\chi}}\end{matrix}\middle| \left(\frac{z_\star}{z_h}\right)^{\frac{4d}{\chi}}\right) \tag{3.65}$$

for the potential of the potential of a quark-antiquark pair. The factor $(L/l_s)^2$ is proportional to $\lambda^{2/\gamma}$, where λ is the 't Hooft coupling of the field theory and $\gamma > 0$. The distance between the quark-antiquark pair is (3.27)

$$\ell = \frac{\sqrt{\pi}z_\star}{2}\sum_{\Delta m=0}^{\frac{4}{\chi}-1}\frac{1}{\Delta m!}\left(\frac{1}{2}\right)_{\Delta m}\left(\frac{z_\star}{z_h}\right)^{\Delta m d}\frac{\Gamma\left(\frac{d}{\chi}a_{1/2}\right)}{\Gamma\left(\frac{d}{\chi}a_1\right)} \\ \times \ {}_{\frac{4+d}{\chi}+1}F_{\frac{4+d}{\chi}}\left(\begin{matrix}1, a_{\frac{1}{2}}, \ldots, a_{\frac{d}{\chi}-\frac{1}{2}}, b_{\frac{1}{2}}, \ldots, b_{\frac{4}{\chi}-\frac{1}{2}} \\ a_1, \ldots, a_{\frac{d}{\chi}}, b_1, \ldots, b_{\frac{4}{\chi}}\end{matrix}\middle| \left(\frac{z_\star}{z_h}\right)^{\frac{4d}{\chi}}\right). \tag{3.66}$$

Therefore, the result can be written in terms of four hypergeometric functions, which simplifies to two terms in even spacetime dimension and to one term in spacetime dimension divisible by four. The results for different spacetime dimensions are shown in Figure 3.8. The results are shown in comparison to the zero-temperature result, which is independent of the spacetime dimension.

Again, we analyze the low- and high-temperature limit similar to the discussion for the two-point function. For the low-temperature limit, the leading term yields the low-temperature result

$$V_q = -\frac{4\pi^2 L^2}{l_s^2\Gamma\left(\frac{1}{4}\right)^4}\,\frac{1}{\ell}\left[1 + \mathcal{O}(\ell\Lambda)^d\right]. \tag{3.67}$$

The result is UV-finite since the term containing the bulk-cut off is removed. In principle, the temperature introduces an additional length-scale in the theory and one could also remove a finite term proportional to $\tilde{\ell}T$. However, the regularization has to be chosen in such a way that the UV-behavior is temperature-independent [111]. Therefore, this renormalized potential is unique.

Since my result applies to any value for the width, it allows to examine the high-temperature limit. The hypergeometric functions appearing in (3.65) diverge in this limit, which results in a potential proportional to the distance. While a

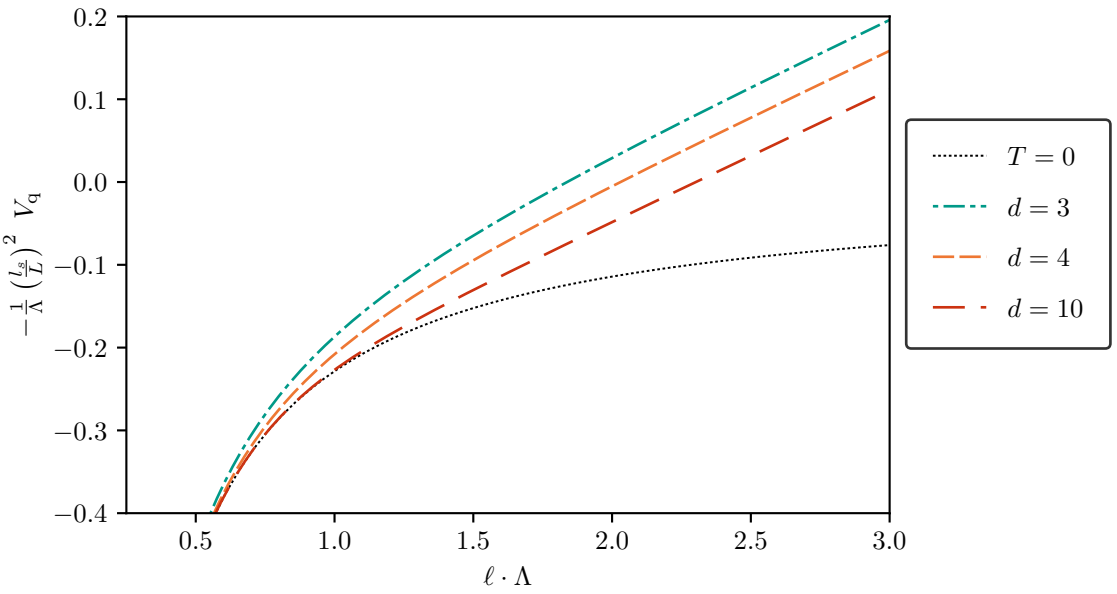

Figure 3.8: Result for Quark-Antiquark Potential at finite Temperature.

systematic expansion in inverse temperature is not possible, the properties of the hypergeometric functions allow an alternative form of my result, which expresses the potential as

$$V_q = \frac{L^2}{2{z_\star}^2 \pi l_s^2} \cdot \ell + \frac{\sqrt{\pi} L^2}{8\pi l_s^2} \frac{1}{z_\star} \sum_{\Delta m=0}^{\frac{4}{\chi}-1} \frac{1}{\Delta m!} \left(\frac{1}{2}\right)_{\Delta m} \left(\frac{z_\star}{z_h}\right)^{\Delta m d} \frac{\Gamma\left(\frac{d}{\chi} a_{-1/2}\right)}{\Gamma\left(\frac{d}{\chi} a_1\right)} \tag{3.68}$$
$$\times \ {}_{\frac{d+4}{\chi}+1}F_{\frac{d+4}{\chi}} \left(\begin{matrix} 1, a_{-\frac{1}{2}}, \ldots, a_{\frac{d}{\chi}-\frac{3}{2}}, b_{\frac{1}{2}}, \ldots, b_{\frac{4}{\chi}-\frac{1}{2}} \\ a_1, \ldots, a_{\frac{d}{\chi}}, b_1, \ldots, b_{\frac{4}{\chi}} \end{matrix} \middle| \left(\frac{z_\star}{z_h}\right)^{\frac{4d}{\chi}} \right).$$

In this result, the divergent is contained in the width and the remaining hypergeometric functions converge in the high-temperature/large-distance limit. Since the distance diverges logarithmically in the high-temperature limit

$$\ell \propto -\ln\left(1 - \frac{z_\star}{z_h}\right),$$

corrections to the turning point $z_\star$ decay exponentially. Therefore, the high-temperature limit can be written as

$$V_q = \frac{L^2 \Lambda^2}{2\pi l_s^2} \cdot \ell - 2\kappa + \cdots, \tag{3.69}$$

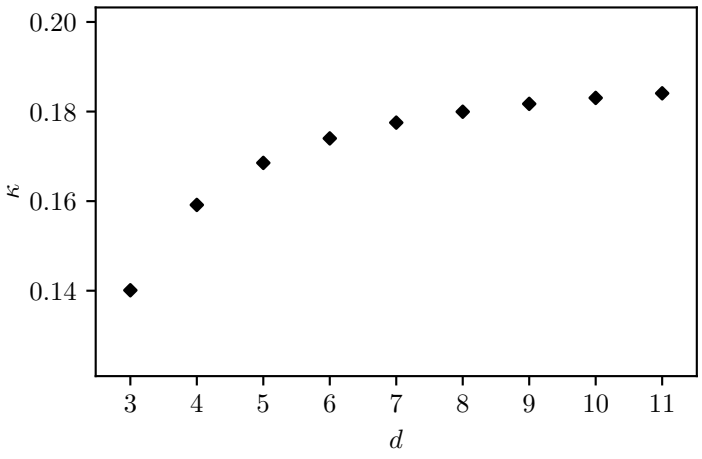

d	$\left(\frac{l_s}{L}\right)^2 \frac{1}{\Lambda} \cdot \kappa$
3	0.14010
4	0.15915
	$= (2\pi)^{-1}$
5	0.16854
6	0.17401
7	0.17753
8	0.17996
9	0.18172
10	0.18305
11	0.18407

Figure 3.9 & Table 3.3: Subleading Term for the Quark-Antiquark Potential.

where the leading term scales with the quark-antiquark distance ℓ. This is the expected behavior for the potential in a confining background. The first subleading term is a constant and of the same form as the subtracted UV-term. Therefore, κ can be interpreted as a (UV-finite) shift of the mass of the quark. The result for κ is can be derived from (3.68) and yields

$$\kappa = -\frac{\sqrt{\pi}L^2}{16\pi l_s^2}\,\Lambda \sum_{\Delta m=0}^{\frac{4}{\chi}-1} \frac{1}{\Delta m!}\left(\frac{1}{2}\right)_{\Delta m} \frac{\Gamma\left(\frac{d}{\chi}a_{-1/2}\right)}{\Gamma\left(\frac{d}{\chi}a_1\right)} \tag{3.70}$$

$$\times\ {}_{\frac{d+4}{\chi}+1}F_{\frac{d+4}{\chi}}\left(\left.\begin{matrix}1, a_{-\frac{1}{2}}, \ldots, a_{\frac{d}{\chi}-\frac{3}{2}}, b_{\frac{1}{2}}, \ldots, b_{\frac{4}{\chi}-\frac{1}{2}} \\ a_1, \ldots, a_{\frac{d}{\chi}}, b_1, \ldots, b_{\frac{4}{\chi}}\end{matrix}\right| 1\right).$$

The results for κ for different spacetime dimension are presented in Table 3.3 and Figure 3.9. The results show that κ is positive[12]. In particular, this shows that wall induces an increase of the effective IR quark-mass. Keep in mind that $L/l_s \propto \lambda^\gamma$ with $\gamma > 0$ and that Λ is the analog of the QCD length. For the Wilson loop expectation value itself, the high-temperature limit is Figure 3.9 and Table 3.3.

[12]The results show this for specific spacetime dimensions and there is no indication of anything drastically changing at some point.

3.3.4 Results for Entanglement Entropy

Let us turn to our final observable: the entanglement entropy and observables related to it. In the following, we restrict ourselves to spacetime dimension larger than two, i.e. to the case $d > 2$. For the two-dimensional case, the Ryu-Takayanagi corresponds to the geodesic considered for the two-point function. The closed form of this results is well-known and as showed earlier a simplification of my result for general dimension.

We saw that the entanglement entropy is proportional to the minimal area of a $(d-1)$-dimensional bulk surface. This corresponds to $n = (d-1)$ in our notation. Since the results simplify for even spacetime dimension, let us introduce the parameter

$$\chi = \begin{cases} 2 & \text{for even dimension } d, \\ 1 & \text{else,} \end{cases} \tag{3.71}$$

to be able to phrase the results in a general fashion.

This allows to write the width of the strip and the minimal area of the attached surface as functions of the turning point $z_\star$. In terms of hypergeometric functions, the width is

$$\begin{aligned} \ell = \frac{\sqrt{\pi} z_\star}{d-1} \sum_{\Delta m=0}^{\frac{2(d-1)}{\chi}-1} \frac{1}{\Delta m!} \left(\frac{1}{2}\right)_{\Delta m} \left(\frac{z_\star}{z_h}\right)^{\Delta m d} \frac{\Gamma\left(\frac{d}{\chi} a_{1/2}\right)}{\Gamma\left(\frac{d}{\chi} a_1\right)} \\ \times \ {}_{\frac{3d-2}{\chi}+1}F_{\frac{3d-2}{\chi}} \left(\begin{matrix} 1, a_{\frac{1}{2}}, \ldots, a_{\frac{d}{\chi}-\frac{1}{2}}, b_{\frac{1}{2}}, \ldots, b_{\frac{2(d-1)}{\chi}-\frac{1}{2}} \\ a_1, \ldots, a_{\frac{d}{\chi}}, b_1, \ldots, b_{\frac{2(d-1)}{\chi}} \end{matrix} \middle| \left(\frac{z_\star}{z_h}\right)^{\frac{2(d-1)d}{\chi}} \right) \end{aligned} \tag{3.72a}$$

and the entanglement entropy is

$$\begin{aligned} S_{EE} = \frac{L^{d-1}\left(\tilde{\ell}/\epsilon\right)^{d-2}}{2(d-2)G_N} + \frac{\sqrt{\pi} L^{d-1}}{4(d-1)G_N} \frac{\tilde{\ell}^{d-2}}{{z_\star}^{d-2}} \sum_{\Delta m=0}^{\frac{2(d-1)}{\chi}-1} \frac{(1/2)_{\Delta m}}{\Delta m!} \frac{\Gamma\left(\frac{d}{\chi} a_{-1/2}\right)}{\Gamma\left(\frac{d}{\chi} a_0\right)} \left(\frac{z_\star}{z_h}\right)^{\Delta m d} \\ \times \ {}_{\frac{3d-2}{\chi}+1}F_{\frac{3d-2}{\chi}} \left(\begin{matrix} 1, a_{-\frac{1}{2}}, \ldots, a_{\frac{d}{\chi}-\frac{3}{2}}, b_{\frac{1}{2}}, \ldots, b_{\frac{2(d-1)}{\chi}-\frac{1}{2}} \\ a_0, \ldots, a_{\frac{d}{\chi}-1}, b_1, \ldots, b_{\frac{2(d-1)}{\chi}} \end{matrix} \middle| \left(\frac{z_\star}{z_h}\right)^{\frac{2(d-1)d}{\chi}} \right). \end{aligned} \tag{3.72b}$$

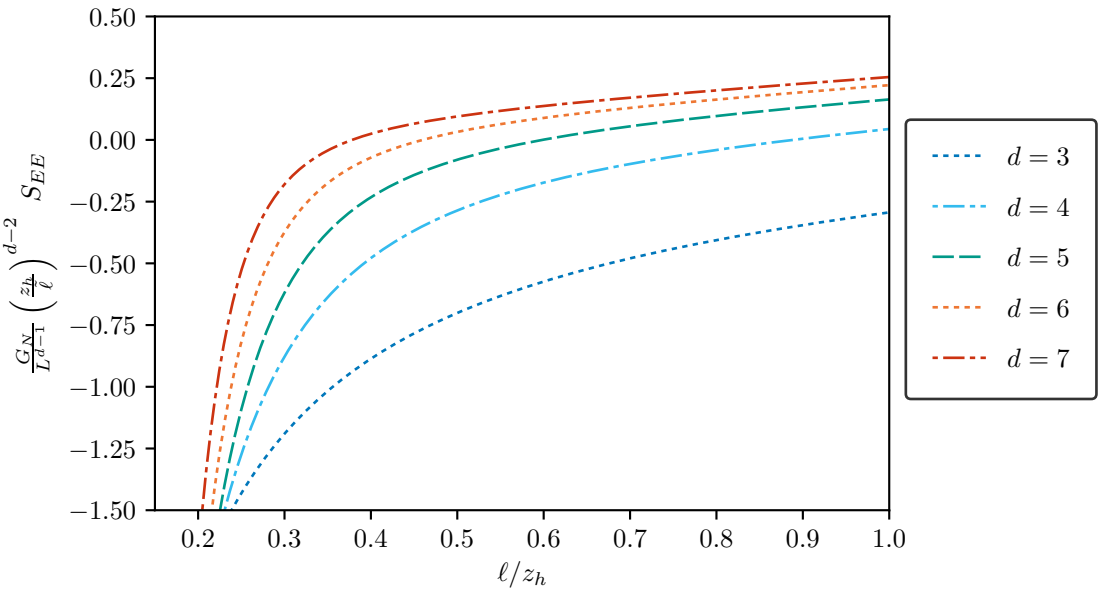

Figure 3.10: Result for Entanglement Entropy at finite Temperature.

The parameters used are introduced in Equations (3.24) and reduce to

$$a_i = \frac{\chi}{2(d-1)d}\Big(\Delta m d + 1 + 2(d-1)i\Big), \tag{3.73a}$$

$$b_j = \frac{\chi}{2(d-1)}\Big(\Delta m + j\Big). \tag{3.73b}$$

The results for different spacetime dimensions are shown Figure 3.10. The zero-temperature result depends on the spacetime dimension and not shown. The prefactor L^{d-1}/G_N is proportional to the central charge of the theory.

If we study the low-temperature limit as discussed in Section 3.2.2, the leading correction has the following form

$$\begin{aligned} S_{EE} = &\frac{L^{d-1}}{2(d-2)G_N}\left(\frac{\tilde{\ell}}{\epsilon}\right)^{d-2} - \frac{L^{d-1}}{4(d-2)G_N}\left(\frac{2\sqrt{\pi}\Gamma\left(\frac{d}{2(d-1)}\right)}{\Gamma\left(\frac{1}{2(d-1)}\right)}\right)^{d-1}\cdot\left(\frac{\tilde{\ell}}{\ell}\right)^{d-2} \\ &+ \underbrace{\frac{d}{d+1}\frac{\sqrt{\pi}\Gamma\left(\frac{d}{d-1}\right)}{2d\Gamma\left(\frac{d+1}{2(d-1)}\right)}\left(\frac{\Gamma\left(\frac{d}{2(d-1)}\right)}{\Gamma\left(\frac{1}{2(d-1)}\right)}\right)^{-2}\ell}_{T_{\text{ent}}^{-1}}\cdot\underbrace{\frac{(d-1)L^d\ell\tilde{\ell}^{d-2}}{16\pi G_N {z_h}^d}}_{\Delta E}, \end{aligned} \tag{3.74}$$

where ΔE is the energy contained in the strip region. This limit is related to entanglement thermodynamics [123, 124]. This first law of entanglement thermodynamics

applies when we consider a small temperature. It yields a law analogous to the second law of thermodynamics

$$T_{\text{ent}}\delta S_{EE} = \delta E, \tag{3.75}$$

which applies to any perturbation of the state. In particular, the entanglement temperature T_{ent} only depends on the geometry of the entangling surface and not on the excitation, i.e. on our case, it does not depend on the temperature. From our result, this limit can be obtained by expanding the hypergeometric functions in terms of power series.

Taking the high-temperature limit is more involved. The generalized hypergeometric functions appearing in the result (3.72) are diverging in the high-temperature limit $z_\star \to z_h$. It is more convenient to work with the alternative form of the result for the entanglement entropy as derived in (3.38)

$$\begin{aligned} S_{EE} = {} & \frac{L^{d-1}}{2(d-2)G_N}\left(\frac{\tilde{\ell}}{\epsilon}\right)^{d-2} + \frac{L^{d-1}\tilde{\ell}^{d-2}}{4{z_\star}^{d-1}G_N}\ell \\ & + \frac{\sqrt{\pi}L^{d-1}}{8(d-1)G_N}\frac{\tilde{\ell}^{d-2}}{{z_\star}^{d-2}}\sum_{\Delta m=0}^{\frac{2(d-1)}{\chi}-1}\frac{1}{\Delta m!}\left(\frac{1}{2}\right)_{\Delta m}\left(\frac{z_\star}{z_h}\right)^{\Delta m d}\frac{\Gamma\left(\frac{d}{\chi}a_{-\frac{1}{2}}\right)}{\Gamma\left(\frac{d}{\chi}a_1\right)} \\ & \times {}_{\frac{3d-2}{\chi}+1}F_{\frac{3d-2}{\chi}}\left(\left.\begin{matrix}1, a_{-\frac{1}{2}}, \ldots, a_{\frac{d}{\chi}-\frac{3}{2}}, b_{\frac{1}{2}}, \ldots, b_{\frac{2(d-1)}{\chi}-\frac{1}{2}} \\ a_1, \ldots, a_{\frac{d}{\chi}}, b_1, \ldots, b_{\frac{2(d-1)}{\chi}}\end{matrix}\right| \left(\frac{z_\star}{z_h}\right)^{\frac{2(d-1)d}{\chi}}\right) \end{aligned} \tag{3.76}$$

This can be brought to the form

$$S_{EE} = \frac{L^{d-1}\tilde{\ell}^{d-2}}{2(d-2)G_N\epsilon^{d-2}} + \frac{L^{d-1}}{4G_N}\frac{\tilde{\ell}^{d-2}}{{z_\star}^{d-2}}\cdot\frac{\ell}{z_\star} + \frac{L^{d-1}}{2G_N}\frac{\tilde{\ell}^{d-2}}{{z_\star}^{d-2}}\,C\left(\frac{z_\star}{z_h}\right). \tag{3.77a}$$

where the function C is defined as

$$\begin{aligned} C\left(\frac{z_\star}{z_h}\right) = {} & \frac{\sqrt{\pi}}{4(d-1)}\sum_{\Delta m=0}^{\frac{2(d-1)}{\chi}-1}\frac{1}{\Delta m!}\left(\frac{1}{2}\right)_{\Delta m}\left(\frac{z_\star}{z_h}\right)^{\Delta m d}\frac{\Gamma\left(\frac{d}{\chi}a_{-\frac{1}{2}}\right)}{\Gamma\left(\frac{d}{\chi}a_1\right)} \\ & \times {}_{\frac{3d-2}{\chi}+1}F_{\frac{3d-2}{\chi}}\left(\left.\begin{matrix}1, a_{-\frac{1}{2}}, \ldots, a_{\frac{d}{\chi}-\frac{3}{2}}, b_{\frac{1}{2}}, \ldots, b_{\frac{2(d-1)}{\chi}-\frac{1}{2}} \\ a_1, \ldots, a_{\frac{d}{\chi}}, b_1, \ldots, b_{\frac{2(d-1)}{\chi}}\end{matrix}\right| \left(\frac{z_\star}{z_h}\right)^{\frac{2(d-1)d}{\chi}}\right). \end{aligned} \tag{3.77b}$$

The divergent part of the entanglement entropy is completely contained in the term containing the width ℓ explicitly. The remaining hypergeometric functions have one

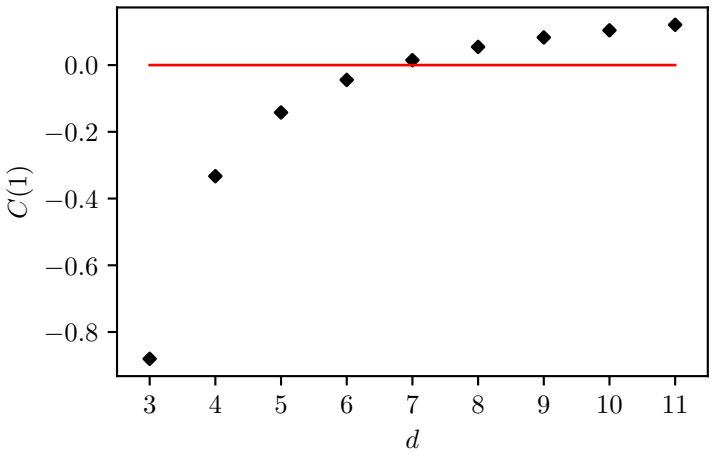

d	$C(1)$
3	-0.880
4	-0.333
5	-0.142
6	-0.0444
7	0.0148
8	0.0545
9	0.0829
10	0.104
11	0.121

Figure 3.11 & Table 3.4: Subleading Term of the Entanglement Entropy.

denominator parameter shifted. In particular, this shift causes the hypergeometric functions to converge to a finite value at unit argument. Furthermore, corrections to the turning point decay exponentially in this limit.

The high-temperature limit therefore reduces to

$$S_{EE} = \frac{L^{d-1}\tilde{\ell}^{d-2}}{2(d-2)G_N\epsilon^{d-2}} + \frac{L^{d-1}}{4G_N}\frac{\tilde{\ell}^{d-2}}{{z_h}^{d-2}} \cdot \frac{\ell}{z_h} + \frac{L^{d-1}}{2G_N}\frac{\tilde{\ell}^{d-2}}{{z_h}^{d-2}}\, C(1). \tag{3.78}$$

The results for $C(1)$ are shown in Figure 3.11 and Table 3.4. In contrast to the previous observables, the subleading term in the high-temperature limit changes sign. We see that the term is negative for field theory dimension $d < 7$ and positive for $d \geq 7$. To study this more closely, let us look at other measures derived from the entanglement entropy.

Entanglement Negativity

The problem with the entanglement entropy as a measure for entanglement is that it also measures classical correlations. In the thermal state we consider, we observed that the entanglement entropy becomes extensive for high-temperature/large-width. Therefore, the entanglement entropy approaches the thermal entropy and is governed by classical correlations. A proper measure for entanglement of mixed states is the entanglement negativity. In general, it cannot be expressed in terms of entanglement entropies, but for holographical theories it can. For the setup considered, it reduces

to

$$\varepsilon(A) = \frac{3}{2}\left(S_{EE}(A) - S^{th}(A)\right) = \frac{3}{2}\left(S_{EE}(A) - \frac{L^{d-1}}{4G_N}\frac{\tilde{\ell}^{d-2}\ell}{{z_h}^{d-1}}\right),$$

i.e. we subtract the thermal entropy and therefore classical correlations arising from it. If we write our result for the entanglement entropy as expressed in Equation (3.76), the entanglement negativity is

$$\varepsilon = \cdots + \frac{3L^{d-1}\tilde{\ell}^{d-2}\ell}{8{z_\star}^{d-1}G_N}\left(1 - \left(\frac{z_\star}{z_h}\right)^{d-1}\right) + \frac{3L}{4G_N}\left(\frac{\tilde{\ell}}{z_\star}\right)^{d-2} C\left(\frac{z_\star}{z_h}\right), \tag{3.79}$$

where the dots represent the usual UV-divergent term. We discussed previously that the low-temperature correction to the entanglement entropy is positive and of order $\mathcal{O}(\ell \cdot T)^2$. This term is subleading to the extensive subtracted term of the order $\mathcal{O}(\ell \cdot T)$. Consequently, the low-temperature result of the entanglement negativity reduces to

$$\begin{aligned}\varepsilon =& \frac{3L^{d-1}}{4(d-2)G_N}\left(\frac{\tilde{\ell}}{\epsilon}\right)^{d-2} - \frac{3L^{d-1}}{8(d-2)G_N}\left(\frac{2\sqrt{\pi}\,\Gamma\left(\frac{d}{2(d-1)}\right)}{\Gamma\left(\frac{1}{2(d-1)}\right)}\right)^{d-1} \cdot \left(\frac{\tilde{\ell}}{\ell}\right)^{d-2} \\ & - \frac{3L^{d-1}}{8G_N}\frac{\tilde{\ell}^{d-2}\ell}{{z_h}^{d-1}}\end{aligned} \tag{3.80}$$

and the leading correction is related to the thermal entropy of the considered strip. Therefore, turning on the temperature reduces short-range entanglement. Since the entanglement negativity is related to the mutual information (see (2.101))

$$\varepsilon = \frac{3}{2}\mathcal{I}(A : B_i).$$

A is the strip and the regions B_1 and B_2 are the regions to the left ($x < -\ell/2$) and to the right ($x > \ell/2$) of the it. The mutual information implies an upper bound on correlations between the A and B_i. The leading temperature correction is positive and places therefore a stricter upper bound on the correlations. The results for the two-point functions showed a similar behavior: The leading order correction is negative and reduces correlation (3.49). There are however to points to keep in mind: the result for the two point function is of order $\mathcal{O}(c)^0$ and therefore satisfies any bound of order $\mathcal{O}(c)^1$ in the large c limit. Furthermore, the result for the two-point function applies exclusively to special operators: the one with large scaling

dimension. The upper bound from the mutual information applies to any operator.

Let us turn to the high-temperature limit. The entanglement negativity reduces to

$$\varepsilon = \frac{3L^{d-1}}{4(d-2)G_N} \cdot \frac{\tilde{\ell}^{d-2}}{\epsilon^{d-2}} + \frac{3L^{d-1}\tilde{\ell}^{d-2}}{4G_N {z_h}^{d-2}} C(1), \tag{3.81}$$

where $C(1)$ is a temperature-independent constant obtained by evaluating the function defined in (3.77) at $z_\star = z_h$. Therefore, an area remains as leading order term after removing the extensive, thermal contribution from the entanglement entropy. Keep in mind that at zero temperature, the entanglement negativity is

$$\varepsilon = \frac{3L^{d-1}}{4(d-2)G_N} \left(\frac{\tilde{\ell}}{\epsilon}\right)^{d-2} - \frac{3L^{d-1}}{8(d-2)G_N} \left(\frac{2\sqrt{\pi}\Gamma\left(\frac{d}{2(d-1)}\right)}{\Gamma\left(\frac{1}{2(d-1)}\right)}\right)^{d-1} \cdot \left(\frac{\tilde{\ell}}{\ell}\right)^{d-2},$$

i.e. $C(1)$ is a temperature depending shift of the area term at finite temperature compared to the zero temperature result. This area term arises from short-range correlation across the entangling surface [32–34], i.e. the boundary of the strip. As we already saw in Table 3.4, the constant $C(1)$ changes sign depending on the spacetime dimension. For spacetime dimension $d < 7$, the shift is negative. Therefore, even for large strips the entanglement entropy (and hence entanglement and correlations) are reduced due to the temperature. In contrast, $C(1)$ is positive for $d \geq 7$. Consequently, long-range entanglement is increased due to the temperature. In particular, there has to be a transition between the $\varepsilon < \varepsilon|_{T=0}$ behavior at small-temperature/small-width and the $\varepsilon > \varepsilon|_{T=0}$ behavior for high-temperature/large-width. The size of the strip ℓ can also be interpreted as an inverse energy scale. Therefore, the low-temperature limit $T \ll \ell^{-1}$ corresponds to the UV where the theory is effectively massless and the area term is given by the UV cutoff. The high-temperature limit $T \gg \ell^{-1}$ corresponds to the IR. Since the fields obtain a thermally induced mass, this theory has a mass-gap. My result show that there is a shift of the area term. Intuition tells us that at low-temperature, there are effectively less degrees of freedom which should reduce short-range correlations. However, my analytic result show an increase in short-range correlations for $d \geq 7$.

The result for the entanglement negativity is shown in Figure 3.12. The results for spacetime dimension $d < 7$ is always smaller than the corresponding finite temperature result. In contrast, there is a transition for higher dimensions as discussed above.

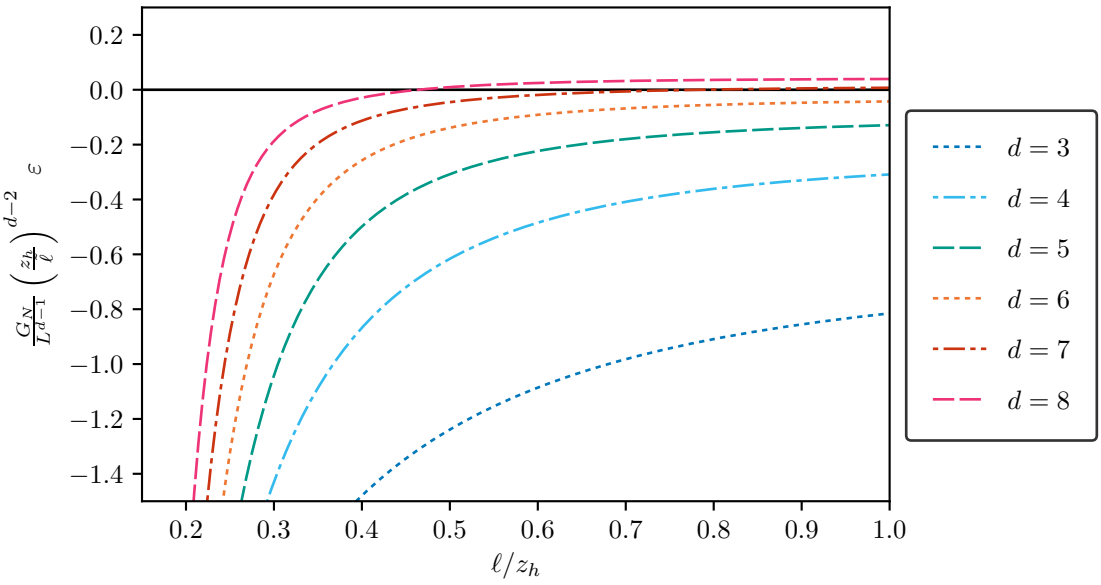

Figure 3.12: Result for the Entanglement Negativity at finite Temperature.

Entanglement Density

Another measure derived from the entanglement entropy is the entanglement density σ as defined by [125]. It is defined as the change of entanglement entropy per strip volume, i.e.

$$\sigma = \frac{1}{\tilde{\ell}^{d-2}\ell}\left[S_{EE}(\ell) - S_{EE}(\ell)|_{T=0}\right]. \tag{3.82}$$

It can be understood as a generalization of the entanglement temperature (3.75) to general states. With the previously presented result for the entanglement entropy, the entanglement density can be written as

$$\sigma = \frac{L^{d-1}}{4(d-2)G_N}\left(\frac{2\sqrt{\pi}\Gamma\left(\frac{d}{2(d-1)}\right)}{\Gamma\left(\frac{1}{2(d-1)}\right)}\right)^{d-1}\cdot\left(\frac{1}{\ell}\right)^{d-1} + \frac{L^{d-1}}{4G_N}\frac{1}{{z_\star}^{d-2}}\cdot\frac{1}{z_\star}$$
$$+ \frac{L^{d-1}}{2G_N}\frac{1}{{z_\star}^{d-2}}\frac{1}{\ell}\,C\left(\frac{z_\star}{z_h}\right). \tag{3.83}$$

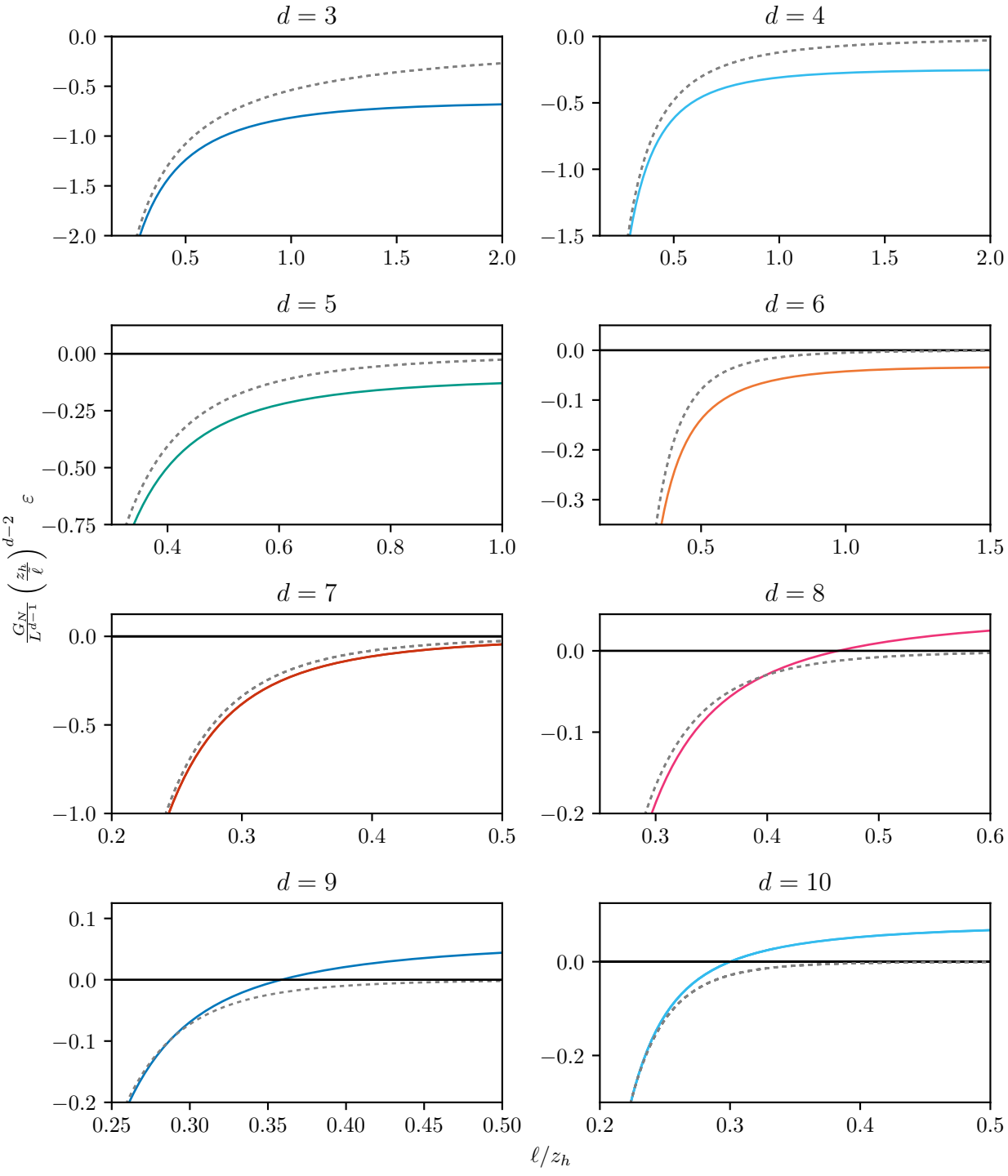

Figure 3.13: Entanglement Negativity for different Dimensions.

Since the zero-temperature result is subtracted, the result is UV-finite. Considering the low-temperature limit, the entanglement entropy behaves as (see (3.74))

$$S_{EE} = S_{EE}|_{T=0} + \langle T_{tt} \rangle \ \ell \tilde{\ell}^{d-2} \cdot \underbrace{T_{\text{ent}}^{-1}}_{\frac{2\pi}{d+1}\ell}.$$

Consequently, the entanglement negativity behaves as

$$\sigma = \langle T_{tt} \rangle \ \cdot \underbrace{T_{\text{ent}}^{-1}}_{\frac{2\pi}{d+1}\ell}.$$

Therefore, it is linear in the width of the strip for a small entangling region. In contrast, the entanglement density in the high-temperature limit behaves as

$$\sigma = \frac{L^{d-1}}{4G_N} \frac{1}{{z_h}^{d-1}} + \frac{L^{d-1}}{2G_N} \frac{1}{{z_h}^{d-2}\ell} \ C(1), \tag{3.84}$$

where the first term is the density of the thermal entropy. Therefore, the entanglement density approaches the thermal entropy. The sign of $C(1)$ determines whether this asymptotic value is approached from below $C(1) < 1$ or from above $C(1) > 1$.

This shows how the sign of the subleading area term determines the behavior of the entanglement density: for low spacetime dimension the entanglement density can approach the thermal entropy density monotonically from below, whereas for large spacetime dimension the entanglement density reaches a maximum and then approaches the thermal entropy from above. Therefore, the entanglement density is a useful tool to study the area term. This area term is related to a variant of the c-theorem [37], the so called area theorem. This theorem states that for an RG-flow from a UV to an IR fixed point, the coefficient of the area law term has to be lower in the IR than in the UV[13]. For field theories, there exist proofs for spherical regions, for $d = 3$ using strong subadditivity [35] and for $d \geq 3$ using the positivity of the relative entropy [36]. The high-temperature behavior of the entanglement density captures the area term as subleading term

$$\sigma = s - \Delta\alpha \underbrace{\frac{\text{Boundary-Area}}{\text{Volume}}}_{\ell^{-1}} + \cdots, . \tag{3.85}$$

[13]This is a weak c-theorem, where the term does not have to decrease monotonically along the RG-flow.

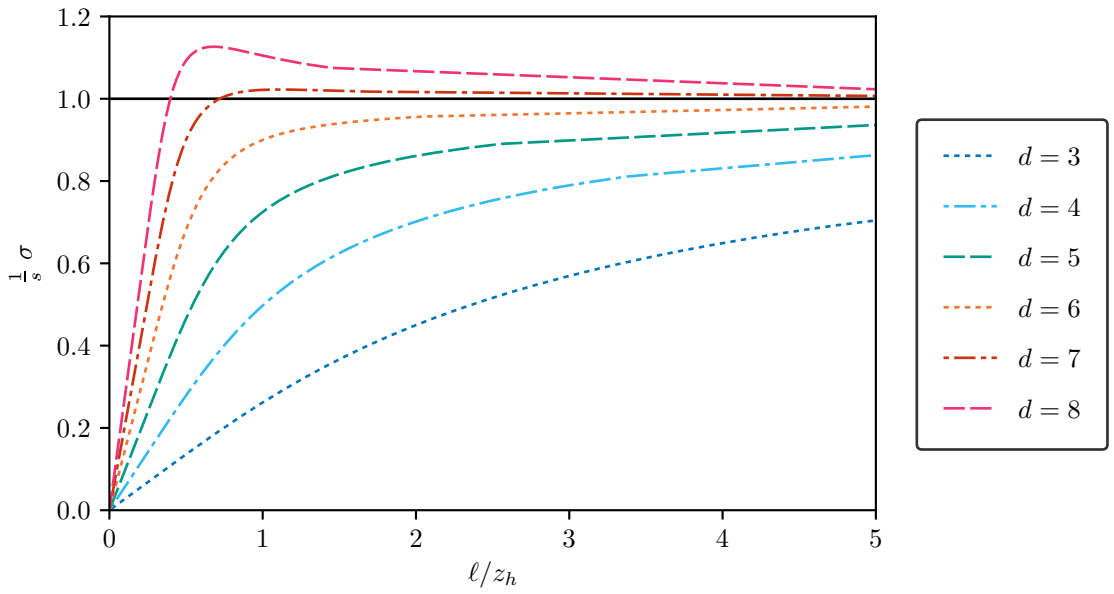

Figure 3.14: Result for the Entanglement Density at finite Temperature.

It is useful to look at the dimensionless quantity

$$\Delta\hat{\alpha} = \frac{T}{s}\Delta\alpha = -2C(1). \tag{3.86}$$

Therefore, for small spacetime dimension $d < 7$, $\Delta\hat{\alpha}$ is positive and the area term complies with the area theorem. In contrast, for $d \geq 7$, $\Delta\hat{\alpha}$ becomes negative, which results in a violation of the area theorem.

Having the coefficient $\Delta\hat{\alpha}$ satisfying a c-theorem for RG-flows suggest to interpret this quantity as a measure for the number of effective degrees of freedom at an energy scale $E \propto \ell^{-1}$. Therefore, our results hint to the appearance of new degrees of freedom in the IR for CFTs with an AdS dual for dimension $d \geq 7$. Interestingly, there is also something happening on the CFT side: there exist no superconformal field theories in spacetime dimensions $d \geq 7$ [126–128]. There also does not exist a string theory embedding of AdS/CFT in these dimensions. Therefore, we do not know what the dual field theory would be for these geometries. These new degrees of freedom could also be related to the fact that non-extremal black hole approach a two-dimensional black hole in the near-horizon limit [129, 130]. This gives rise to an additional conformal symmetry.

3.3.5 Summary and Discussion

In AdS/CFT, AdS Schwarzschild black holes are dual to finite temperature states on the CFT side. We examined boundary anchored surfaces anchored on strips of various dimensionality. From the gravity side, these covariantly assign an area to the considered boundary strip. The AdS/CFT dictionary relates the area of such surfaces to different non-local observables on the field theory side: the spatial two-point correlation function, the spatial Wilson loop and the entanglement entropy.

The previous sections present my analytic results for the area of such boundary anchored surfaces in terms of generalized hypergeometric functions. Properties of hypergeometric functions allow to analyze the behavior of the result. Furthermore, the results can be evaluated using conventional computer algebra systems.

Special focus is put on the high-temperature/large-width limit. The leading term follows trivially from the geometry at the behavior and the area is becomes extensive. Since the hypergeometric functions diverge in this limit, it is not possible to perform a systematic expansion in $(\ell T)^{-1}$. However, the properties of the specific hypergeometric functions allow to determine a closed result for the subleading term, which is proportional to the boundary of the strip. This term is highly non-trivial and depends on the entire spacetime geometry.

The interpretation for this subleading term various depending on which observable is considered. For the two-point correlation function, this subleading constant produced a rescaling of the two-point correlation function and therefore an increase in long-distance correlations.

Of particular interest is studying the subleading term for the entanglement entropy. For this observable, we have an unexpected behavior: the subleading term changes sign between $d = 6$ and $d = 7$. Studying this in terms of the entanglement negativity and entanglement density, this shows unexpected behavior for field theory dimension $d \geq 7$: finite temperature produces additional IR degrees of freedom and increases long-range entanglement. This contradicts the behavior of field theories. However, it is well-known that there are no superconformal field theories in these dimension. Therefore, a potential field theory dual has to be described by a different theory. A similar behavior was found numerically in [125] also for Reissner-Nordström solutions as well as further examples. In particular, they found that this phenomenon occurs when the near-horizon geometry approaches $\mathrm{AdS}2 \times \ldots$ in some limit and hence an additional conformal symmetry emerges in the IR. These additionally appearing degrees of freedom may therefore be related to massless degrees of freedom appearing when approaching these limiting cases.

For the Wilson loop, my results apply to spatial Wilson loops in AdS Schwarzschild. A double-Wick rotation transforms them into temporal Wilson loops of a different geometry: AdS-Soliton. This geometry has a compact spatial direction which shrinks to zero at radial position $z = z_h$. This introduces an analog of the QCD length scale and makes the theory confining. In this theory, the Wilson loop is related to the quark-antiquark potential. The subleading term corresponds to a renormalization of the mass of the probe quark.

Furthermore, the method I applied to AdS Schwarzschild can be easily generalized. The main part is expressing a power series in terms of hypergeometric functions by reordering it, splitting it and summing it up separately. This is possible when the series obtained after splitting in a certain way are rational functions of the index of summation. The reordering is only allowed when the original series converges absolutely. The analytic continuation of hypergeometric function is known: Meijer G-functions. While I did not phrase the result for the considered observables in terms of these functions, the result for the area of surfaces of arbitrary dimension in terms of these functions is discussed in Section 3.2.4. Therefore, the condition that the power series has to be absolutely convergent can be bypassed.

Chapter 4

Subregion Complexity at finite Temperature

In the previous chapter, we studied non-local observables in AdS/CFT. For static spacetimes, they are related to minimal surfaces in a constant time slice. In particular, the entanglement entropy is proportional to the area of the Ryu-Takayanagi surface, i.e. the minimal co-dimension one surface in this slice. This associates a unique bulk region to the given boundary region. This motivates studying the volume enclosed by the Ryu-Takayanagi surface [131]. In analogy to the holographic complexity, the *holographic subregion complexity* is defined as

$$\mathcal{C}_A = \frac{1}{G_N L}\mathcal{V}_A, \tag{4.1}$$

where $\mathcal{V}$ is the volume inside the Ryu-Takayanagi surface anchored on ∂A, G_N the Newton constant and L the AdS-radius[1]. Motivated by previous work which considered the entire spacetime [39, 41] and reviewed in Section 2.5.3, this quantity has the interpretation of complexity, a measure of the difficulty of constructing a state ρ. The volume inside the Ryu-Takayanagi surface is the generalization complexity to reduced states ρ_A.

In particular, I consider the volume inside the subregion complexity in AdS Schwarzschild. The authors of [132] showed that the *complexity of formation*, i.e. the additional complexity required to construct the thermal state, is proportional to the thermal entropy. This can be motivated by considering the dual tensor network picture, see Section 2.5.4. In the following, I extend this discussion to subregion complexity. While the complexity of the state only allows us to study

[1]The proportionality factor in this expression is a mater of convention.

the complexity of the whole network, studying the subregion complexity also allows drawing conclusions about how the complexity is distributed in the network.

The structure of this chapter is as follows. In Section 4.1 we take a look at reduced states. The treatment in the field theory as well as the holographic realization is reviewed. Afterwards, I present my analytic results using the methods applied in Chapter 3. To gain some intuition, I take a look at the corresponding MERA network in Section 4.3, use a hard wall gravity model corresponding to this and compare results in this setup to the one for AdS Schwarzschild derived above. Afterwards, the chapter concludes with a summary and outlook.

4.1 Reduced States in AdS/CFT

This section reviews reduced states and their treatment in AdS/CFT. It is based on [75, 80, 133].

In a field theory, the degrees of freedom on a constant time-slice[2] can be split into the degrees of freedom living on a region A and the one living on the complement A^c. Therefore, the Hilbert space is a product space $\mathcal{H}_A \otimes \mathcal{H}_{A^c}$. The degrees of freedom are described by the reduced density matrix (2.94)

$$\rho_A = \mathrm{Tr}_{A^c}\, \rho.$$

Knowledge of ρ_A is sufficient to calculate observables in the region A. In fact, knowledge of ρ_A and the Hamiltonian acting on A allows to calculate observables in a larger spacetime region using unitary time evolution. The region in which this is possible is the so-called *domain of dependence*, which is defined as

$$D[A] = \left\{ p \in \mathbb{R}^{1,d-1} |\ \forall \text{ causal curves through } p \text{ intersect } A \text{ exactly once} \right\}, \quad (4.2)$$

where we consider the spacetime to be d-dimensional Minkowski space $\mathbb{R}^{1,d-1}$. A given region A defines a splitting of the spacetime into four regions

$$\text{boundary} = D[A] \cup D[A^c] \cup J^+[\partial A] \cup J^-[\partial A],$$

where $J^\mp$ are the causal past and causal future respectively. These regions do not intersect except at $\partial A = J^+[\partial A] \cap J^-[\partial A]$. This splitting is shown in Figure 4.1.

[2] More exactly, a Cauchy slice, i.e. a slice which is intersected by any causal curve exactly once.

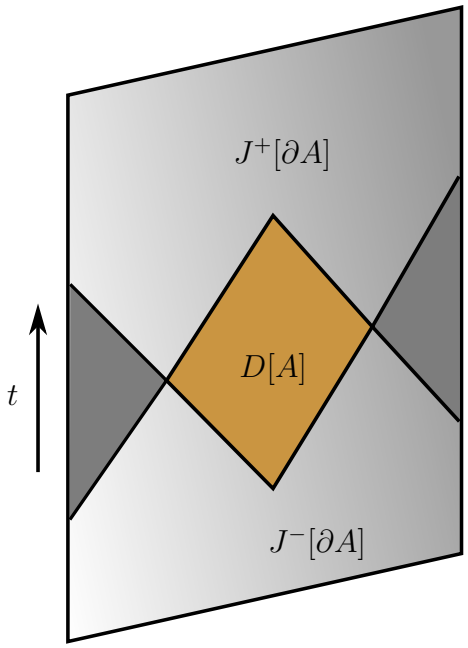

Figure 4.1: Causal Splitting of Boundary Spacetime.

In particular, if two regions A and A' have the same domain of dependence, the reduced states can be obtained by a unitary transformation from each other. Since the entanglement entropy (2.90)

$$S_{EE} = -\operatorname{Tr} \rho_A \ln \rho_A$$

is not changed by unitary transformations, it strictly speaking only depends on $D[A]$. Therefore, it is a so-called *wedge observable*[3].

To understand the emergence of geometry, it is of interest what gravity region corresponds to the reduces state. In particular this requires that ρ_A can be uniquely determined from this gravity region and vice-versa. If we consider different states ρ and $\hat{\rho}$ which have the same reduced state, i.e. they are different purifications of the same reduced state, their gravity duals (if existent) shares this region. The first guess would be the *causal wedge* $\mathcal{W}_\mathcal{C}[A]$, which is defined as the spacetime region which can send signals and receive signals from $D[A]$. This region can be written as

$$\mathcal{W}_\mathcal{C}[A] := \mathcal{J}^+[D[A]] \cap \mathcal{J}^-[D[A]],$$

where $\mathcal{J}^\mp$ are the bulk causal past and causal future. In AdS/CFT, this gravity

[3]Even if it is not an observable in the usual sense.

region can be constructed from knowing correlation functions on $D[A]$. Therefore, this is the minimal region has to be covered by the region dual of the reduced state.

However, it was shown in [118] that the Ryu-Takayanagi surface is a better observable to probe the geometry. Let us donate its covariant generalization, i.e. the minimal extremal surface anchored on the entangling surface ∂A, as $\mathcal{E}$. In general, this surface lies outside of the causal wedge $\mathcal{W}_{\mathcal{C}}$. For the Ryu-Takayanagi proposal, it is important that the minimal surface is homologous to A. In the covariant case, this translates to the existence of a so called homology surface $\mathcal{R}_A$, which is a Cauchy surface interpolating between A and $\mathcal{E}$. The *entanglement wedge* is defined as the bulk domain of dependence of the homology surface, i.e. as

$$\mathcal{W}[A] := \mathcal{D}\left[\mathcal{R}_A\right]. \tag{4.3}$$

An alternative definition is that the causal wedge consists of the points which are spacelike separated from $\mathcal{E}$ and connected to $D[A]$. This definition does not require to consider a homology surface. This entanglement wedge $\mathcal{W}[A]$ is conjectured to be the correct holographic dual for the reduced state. In particular, the entanglement wedge is its own domain of dependence, i.e. the region where we can construct the state by knowledge of the reduced state. This is not in general the cause for the causal wedge, but a necessary condition to obtain the correct bulk dual of the reduced state: the region is the one being constructible from knowledge of ρ_A. Complete knowledge of a region implies complete knowledge of its domain of dependence. Therefore, the region dual to a reduced state should be its own domain of dependence.

Analog to the causal splitting of the boundary by ∂A, the extremal surface $\mathcal{E}$ defines a causal splitting of the bulk spacetime into four parts:

$$\text{bulk } = \mathcal{W}[A] \cup \mathcal{J}^+\left[\mathcal{E}_A\right] \cup \mathcal{J}^-\left[\mathcal{E}_A\right] \cup C$$

where the region C are the points spacelike separated from $\mathcal{E}$ but not connected to $D[A]$. The region C is in general larger than $\mathcal{W}[A^c]$, e.g. when considering geometries with a horizon. This causal splitting corresponds to the causal splitting of the boundary (4.3) . In particular, we have

$$\begin{aligned} \mathcal{W}[A] \cap \text{boundary } &= D[\mathcal{A}], \\ \mathcal{J}^{\pm}\left[\mathcal{E}_A\right] \cap \text{boundary } &= J^{\pm}[\partial A]. \end{aligned}$$

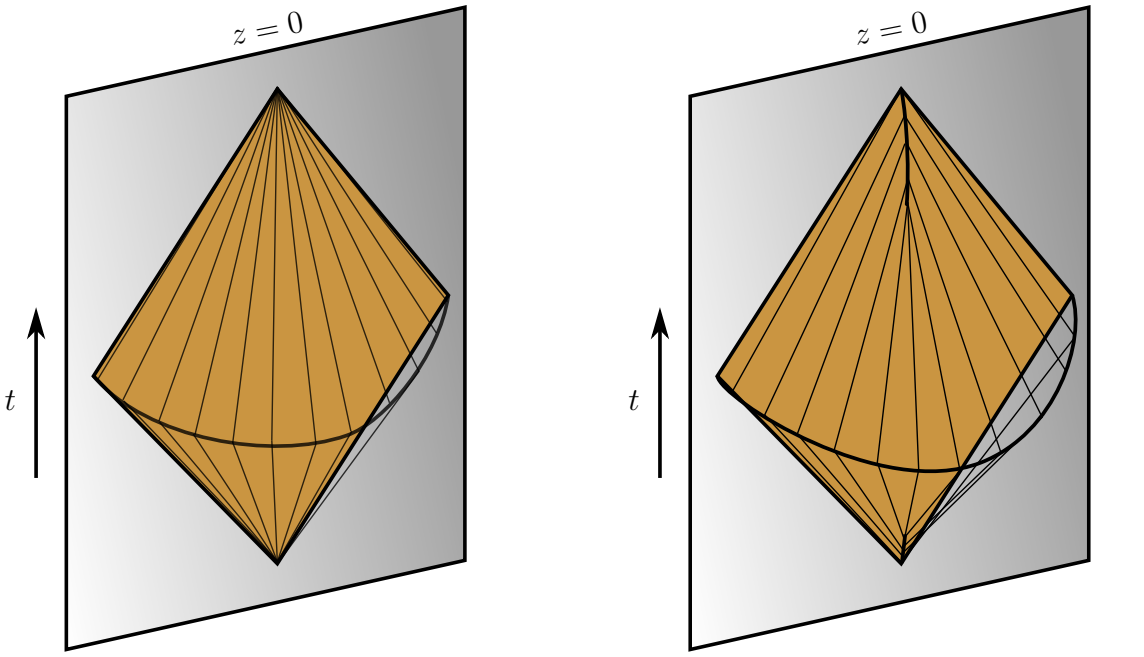

(a) Causal Wedge.
Constructed by sending lightrays from $\partial D[A]$ into the bulk.

(b) Entanglement Wedge.
Constructed by sending lightrays from ε_A to the boundary.

Figure 4.2: Bulk Regions associated to a Reduced State.

The naive intuition would be that since the extremal surface lies outside of the causal wedge $\mathcal{W}_{\mathcal{C}}[A]$, the intersection between the entanglement wedge and the boundary $\mathcal{W}[A]$ could contain more of the boundary spacetime than the domain of dependence $D[\mathcal{A}]$. A detailed study on null-congruences, i.e. the set of null curves starting on a general spatial co-dimension two surface anchored on ∂A, shows why this cannot be the case. In the case that the surface lies inside the causal wedge, the congruence intersects the boundary inside $D[A]$. If the surface lies at the boundary of $\mathcal{W}_{\mathcal{C}}[A]$, the congruence exactly intersects the boundary at the boundary of $\partial D[A]$, as one would intuitively expect. If one now considers a surface outside of the causal wedge, the intersection does not move outside of the domain of dependence. Rather, nearby curves start intersecting, which results in caustics outside the boundary and a termination of the congruence. Therefore, the kind of construction used for the entanglement wedge for any spacelike surface anchored on ∂A does not yield an intersection with the boundary larger than $D[A]$. This causal wedge and the entanglement wedge are shown in Figure 4.2.

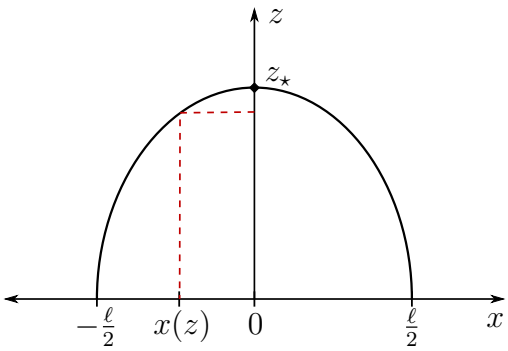

Figure 4.3: Entangling Region and Ryu-Takayanagi Surface.
The strip has the width ℓ in the spatial direction x. The $(d-2)$ remaining spatial directions are not shown, since the shape of the surface is independent of these coordinates.

4.2 Subregion Complexity in AdS Schwarzschild

The bulk dual to a reduced state is the entanglement wedge. Therefore, holography automatically assigns a unique volume to the reduced state: the volume of the maximal extremal slice in this wedge. For static spacetimes, this reduces to the volume inside the Ryu-Takayanagi surface on the constant time slice. The volume is proportional to the holographic subregion complexity (4.1).

Based on my study of the entanglement entropy in the previous Chapter 3, I study the subregion complexity for strips at finite temperature. Therefore, the considered bulk geometry is AdS Schwarzschild

$$\mathrm{d}s^2 = \left(\frac{L}{z}\right)^2 \left(-b(z)\mathrm{d}t^2 + \mathrm{d}\vec{x}^2 + b(z)^{-1}\mathrm{d}z^2\right), \tag{4.4a}$$

$$b(z) = 1 - \left(\frac{z}{z_h}\right)^d. \tag{4.4b}$$

In the previous chapter, I calculated the area of the Ryu-Takayanagi surface, i.e. the co-dimension one surface anchored on the boundary in a constant time slice as shown in Figure 4.3. In the following, I derive an analytic expression for the volume inside this surface. For the AdS Schwarzschild metric (4.4), the integral expression

for the volume is

$$\begin{aligned}\mathcal{V} &= L^d \tilde{\ell}^{d-2} \int_\epsilon^{z_\star} \mathrm{d}z \int_{x(z)}^{-x(z)} \mathrm{d}x \; z^{-d} \sqrt{b(z)}^{-1}, \\ &= -2L^d \tilde{\ell}^{d-2} \int_\epsilon^{z_\star} \mathrm{d}z \; x(z) z^{-d} \sqrt{b(z)}^{-1}, \end{aligned} \tag{4.5}$$

where $x(t)$ is the embedding (3.18) of the Ryu-Takayanagi surface. Since the metric is independent of the spatial coordinates, the volume reduces to a one-dimensional integral. The volume is divergent and has to be regulated by considering the bulk cutoff ϵ. The conventions in this expression are that the left branch of the minimal surface is considered, i.e. where $x < 0$ and $x'(z) > 0$. As derived in (4.6), the differential expression for the embedding of the $(d-1)$-dimensional surface is

$$x'(t) = \left(\frac{z}{z_\star}\right)^{d-1} \frac{1}{\sqrt{b(z)}} \frac{1}{\sqrt{1-(z/z_\star)^{2(d-1)}}}. \tag{4.6}$$

In my previous study of the entanglement entropy, I did not solve the embedding explicitly. This is also not necessary to determine the volume. In order to obtain an integrand which only depends on the derivative of the embedding, I partially integrate the expression obtained in (4.5). For this, I define κ via the differential equation

$$\kappa'(z) = z^{-d} \sqrt{b(z)}^{-1}, \tag{4.7a}$$

which has the solution

$$\kappa(z) = -\frac{z^{1-d}}{d-1} \; {}_2F_1\left(\left. \begin{matrix} \frac{1}{2}, \frac{1}{d}-1 \\ \frac{1}{d} \end{matrix} \right| \left(\frac{z}{z_h}\right)^d \right). \tag{4.7b}$$

Therefore, the volume inside the Ryu-Takayanagi surface is

$$\begin{aligned}\mathcal{V} &= -2L^d \tilde{\ell}^{d-2} \int_\epsilon^{z_\star} \mathrm{d}z \; x(z) \kappa'(z), \\ &= 2L^d \tilde{\ell}^{d-2} \int_\epsilon^{z_\star} \mathrm{d}z \; x'(z) \kappa(z) - 2L^d \tilde{\ell}^{d-2} [x(z)\kappa(z)]_\epsilon^{z_\star}. \end{aligned} \tag{4.8}$$

This formulates the volume in a way which enables us to directly use the differential equation for the embedding (4.6).

The boundary term depends on the near-boundary behavior of κ and $x(z)$. Expanding both expressions as a power series yields

$$\kappa(z) = -\frac{z^{1-d}}{d-1}\left(1 + \mathcal{O}\left(\frac{z}{z_h}\right)^d\right), \tag{4.9a}$$

$$x(z) = -\ell + z_\star \cdot \mathcal{O}\left(\frac{z}{z_\star}\right)^d. \tag{4.9b}$$

These limits are obtained by expanding the hypergeometric function in (4.7) and expanding the differential equation for the embedding (4.6). The boundary term reduces to

$$\mathcal{V} = 2L^d\tilde{\ell}^{d-2}\int_\epsilon^{z_\star} \mathrm{d}z\; x'(z)\kappa(z) + \frac{L^d}{d-1}\cdot\overbrace{\frac{\ell\tilde{\ell}^{d-2}}{\epsilon^{d-1}}}^{\text{Volume of strip}}. \tag{4.10}$$

Therefore, the UV-divergent term for the volume arises from the boundary term. The term agrees with the UV-divergent term of the vacuum result [134]. The additional integral expression if UV-finite and allows to take the bulk cutoff to zero. The integrand can be simplified using the Euler transform of the hypergeometric function (see (B.10) of the appendix) in order to simplify the integrand by absorbing one of the square roots. This results in

$$\mathcal{V}_{\text{finite}} = -\frac{2L^d\tilde{\ell}^{d-2}}{(d-1){z_\star}^{d-1}}\int_0^{z_\star}\mathrm{d}z\;\; {}_2F_1\left(\begin{matrix}1, \frac{1}{d}-\frac{1}{2}\\ \frac{1}{d}\end{matrix}\middle|\left(\frac{z}{z_h}\right)^d\right)\sqrt{1-\left(\frac{z}{z_\star}\right)^{2(d-1)}}^{-1}. \tag{4.11}$$

Therefore, I reduces the calculation of the volume to solving this integral. The integral can be solved using the same method as I used to derive a result for the minimal area: it can be written as an absolutely converging power series, which I integrate term by term and reconstruct in terms of generalized hypergeometric functions.

4.2.1 Analytic Result for the Subregion Complexity

The integral of interest is

$$\mathcal{I} = \int_0^{z_\star} \mathrm{d}z \;\; {}_2F_1\left(\left.\begin{matrix}1, \frac{1}{d} - \frac{1}{2} \\ \frac{1}{d}\end{matrix}\right| \left(\frac{z}{z_h}\right)^d\right) \sqrt{1 - \left(\frac{z}{z_\star}\right)^{2(d-1)}}^{-1}. \tag{4.12}$$

Both the hypergeometric function and the square-root can be written as absolutely convergent power series in $(z/z_h)^d$ and $(z/z_\star)^{2(d-1)}$ respectively. Integrating this power series yields

$$\begin{aligned}\mathcal{I} &= z_\star \sum_{m_1,m_2=0}^{\infty} \frac{\left(\frac{1}{2}\right)_{m_1} \left(\frac{1}{d} - \frac{1}{2}\right)_{m_2}}{m_1! \left(\frac{1}{d}\right)_{m_2}} \frac{1}{dm_2 + 2(d-1)m_1 + 1} \left(\frac{z_\star}{z_h}\right)^{dm_2}, \\ &= \frac{z_\star \sqrt{\pi}}{2(d-1)} \sum_{m=0}^{\infty} \frac{\left(\frac{1}{d} - \frac{1}{2}\right)_m}{\left(\frac{1}{d}\right)_m} \frac{\Gamma\left(\frac{dm+1}{2(d-1)}\right)}{\Gamma\left(\frac{dm+1}{2(d-1)} + \frac{1}{2}\right)} \left(\frac{z_\star}{z_h}\right)^{dm},\end{aligned} \tag{4.13}$$

where the sum over m_2 reduces to a hypergeometric function ${}_2F_1$, which is evaluated at unit argument and simplifies in terms of Gamma functions as described in (B.7).

Let us take a short detour and consider the case $d = 2$ separately. The integral reduces to

$$\mathcal{I} = \frac{\pi z_\star}{2}. \tag{4.14}$$

Therefore, the two-dimensional case is trivial as the volume is constant

$$\mathcal{V} = -\frac{\pi L^d \tilde{\ell}^{d-2}}{d-1} + \frac{L^d}{d-1} \cdot \frac{\ell \tilde{\ell}^{d-2}}{\epsilon^{d-1}}. \tag{4.15}$$

It was shown in [135] that this arises because in three dimensional gravity the Gauss-Bonnet theorem applies and renders the complexity a topological quantity. Therefore, the following discussion only treats $d > 2$.

The problem with constructing hypergeometric functions from Equation (4.13) is that subsequent coefficients do not have to correct form. As before, I first have to reorder the series. This is done by redefining the index. Analog to the case for a

minimal surface of general dimension discussed in Equation (3.21), I define

$$m = \Delta m + \frac{2(d-1)}{\chi}\delta m, \tag{4.16a}$$

$$\delta m = 0, \ldots, \infty, \qquad \Delta m = 0, \ldots, \frac{2(d-1)}{\chi} - 1, \tag{4.16b}$$

where the parameter χ

$$\chi = \gcd(2(d-1), d) = \begin{cases} 1 & d \text{ odd} \\ 2 & d \text{ even} \end{cases}$$

incorporates possible simplification for even spacetime dimension d. This splits the series into $2(d-1)/\chi$ ones which are labeled by Δm. The coefficients of these are

$$\hat{c}_{\delta m} = c_m\big|_{\Delta m + \frac{2(d-1)}{\chi}\delta m} \qquad c_m = \frac{1}{\left(\frac{1}{d}\right)_m}\left(\frac{1}{d} - \frac{1}{2}\right)_m \left(\frac{z_\star}{z_h}\right)^{md} \frac{\Gamma\left(\frac{md+1}{2(d-1)}\right)}{\Gamma\left(\frac{md+d}{2n}\right)}.$$

In order to construct hypergeometric functions, the ratio between successive coefficients has to have the form

$$\frac{\hat{c}_{\delta m+1}}{\hat{c}_{\delta m}} = u \cdot \frac{P(-\delta m)}{Q(-\delta m)} \frac{1}{\delta m},$$

where P and Q are polynomial functions (see (B.4)). Careful analysis shows that the ratio for $\mathcal{I}$ can be written as

$$\begin{aligned} \frac{\hat{c}_{\delta m+1}}{\hat{c}_{\delta m}} = {} & \frac{\Gamma\left(\frac{1}{d} - \frac{1}{2} + \Delta m + \frac{2(d-1)}{\chi}\delta m + \frac{2(d-1)}{\chi}\right)}{\Gamma\left(\frac{1}{d} - \frac{1}{2} + \Delta m + \frac{2(d-1)}{\chi}\delta m\right)} \frac{\Gamma\left(\frac{1}{d} + \Delta m + \frac{2(d-1)}{\chi}\delta m\right)}{\Gamma\left(\frac{1}{d} + \Delta m + \frac{2(d-1)}{\chi}\delta m + \frac{2(d-1)}{\chi}\right)} \\ & \times \frac{\Gamma\left(\frac{\Delta md+1}{2(d-1)} + \frac{d}{\chi}(\delta m+1)\right)}{\Gamma\left(\frac{\Delta md+1}{2(d-1)} + \frac{d}{\chi}\delta m\right)} \frac{\Gamma\left(\frac{\Delta md+d}{2(d-1)} + \frac{d}{\chi}\delta m\right)}{\Gamma\left(\frac{\Delta md+d}{2(d-1)} + \frac{d}{\chi}(\delta m+1)\right)} \left(\frac{z_\star}{z_h}\right)^{\frac{2(d-1)d}{\chi}\delta m}. \end{aligned} \tag{4.17}$$

The redefinition of the index of summation guarantees that the arguments of the numerator Gamma functions differ by integer values from the denominator Gamma

functions. Therefore, the ratio can be written as products

$$\frac{\hat{c}_{\delta m+1}}{\hat{c}_{\delta m}} = \left(\frac{z_\star}{z_h}\right)^{\frac{2(d-1)d}{\chi}\delta m} \times \prod_{j=0}^{2(d-1)/\chi-1} \left(\frac{\frac{1}{d}-\frac{1}{2}+\Delta m+\frac{2(d-1)}{\chi}\delta m+j}{\frac{1}{d}+\Delta m+\frac{2(d-1)}{\chi}\delta m+j}\right) \times \prod_{k=0}^{d/\chi-1} \left(\frac{\frac{\Delta md+1}{2(d-1)}+\frac{d}{\chi}\delta m+k}{\frac{\Delta md+d}{2(d-1)}+\frac{d}{\chi}\delta m+k}\right).$$

This simplifies to

$$\frac{\hat{c}_{\delta m+1}}{\hat{c}_{\delta m}} = \left(\frac{z_\star}{z_h}\right)^{\frac{2nd}{\chi}\delta m} \times \prod_{j=0}^{2n/\chi-1} \left(\frac{\delta m+c_{j-\frac{1}{2}}}{\delta m+c_j}\right) \cdot \prod_{k=0}^{d/\chi-1} \left(\frac{\delta m+a_{k+\frac{1}{2}}}{\delta m+a_{k+1}}\right). \tag{4.18}$$

where the parameters are defined as

$$a_i = \frac{\chi}{2(d-1)d}\Big(\Delta md+1+2(d-1)i\Big), \tag{4.19a}$$

$$c_j = \frac{\chi}{2(d-1)}\Big(\Delta m+j\Big)+\frac{\chi}{2d(d-1)}. \tag{4.19b}$$

The parameters a_i are already relevant for the minimal surface. The new parameters c_j are up to a constant shift identical to the parameters b_j defined for the minimal surface calculation. Therefore, I simplified the power series $\mathcal{I}$ as $\frac{2(d-1)}{\chi}$ hypergeometric functions

$$\mathcal{I} = \frac{z_\star\sqrt{\pi}}{2(d-1)} \sum_{\Delta m=0}^{\frac{2(d-1)}{\chi}-1} \frac{\left(\frac{1}{d}-\frac{1}{2}\right)_{\Delta m}}{\left(\frac{1}{d}\right)_{\Delta m}} \frac{\Gamma\left(\frac{d}{\chi}a_0\right)}{\Gamma\left(\frac{d}{\chi}a_{\frac{1}{2}}\right)} \left(\frac{z_\star}{z_h}\right)^{d\Delta m} \times {}_{\frac{3d-2}{\chi}+1}F_{\frac{3d-2}{\chi}}\left(\begin{matrix}1, a_0, \ldots, a_{\frac{d}{\chi}-1}, c_{-\frac{1}{2}}, \ldots, c_{\frac{2(d-1)}{\chi}-\frac{3}{2}} \\ a_{\frac{1}{2}}, \ldots, a_{\frac{d}{\chi}-\frac{1}{2}}, c_0, \ldots, c_{\frac{2(d-1)}{\chi}-1}\end{matrix}\middle| \left(\frac{z_\star}{z_h}\right)^{\frac{2(d-1)d}{\chi}}\right). \tag{4.20}$$

The finite part of the volume simplifies to

$$\mathcal{V}_{\text{finite}} = -\frac{\sqrt{\pi}L^d}{(d-1)^2}\frac{\tilde{\ell}^{d-2}}{{z_\star}^{d-2}} \sum_{\Delta m=0}^{\frac{2(d-1)}{\chi}-1} \frac{\left(\frac{1}{d}-\frac{1}{2}\right)_{\Delta m}}{\left(\frac{1}{d}\right)_{\Delta m}} \frac{\Gamma\left(\frac{d}{\chi}a_0\right)}{\Gamma\left(\frac{d}{\chi}a_{1/2}\right)} \left(\frac{z_\star}{z_h}\right)^{\Delta md} \times {}_{\frac{3d-2}{\chi}+1}F_{\frac{3d-2}{\chi}}\left(\begin{matrix}1, a_0, \ldots, a_{\frac{d}{\chi}-1}, c_{-\frac{1}{2}}, \ldots, c_{\frac{2(d-1)}{\chi}-\frac{3}{2}} \\ a_{\frac{1}{2}}, \ldots, a_{\frac{d}{\chi}-\frac{3}{2}}, c_0, \ldots, c_{\frac{2(d-1)}{\chi}-1}\end{matrix}\middle| \left(\frac{z_\star}{z_h}\right)^{\frac{2(d-1)d}{\chi}}\right). \tag{4.21}$$

I derived the corresponding width of the strip in the previous section (3.72a) as

$$\ell = \frac{\sqrt{\pi} z_\star}{d-1} \sum_{\Delta m=0}^{\frac{2(d-1)}{\chi}-1} \frac{1}{\Delta m!} \left(\frac{1}{2}\right)_{\Delta m} \left(\frac{z_\star}{z_h}\right)^{\Delta m d} \frac{\Gamma\left(\frac{d}{\chi} a_{1/2}\right)}{\Gamma\left(\frac{d}{\chi} a_1\right)}$$
$$\times \ {}_{\frac{3d-2}{\chi}+1}F_{\frac{3d-2}{\chi}} \left(\begin{matrix} 1, a_{\frac{1}{2}}, \ldots, a_{\frac{d}{\chi}-\frac{1}{2}}, b_{\frac{1}{2}}, \ldots, b_{\frac{2(d-1)}{\chi}-\frac{1}{2}} \\ a_1, \ldots, a_{\frac{d}{\chi}}, b_1, \ldots, b_{\frac{2(d-1)}{\chi}} \end{matrix} \middle| \left(\frac{z_\star}{z_h}\right)^{\frac{2(d-1)d}{\chi}} \right), \tag{4.22}$$

where the parameter b_i is defined as

$$b_j = \frac{\chi}{2(d-1)} \Big(\Delta m + j\Big). \tag{4.23}$$

Figure 4.4 shows the results for different spacetime dimensions in comparison to the zero-temperature result.

4.2.2 High-Temperature/Large-Strip Limit and Comparison to Area

In Equation (3.72b) of chapter 3, I presented my analytic result for the entanglement entropy or equivalently for the area of the Ryu-Takayanagi surface as

$$\mathcal{A} = \frac{2L^{d-1}}{d-2} \left(\frac{\tilde{\ell}}{\epsilon}\right)^{d-2} + \frac{\sqrt{\pi} L^{d-1}}{d-1} \frac{\tilde{\ell}^{d-2}}{z_\star{}^{d-2}} \sum_{\Delta m=0}^{\frac{2(d-1)}{\chi}-1} \frac{(1/2)_{\Delta m}}{\Delta m!} \frac{\Gamma\left(\frac{d}{\chi} a_{-1/2}\right)}{\Gamma\left(\frac{d}{\chi} a_0\right)} \left(\frac{z_\star}{z_h}\right)^{\Delta m d}$$
$$\times \ {}_{\frac{3d-2}{\chi}+1}F_{\frac{3d-2}{\chi}} \left(\begin{matrix} 1, a_{-\frac{1}{2}}, \ldots, a_{\frac{d}{\chi}-\frac{3}{2}}, b_{\frac{1}{2}}, \ldots, b_{\frac{2(d-1)}{\chi}-\frac{1}{2}} \\ a_0, \ldots, a_{\frac{d}{\chi}-1}, b_1, \ldots, b_{\frac{2(d-1)}{\chi}} \end{matrix} \middle| \left(\frac{z_\star}{z_h}\right)^{\frac{2(d-1)d}{\chi}} \right). \tag{4.24}$$

Let us compare the result for the area to the result for the volume inside the Ryu-Takayanagi surface. The UV-divergent part of the minimal area and the one of the volume inside it are different: it is proportional to the area of the boundary of the strip for the area whereas for it is proportional to the volume of the strip for the volume. However, the structure of the power series for the UV-finite part is the same[4], but the coefficients are different. This similarity between the power series is discussed in [134].

Similarly as before, I put special focus on the high-temperature limit. In Chapter 3, I showed how the width and the area both diverge logarithmically. Hence, the

[4]The hypergeometric functions can be expressed as power series in $(z_\star/z_h)^{2(d-1)d/\chi}$.

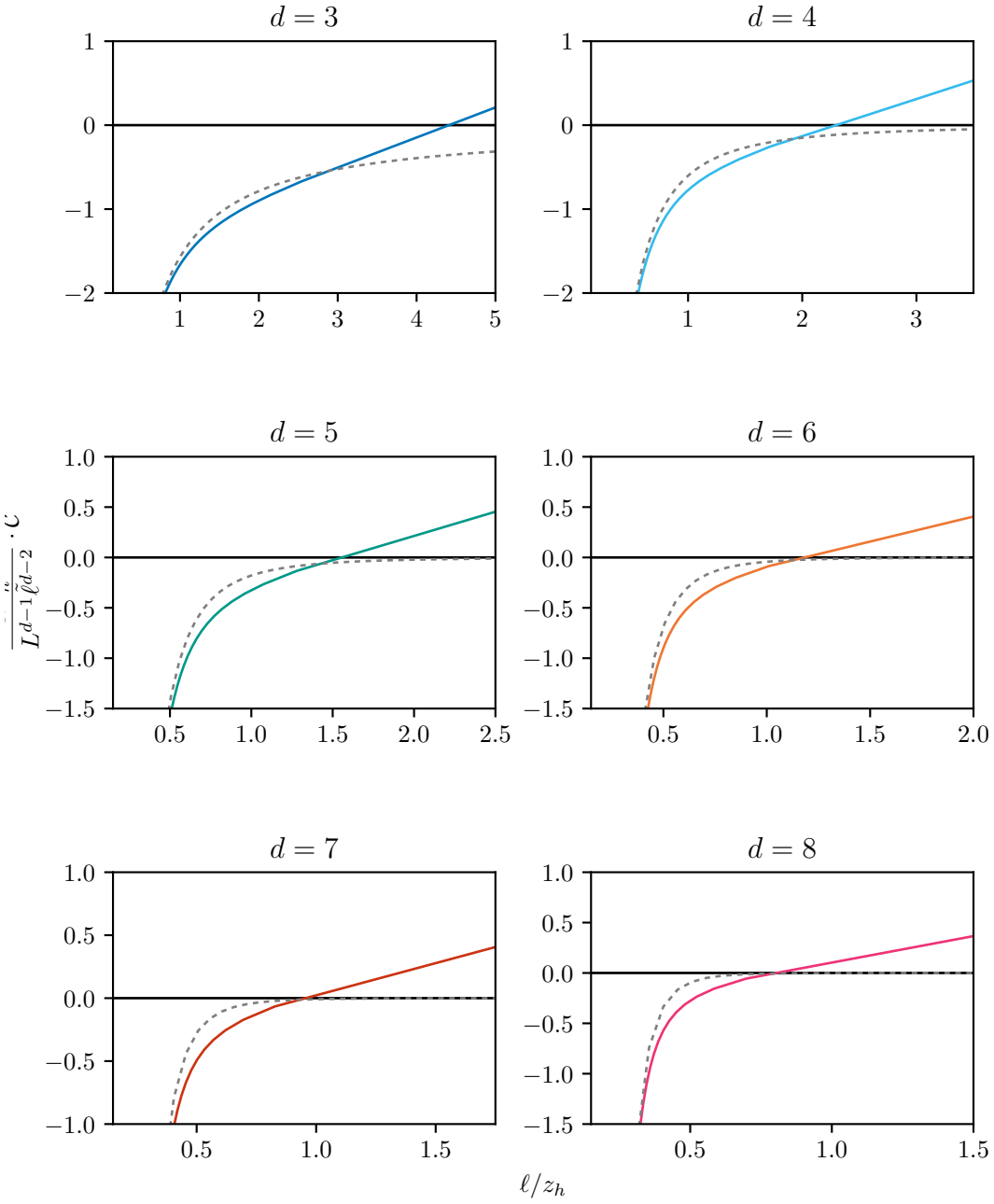

Figure 4.4: Subregion Complexity for different Dimensions.
We subtracted the cutoff term. The dotted grey line is the zero-temperature result.

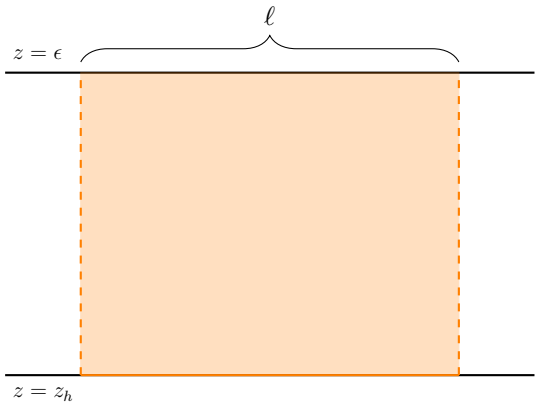

Figure 4.5: Rectangular approximation of the Ryu-Takayanagi surface.

area becomes extensive and the entanglement entropy is in leading order the thermal entropy of the region. While the hypergeometric functions for the volume have different parameters then the one for the volume (4.21), the divergent behavior (c.f. (B.8)) is the same. Therefore, the volume diverges logarithmically as the turning point approaches the horizon and has the same divergent behavior as the width of the strip. The leading contribution in the high-temperature limit is a therefore a volume behavior. The coefficient can be obtained by careful analysis of the divergent behavior described in Equation (B.8) in the appendix.

I take an alternative approach in the following: I obtain it by considering the rectangular approximation as discussed for the area in Section 3.2.3. The Ryu-Takayanagi surface in the high-temperature/large-width limit is approximated by a rectangular surface with two vertical pieces falling from a boundary to the horizon and a horizontal piece along the horizon. Figure 4.5 shows this construction. The volume inside this rectangular surface is

$$\begin{aligned}\mathcal{V}_{\text{disc.}} &= \ell\tilde{\ell}^{d-2}\int_{\epsilon}^{z_h}\frac{L^d}{z^d}\sqrt{b(z)}^{-1},\\ &= L^d\ell\tilde{\ell}^{d-2}\left(\frac{\sqrt{\pi}\Gamma\left(\frac{1}{d}-1\right)}{d\Gamma\left(\frac{1}{d}-\frac{1}{2}\right){z_h}^{d-1}}+\frac{\epsilon^{1-d}}{d-1}\right).\end{aligned} \tag{4.25}$$

Therefore, the high-temperature/large-volume limit is in leading order

$$\mathcal{V}_{\text{disc.}} \approx \left(\frac{L^d}{d-1}\cdot\frac{1}{\epsilon^{d-1}}+\frac{L^d}{z_h^{d-1}}\frac{\sqrt{\pi}\Gamma\left(\frac{1}{d}-1\right)}{d\cdot\Gamma\left(\frac{1}{d}-\frac{1}{2}\right)}\right)\ell\tilde{\ell}^{d-2}. \tag{4.26}$$

This extensive behavior is also observed for the complexity of formation for the whole

system [132]. The authors introduced the complexity of formation as difference to the vacuum AdS result, i.e.

$$\Delta\mathcal{C} = \mathcal{C} - \mathcal{C}|_{T=0}. \tag{4.27}$$

In particular, the extensive behavior also observed above implies that the complexity of formation is proportional to the thermal entropy[5]. Written out, the authors found

$$\Delta\mathcal{C} = k_d S_{\text{therm.}}, \qquad k_d = 4\sqrt{\pi}\frac{d-2}{d-1}\frac{\Gamma\left(1+\frac{1}{d}\right)}{\Gamma\left(\frac{1}{2}+\frac{1}{d}\right)} \tag{4.28}$$

for AdS Schwarzschild, which agrees with the extensive behavior discussed above.

For the entanglement entropy, I was able to write the result in an alternative form (3.76): the divergent behavior is completely expressed in terms of the width and the remaining part is finite in the large-width/high-temperature limit. This was possible because the parameter of the hypergeometric functions appearing in the area result only differ by integer values from the result for the width. Properties of hypergeometric functions then give a linear relationship between these. This is not possible for the volume. Since the parameter appearing in the hypergeometric functions is c_j instead of b_j, there is an additional shift of $\frac{1}{d}$, which prohibits to use the same procedure as for the area.

As shown above, the high-temperature behavior of area and volume is the same: both are extensive and therefore proportional to the thermal entropy. Furthermore, we discussed how the structure of area and volume as power series are the same, but have different coefficient. This gives rise to one crucial difference: the leading correction to the area is positive, whereas the leading correction to the volume is negative. Explicitly, the leading order corrections are both of the same form

$$\mathcal{A} = \mathcal{A}|_{T=0} + c_{\mathcal{A}} \cdot (\ell T)^2 + \mathcal{O}(\ell T)^{d+2}, \tag{4.29a}$$

$$\mathcal{V} = \mathcal{V}|_{T=0} + c_{\mathcal{V}} \cdot (\ell T)^2 + \mathcal{O}(\ell T)^{d+2}. \tag{4.29b}$$

As discussed in Equation (3.74), the coefficient $c_{\mathcal{A}}$ is positive and related to the entanglement temperature (see [124]). The corresponding coefficient for the volume $c_{\mathcal{V}}$ is negative. Furthermore, we discussed in Section 3.3.4 that the entanglement entropy is increased due to the temperature. This is not the case for the volume inside

[5]For other geometries, this is only valid in the high-temperature limit [132].

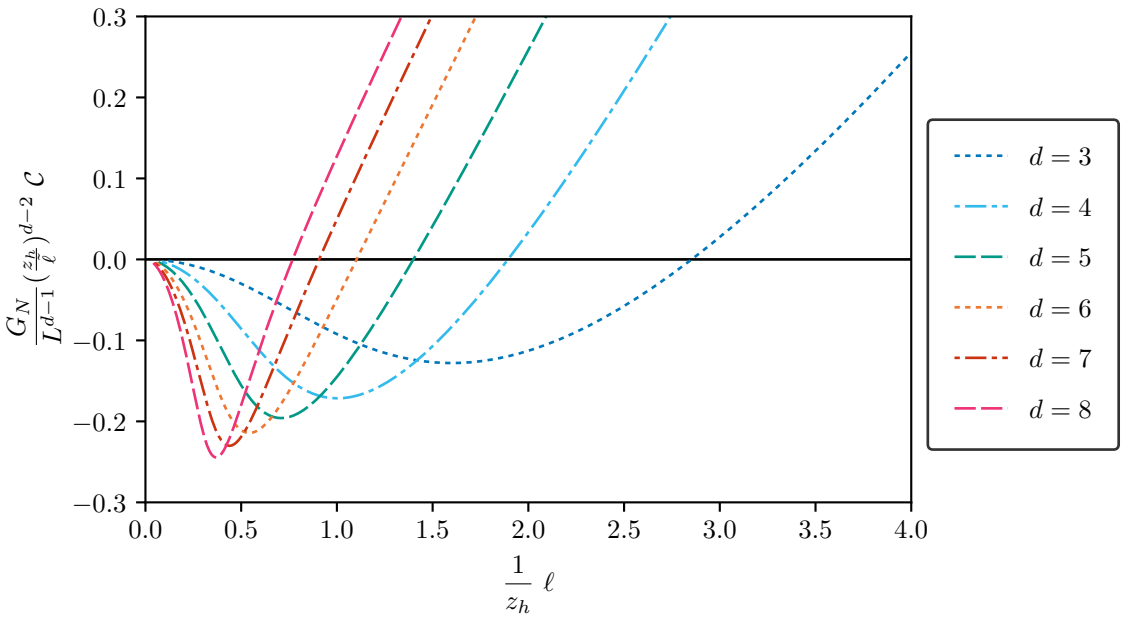

Figure 4.6: Result for Subregion Complexity of Formation at finite Temperature.

the Ryu-Takayanagi surface. Since the leading order correction at low-temperature is negative and the leading order behavior at high-temperature is extensive and positive, there is a transition between reduced complexity due to temperature at low-temperature/small-width and increased complexity at high-temperature/large-strip. This was already discovered qualitatively in [136]. This difference can be studied by looking at the complexity of formation, i.e.

$$\Delta\mathcal{C} = \mathcal{C} - \mathcal{C}|_{T=0}. \tag{4.30}$$

for the reduced states. Figure 4.6 shows the complexity of formation for my result presented in Equation (4.21).

Therefore, there is a critical width at which the subregion complexity at finite temperature agrees with the subregion complexity at zero temperature. At this critical width the sign of $\Delta\mathcal{C}$ changes. Using my analytic result, I determined it numerically for different spacetime dimension d. The result is shown in Figure 4.7.

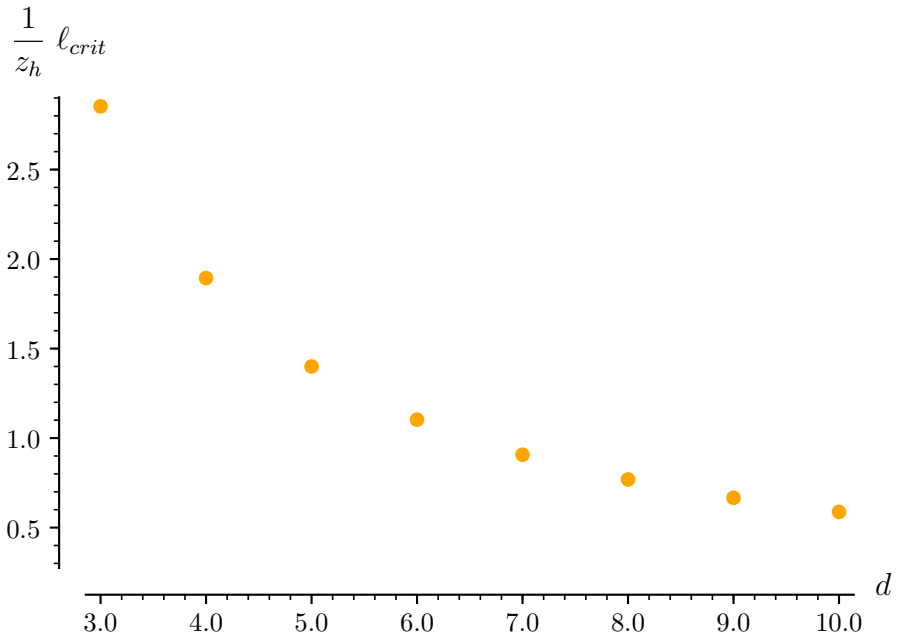

Figure 4.7: Critical Length.
For AdS Schwarzschild, the subregion complexity becomes larger at the critical length than the subregion complexity for the vacuum solution.

4.3 MERA Approximation

To gain some intuition, let us take a look at the corresponding MERA network. Tensor networks and MERA in particular are reviewed in Section 2.5.4. In particular, MERA can be understood as reproducing a discrete version of AdS/CFT. The tensor network model dual to a thermal state is proposed in [100, 101, 137] and shown in Figure 4.8. The network corresponds to a spatial slice in the two-sided AdS black hole. The open indices at the top and at the bottom correspond to the two CFTs of the TFD state. The discrete spins are grouped into blocks of two, on which then a coarse graining operation is applied. These are the isometries in the network. Additionally, disentanglers act on neighboring spins in separate blocks to remove short-range correlations appropriately. These are not shown explicitly here. In the UV, the tensors in the MERA network for the finite temperature state are the same as for the ground state. They coarse-grain the state layer by layer. The obtained reduced states become more and more mixed. At some point, the effective temperature becomes infinite and the state infinitely mixed. At this point, the tensor network ends in fixed point tensors, which are responsible for the thermal

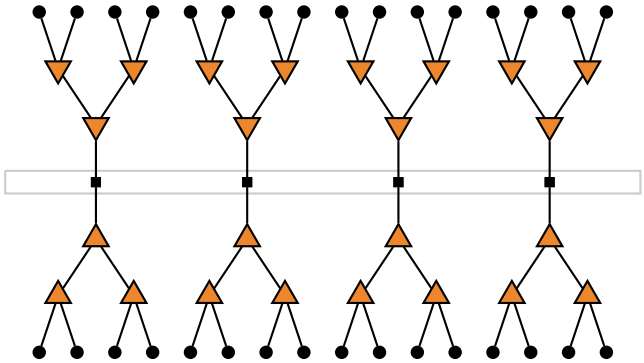

Figure 4.8: MERA Network for a Thermal State.

correlations and glue the two networks starting from the different boundaries together. These fixed point tensors form the bridge layer. The comparison between the MERA network and the gravity dual is summarized in Table 4.1.

The advantage of tensor network is that they give some intuition about complexity. The analog of the Ryu-Takayanagi surface, i.e. the minimal surface anchored on the boundary is the minimal-cut surface. Complexity in tensor networks is measured by the number of tensors (i.e. isometries and disentanglers). Therefore, there is also a notion of subregion complexity as the number of tensors inside the minimal-cut surface. Instead of doing numerical calculations in MERA, I use the tensor network picture to obtain a gravity setup corresponding to it: a AdS hard wall model. Afterwards, I calculate the subregion complexity in this setup and compare it to my previous results.

Table 4.1: Comparison between MERA and AdS Picture.

open indices at top and bottom	$\longleftrightarrow$	two entangled CFTs
tensor network	$\longleftrightarrow$	spacelike cross-section of black hole
coarse graining direction	$\longleftrightarrow$	radial direction
bridge layer of fixed point tensors	$\longleftrightarrow$	Einstein-Rosen bridge, horizon at z_h

4.3.1 Dual Gravity Picture

The tensor network for the thermal states consists of two truncated vacuum networks glued together along a bridge layer. This can be translated into a gravity picture. The transition is shown in Table 4.2. The corresponding metric is

$$\mathrm{d}s^2 = \frac{L^2}{z^2}\left(-\mathrm{d}t^2 + \mathrm{d}z^2 + \mathrm{d}\vec{x}^2\right), \tag{4.31a}$$

$$z \leq z_h \tag{4.31b}$$

and describes vacuum AdS with a hard wall at radial position z_h. In the following, I use this hard wall model to calculate the subregion complexity. Later, the result is compared to the previous results for AdS Schwarzschild. In particular, I empathize how the bridge tensors influence the complexity and how this fixes the sign change of $\Delta\mathcal{C}$.

To analyze the Ryu-Takayanagi surfaces and the complexity in this setup, we first take a look at the vacuum results. These are valid as long as the (vacuum) minimal surface does not reach past z_h. If the vacuum turning point lies deeper in the bulk, the minimal surface in this geometry is truncated at the horizon and connected along the horizon. This truncated surface is shown in Figure 4.9.

In the following, I fist consider the vacuum AdS calculation which applies to small boundary regions. Afterwards, I calculate the minimal area and enclosed volume of the truncated surface discussed above. Furthermore, there is a competing surface: the rectangular one. I show how this surface is always larger than the truncated one and there is no phase transition.

Table 4.2: Inspiration for Gravity Dual from MERA.

UV part identical to vacuum	$\rightarrow$	geometry unchanged for $0 < z < z_h$
IR part removed	$\rightarrow$	hard IR wall at z_h
fixed point tensors of bridge	$\rightarrow$	additional contribution to complexity

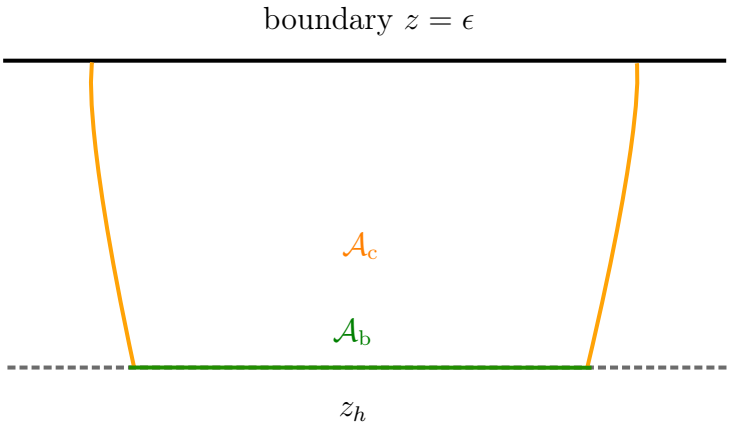

Figure 4.9: Ryu-Takayanagi Surface in hard wall Geometry.
The discussed MERA network for the TFD state inspires to consider the following setup: we consider pure AdS with a hard-wall at $z = z_h$ (dashed line). The minimal surfaces consists of two parts: the minimal surface for the zero-temperature case which is cut off at z_h (orange) and a piece along z_h (green). These correspond to $\mathcal{A}_c$ and $\mathcal{A}_b$.

4.3.2 Ryu-Takayanagi Surface in pure AdS

In the following, we rederive the vacuum result which applies to the hard wall geometry as long as the surface stays outside the wall. I start with the integral expressions for the width of the strip and the area of the minimal surface derived in Chapter 3. The results (3.19) reduce to

$$\ell = 2\int_0^{z_\star} \mathrm{d}z \, \left(\frac{z}{z_\star}\right)^{d-1} \frac{1}{\sqrt{1-(z/z_\star)^{2(d-1)}}} = 2z_\star\sqrt{\pi}\cdot\frac{\Gamma\left(\frac{d}{2(d-1)}\right)}{\Gamma\left(\frac{1}{2(d-1)}\right)} \tag{4.32a}$$

when we integrate over the whole range. The indefinite integral evaluates to

$$\ell = \left[\frac{2}{d}z_\star\left(\frac{z}{z_\star}\right)^d {}_2F_1\left(\frac{1}{2},\frac{d}{2(d-1)};\frac{d}{2(d-1)}+1;\left(\frac{z}{z_\star}\right)^{2(d-1)}\right)\right]_0^{z_\star}, \tag{4.32b}$$

and will be useful later. For the minimal area, we obtain

$$\mathcal{A} = \int_\epsilon^{z_\star} \mathrm{d}z \; z^{1-d}\frac{2L^{d-1}\tilde{\ell}^{d-2}}{\sqrt{1-(z/z_\star)^{2(d-1)}}} = \cdots + \frac{\sqrt{\pi}L^{d-1}\tilde{\ell}^{d-2}}{(d-1){z_\star}^{d-2}}\frac{\Gamma\left(\frac{2-d}{2(d-1)}\right)}{\Gamma\left(\frac{2-d}{2(d-1)}+\frac{1}{2}\right)}, \tag{4.33a}$$

where the dots represent the usual UV-divergent term. Before evaluating the expression on the boundary points, the indefinite integral reduces to[6]

$$\mathcal{A} = -\frac{2L^{d-1}\tilde{\ell}^{d-2}}{(d-2){z_\star}^{d-2}}\left[\left(\frac{z}{z_\star}\right)^{2-d}{}_2F_1\left(\frac{1}{2},\frac{2-d}{2(d-2)};\frac{d}{2(d-1)};\left(\frac{z}{z_\star}\right)^{2(d-1)}\right)\right]_\epsilon^{z_\star}. \quad (4.33b)$$

For the volume calculation, κ reduces to $\kappa = -z^{1-d}/(d-1)$. Using our previous results (4.8), the volume can be written as

$$\begin{aligned}\mathcal{V} &= -2L^d\tilde{\ell}^{d-2}[x(z)\kappa(z)]_\epsilon^{z_\star} - \frac{2L^d\tilde{\ell}^{d-2}}{(d-1)z_\star^{d-1}}\int_0^{z_\star}\mathrm{d}z\sqrt{1-\left(\frac{z}{z_\star}\right)^{2(d-1)}}^{-1},\\ &= \text{UV term} - \frac{2\sqrt{\pi}L^d\tilde{\ell}^{d-2}\Gamma\left(1+\frac{1}{2(d-1)}\right)}{(d-1)\Gamma\left(\frac{1}{2}+\frac{1}{2(d-1)}\right){z_\star}^{d-2}},\end{aligned} \quad (4.34a)$$

where the UV-divergent term is the usual power-law dependent term. If we consider the intermediate step after determining the indefinite integral and before plugging in the boundary values, we obtain

$$\mathcal{V} = \frac{2L^d\tilde{\ell}^{d-2}}{d-1}\left[x(z)z^{1-d}\right]_\epsilon^{z_\star} - \left[\frac{2L^d\tilde{\ell}^{d-2}\,z}{(d-1)z_\star^{d-1}}\,{}_2F_1\left(\left.\begin{matrix}\frac{1}{2},\frac{1}{2(d-1)}\\ 1+\frac{1}{2(d-1)}\end{matrix}\right|\left(\frac{z}{z_\star}\right)^{2(d-1)}\right)\right]_0^{z_\star} \quad (4.34b)$$

At zero temperature, we can invert the result for the width (4.32a). This has the consequence that both the area and the enclosed volume can be expressed directly in terms of the width ℓ. While these results are only valid for $z_\star < z_h$ in the wall geometry, we can still use $z_\star$ as a parameter for larger regions. Therefore, if we use the parameter $z_\star$ in the following, we consider a strip with the width $\ell(z_\star)$ as given in the vacuum result (4.32a).

[6]Notice the alternative notation for hypergeometric functions

$${}_pF_q\left(a_1,\ldots,a_p;b_1,\ldots,b_q;u\right) = {}_pF_q\left(\left.\begin{matrix}a_1,\ldots,a_p\\ b_1,\ldots,b_q\end{matrix}\right|u\right),$$

which is sometimes used to save space.

4.3.3 Ryu-Takayanagi Surface in Wall Geometry

The zero-temperature result is valid for minimal surfaces with vacuum turning point $z_\star < z_h$, i.e. for

$$\ell < \ell_{\text{crit}} = 2z_h\sqrt{\pi}\cdot\frac{\Gamma\left(\frac{d}{2(d-1)}\right)}{\Gamma\left(\frac{1}{2(d-1)}\right)}. \tag{4.35}$$

Therefore, we have to consider a different result for the strips wider than a critical width ℓ_{crit}: the truncated Ryu-Takayanagi surface. This is shown in Figure 4.9. There are two contributions to the area of this surface. First, I calculate the area arising from parts connecting the boundary to the wall. Using the indefinite integral in (4.33b) and only integrating up to the wall yields

$$\mathcal{A}_{\text{c}} = \text{UV term} - \frac{2L^{d-1}\tilde{\ell}^{d-2}}{(d-2){z_h}^{d-2}}\,{}_2F_1\left(\frac{1}{2},\frac{2-d}{2(d-1)};\frac{d}{2(d-1)};\left(\frac{z_h}{z_\star}\right)^{2(d-1)}\right). \tag{4.36}$$

Furthermore, I have to determine the width along the wall we still have to close. Using (4.32b) and integrating from z_h to $z_\star$ yields

$$\left[\ell(z_\star) - \frac{2}{d}z_\star\left(\frac{z_h}{z_\star}\right)^{d}\,{}_2F_1\left(\frac{1}{2},\frac{d}{2(d-1)};\frac{d}{2(d-1)}+1;\left(\frac{z_h}{z_\star}\right)^{2(d-1)}\right)\right]$$

for the width along the wall. Using the geometry of the wall, this piece has the area

$$\begin{aligned}\mathcal{A}_{\text{b}} &= \left[\frac{2}{d}z_\star\left(\frac{z}{z_\star}\right)^{d}\,{}_2F_1\left(\frac{1}{2},\frac{d}{2(d-1)};\frac{d}{2(d-1)}+1;\left(\frac{z}{z_\star}\right)^{2(d-1)}\right)\right]_{z_h}^{z_\star}\cdot\frac{\tilde{\ell}^{d-2}L^{d-1}}{{z_h}^{d-1}},\\ &= \left[\frac{\ell}{z_h} - \frac{2}{d}\left(\frac{z_h}{z_\star}\right)^{d-1}\,{}_2F_1\left(\frac{1}{2},\frac{d}{2(d-1)};\frac{3d-2}{2(d-1)};\left(\frac{z_h}{z_\star}\right)^{2(d-1)}\right)\right]\frac{\tilde{\ell}^{d-2}L^{d-1}}{{z_h}^{d-2}}.\end{aligned} \tag{4.37}$$

Combining these results, the area of the surface is given by

$$\begin{aligned}\mathcal{A} = &-\frac{2L^{d-1}\tilde{\ell}^{d-2}}{(d-2){z_h}^{d-2}}\,{}_2F_1\left(\frac{1}{2},\frac{2-d}{2(d-1)};\frac{d}{2(d-1)};\left(\frac{z_h}{z_\star}\right)^{2(d-1)}\right) + \frac{\ell\tilde{\ell}^{d-2}L^{d-1}}{{z_h}^{d-1}}\\ &- \frac{2}{d}\left(\frac{z_h}{z_\star}\right)^{d-1}\,{}_2F_1\left(\frac{1}{2},\frac{d}{2(d-1)};\frac{3d-2}{2(d-1)};\left(\frac{z_h}{z_\star}\right)^{2(d-1)}\right)\frac{\tilde{\ell}^{d-2}L^{d-1}}{{z_h}^{d-2}}\\ &+ \text{UV term}.\end{aligned} \tag{4.38}$$

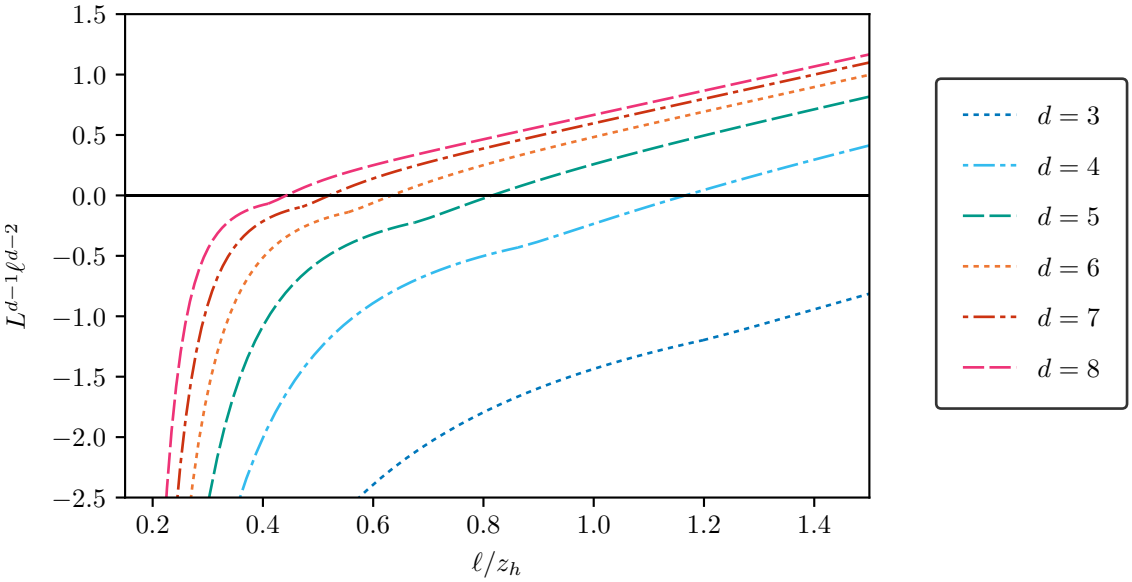

Figure 4.10: Area of Ryu-Takayanagi Surface in hard-wall Geometry.

For these surfaces the width of the strip is given by (4.32a). However, the parameter $z_\star$ does no longer have the interpretation of the turning point, but is only the comparable vacuum turning point. The large-strip/high-temperature limit corresponds to $z_\star/z_h \to \infty$. In this limit, the first term containing a hypergeometric function approaches a constant, whereas the second one goes to zero because of the prefactor. The area therefore behaves as

$$\mathcal{A} \approx \text{UV term} - \frac{2L^{d-1}\tilde{\ell}^{d-2}}{(d-2){z_h}^{d-2}} + \frac{\ell\tilde{\ell}^{d-2}L^{d-1}}{{z_h}^{d-1}} \tag{4.39}$$

and becomes extensive. The extensive term arises from the piece along the bridge. This is in particular important because it produces the contribution from the thermal entropy. The results of the area of th Ryu-Takayanagi surface in the hard-wall geometry are shown in Figure 4.10.

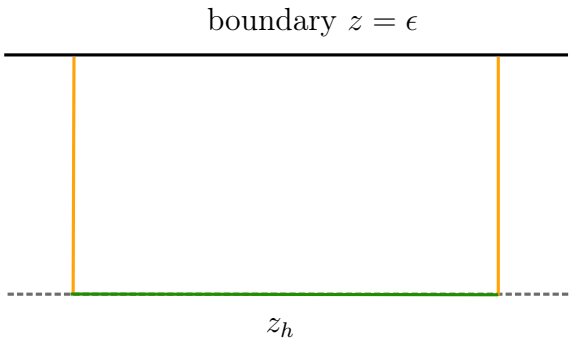

Figure 4.11: Rectangular Surface in hard wall Geometry.

4.3.4 Potential Phase Transition

In principle, there is a competing piecewise-smooth surface: the rectangular one. Figure 4.11 shows how this surface consists of three surfaces: two falling from the boundary to the wall and one along the wall. The area can be calculated as

$$\begin{aligned}\mathcal{A}_{\text{rec}} &= 2\tilde{\ell}^{d-2}\int_{\epsilon}^{z_h} \mathrm{d}z \left(\frac{L}{z}\right)^{d-1} + \frac{L^{d-1}\tilde{\ell}^{d-2}\ell}{{z_h}^{d-2}}, \\ &= \frac{2L^{d-1}}{d-2}\left(\frac{\tilde{\ell}^{d-2}}{\epsilon^{d-2}} - \frac{\tilde{\ell}^{d-2}}{{z_h}^{d-2}}\right) + \frac{L^{d-1}\tilde{\ell}^{d-2}\ell}{{z_h}^{d-2}}. \end{aligned} \tag{4.40}$$

Therefore, I obtain the usual UV-divergent term, an extensive term and a constant shift. This rectangular surface therefore agrees to the high-temperature behavior of the one obtained by truncating the vacuum Ryu-Takayanagi surface.

The difference between the truncated of minimal surface and the rectangular one is

$$\begin{aligned}\Delta\mathcal{A} &= \mathcal{A} - \mathcal{A}_{\text{rec}} \\ &= -\frac{2L^{d-1}\tilde{\ell}^{d-2}}{(d-2){z_h}^{d-2}}\,{}_2F_1\left(\frac{1}{2}, \frac{2-d}{2(d-1)}; \frac{d}{2(d-1)}; \left(\frac{z_h}{z_\star}\right)^{2(d-1)}\right) + \frac{2L^{d-1}\tilde{\ell}^{d-2}}{(d-2){z_h}^{d-2}} \\ &\quad - \frac{2}{d}\left(\frac{z_h}{z_\star}\right)^{d-1}{}_2F_1\left(\frac{1}{2}, \frac{d}{2(d-1)}; \frac{3d-2}{2(d-1)}; \left(\frac{z_h}{z_\star}\right)^{2(d-1)}\right)\frac{\tilde{\ell}^{d-2}L^{d-1}}{{z_h}^{d-2}}\end{aligned}$$

and approaches zero in the large-strip limit $z_\star \to \infty$. Taking the derivative with

respect to the length yields

$$\begin{aligned}\frac{\mathrm{d}}{\mathrm{d}\ell}\Delta\mathcal{A} &\propto \frac{\mathrm{d}}{\mathrm{d}z_\star}\Delta\mathcal{A} \propto -\frac{z_\star}{u}\frac{\mathrm{d}}{\mathrm{d}u}\Delta\mathcal{A} \\ &= -\frac{z_\star}{u}\frac{L^{d-1}\tilde{\ell}^{d-2}}{{z_h}^{d-2}}\,{}_2F_1\left(\frac{1}{2},\frac{2-d}{2(d-1)};\frac{d}{2(d-1)};u\right)\underbrace{\left(1-u^{-\frac{1}{2}}\right)}_{\leq 0} \geq 0, \end{aligned} \tag{4.41}$$

where we defined

$$u = \left(\frac{z_h}{z_\star}\right)^{2(d-1)} < 1.$$

We used the known derivatives of hypergeometric functions, see (B.5) in the appendix. Therefore, the truncated surface approaches the rectangular one monotonically from below and is always the smaller surface. This proves that there is no phase transition for any dimension.

It is interesting to see that $\Delta\mathcal{A}$ approaches zero in this MERA inspired hard wall model for the finite temperature state. In Section 3.2.3 I examined the analog rectangular surface in AdS Schwarzschild and found a constant shift to the area of the real minimal surface.

4.3.5 Volume in the Wall Geometry

Now that I have determined minimal surface, I calculate the volume inside it. Using the intermediate result in (4.34b) and integrating up to the wall yields

$$\begin{aligned}\mathcal{V}_{\text{cupped}} = \text{UV term} &- \frac{2L^d\tilde{\ell}^{d-2}x(z_h)}{(d-1){z_h}^{d-1}} \\ &- \frac{2L^d\tilde{\ell}^{d-2}z_h}{(d-1){z_\star}^{d-1}}\,{}_2F_1\left(\frac{1}{2},\frac{1}{2(d-1)};\frac{2d-1}{2(d-1)};\left(\frac{z_h}{z_\star}\right)^{2(d-1)}\right).\end{aligned}$$

The second term arises from the boundary term after partially integrating. Using that $2x(z_h)$ is the size of the horizontal piece along the horizon, I write the second term in terms of $\mathcal{A}_\text{b}$. This results in

$$\mathcal{V} = \text{UV term} - \frac{\mathcal{A}_\text{b}}{d-1} - \frac{2L^d\tilde{\ell}^{d-2}z_h}{(d-1){z_\star}^{d-1}}\;{}_2F_1\left(\left.\begin{matrix}\frac{1}{2},\frac{1}{2(d-1)}\\ \frac{2d-1}{2(d-1)}\end{matrix}\right|\left(\frac{z_h}{z_\star}\right)^{2(d-1)}\right). \tag{4.42}$$

Without restricting the form of the fixed-term tensors, the complexity contribution arising from the bridge layer has to be proportional to the vertical piece along the bridge

$$\mathcal{V}_{\mathrm{b}} = \left(\alpha + \frac{1}{d-1}\right)\mathcal{A}_{\mathrm{b}}, \tag{4.43}$$

with a not determined constant α. This follows from the picture of having a constant density of the same fixed point tensor forming the bridge. Combining these two results, the analog of the subregion complexity in this MERA approximation is

$$\mathcal{V} = \text{UV term} + \alpha\mathcal{A}_{\mathrm{b}} - \frac{2L^d\tilde{\ell}^{d-2}z_h}{(d-1){z_\star}^{d-1}}\ {}_2F_1\left(\left.\begin{matrix}\frac{1}{2},\frac{1}{2(d-1)}\\ \frac{2d-1}{2(d-1)}\end{matrix}\right|\left(\frac{z_h}{z_\star}\right)^{2(d-1)}\right). \tag{4.44}$$

To be in compliance with [132], the extensive term in the large-width limit should be related to the complexity of formation of the whole state. Therefore, I fix the constant α appropriately and obtain

$$\mathcal{V} = \cdots + \frac{\sqrt{\pi}\Gamma\left(\frac{1}{d}-1\right)}{d\Gamma\left(\frac{1}{d}-\frac{1}{2}\right)}\mathcal{A}_{\mathrm{b}} - \frac{2L^d\tilde{\ell}^{d-2}z_h}{(d-1){z_\star}^{d-1}}\ {}_2F_1\left(\left.\begin{matrix}\frac{1}{2},\frac{1}{2(d-1)}\\ \frac{2d-1}{2(d-1)}\end{matrix}\right|\left(\frac{z_h}{z_\star}\right)^{2(d-1)}\right), \tag{4.45}$$

where the dots are the usual UV-term. The result is shown in Figure 4.12.

4.4 Summary and Discussion

To summarize this chapter, I first reviewed the tensor network for a thermal state and considered the analogue model on the gravity side: vacuum AdS with a hard wall at radial position $z = z_h$. In particular, the structure in the UV is unchanged, the IR is removed and the wormhole connecting two CFTs of the thermofield double state is encoded as a bridge layer. This layer gives an additional contribution to the complexity. This tensor networks corresponds to a hard wall model in pure AdS.

As shown above, the complexity obtained by considering the hard wall model yields a higher subregion complexity than AdS Schwarzschild, see Figure 4.12. For a small strip, this is obvious: the Ryu-Takayanagi surface does not reach the wall and only probes the pure AdS spacetime. Therefore, the result agrees to the zero temperature result, which is larger than the one obtained for AdS Schwarzschild. This shows that the MERA network for a thermal state is more complex than the

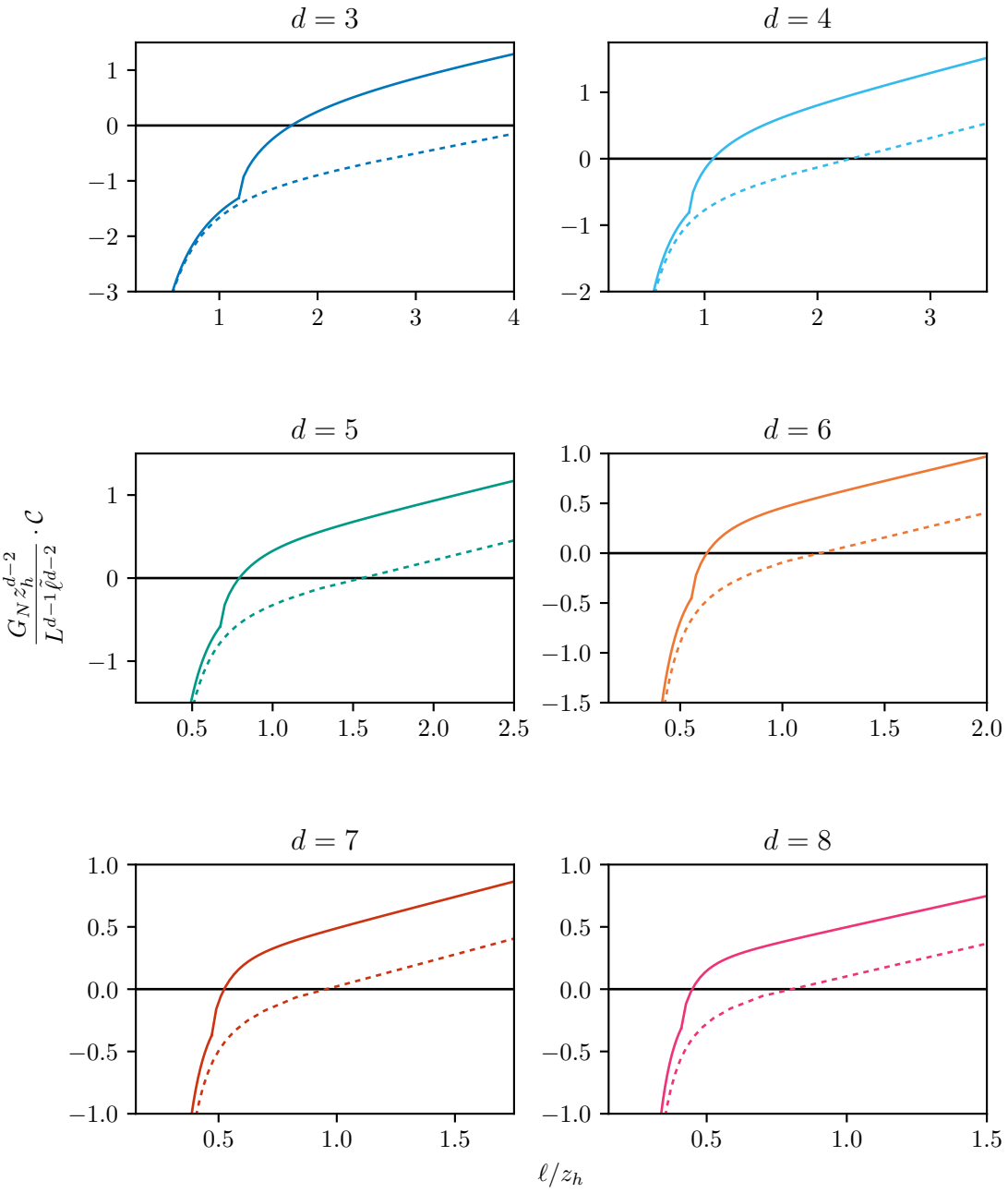

Figure 4.12: Subregion Complexity for hard wall Model.
We subtracted the cutoff term. The dashed line is the AdS Schwarzschild result.

holographic description. Considering larger strips, the minimal surfaces start probing the wall. The subregion complexity for such strips obtains contributions from the bridge. This contribution is in particular responsible for the extensive behavior in the large-strip/high-temperature limit. The comparison presented in Figure 4.12 shows that due to this contribution, the result from the hard wall geometry is larger than the one obtained for AdS Schwarzschild.

In particular, my results show where the tensor network is not optimally efficient in encoding the state. The model was obtained by considering two copies of the MERA network optimized for the vacuum state, truncating them and gluing them together. In particular, the tensors are not changed in the UV. Therefore, further optimization might be possible. This can be seen in the results, where the subregion complexity for the hard wall model is always larger. However, the tremendous difference arises when the minimal surface reaches the wall.

As remarked previously, there is a critical width $\ell_{\text{crit.}}$ at which the subregion complexity at finite temperature becomes larger than the zero temperature result. As discussed above, it is more meaningful to compare our result to the one for the hard wall model then to compare it to the vacuum result. For this MERA inspired model, there is also a critical width, under which the result is given by the vacuum result and above which the bridge layer comes into play. Figure 4.13 compares the values for different spacetime dimension. It shows in particular that the transition from the vacuum minimal surface to the truncated surface always takes place before the critical width of AdS Schwarzschild is reached.

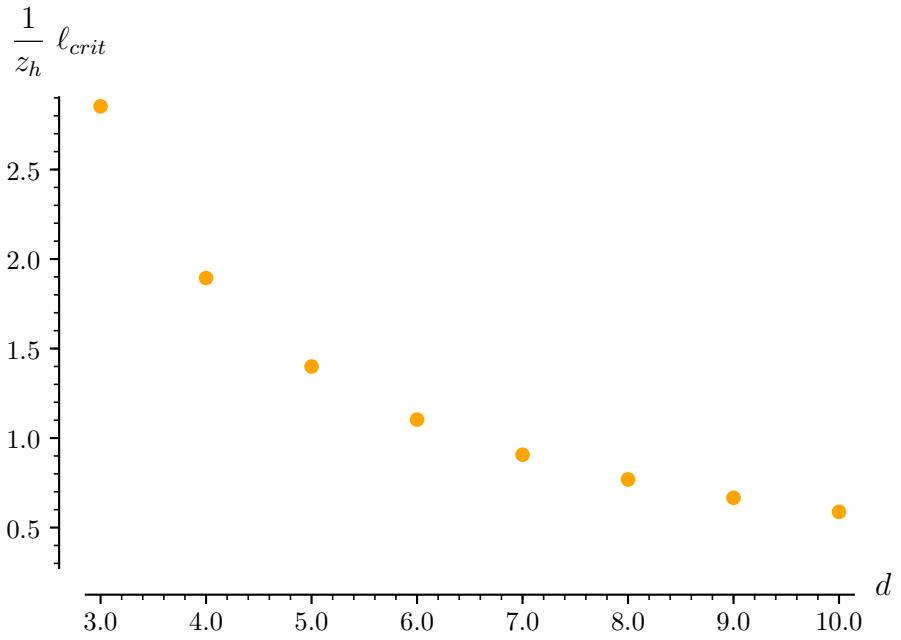

Figure 4.13: Critical Length.
For AdS Schwarzschild, the subregion complexity becomes larger at the critical length than the subregion complexity for the vacuum solution.

Chapter 5

Conformal Transformations and Complexity in AdS_3/CFT_2

In the previous chapter, we examined subregion complexity. It arises as a natural quantity since the Ryu-Takayanagi surface automatically associates a unique bulk volume to a boundary region. However, considering complexity in AdS/CFT is tricky since the field theory definition is not known. To make the problem less involved, we consider the complexity of the pure total state, rather than restricting ourselves to mixed reduced states.

For pure states, quantum information theory defines complexity as difficulty to construct a state from a given reference state. The considered state $|\psi_U\rangle$ is obtained from the reference state $|\mathcal{R}\rangle$ via

$$|\psi_U\rangle = U\,|\mathcal{R}\rangle\,, \tag{5.1}$$

where U is a unitary operator. The *complexity of an operator* is the minimal number of required gates to construct it, i.e.

$$U = \mu_1 \dots \mu_{\mathcal{C}}, \tag{5.2}$$

where the gates μ_i are from the set of allowed gates. Consequently, the *complexity of a state* $|\Psi\rangle$ is defined as the minimal complexity of operators synthesizing it

$$\mathcal{C} = \min_{U \text{ with } |\Psi\rangle = U|\mathcal{R}\rangle} \mathcal{C}(U). \tag{5.3}$$

Every definition of complexity depends implicitly on the chosen reference state and gate set.

The success of the holographic entanglement entropy spiked interest into other

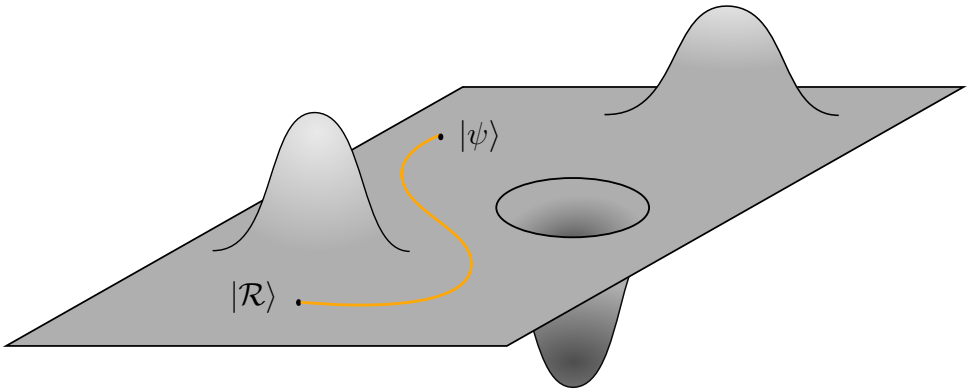

Figure 5.1: Curved Space of States.

quantum information measures such as the complexity [38, 41, 94]. In the following, we follow the holographic *complexity=volume proposal* [38–42]. For the total state, the considered volume is the volume of the maximal co-dimension one slice anchored on the boundary equal time slice. The complexity is conjectured to be

$$\mathcal{C} \propto \frac{\mathcal{V}}{LG_N}. \tag{5.4}$$

The AdS radius L is included for dimensional reasons [39, 40, 47, 48]. In particular, this makes the complexity proportional to the central charge of the field theory.

However, it is an open question whether the maximal volume is an appropriate measure for complexity and what the implicit choices for reference state and gate set are. Therefore, it is of interest to study states for which we know how to construct them. This work focuses on states obtained by conformal transformations in AdS_3/CFT_2. In this lower dimensional example, the conformal group is infinite dimensional and the corresponding operators are known. Considering such a transformation can be done for any CFT without restriction on the particle content. Thus, studying these a state gives insights into the validity of the complexity=volume proposal.

Furthermore, complexity defines a *distance* to the reference state and hence induces a geometry in the space of states. States obtained by conformal transformations applied to the vacuum state are a submanifold in this geometry. Studying small conformal transformations helps to locally map out the geometry of the submanifold. In particular, it is interesting to study whether the vacuum state is in any way exceptional and whether complexity is a good tool to characterize states.

5.1 Conformal Transformations in AdS_3/CFT_2

In this chapter, we focus on AdS_3/CFT_2. The metric dual to the vacuum state of the CFT is

$$ds^2 = \frac{1}{z^2}\left(dz^2 - dx^+ \cdot dx^-\right) = \frac{1}{z^2}\left(dz^2 - dt^2 + dx^2\right). \tag{5.5}$$

In two dimensions, it is convenient to use light-cone coordinates on the boundary, i.e. $x^\pm = t \pm x$. The advantage of considering this lower-dimensional example is that the asymptotic symmetry group is infinitely dimensional. In particular, we can consider conformal transformations $x^\pm = G_\pm(\tilde{x}^\pm)$ with arbitrary functions $G_\pm$. As discussed in Section 2.4.3, these can be realized as a coordinate transformation. Following the conventions of [138, 139], we consider the coordinate transformation

$$x^+ = G_+(\tilde{x}^+), \tag{5.6a}$$
$$x^- = G_-(\tilde{x}^-) \tag{5.6b}$$

for the light-cone coordinates and

$$z = \tilde{z} \cdot \sqrt{|G_+'(\tilde{x}^+)G_-'(\tilde{x}^-)|} \tag{5.6c}$$

for the radial coordinate. The transformation of the radial coordinate is such that a UV cutoff in the field theory corresponds to a cutoff surface $\tilde{z} = \epsilon$ in the new, tilted coordinates. The resulting metric is

$$ds^2 = \frac{d\tilde{z}^2}{\tilde{z}^2} - \frac{d\tilde{x}^+ d\tilde{x}^-}{\tilde{z}^2} + \left(A_+ d\tilde{x}^+ + A_- d\tilde{x}^-\right)^2 - \frac{2d\tilde{z}}{\tilde{z}} \cdot \left(A_+ d\tilde{x}^+ + A_- d\tilde{x}^-\right), \tag{5.7a}$$

with

$$A_\pm = -\frac{1}{2}\frac{G_\pm''(\tilde{x}^\pm)}{G_\pm'(\tilde{x}^\pm)}. \tag{5.7b}$$

This type of geometry is known as Bañados geometries. With the metric in this form, it is not directly obvious why the metric is asymptotically AdS as defined by Brown and Henneaux in [62]. It can be checked that the metric has the right boundary behavior when going to coordinates $\hat{x}^\pm = \tilde{x}^+ \mp A_\mp \cdot z^2$. The metric in the used form has the advantage that we avoid a change of the radial component δg_{zz}.

The special feature of three-dimensional gravity is that is has no propagating

degrees of freedom. Thus, all solutions are locally equivalent up to coordinate transformations. However, there are subtleties when considering spacetimes with boundaries. The transformations we consider here act non-trivially on the boundary. Furthermore, while we see from the transformed metric (5.7) that the boundary metric is not changed, the asymptotic fall-off of the metric is changed. These determine the stress-energy tensor. In the transformed state, we have

$$8\pi G_3 T_{++} = \frac{1}{4G_+'(\tilde{x}^+)^2}\left(3G_+''(\tilde{x}^+)^2 - 2G_+'(\tilde{x}^+)G_+'''(\tilde{x}^+)\right), \tag{5.8a}$$

$$8\pi G_3 T_{--} = \frac{1}{4G_-'(\tilde{x}^-)^2}\left(3G_-''(\tilde{x}^-)^2 - 2G_-'(\tilde{x}^-)G_-'''(\tilde{x}^-)\right), \tag{5.8b}$$

$$8\pi G_3 T_{+-} = 0. \tag{5.8c}$$

As can be seen from Equation (5.8), the resulting states violate the null energy condition (NEC). However, that is not surprising in a quantum field theory [140]: the energy density at a point can be arbitrarily negative, i.e. it is not bounded from below. However, for quantum theories the quantum NEC [141] (QNEC) holds, which bounds the energy density using expressions involving entanglement entropy. Following [142], Bañados geometries in fact saturate the QNEC. The energy of the transformed state is

$$\begin{aligned} E &= \int_{-\infty}^{\infty} \mathrm{d}\tilde{x}\, T_{tt} = \int_{-\infty}^{\infty} \mathrm{d}\tilde{x}\, [T_{++} + T_{--} + 2\,T_{+-}]\,, \\ &= \frac{1}{32\pi G_3}\int_{-\infty}^{\infty} \mathrm{d}x \left[\left(\frac{G_-''(\tilde{x}^-)}{G_-'(\tilde{x}^-)}\right)^2 + \left(\frac{G_+''(\tilde{x}^+)}{G_+'(\tilde{x}^+)}\right)^2\right] > 0. \end{aligned} \tag{5.9}$$

Therefore, we obtain states with positive energy,

The conformal transformation changes the holographic calculation of the complexity in two aspects. Firstly, due to the conformal transformation on the boundary we have to consider a different equal-time slice. Expressing the old time coordinate t in terms of the new coordinates yields a space-dependence

$$t = \frac{1}{2}\left(G_+(\tilde{t}+\tilde{x}) + G_-(\tilde{t}-\tilde{x})\right).$$

It follows that we have different boundary condition for the extremal surface. Secondly, the transformation changes the cutoff surface. Since the complexity is a UV-divergent quantity, a UV cutoff has to be used to regularize it. The conformal

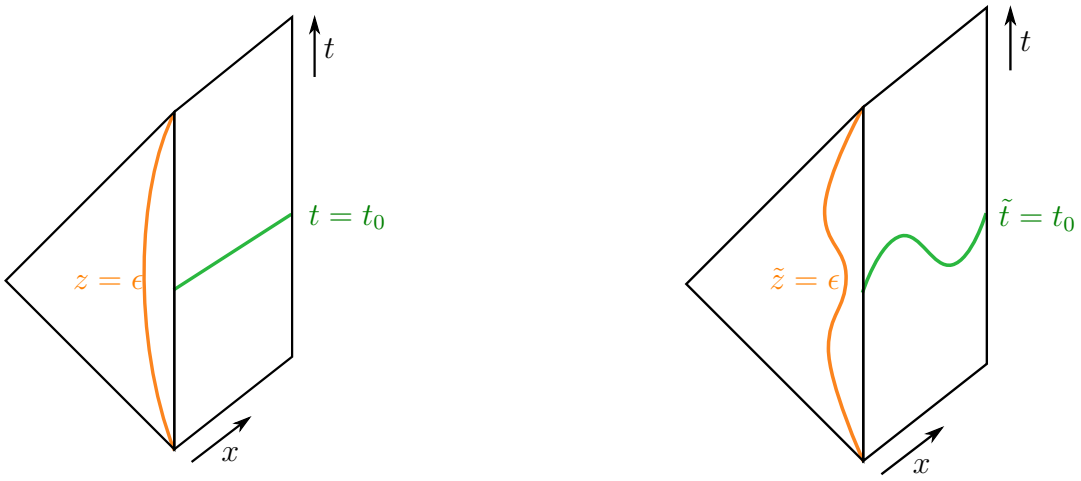

(a) Vacuum State.

(b) Excited State.

Figure 5.2: Bulk Picture of Conformal Transformation.
The excited state can be shown in the original Poincare diagram. The boundary equal time-slice is now curved, i.e. the extremal volume slice is anchored differently on the boundary. Additionally, the radial cutoff is changed.

transformation changes the cutoff to

$$\tilde{z} = \epsilon, \qquad \Longleftrightarrow \qquad z = \epsilon \sqrt{G_+{}'(\tilde{x}^+) G_-{}'(\tilde{x}^-)}. \tag{5.10}$$

These effects are shown in Figure 5.2.

The general problem is highly non-trivial. I considered the simplified case of a small conformal transformation

$$x^+ = G_+(\tilde{x}^+) = \tilde{x}^+ + \sigma\ g_+(\tilde{x}^+), \tag{5.11a}$$
$$x^- = G_-(\tilde{x}^-) = \tilde{x}^- + \sigma\ g_-(\tilde{x}^-), \tag{5.11b}$$

where the expansion parameter is $\sigma \ll 1$. The metric simplifies to

$$\begin{aligned} \mathrm{d}s^2 = {} & \frac{1}{\tilde{z}^2}\,\mathrm{d}\tilde{z}^2 - \frac{1}{\tilde{z}^2}\,\mathrm{d}\tilde{t}^2 + \frac{1}{\tilde{z}^2}\,\mathrm{d}\tilde{x}^2 \\ & + \frac{\sigma}{\tilde{z}}\Big[\Big(g_+{}''\left(\tilde{x}^+\right) + g_-{}''\left(\tilde{x}^-\right)\Big)\mathrm{d}\tilde{t} + \Big(g_+{}''\left(\tilde{x}^+\right) - g_-{}''\left(\tilde{x}^-\right)\Big)\mathrm{d}\tilde{x}\Big]\mathrm{d}\tilde{z} \\ & + \frac{\sigma^2}{4}\left(g_-{}''\left(\tilde{x}^-\right) + g_+{}''\left(\tilde{x}^+\right)\right)\mathrm{d}\tilde{t}^2 + \frac{\sigma^2}{4}\left(g_+{}''\left(\tilde{x}^+\right) - g_-{}''\left(\tilde{x}^-\right)\right)\mathrm{d}\tilde{x}^2 + \ldots. \end{aligned} \tag{5.12}$$

The dots contain off-diagonal terms of order σ^2 and diagonal terms of order σ^3. Ad-

ditionally, the energy momentum tensor is of first order in the expansion parameter

$$8\pi G_3 T_{++} = -\frac{\sigma}{2} g_+'''(\tilde{x}^+) + \frac{\sigma^2}{4}\left(3g_+''(\tilde{x}^+)^2 + 2g_+'(\tilde{x}^+)g_+'''(\tilde{x}^+)\right) + \mathcal{O}(\sigma^3), \quad (5.13a)$$

$$8\pi G_3 T_{--} = -\frac{\sigma}{2} g_-'''(\tilde{x}^-) + \frac{\sigma^2}{4}\left(3g_-''(\tilde{x}^+)^2 + 2g_-'(\tilde{x}^+)g_+'''(\tilde{x}^-)\right) + \mathcal{O}(\sigma^3). \quad (5.13b)$$

The leading order term is an energy fluctuation, which does not contribute to the total energy. In contrast, the second order term produces

$$E = \frac{\sigma^2}{32\pi G_3} \int_{-\infty}^{\infty} \mathrm{d}x \left[g_-''(\tilde{x}^-)^2 + g_+''(\tilde{x}^+)^2\right] > 0. \quad (5.14)$$

To summarize this section, we reviewed how the conformal transformation on the gravity side is realized by a coordinate transformation acting non-trivially on the boundary. Furthermore, we looked more closely on small conformal transformations.

5.2 Operator for Conformal Transformation

In this section, we take a look at the operator corresponding to the conformal transformation. We start by considering a compact spatial direction, i.e. $x \in [0, \ell]$. In this setup, it is more convenient to go to complex coordinates

$$w = \exp\left(i\frac{2\pi}{\ell}\cdot x^+\right), \qquad \bar{w} = \exp\left(i\frac{2\pi}{\ell}\cdot x^-\right). \quad (5.15)$$

In Minkowski signature, these satisfy

$$|w| = 1, \qquad w^\dagger = w^{-1}$$

to ensure $x^\pm \in \mathbb{R}$. The holomorphic component of the stress-energy tensor can be expanded as a power series

$$T_{ww} = T(w) = \sum_n L_n w^{-n-2}. \quad (5.16a)$$

Going back to light-cone coordinates $x^\pm$, the corresponding stress-energy tensor is

$$T_{++} = -\frac{4\pi^2}{\ell^2}\left(w^2 T(w) + const.\right) \quad (5.16b)$$

and the analog expression for T_{--}. The off-diagonal components vanish. Since T_{++} is real, the conditions on L_n are

$$L_n^\dagger = L_{-n}.$$

These coefficients are called Virasoro generators and satisfy the Virasoro algebra, i.e.

$$[L_m, L_n] = (m-n)L_{m+n} + \frac{c}{12}(m^3 - m)\delta_{m+n,0}. \tag{5.17}$$

A small[1] conformal transformation is a transformation of the form

$$w \to w' = w + \varepsilon(w). \tag{5.18}$$

The Fourier decomposition of ε is

$$\varepsilon = \sum_n \varepsilon_n w^{-n+1}. \tag{5.19}$$

The light-cone coordinate x'^+ is real, hence we have

$$\varepsilon_n^* = -\varepsilon_{-n} + \sum_{n_1=-\infty}^{\infty} \varepsilon_{-n_1} \cdot \varepsilon_{n_1-n} + \mathcal{O}(\varepsilon)^3. \tag{5.20}$$

The stress energy tensor is changed by the conformal transformation. The transformation behavior is

$$\tilde{T}(w') = \left(\frac{\partial w'}{\partial w}\right)^{-2} \left(T(w) - \frac{c}{12} S(w', w)\right), \tag{5.21a}$$

where the *Schwarzian derivative* is

$$S(w', w) = \left(\frac{\partial^3 w'}{\partial w^3}\right)\left(\frac{\partial w'}{\partial w}\right)^{-1} - \frac{3}{2}\left(\frac{\partial^2 w'}{\partial w^2}\right)^2 \left(\frac{\partial w'}{\partial w}\right)^{-2}. \tag{5.21b}$$

In [P3], we calculate the change of the stress energy tensor for a small conformal

[1] We talk about a small infinitesimal transformation and not an infinitesimal one since we also consider subleading terms. In particular, we will keep the transformation behavior of $x^\pm$ exact.

transformation

$$\begin{aligned}\delta T(w) \equiv& \tilde{T}(w) - T(w) \\ =& -\varepsilon(w)T'(w) - 2T(w)\varepsilon'(w) - \frac{1}{12}c\varepsilon^{(3)}(w) \\ &+ \frac{1}{12}c\varepsilon^{(4)}(w)\varepsilon(w) + \frac{1}{8}c\varepsilon''(w)^2 + \frac{1}{4}c\varepsilon^{(3)}(w)\varepsilon'(w) + \frac{1}{2}\varepsilon(w)^2T''(w) \\ &+ 3\varepsilon(w)T'(w)\varepsilon'(w) + 2T(w)\varepsilon(w)\varepsilon''(w) + 3T(w)\varepsilon'(w)^2. \end{aligned} \tag{5.22}$$

This extends the already known first order result [138] to second order in ε. We want to express the change of the energy momentum tensor as unitary transformations of its Fourier modes. The corresponding condition is

$$\begin{aligned}\delta T(w) &= \sum_n \delta L_n w^{-n-2} \\ \delta L_k, &\stackrel{!}{=} U^\dagger L_k U - L_k.\end{aligned}$$

The operator implementing this transformation is

$$U = e^{\mathcal{L}+\mathcal{B}}. \tag{5.24}$$

The leading order term ε was already known [138] and my collaborator determined the subleading term [P3], resulting in

$$\mathcal{L} = \sum_n \varepsilon_n L_{-n}, \tag{5.25a}$$

$$\mathcal{B} = \sum_{m,n} \frac{m+n-2}{4}\varepsilon_m\varepsilon_n L_{-n-m}. \tag{5.25b}$$

This expands the CFT operator implementing the conformal transformation up to second order in epsilon. The spatial direction is compact and the result is expressed in terms of the Fourier coefficients.

Let me transform this back into our previous notation. First, we leave the spatial direction compact and express everything in terms of $g_\pm$. The considered conformal transformation is

$$x^+ = G_+(\tilde{x}^+) = \tilde{x}^+ + \sigma\ g_+(\tilde{x}^+). \tag{5.26}$$

The function g_+ is related to the previously defined ε via (see (5.15) and (5.18))

$$\exp\left(-\sigma\ \tfrac{2\pi i}{\ell}\cdot g_+\right) = 1 + \tfrac{\varepsilon}{w}. \tag{5.27}$$

Using the Fourier decomposition of g_+

$$g_+ = \sum_n g_{+,n} w'^{-n}, \qquad\qquad g^*_{+,n} = g_{+,-n}, \tag{5.28}$$

the relationship between ε_n and $g_{+,n}$ is

$$\varepsilon_n \approx -\sigma\ \frac{2\pi i}{\ell} g_{+,n} + \sigma^2\ \frac{2(n-1)\pi^2}{\ell^2} \sum_{n_1} g_{+,n_1} g_{+,n-n_1} + \mathcal{O}(\sigma)^3. \tag{5.29}$$

One has to keep in mind the Fourier decomposition of ε is with respect to w, whereas the Fourier decomposition of g_+ is with respect to w'. This is relevant for obtaining the correct second order term.

The unitary operator can consequently be written as

$$\begin{aligned} U(g_+) = 1 &- \sigma\ \frac{2\pi i}{\ell} \sum_n g_{+,n} L_{-n} - \sigma^2\ \frac{2\pi^2}{\ell^2} \sum_{n_i} g_{+,n_1} g_{+,n_2} L_{-n_1} L_{-n_2} \\ &+ \sigma^2\ \frac{\pi^2}{\ell^2} \sum_{n_i} (n_1 + n_2) g_{+,n_1} g_{+,n_2} L_{-n_1-n_2} + \mathcal{O}(\sigma)^3. \end{aligned} \tag{5.30}$$

The last step is to decompactify the spatial direction, i.e. taking the limit $\ell \to \infty$. This is done by defining

$$\xi = \frac{n}{\ell}, \qquad\qquad \mathrm{d}\xi = \frac{1}{\ell}. \tag{5.31}$$

The expansions in w and w' turn into Fourier transformations for $g_\pm$

$$g_+(\tilde{x}^+) = \int \mathrm{d}\xi\ \underbrace{\ell \cdot g_{+,\ell\xi}}_{\hat{g}_+(\xi)} \exp\bigl(-2\pi i \cdot \tilde{x}^+ \cdot \xi\bigr) \tag{5.32a}$$

and for the stress energy tensor

$$T_{++}(x^+) = -\,4\pi^2 \int \mathrm{d}\xi\ \underbrace{\frac{1}{\ell^2} \ell \cdot L_{\ell\xi}}_{\hat{L}(\xi)}\ \exp\bigl(-2\pi i \cdot x^+ \cdot \xi\bigr). \tag{5.32b}$$

It follows that the operator can be written as

$$U(g_+) = \exp\left(-\sigma\ 2\pi i \int \mathrm{d}\xi\ \hat{g}_+(\xi)\hat{L}(-\xi)\right. \tag{5.33a}$$
$$\left. +\sigma^2\ \pi^2 \iint \mathrm{d}\xi_1 \mathrm{d}\xi_2\ (\xi_1+\xi_2)\hat{g}_+(\xi_1)\hat{g}_+(\xi_2)\hat{L}(-\xi_1-\xi_2)\right) + \mathcal{O}(\sigma)^3$$

or equivalently

$$U(g_+) = \exp\left(\sigma\ \frac{i}{2\pi}\int \mathrm{d}x\ g_+(x)\cdot T_{++}(x)\right. \tag{5.33b}$$
$$\left. -\sigma^2\ \frac{i}{8\pi}\iint \mathrm{d}x_1\mathrm{d}x_2\ g'_+(x_1)g_+(x_2)\cdot T_{++}(x_1+x_2)\right) + \mathcal{O}(\sigma)^3$$

The analog expression is obtained for $U(g_-)$. This differs from the usual CFT approach: usually $U = e^{\mathcal{L}}$ is taken as exact, i.e. higher order corrections do not appear in U but in the transformation behavior of $x^{\pm}$. We approached this differently to keep the transformation behavior of $x^{\pm}$ and hence the diffeomorphism applied on the gravity side exact.

5.3 Change of Holographic Complexity

In this section, I calculate the change of the volume perturbatively for a small conformal transformation. The expansion parameter is σ. The integral expression for the volume is

$$\mathcal{V} = \int_{\epsilon}^{\infty} \mathrm{d}\tilde{z} \int_{\infty}^{\infty} \mathrm{d}\tilde{x}\ \sqrt{\gamma}, \tag{5.34}$$

where γ is the induced metric on the slice and depends on the embedding $\tilde{t}(\tilde{x},\tilde{\lambda})$ implicitly. In lowest order in σ, we obtain the vacuum result

$$\begin{aligned}\mathcal{V}|_{\sigma=0} &= \int \mathrm{d}\tilde{z} \int \mathrm{d}\tilde{x} \frac{1}{\tilde{z}^2}\sqrt{1-\tilde{t}^{(0,1)}(\tilde{x},\tilde{z})^2 - \tilde{t}^{(1,0)}(\tilde{x},\tilde{z})^2},\\ &= \int \mathrm{d}\tilde{z} \int \mathrm{d}\tilde{x} \frac{1}{\tilde{z}^2} = \frac{\mathrm{Vol}(\mathbb{R})}{\epsilon},\end{aligned} \tag{5.35}$$

where the embedding is given by the constant time slice $\tilde{t} = t_0$. The embedding can be expanded as

$$\tilde{t}(\tilde{x}, \tilde{z}) = t_0 + \sigma\, t_1(\tilde{x}, \tilde{z}) + \sigma^2\, t_2(\tilde{x}, \tilde{z}) + \mathcal{O}(\sigma)^3. \tag{5.36}$$

I now expand the volume in powers of σ, i.e.

$$\mathcal{V} = \mathcal{V}_{(0)} + \sigma \mathcal{V}_{(1)} + \sigma^2 \mathcal{V}_{(2)} + \mathcal{O}(\sigma^3) \tag{5.37}$$

where $\mathcal{V}_{(0)} = \mathcal{V}|_{\sigma=0}$. The first order correction is

$$\begin{aligned} \mathcal{V}_{(1)} &= \left.\frac{\delta \mathcal{V}}{\delta t}\right|_{\delta=0} \delta t + \left.\frac{\delta \mathcal{V}}{\delta \gamma_{\mu\nu}}\right|_{\delta=0} \delta\gamma_{\mu\nu}, \\ &= \int \mathrm{d}z (\sqrt{\gamma}\, \gamma^{\mu\nu})\big|_{\delta=0} \delta\gamma_{\mu\nu}, \\ &= 0. \end{aligned} \tag{5.38}$$

The variation with respect of the embedding t vanishes automatically since we consider an extremal embedding. The variation with respect with the induced metric does not vanish, however since γ is diagonal and $\delta\gamma$ only has off-diagonal contributions at leading order, this term also vanishes for the considered metric. Therefore, the term of interest is the term of order σ^2. Calculating it yields

$$\begin{aligned} \mathcal{V}_{(2)} &= \left.\frac{\delta^2 \mathcal{V}}{\delta^2 t}\right|_{\delta=0} \delta t^2 + 2 \left.\frac{\delta^2 \mathcal{V}}{\delta\gamma_{\mu\nu}\delta t}\right|_{\delta=0} \delta\gamma_{\mu\nu}\, \delta t + \left.\frac{\delta^2 \mathcal{V}}{\delta\gamma_{\mu\nu}\delta\gamma_{\eta\omega}}\right|_{\delta=0} \delta\gamma_{\mu\nu}\, \delta\gamma_{\eta\omega}, \\ &= \int_0^\infty \mathrm{d}\tilde{z} \int_{-\infty}^\infty \mathrm{d}\tilde{x} \left[\frac{1}{4\tilde{z}}\, \tilde{t}_1{}^{(0,1)}(\tilde{x}, \tilde{z}) \left(g''_-\left(\tilde{t}_0 - \tilde{x}\right) + g''_+\left(\tilde{t}_0 + \tilde{x}\right)\right) \right. \\ &\quad \left. - \frac{1}{4\tilde{z}^2}\, \tilde{t}_1{}^{(0,1)}\big(\tilde{x}, \tilde{z}\big)^2 - \frac{1}{4\tilde{z}^2}\, \tilde{t}_1{}^{(1,0)}\big(\tilde{x}, \tilde{z}\big)^2 \right]. \end{aligned} \tag{5.39}$$

I obtain contributions arising from varying with respect to the embedding twice and from varying with respect to the embedding and the induced metric. There is no contribution arising from varying with respect of the metric twice. This is due to the form of the metric and its perturbation. Having a metric γ with a small perturbation $\delta\gamma$, the integrand can be written as

$$\sqrt{\det(\gamma + \delta\gamma)} = \sqrt{\det(\gamma)} \left(1 + \frac{\mathrm{Tr}\,(\gamma^{-1}\delta\gamma)}{2} + \frac{\mathrm{Tr}\,(\gamma^{-1}\delta\gamma)^2}{8} - \frac{\mathrm{Tr}\,((\gamma^{-1}\delta\gamma)^2)}{4} \right) + \dots.$$

For the metric I consider (5.13a), the leading order correction is off-diagonal, whereas γ is diagonal. Consequently, the second term only yields a subleading contribution i.e. $\mathrm{Tr}\,\gamma^{-1}\delta\gamma = \mathcal{O}(\sigma)^2$. The leading order term of $\delta\gamma$ contributes to $\mathrm{Tr}((\gamma^{-1}\delta\gamma)^2)$, but this term is exactly canceled from the trace of the second order term arising from $\gamma^{-1}\delta\gamma$.

5.3.1 Embedding of Extremal Slice

The differential equation for t_1 arising from extremizing the volume (5.39) is

$$2{t_1}^{(0,2)}(\tilde{x},\tilde{z}) - \frac{4}{\tilde{z}}\,{t_1}^{(0,1)}(\tilde{x},\tilde{z}) + 2{t_1}^{(2,0)}(\tilde{x},\tilde{z}) = -g_+''(\tilde{x}+t_0) - g_-''(t_0-\tilde{x})\,. \quad (5.40)$$

Since I consider a spacetime with a boundary, the variational principle is only well defined if no boundary term arises. For the integral expression I consider, this requires

$$\lim_{\tilde{z}\to 0}\ \frac{1}{2\tilde{z}}\left(-\frac{4}{\tilde{z}^4}t_1{}^{(0,1)}(\tilde{x},\tilde{z}) - g_-''(t_0-\tilde{x}) - g_+''(t_0+\tilde{x})\right) = 0. \quad (5.41)$$

This constrains the near boundary behavior of t_1. Additionally, I have the boundary condition from demanding that the extremal surface is anchored at $\tilde{t}(\tilde{x},0) = t_0$.

To avoid having to solve this partial differential equation, I use the Fourier transform

$$t_1(\tilde{x},\tilde{z}) = \int_{-\infty}^{\infty} \mathrm{d}\xi\ \hat{t}(\xi,\tilde{z})\ \exp(2\pi i\xi\tilde{x}). \quad (5.42)$$

Furthermore, for the infinitesimal transformation we define

$$g_\pm(\tilde{x}^\pm) = \int_{-\infty}^{\infty} \mathrm{d}\xi\ \hat{g}_\pm(\xi)\exp\big(-2\pi i\cdot\tilde{x}^\pm\cdot\xi\big). \quad (5.43a)$$

$$= \int_{-\infty}^{\infty} \mathrm{d}\xi\ \hat{g}_\pm(-\xi)e^{2\pi i\xi\tilde{t}}\ \exp(\pm 2\pi i\xi\cdot\tilde{x}). \quad (5.43b)$$

The Fourier modes $\hat{g}_\pm$ and $\hat{t}$ have to satisfy

$$\hat{g}_\pm(\xi)^* = \hat{g}_\pm(-\xi), \qquad \hat{t}(\xi)^* = \hat{t}(-\xi) \quad (5.44)$$

for $g_\pm$ and t_1 to be real. To keep the expansion in σ well defined, I assume that $g_\pm$ and $\hat{g}$ are bounded.

This reduces the partial differential equation to an ordinary differential equation

$$2\hat{t}^{(0,2)}(\xi,\tilde{z}) - \frac{4}{\tilde{z}}\hat{t}^{(0,1)}(\xi,\tilde{z}) - 8\pi^2\xi^2\hat{t}(\xi,\tilde{z}) = 4\pi^2\xi^2\left(\hat{g}_+(-\xi)e^{2i\pi\xi t_0} + \hat{g}_-(\xi)e^{-2i\pi\xi t_0}\right). \tag{5.45}$$

Thus, we have a second order differential equation and need two boundary conditions. These are given by having the surface anchored at t_0 and the appropriate boundary behavior to make the variational principle well defined. In this differential equation, ξ reduces to a parameter. I have to consider $\xi > 0$ and $\xi < 0$ separately when fixing the constants of integration. This results in

$$\hat{t}(\xi,\tilde{\lambda}) = \begin{cases} \left(\frac{1}{2}\left(1-e^{2\pi\xi\tilde{z}}\right) + \pi\xi\tilde{z}\right)\left(\hat{g}_-(\xi)e^{-2i\pi\xi t_0} + \hat{g}_+(-\xi)e^{2i\pi\xi t_0}\right)e^{-2\pi\xi\tilde{z}} & \xi > 0, \\ -\left(\frac{1}{2}\left(1-e^{2\pi\xi\tilde{z}}\right) + \pi\xi\tilde{z}e^{2\pi\xi\tilde{z}}\right)\left(\hat{g}_-(\xi)e^{-2i\pi\xi t_0} + \hat{g}_+(-\xi)e^{2i\pi\xi t_0}\right) & \xi < 0. \end{cases}$$

The change of the embedding can be written in the compact form

$$\hat{t}(\xi,\tilde{z}) = \left(\frac{1}{2}\left(e^{-2\pi|\xi|\tilde{z}}-1\right) + \pi|\xi|\tilde{z}e^{-2\pi|\xi|\tilde{z}}\right)\left(\hat{g}_-(\xi)e^{-2i\pi\xi t_0} + \hat{g}_+(-\xi)e^{2i\pi\xi t_0}\right). \tag{5.46}$$

The embedding is not smooth at $\chi = 0$, but itself as well as its first and second derivative with respect to $\tilde{z}$ are continuous at this point. Therefore, the piecewise definition does not cause problems with the differential equation (5.45). We see that the part depending on the radial coordinate is bounded. For $\tilde{z} \in (0,\infty)$, it lies in the range

$$-\frac{1}{2} \leq \frac{1}{2}\left(e^{-2\pi|\xi|\tilde{z}}-1\right) + \pi|\xi|\tilde{z}e^{-2\pi|\xi|\tilde{z}} \leq 0,$$

where the lower bound is reached at the Poincaré horizon at $\tilde{z} = \infty$ and the upper bound at the boundary $\tilde{z} = 0$. This boundedness is necessary to keep the expansion in σ well-defined. The change of embedding can be transformed back to determine

the leading order shift of the embedding

$$t_1(\tilde{x},\tilde{z}) = -\frac{1}{2}\Big(g_+(t_0+\tilde{x}) + g_-(t_0-\tilde{x})\Big) + \frac{1}{\pi}\int_{-\infty}^{\infty} \mathrm{d}\tilde{t}\, \frac{\tilde{z}^3}{(\tilde{t}^2+\tilde{z}^2)^2}\Big(g_+(t_0+\tilde{t}+\tilde{x}) + g_-(t_0+\tilde{t}-\tilde{x})\Big). \tag{5.47}$$

One may wonder how the boundary condition $t_1(x,0) = 0$ is incorporated in this expression. The integral is an integral transform of the function

$$g_+(\cdot + t_0 + x) + g_-(\cdot + t_0 - x).$$

The integral kernel approaches $\pi\delta(t)/2$ in the near-boundary limit. Therefore both terms cancel each other and we have the desired boundary condition.

5.3.2 Volume of Extremal Slice

Let us return to the volume. As I derived in (5.39), the volume can be written as

$$\mathcal{V}_{(2)} = \int_0^\infty \mathrm{d}\tilde{z} \int_{-\infty}^{\infty} \mathrm{d}\tilde{x} \left[\frac{1}{4\tilde{z}}\, \tilde{t}_1{}^{(0,1)}\,(\tilde{x},\tilde{z})\left(g_-''\left(\tilde{t}_0-\tilde{x}\right) + g_+''\left(\tilde{t}_0+\tilde{x}\right)\right) - \frac{1}{4\tilde{z}^2}\, \tilde{t}_1{}^{(0,1)}\big(\tilde{x},\tilde{z}\big)^2 - \frac{1}{4\tilde{z}^2}\, \tilde{t}_1{}^{(1,0)}\big(\tilde{x},\tilde{z}\big)^2\right]. \tag{5.48}$$

I get rid of the last two terms by integration by parts. This allows to express them in terms of $\hat{g}_\pm{}''$ using (5.40)

$$\begin{aligned}\mathcal{V}_{(2)} &= \int_0^\infty \mathrm{d}\tilde{z} \int_{-\infty}^{\infty} \mathrm{d}\tilde{x} \left[\frac{1}{4\tilde{z}}\, \tilde{t}_1{}^{(0,1)}\,(\tilde{x},\tilde{z}) - \frac{\tilde{t}_1\,(\tilde{x},\tilde{z})}{8z^2}\right]\left(g_-''\left(\tilde{t}_0-\tilde{x}\right) + g_+''\left(\tilde{t}_0+\tilde{x}\right)\right), \\ &= \int_0^\infty \mathrm{d}\tilde{z} \int_{-\infty}^{\infty} \mathrm{d}\tilde{x}\, \frac{1}{8z^2}\, \tilde{t}_1\,(\tilde{x},\tilde{z})\left(g_-''\left(\tilde{t}_0-\tilde{x}\right) + g_+''\left(\tilde{t}_0+\tilde{x}\right)\right).\end{aligned} \tag{5.49}$$

At this point, we can plug in our solution for the embedding $\tilde{t}_1$ (5.46). After expressing the integrand in terms of the Fourier transform for $g_\pm$ (5.43) and $\tilde{t}_1$ (5.42),

the integral reduces to

$$\mathcal{V}_{(2)} = \pi^3 \int_{-\infty}^{\infty} \mathrm{d}\xi \ |\xi|^3 \left(\hat{g}_+(\xi)e^{-2i\pi\xi t_0} + \hat{g}_-(-\xi)e^{2i\pi\xi t_0}\right)\left(\hat{g}_-(\xi)e^{-2i\pi\xi t_0} + \hat{g}_+(-\xi)e^{2i\pi\xi t_0}\right).$$

Since the functions $g_\pm$ are real, their Fourier transforms satisfy $\hat{g}_\pm(-\xi) = \hat{g}_\pm(\xi)^*$. Hence, the change of volume reduces to

$$\mathcal{V}_{(2)} = \pi^3 \int_{-\infty}^{\infty} \mathrm{d}\xi \ |\xi|^3 \left|\hat{g}_-(\xi)e^{-2i\pi\xi t_0} + \hat{g}_+(-\xi)e^{2i\pi\xi t_0}\right|^2. \tag{5.50}$$

As noted by [50], this can be transformed back into $g_\pm$. For a general boundary time t_0, this yields

$$\mathcal{V}_{(2)} = \frac{3}{4\pi}\int \mathrm{d}x\mathrm{d}y \frac{1}{(x-y)^4}\Big(g_+(t_0+x) + g_-(t_0-x)\Big)\Big(g_+(t_0+y) + g_-(t_0-y)\Big).$$

The sum $(g_+ + g_-)$ has a physical interpretation. Expressing the new time coordinate $\tilde{t}$ in terms of the old one, we obtain

$$\tilde{t} = t - \frac{\sigma}{2}\left(g_+(\tilde{x}^+) + g_-(\tilde{x}^-)\right). \tag{5.51}$$

Consequently, $(g_+ + g_-)$ is proportional to the shift of the embedding in the old coordinates.

5.3.3 Properties of Volume Change

In the following, I analyze the obtained expression more closely. In the form given in Equation (5.50), one property is already obvious: the change of volume is always non-negative and does not depend on the sign of σ. To have a vanishing change of volume at a certain time t_0, the transformation has to satisfy

$$\hat{g}_-(\xi) = -\hat{g}_+(-\xi)\exp(4i\pi t_0\xi) \qquad \forall\xi \in (-\infty, \infty). \tag{5.52a}$$

In this case, the change of volume is positive for any other time. In particular, it follows

$$g_-(t_0 - x) = -g_+(t_0 + x), \tag{5.52b}$$

i.e. for the timeslice is unchanged and only the spatial direction is transformed. This implies the following: the extremal volume slice stays the same, only the cutoff changes. Therefore, it is also possible to use the vacuum result for the embedding (5.35) but a different regularization (see (5.10)). In this case, one does not have to solve a complicated embedding and can also consider this setup for finite conformal transformation. The conditions translate to

$$t_0 = \frac{1}{2}\left(G_+(\tilde{x}^+) + G_-(\tilde{x}^-)\right)|_{\tilde{t}=t_0}, \tag{5.53}$$

$$x = \frac{1}{2}\left(G_+(\tilde{x}^+) - G_-(\tilde{x}^-)\right)|_{\tilde{t}=t_0} = G_+(\tilde{x}^+)|_{\tilde{t}=t_0} - t_0. \tag{5.54}$$

Starting with the vacuum result (5.35), the volume for the transformed state is

$$\mathcal{V}(t_0) = \int \mathrm{d}x\, \frac{1}{z_\epsilon},$$

where the cutoff is spacetime dependent $z_\epsilon = z(\tilde{z} = \epsilon, \tilde{x})$ (5.10). Furthermore, it is more convenient to integrate over $\tilde{x}$. These transformations result in

$$\mathrm{d}x = |G_+{}'(\tilde{x}^+)|\mathrm{d}x \tag{5.55a}$$

$$z_\epsilon = \epsilon\sqrt{|G_+{}'(\tilde{x}^+)G_-{}'(\tilde{x}^+)|}|_{\tilde{t}=t_0} = \epsilon|G_+{}'(\tilde{x}^+)| \tag{5.55b}$$

Both contributions cancel each other. The volume is consequently does not change, i.e.

$$\mathcal{V}(t_0) = \int \mathrm{d}\tilde{x}\, \frac{1}{\epsilon}\frac{|G_+{}'(\tilde{x}^+)|}{|G_+{}'(\tilde{x}^+)|} = \mathcal{V}_{(0)}(t_0). \tag{5.56}$$

This is interesting. It implies that there are excited states with the same complexity as the vacuum state. In particular, their energy can be arbitrary high. However, the complexity for these states is time-dependent and only vanishes at a fixed time t_0.

Let us return to the result for an infinitesimal conformal transformation. The volume change can be split into three parts: one term only depending on g_+, one term only depending on g_- and one mixed term

$$\mathcal{V}_{(2)} = \mathcal{V}_{(2),\mathrm{pure}}(\hat{g}_+) + \mathcal{V}_{(2),\mathrm{pure}}(\hat{g}_-) + \mathcal{V}_{(2),\mathrm{mixed}}(\hat{g}_+, \hat{g}_-), \tag{5.57a}$$

where the different terms are defined as

$$\mathcal{V}_{(2),\text{pure}}(\hat{g}) = \pi^3 \int_{-\infty}^{\infty} d\xi \ |\xi|^3 \cdot \hat{g}(-\xi)\hat{g}(\xi), \tag{5.57b}$$

$$\mathcal{V}_{(2),\text{mixed}}(\hat{g}_+, \hat{g}_-) = 2\pi^3 \int_{-\infty}^{\infty} d\xi \ |\xi|^3 \cdot \hat{g}_+(\xi)\hat{g}_-(\xi)e^{-4i\pi\xi t_0}. \tag{5.57c}$$

In particular, the change of complexity is time-independent if only one light-cone coordinate is transformed. The reason for that is that such a transformation preserves the translational invariance in the untransformed light-cone coordinate. This translates into the time-independence of the result. The result in this form shows an interesting behavior: there is a positive, time-independent part arising from the pure terms and a time-dependent fluctuation arising from the mixed term. The fluctuation changes sign if the sign of $\hat{g}_+$ or $\hat{g}_-$ is changed, whereas the pure term is invariant. Since the complexity change is always non-negative, this implies

$$\left|\mathcal{V}_{(2),\text{mixed}}(\hat{g}_+, \hat{g}_-)\right| \leq \mathcal{V}_{(2),\text{pure}}(\hat{g}_+) + \mathcal{V}_{(2),\text{pure}}(\hat{g}_-) \tag{5.58}$$

for any transformation. From the definitions of both terms (5.57), it can be seen that the bound is only saturated for

$$\hat{g}_-(\xi) = \pm\hat{g}_+(-\xi)\exp(4i\pi t_0) \qquad \forall\xi \in (-\infty, \infty), \tag{5.59a}$$

$$g_-(t_0 - x) = \pm g_+(t_0 + x). \tag{5.59b}$$

Furthermore, it is interesting to observe how $\mathcal{V}_{(2)}$ (5.57) changes under manipulation of $g_\pm$. One interesting case is a rescaling of the argument of $g_\pm$. It follows directly from my result that the change of complexity behaves as

$$g_\pm(x) \to g_\pm(\lambda x), \qquad \hat{g}_\pm(\xi) \to \frac{1}{|\lambda|}\hat{g}_\pm(\xi/\lambda) \tag{5.60a}$$

$$\mathcal{V}_{(2)} \to \lambda^2 \mathcal{V}_{(2)}|_{t_0 \to \lambda t_0}. \tag{5.60b}$$

This can be understood by performing the replacement

$$\begin{aligned} x^\pm &= \tilde{x}^\pm + \sigma g^\pm(\tilde{x}^\pm), \\ \to \lambda x^\pm &= \lambda\tilde{x}^\pm + \sigma\lambda\, g^\pm(\lambda\tilde{x}^\pm). \end{aligned}$$

Therefore, we can consider it as the initial transformation from old coordinates λx with new coordinates $\lambda\tilde{x}$. Since the vacuum state is invariant under dilatation, this factor λ on the left does not change the complexity. The Weyl rescaling on the right-hand side only translates into a rescaling of t_0. Additionally, the expansion parameter is multiplied with λ.

Another interesting transformation are coordinate shifts

$$g_\pm(x^\pm) \to g_\pm(x^\pm + \delta_\pm). \tag{5.61}$$

These transformations add a local phase to the Fourier transforms

$$\hat{g}_\pm(\xi) \to \hat{g}_\pm(\xi) e^{-2\pi i\xi\delta_\pm}. \tag{5.62}$$

In particular, this leaves the pure terms invariant since they only depend on the absolute values. For the mixed term, this complex phases result in a shift of t_0

$$\Rightarrow V_{(2)}(\hat{g}_+(\xi)e^{-2\pi i\xi\delta_+}, \hat{g}_+(\xi)e^{-2\pi i\xi\delta_-}) = V_{(2)}(\hat{g}_+(\xi), \hat{g}_-(\xi))\big|_{t_0\to t_0+(\delta_++\delta_-)/2}. \tag{5.63}$$

This transformation is special when $\delta^\pm$ are identical up to the sign. In these cases, the transformation describe time-shifts and translations

time-shift:	translation:	
$g_\pm(x^\pm) \to g_\pm(x^\pm + \delta)$,	$g_\pm(x^\pm) \to g_\pm(x^\pm \pm \delta)$,	(5.64a)
$\hat{g}_\pm(\xi) \to \hat{g}_\pm(\xi)e^{-2\pi i\xi\delta}$,	$\hat{g}_\pm(\xi) \to \hat{g}_\pm(\xi)e^{\mp 2\pi i\xi\delta}$,	(5.64b)
$V_{(2)} \to V_{(2)}\big\vert_{t_0\to t_0+\delta}$,	$V_{(2)} \to V_{(2)}$.	(5.64c)

Translations leave as expected the complexity invariant, while time-shifts only result in a shift of t_0.

5.4 Examples

In the following my result is applied to calculable examples. In particular, the transformations are chosen to have a power law behavior at infinity, which makes them approximately localized. Therefore, they can be interpreted as localized wave packages.

To keep the notation simple, the tildes over the new coordinates are skipped in

this section.

Example 1

First, I consider

$$g_+\left(x^+\right) = \frac{a_+ c_+}{a_+^2 + \left(x^+\right)^2} \quad \Longleftrightarrow \quad \hat{g}_+(\xi) = c_+ e^{-2a_+\pi|\xi|}\pi, \tag{5.65a}$$

$$g_-\left(x^-\right) = \frac{a_- c_-}{a_-^2 + \left(x^-\right)^2} \quad \Longleftrightarrow \quad \hat{g}_-(\xi) = c_- e^{-2a_-\pi|\xi|}\pi. \tag{5.65b}$$

The convention is that $a_\pm$ are positive and the sign is encoded in $c_\pm$. Therefore, the Fourier transforms are exponentially decaying. The leading order contribution to the energy density (see (5.14)) is shown in Figure 5.3.

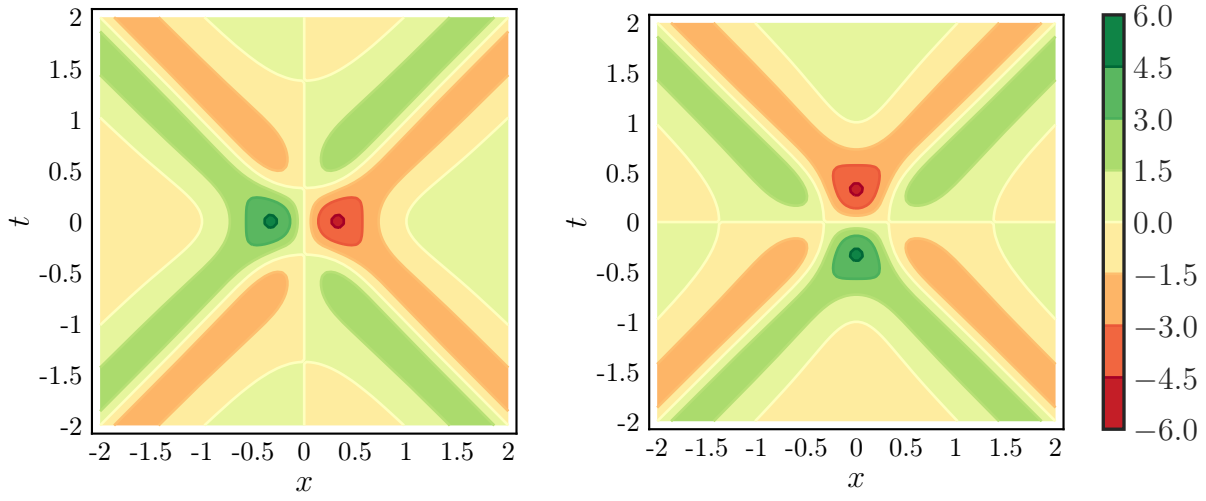

(a) $c_+ = -c_- = 1$ **(b)** $c_+ = c_- = 1$

Figure 5.3: First order term of the Energy Density for Example 1.
Here, I consider $a_\pm = c_+ = 1$ and $c_- = \mp 1$.

The embedding of the extremal surface can be derived from (5.36) and is

$$\begin{aligned} t_1(x,z) =& c_- \frac{2z^{-1}\left((t_0-x)^2 - a_-^2\right) - z^{-2}a_-\left(a_-^2 - 3(t_0-x)^2\right) - a_-}{2\left(a_-^2 + (t_0-x)^2\right)\left(2a_- z^{-1} + z^{-2}\left(a_-^2 + (t_0-x)^2\right) + 1\right)^2} \\ &+ c_+ \frac{2z^{-1}\left((t_0+x)^2 - a_+^2\right) - z^{-2}a_+\left(a_+^2 - 3(t_0+x)^2\right) - a_+}{2\left(a_+^2 + (t_0+x)^2\right)\left(2a_+ z^{-1} + z^{-2}\left(a_+^2 + (t_0+x)^2\right) + 1\right)^2}. \end{aligned} \tag{5.66}$$

The correction to the volume is given by

$$\mathcal{V}_{(2)} = c_+^2 \cdot \frac{3\pi}{64a_+^4} + c_-^2 \cdot \frac{3\pi}{64a_-^4} + \frac{c_- c_+}{(a_+ + a_-)^4} \cdot \frac{3\pi\left(16t_a^4 - 24t_a^2 + 1\right)}{2\left(4t_a^2 + 1\right)^4}, \tag{5.67}$$

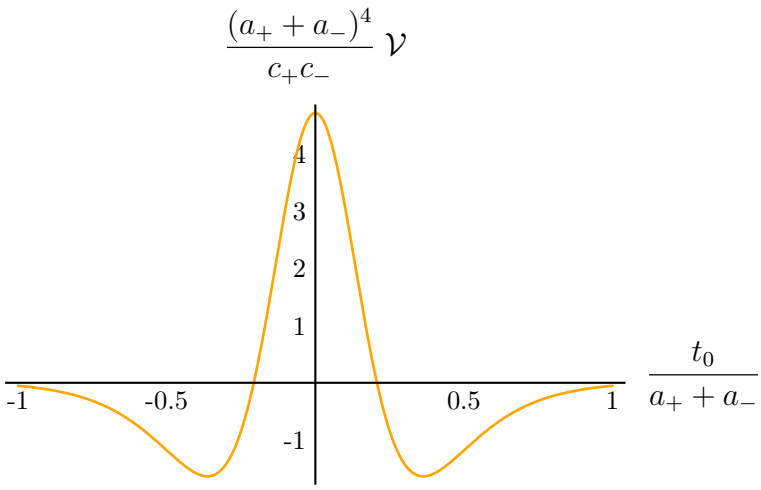

Figure 5.4: Change of Complexity for Example 1 and Example 2.
The mixed, time-dependent term of the change of volume is plotted. The volume is is related to the complexity by $\delta\mathcal{C} = \mathcal{V}/G_N L$.

where t_a is defined as $t_a = \frac{t_0}{a_+ + a_-}$. The result nicely displays the structure derived in (5.57a). The mixed term $\mathcal{V}_{(2),\text{mixed}}$ is shown in figure 5.4.

This transformation yields $V_{(2)} = 0$ at time $t_0 = 0$ for $a_+ = a_-$ and $c_+ = -c_-$. This can be seen from checking the conditions on the Fourier transforms $\hat{g}_\pm$ (5.52).

Example 2

As a second example, I consider

$$g_+\left(x^+\right) = -\frac{c_+ x^+}{a_+^2 + \left(x^+\right)^2} \Leftrightarrow \hat{g}_+(\xi) = -ic_+ e^{-2a_+\pi|\xi|}\pi\,\text{sgn}(\xi), \tag{5.68a}$$

$$g_-\left(x^-\right) = -\frac{c_- x^-}{a_-^2 + \left(x^-\right)^2} \Leftrightarrow \hat{g}_-(\xi) = -ic_- e^{-2a_-\pi|\xi|}\pi\,\text{sgn}(\xi). \tag{5.68b}$$

The embedding of the new extremal surface is

$$\begin{aligned} t_1(x,\lambda) = &-c_- \frac{(t_0 - x)\left(-4a_- z^{-1} + z^{-2}\left(-3a_-^2 + (t_0 - x)^2\right) - 1\right)}{2\left(a_-^2 + (t_0 - x)^2\right)\left(2a_- z^{-1} + z^{-2}\left(a_-^2 + (t_0 - x)^2\right) + 1\right)^2} \\ &-c_+ \frac{(t_0 + x)\left(-4a_+ z^{-1} + z^{-2}\left(-3a_+^2 + (t_0 + x)^2\right) - 1\right)}{2\left(a_+^2 + (t_0 + x)^2\right)\left(2a_+ z^{-1} + z^{-2}\left(a_+^2 + (t_0 + x)^2\right) + 1\right)^2}. \end{aligned} \tag{5.69}$$

The volume change caused by the transformation is

$$\mathcal{V}_{(2)} = c_+^2 \cdot \frac{3\pi}{64a_+^4} + c_-^2 \cdot \frac{3\pi}{64a_-^4} - \frac{c_- c_+}{(a_+ + a_-)^4} \cdot \frac{3\pi\left(16t_a^4 - 24t_a^2 + 1\right)}{2\left(4t_a^2 + 1\right)^4} \tag{5.70}$$

with time $t_a = \frac{t_0}{a_+ + a_-}$. The change of volume and hence complexity is identical to the result in example 1 (5.67) up to a sign change in the mixed term. See figure 5.4 for a plot of this quantity. However, the transformed state itself is quite different. In particular, the energy density is shown in Figure 5.5.

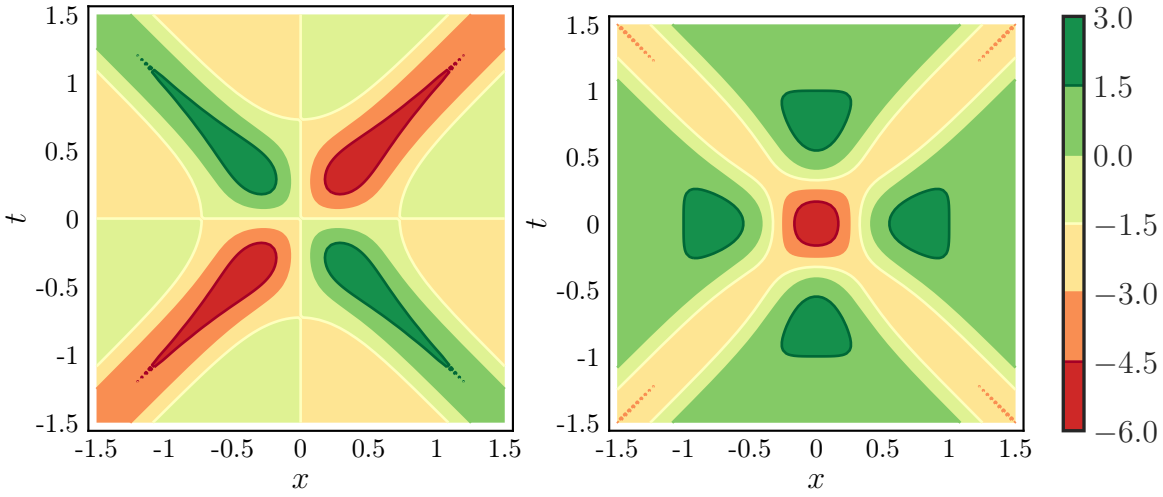

(a) $c_+ = -c_- = 1$ **(b)** $c_+ = c_- = 1$

Figure 5.5: First order term of the Energy Density for Example 2.
Here, I consider $a_\pm = c_+ = 1$ and $c_- = \mp 1$.

Example 3

As a final example, I consider a combination of the previous two examples

$$g_+\left(x^+\right) = \frac{c_+ x^+}{a_+^2 + \left(x^+\right)^2} \Leftrightarrow \hat{g}_+(\xi) = ic_+ e^{-2a_+\pi|\xi|}\pi\,\mathrm{sgn}(\xi), \tag{5.71a}$$

$$g_-\left(x^-\right) = \frac{a_- c_-}{a_-^2 + \left(x^-\right)^2} \Leftrightarrow \hat{g}_-(\xi) = c_- e^{-2a_-\pi|\xi|}\pi. \tag{5.71b}$$

The change of complexity is

$$\mathcal{V}_{(2)} = c_+^2 \cdot \frac{3\pi}{64a_+^4} + c_-^2 \cdot \frac{3\pi}{64a_-^4} - \frac{c_- c_+}{(a_+ + a_-)^4} \cdot \frac{12\pi t_a\left(1 - 4t_a^2\right)}{\left(4t_a^2 + 1\right)^4} \tag{5.72}$$

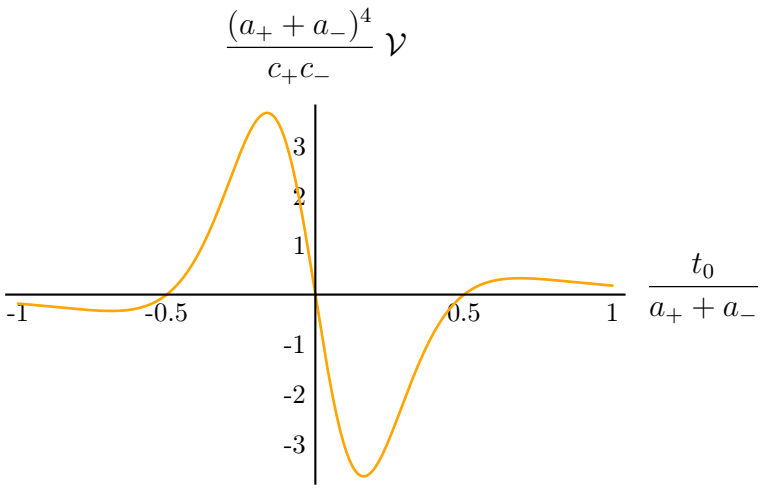

Figure 5.6: Change of Complexity for Example 3.
The mixed, time-dependent term of the change of volume is plotted. The volume is is related to the complexity by $\delta\mathcal{C} = \mathcal{V}/G_N L$.

with $t_a = \frac{t_0}{a_+ + a_-}$. The time-dependent part of the mixed term is shown in Figure 5.6. In this example, the metric perturbation does not satisfy the condition (5.52) for the change of complexity to vanish at a certain time t_0. Taking a closer look at (5.52), a necessary condition for $V_{(2)} = 0$ is that the absolute value of the mixed term has a unique maximum. We derived in (5.59a) the condition on the functions $\hat{g}_\pm$ for

$$\mathcal{V}_{(2),\text{mixed}} = \pm \left(\mathcal{V}_{(2),\text{pure}}(\hat{g}_+) + \mathcal{V}_{(2),\text{pure}}(\hat{g}_-) \right) .$$

However, this condition can at most be satisfied for a particular time t_0. Consequently, the result for $\mathcal{V}_{(2),\text{mixed}}$ as shown in Figure 5.6 directly forbids $\mathcal{V}_{(2)} = 0$.

The energy density of this example is presented in Figure 5.7.

5.5 Summary and Discussion

The complexity of a state induces a *notion of distance* on the space of states. Let us denote

$$\mathcal{C}\left(|\Psi\rangle, |\hat{\Psi}\rangle\right)$$

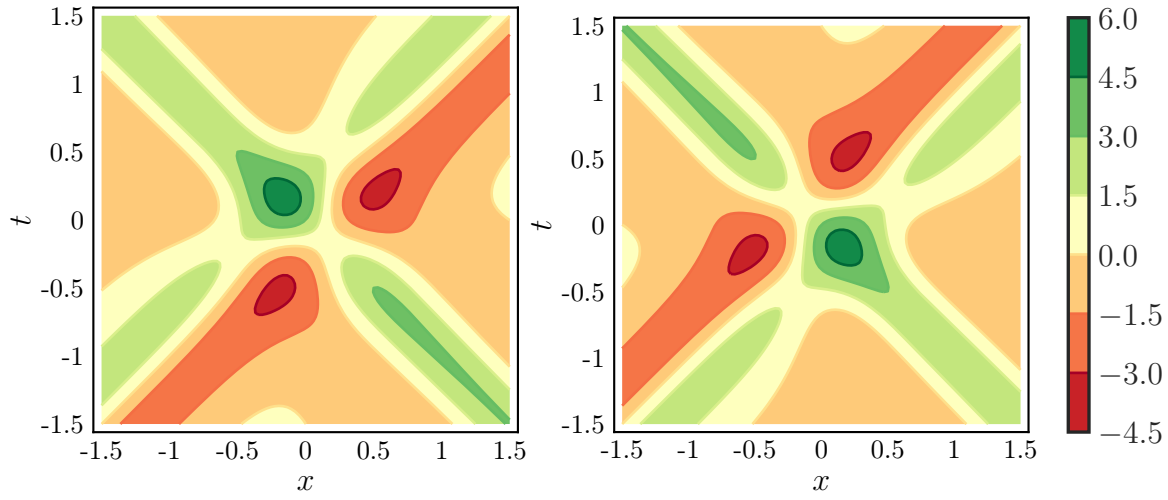

(a) $c_+ = -c_- = 1$ **(b)** $c_+ = c_- = 1$

Figure 5.7: First order term of the Energy Density for Example 3.
Here, I consider $a_\pm = c_+ = 1$ and $c_- = \mp 1$.

as complexity of the state $|\Psi\rangle$ with respect to the reference state $|\hat{\Psi}\rangle$. In this chapter, we study conformal transformation of the form

$$x^+ = G_+(\tilde{x}^+), \qquad t = \frac{1}{2}\left(G_+(\tilde{x}^+) + G_-(\tilde{x}^-)\right),$$
$$x^- = G_-(\tilde{x}^-), \qquad x = \frac{1}{2}\left(G_+(\tilde{x}^+) - G_-(\tilde{x}^-)\right).$$

They correspond to local conformal transformation and are generating new states. The corresponding operator are denoted as $U_\pm$ in the following. There is a well-defined notion how this transformation is described by a diffeomorphism on the gravity side. For the calculation following the complexity=volume proposal, the transformation changes two aspects:

- The volume slices are anchored on a different equal timeslice $\tilde{t} = t_0$.
- The bulk cutoff used to regularize the volume is different.

For a general conformal transformation, it is a non-trivial problem to solve the embedding of the extremal surface. For the special case where the conformal transformation does not change the considered equal time slice, i.e. for

$$t(\tilde{t}, \tilde{x}) = t_0|_{\tilde{t}=t_0}, \qquad \Longrightarrow \qquad G_-(y) = t_0 - G_+(2t_0 - y), \tag{5.73}$$

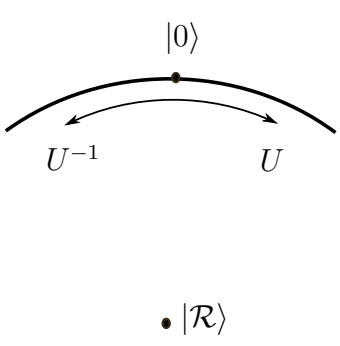

(a) Vacuum State and adjoint Minima.

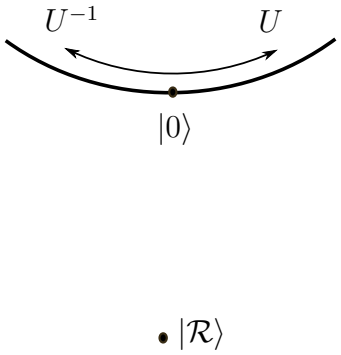

(b) Vacuum State as Minimum.

Figure 5.8: Geometry of Space of States for Different Transformations.
Conformal transformations satisfying (5.73) do not change the distance to the reference state. Infinitesimally, conformal transformations not satisfying this condition cause a positive, symmetric complexity change.

we avoid this problem. For these transformations, the only complexity change arises from the change of the bulk cutoff. I showed in (5.56) that this contribution also vanishes. Therefore, there is a continuous set of states

$$U_+U_-|0\rangle \text{ with } G_-(y) = t_0 - G_+(2t_0 - y)$$

parameterized by G_+ which have the same distance to the reference state $|\mathcal{R}\rangle$ as the vacuum state. This situation is shown in Figure 5.8a.

For any conformal transformation not satisfying (5.73), we calculated the change of complexity perturbatively by considering

$$\begin{aligned} x^+ &= \tilde{x}^+ + \sigma g_+(\tilde{x}^+), \\ x^- &= \tilde{x}^- + \sigma g_-(\tilde{x}^-), \end{aligned}$$

where the functions $g_\pm$ are bounded and σ is a small expansion parameter. For such transformations, we found that the change of complexity is of second order and positive, i.e. it is of the form

$$\delta\mathcal{C} = \sigma^2\mathcal{C}_{(2)} + \mathcal{O}(\sigma^3) \text{ with } \mathcal{C}_{(2)} > 0.$$

Therefore, the vacuum state is a local minimum in the direction corresponding to these transformations. In particular, the change of complexity is invariant under

$$U_\pm \to (U_\pm)^{-1}$$

and the structure of the space of states is reflection invariant. This is shown in Figure 5.8b.

After discussing what our results tell us about the geometry of the space of states, let us take a look what the corresponding operator applied to the vacuum state tells us. We calculated the change of complexity with respect to the reference state $|\mathcal{R}\rangle$

$$\mathcal{C}\big(U(g_+)U(g_-)\,|0\rangle\,,|\mathcal{R}\rangle\,\big) \approx \mathcal{C}\big(\,|0\rangle\,,|\mathcal{R}\rangle\,\big) + \delta\mathcal{C}. \tag{5.74}$$

For $\delta\mathcal{C} \geq 0$ this results in the inequality

$$\mathcal{C}\big(\,|0\rangle\,,|\mathcal{R}\rangle\,\big) \leq \mathcal{C}\big(U(g_+)U(g_-)\,|0\rangle\,,|\mathcal{R}\rangle\,\big). \tag{5.75}$$

Furthermore, the complexity is expected to satisfy a triangle inequality [95, 97], which results in

$$\mathcal{C}\big(U(g_+)U(g_-)\,|0\rangle\,,|\mathcal{R}\rangle\,\big) \leq \mathcal{C}\big(U(g_+)U(g_-)\,|0\rangle\,,|0\rangle\,\big) + \mathcal{C}\big(\,|0\rangle\,,|\mathcal{R}\rangle\,\big). \tag{5.76}$$

Therefore, the triangle inequality yields a bound on the complexity of the transformed state with respect to the vacuum state

$$\delta\mathcal{C} = \frac{\sigma^2}{LG_N}\mathcal{V}_{(2)} \leq \mathcal{C}\big(U(g_+)U(g_-)\,|0\rangle\,,|0\rangle\,\big). \tag{5.77}$$

The complexity of a state is defined as the minimal complexity of an operator transforming the reference state into the desired one. Since we know the exact form of $U_\pm$, we know one operator performing this transformation. The complexity of the operator U_+U_- is bounded by the the complexity change, since it does not have to be the most efficient one. As shown, U can be expanded as a power series in σ, i.e.

$$U \approx \mathbb{1} + \sigma U_1 + \sigma^2 U_2.$$

Definitions of complexity in accordance with Nielsen's approach [95, 97] ought to give a complexity of the form

$$\mathcal{C}(U) \approx \sigma\kappa + \ldots \tag{5.78}$$

for small operators. Therefore, our results are compatible with field theory proposals following this approach. If the lowest order term for the complexity of the operator is non-vanishing, this inequality is automatically satisfied since the expansion parameter σ is small. For conformal transformations with $\kappa = 0$, our results place necessary conditions on the field theory results for this definition of field theory be compatible with the complexity=volume proposal.

On another note, my co-author calculated the complexity change also for the competing complexity=action proposal [49]. Interestingly, the lowest order term has the form

$$\delta\mathcal{C} \propto \sigma \ln \sigma.$$

While this still vanishes in the limit $\sigma \to 0$, it goes to zero slower to than σ. As a consequence, the complexity=action proposal is not compatible with Nielsen's approach. The complexity of the operator has the form (5.78) and the triangle inequality (5.77) would be violated for small σ. Therefore, the complexity=volume proposal is favored as a potential dual to field theory complexity.

Furthermore, our result gives an explicit result which can be compared to field theory results. There exists field theory results for the complexity of the transformed state with respect to the vacuum state [50]. They developed a boundary notion of complexity. When applied to conformal transformations, they found the exact same result as we found for the complexity change. Since we considered the complexity with respect to the reference state $|\mathcal{R}\rangle$, it is related to their result via the triangle inequality (5.76). This suggest that this bound is saturated. This is a powerful confirmation and our results and the complexity=volume proposal.

Chapter 6

Summary and Outlook

We elaborated in the introduction how the AdS/CFT correspondence, as a holographic duality, sheds light on the emergence of gravity from field theory degrees of freedom. In particular, a good way to probe the geometry is to anchor extremal surfaces at the boundary. These correspond to non-local observables in the field theory: the two-point function of certain operators to the geodesic, the Wilson loop expectation value to a two-dimensional surface and the entanglement entropy to the co-dimension two surface, which reduces to a co-dimension one surface in a constant time slice.

These observables were studied in Chapter 3. The examined geometries are AdS Schwarzschild black holes in general spacetime dimensions and correspond to thermal states in the $\mathrm{AdS}_{d+1}/\mathrm{CFT}_d$ duality. We derived analytic solutions for the considered observables in terms of generalized hypergeometric function. In particular the high-temperature limit shows an interesting behavior. In this limit, the extremal surfaces reach deep into the bulk. The leading order contribution only depends on the geometry at the horizon, but the subleading term depends non-trivially on the entire bulk geometry. Our analytic results determine this subleading term in a closed form. Especially the resulting term for the entanglement entropy showed an interesting behavior: the subleading term is an area term and expected to satisfy a variant of the c-theorem, the so-called area theorem. Therefore, it can be interpreted as a measure for the number of degrees of freedom. Our result show that this area term becomes positive for spacetime dimension larger than six. This hints to additional IR degrees of freedom which increase entanglement. Independent numerical studies have shown a similar behavior for various geometries such as AdS Reissner-Nordström black holes [125]. This shows that the high-temperature behavior is an interesting diagnostic tool to examine the dual field theory. Our analytic methods developed can also be applied for more general setups to extend the study of this

area term. One example are semi-local quantum liquids [143], a theory with a finite correlation length and a near-horizon region with a non-relativistic scale invariance. It was suspected in [125] that this might be the origin of the appearing area theorem violation. Additionally to further analytic studies, our results can serve as a testing ground for numerical methods.

Recently, an interpretation of entanglement in terms of *bit threads* was proposed [144, 145]. They reformulated the problem of finding the minimal surface in terms of finding the bulk vector field which maximizes the flux through the corresponding boundary region. This flux has to be divergenceless and has a maximal density determined by the Planck scale. This allows to visualize the flow by its flow lines going from the region to the complement. The bit thread picture suggest new ways to think about the relationship between geometry and quantum information. Our analytic results for the entanglement entropy can be used to construct such vector flow configurations explicitly [146]. While these configurations are not unique and have a priori no physical interpretation, constructing them for examples helps to gain intuition and learn more about how they are related to the emergence of geometry.

The holographic construction for the entanglement entropy associates a bulk region to the boundary region. This is also an interesting observable to study since it encodes 'how much' geometry is associated to a reduced state. Therefore, a natural next step to study the emergence of geometry is to study this volume. We calculate it for AdS Schwarzschild in Chapter 4. The volume has an interesting interpretation when comparing AdS/CFT to MERA tensor networks. Tensor networks are a numerical tool in many-body physics to describe a quantum state by tensors. MERA in particular has an emergent geometry of tensors encoding the entanglement pattern of the state. In analogy to holography, entanglement entropy is determined by minimal cut surfaces in these networks. The volume inside this minimal cut surfaces gives a measure on how optimized the network is to describe the quantum state. A MERA network for the thermal state can be constructed from the vacuum MERA network. We approximated this network by a gravitational dual described by vacuum AdS with a hard IR wall. We calculate the volume inside the Ryu-Takayanagi surface both for AdS Schwarzschild and this hard wall model. In particular, we find that the volume obtained in AdS Schwarzschild is smaller, hinting that thermal MERA could be further optimized. Further MERA calculations would give more insights into the connection between AdS/CFT and MERA.

AdS/CFT relates volume to complexity $\mathcal{C}$, a measure of how difficult it is to

construct a state $|\psi\rangle$. Any definition of complexity encodes implicitly the choice of reference state $|\mathcal{R}\rangle$ from which the state is constructed and the choice of gate set used to construct the corresponding operation $\{\mu_i\}$, i.e.

$$|\psi\rangle = U\,|\mathcal{R}\rangle\,,$$
$$U \approx \mu_1 \dots \mu_{\mathcal{C}}.$$

For the volume considered above, the states are to reduced states which are in general mixed. A proper quantum information definition of such a subregion complexity is lacking. Even for pure states, the notion of complexity of field theory is not well defined. In particular, it is not obvious what the preferred choices for gate set and reference state are. The reference state is usually assumed to be a simple, unentangled state, i.e. a state without gravitational dual. Furthermore, the discussion about a proper holographic dual to complexity are still ongoing: besides the used complexity=volume proposal there also exists a complexity=action proposal, relating the complexity to the gravitational action evaluated on a certain bulk region, and a modified complexity=volume proposal. Recently, also discussions on what complexity these proposals correspond to intensified. Motivated by this, Chapter 5 considers the holographic complexity for states obtained by conformal transformations in $\mathrm{AdS}_3/\mathrm{CFT}_2$. We used the complexity=volume proposal and subsequent work by my collaborator [49] examined the complexity=action proposal. The advantage of such states is that we know how to write them as a unitary operator acting on the vacuum state. This allows to identify differences between the different proposals and to compare these holographic result to field theory calculations. In particular, the holographic results for the complexity of the state give a lower bound on the complexity of the operator corresponding to the conformal transformations. Our results show that the complexity=volume proposal yields a result compatible with this. As shown in [49], the complexity=action proposal yields a different result which is incompatible with usual field theory prescriptions of complexity. Furthermore, our results where confirmed by holography inspired field theory calculations [50]. The study of a proper field theory definition of complexity is ongoing, both using Nielsen's approach [147–149] as well as alternative approaches [150, 151]. Therefore, determining the complexity for well-defined states in the field theories helps to compare them explicitly to the holographic proposal.

While these studies allow us compare the holographic complexity=volume proposals to field theory proposals, there is also a more abstract interpretation of com-

plexity: the complexity of a state $|\Psi_1\rangle$ with respect to a reference state $|\Psi_2\rangle$ gives an abstract notion of distance

$$\mathcal{C}\left(|\Psi_1\rangle, |\Psi_2\rangle\right).$$

This distance measure does not even have to be symmetric, but it is expected to satisfy the triangle inequality

$$\mathcal{C}\left(|\Psi_1\rangle, |\Psi_3\rangle\right) \leq \mathcal{C}\left(|\Psi_1\rangle, |\Psi_2\rangle\right) + \mathcal{C}\left(|\Psi_2\rangle, |\Psi_3\rangle\right).$$

Our studies on the change of complexity due to conformal transformations allows us insight in the local structure of this space of states. In particular, we constructed a continuous set of states with the same complexity as the ground state. In contrast to the vacuum state these states are time-dependent. Motivated by the behavior of complexity close to the vacuum state and also the second law of quantum complexity [152], we expect that the complexity of these states growth with time. Therefore, the moment of minimal complexity is achieved by meticulous fine tuning but not stable. It would be interesting to study finite conformal transformations in this setup. In particular, we are wondering whether there are additional states with the same complexity and how they are related to the states discussed previously. Furthermore, it would be interesting to find the state with minimal complexity. These would bring us closer to the choice of reference state involved in the holographic complexity.

The holographic entanglement entropy was one of the first clues how geometry emerges in AdS/CFT. But it alone was just the tip of the iceberg. After entanglement being identified as the ingredient to build spacetime, it opened the door to study quantum information aspects in holography. The topics discussed in this dissertation are only the starting point to fully understand the interconnections between gravity, field theory and quantum information theory.

Chapter A

Conventions

A.1 Metric

cosmological constant	$\Lambda = -\frac{d(d-1)}{L^2}$
AdS-radius	L
planar AdS_{d+1}	$\mathrm{d}s^2 = \left(\frac{L}{z}\right)^2 \left(-\mathrm{d}t^2 + \mathrm{d}\vec{x}^2 + \mathrm{d}z^2\right),\ \vec{x} \in \mathbb{R}^{d-1},$
	boundary at $z = 0$, UV cutoff $z = \epsilon$
planar AdS Schwarzschild	$\mathrm{d}s^2 = \left(\frac{L}{z}\right)^2 \left(-b(z)\mathrm{d}t^2 + \mathrm{d}\vec{x}^2 + b(z)^{-1}\mathrm{d}z^2\right),$
	$b(z) = 1 - \left(\frac{z}{z_h}\right)^d,$ horizon at $z = z_h$
gravitational action for $\mathrm{AdS}_{d+1}/\mathrm{CFT}_d$	$S = \frac{1}{16\pi G_N^{(d+1)}} \int \mathrm{d}^{d+1}x\sqrt{-g}\left(R + \frac{d(d-1)}{L^2} + \text{matter terms}\right)$
Newton constant	$G_N^{(d+1)} \propto l_p^{d-1}$
Planck constant	l_p
string length	$l_s \propto \sqrt{\alpha'}$

A.2 AdS/CFT Dictionary

central charge	$c \propto \frac{L^{d-1}}{G_N^{(d+1)}} \propto \left(\frac{L}{l_p}\right)^{d-1}$
't Hooft coupling	$\lambda \propto \left(\frac{L}{l_s}\right)^{\gamma},\ \gamma > 0$
Field-Operator-Map	Operator $\mathcal{O}_\Delta$ of dimension Δ
	$\updownarrow$
	Field $\phi(z, x)$ of mass $m = \sqrt{\Delta(\Delta - d)}$

A.3 Indices

$M, N, \ldots$	$0, \ldots, D$	target space coordinates D=26 for bosonic string theory, D=10 for superstring theory
α, β	$0, 1$	worldsheet coordinates of the string
μ, ν	$0, \ldots, p$	coordinates parallel to brane
i, j	$1, \ldots, D - p - 1$	coordinates transverse to brane

Chapter B

Mathematical Functions

B.1 Generalized Hypergeometric Functions

The results for the extremal surfaces can be expressed in terms of generalized hypergeometric functions. In the following, we review these functions and their properties [153–155].

A generalized hypergeometric function is the power series

$$ {}_pF_q\left(\left.\begin{matrix}a_1,\dots,a_p\\ b_1,\dots,b_q\end{matrix}\right| z\right) = \sum_{n=0}^{\infty}\frac{1}{n!}\frac{(a_1)_n\cdots(a_p)_n}{(b_1)_n\cdots(b_q)_n}\ z^n, \tag{B.1a} $$

$$ = \sum_{n=0}^{\infty} c_n, \tag{B.1b} $$

where $(a)_n$ is the (rising) Pochhammer symbol

$$ (a)_n = \begin{cases} 1 & \text{if } n = 0, \\ a\cdot(a+1)\cdot\cdots\cdot(a+n-1) & \text{if } n\in\mathbb{N}. \end{cases} \tag{B.2} $$

The parameters a_i and b_i are the numerator and denominator parameters respectively, whereas z is the variable or argument of the hypergeometric function. Another common notation is

$$ {}_pF_q\left(a_1,\dots,a_p;b_1,\dots,b_q;z\right), \tag{B.3} $$

which we will use occasionally to avoid lengthy expressions. In this work, we construct hypergeometric functions from a known power series, i.e. for known c_n (c.f. Equation (B.1b)) normalized such that $c_0 = 1$. This can be done by calculating the

ratio between successive coefficients

$$\frac{c_{n+1}}{c_n} = z \cdot \frac{\prod_{m=1}^{p} (a_m + n)}{\prod_{m=1}^{q} (b_m + n)} \frac{1}{n+1}. \tag{B.4}$$

It can be shown easily that differentiating with respect to the argument results in

$$\frac{\mathrm{d}}{\mathrm{d}z} {}_pF_q \left(\left. \begin{matrix} a_1, \ldots, a_p \\ b_1, \ldots, b_q \end{matrix} \right| z \right) = \frac{\prod_{i=1}^{p} a_i}{\prod_{j=1}^{q} b_j} {}_pF_q \left(\left. \begin{matrix} a_1 + 1, \ldots, a_p + 1 \\ b_1 + 1, \ldots, b_q + 1 \end{matrix} \right| z \right), \tag{B.5a}$$

$$\frac{\mathrm{d}}{\mathrm{d}z} z^{a_1} {}_pF_q \left(\left. \begin{matrix} a_1, \ldots, a_p \\ b_1, \ldots, b_q \end{matrix} \right| z \right) = a_1 z^{a_1 - 1} {}_pF_q \left(\left. \begin{matrix} a_1 + 1, a_2, \ldots, a_p \\ b_1, \ldots, b_q \end{matrix} \right| z \right). \tag{B.5b}$$

For a power series, the radius of convergence is important. A generalized hypergeometric function converges absolutely

- for all values of $|z|$ if $p \leq q$,
- for $|z| < 1$ if $p = q + 1$,
- for $|z| = 1$ if $p = q + 1$ under the condition that

$$\Psi = \sum_{i=1}^{p} b_i - \sum_{i=1}^{p+1} a_i > 0. \tag{B.6}$$

Let us look closer at the case $p = q + 1$. For ${}_2F_1$, the result at unit argument is known in the case that it is finite

$${}_2F_1 \left(\left. \begin{matrix} a, b \\ c \end{matrix} \right| 1 \right) = \frac{\Gamma(c)\Gamma(c - a - b)}{\Gamma(c - a)\Gamma(c - b)}, \qquad \text{for } \Psi > 0. \tag{B.7}$$

Unfortunately, this is not the case for general ${}_{p+1}F_p$. However, we can examine the divergent behavior, which is

$${}_{p+1}F_p \left(\left. \begin{matrix} a_1, \ldots, a_{p+1} \\ b_1, \ldots, b_p \end{matrix} \right| z \right) = \Gamma(-\Psi) \frac{\prod_{i=1}^{p} \Gamma(b_i)}{\prod_{i=1}^{p+1} \Gamma(a_i)} \cdot (1 - z)^{\Psi} \tag{B.8a}$$

for $\mathrm{Re}(\Psi) < 0$ and

$$ {}_{p+1}F_p\left(\left.\begin{matrix} a_1,\ldots,a_{p+1} \\ b_1,\ldots,b_p \end{matrix}\right| z\right) = -\frac{\prod_{i=1}^{p}\Gamma\left(b_i\right)}{\prod_{i=1}^{p+1}\Gamma\left(a_i\right)}\cdot\ln(1-z) \qquad \text{for } \Psi = 0. \tag{B.8b} $$

Let us finish this section with possible simplifications. From the series representation Equation (B.1a) we notice the trivial one: coinciding numerator and denominator parameter cancel each other

$$ {}_{p+1}F_{q+1}\left(\left.\begin{matrix} a_1,\ldots,a_p,a_{p+1} \\ b_1,\ldots,b_q,a_{p+1} \end{matrix}\right| z\right) = {}_pF_q\left(\left.\begin{matrix} a_1,\ldots,a_p \\ b_1,\ldots,b_q \end{matrix}\right| z\right). \tag{B.9} $$

In some cases, it is possible to absorb a square root in ${}_2F_1$

$$ {}_2F_1(a,b;c;z) = (1-z)^{c-a-b}{}_2F_1(c-a,c-b;c;z). \tag{B.10} $$

Another interesting simplification is possible if two hypergeometric functions are associated or contiguous to each other, i.e. their parameters differ by integer values. One can find a linear relationship between them, so called contiguous relations. One simple case is

$$ \begin{aligned} a_1\cdot{}_pF_q\left(\left.\begin{matrix} a_1+1,a_2,\ldots,a_p \\ b_1,\ldots,b_q \end{matrix}\right| z\right) - (b_1-1)\cdot{}_pF_q\left(\left.\begin{matrix} a_1,\ldots,a_p \\ b_1-1,b_2,\ldots,b_q \end{matrix}\right| z\right) \\ +(b_1-a_1-1)\cdot{}_pF_q\left(\left.\begin{matrix} a_1,\ldots,a_p \\ b_1,\ldots,b_q \end{matrix}\right| z\right) = 0. \end{aligned} \tag{B.11} $$

Finally, for some parameters a closed form for the hypergeometric function or the value at unit argument is known. Examples are presented in Table B.1.

B.2 Meijer G-Function

Another interesting function is the Meijer G-Function

$$ G^{m,n}_{p,q}\left(\left.\begin{matrix} a_1,\ldots,a_p \\ b_1,\ldots,b_q \end{matrix}\right| z\right) = \frac{1}{2\pi i}\int_L \mathrm{d}s\, \frac{\prod_{j=1}^{m}\Gamma(b_j-s)\prod_{j=1}^{n}\Gamma(1-a_j+s)}{\prod_{j=m+1}^{q}\Gamma(1-b_j+s)\prod_{j=n+1}^{p}\Gamma(a_j-s)}\, z^s \tag{B.13} $$

$$
\begin{aligned}
{}_1F_0\left(a;;z\right) &= (1-z)^{-a}, && \text{(B.12a)}\\
{}_2F_1\left(1,\tfrac{1}{2};\tfrac{3}{2};z\right) &= \frac{1}{\sqrt{z}}\operatorname{artanh}\left(\sqrt{z}\right), && \text{(B.12b)}\\
{}_2F_1\left(1,1;2;z\right) &= -\frac{1}{z}\log(1-z), && \text{(B.12c)}\\
{}_3F_2\left(1,1,\tfrac{3}{2};2,\tfrac{5}{2};z\right) &= -\frac{6\tanh^{-1}\left(\sqrt{z}\right)}{z^{3/2}} + \frac{6}{z} - \frac{3\log(1-z)}{z}, && \text{(B.12d)}\\
{}_3F_2\left(1,1,\tfrac{3}{2};2,2;1\right) &= 4\ln 2, && \text{(B.12e)}\\
{}_3F_2\left(1,1,\tfrac{3}{2};2,\tfrac{5}{2};1\right) &= 3(2-\ln 4). && \text{(B.12f)}
\end{aligned}
$$

Table B.1: Examples of Hypergeometric Functions.

which is well defined for

$$
\begin{aligned}
&0 \le m \le q,\ 0 \le n \le p && , && \text{(B.14a)}\\
&a_k - b_j \notin \mathbb{N} && \forall k = 1,\dots,n \text{ and } j = 1,\dots,m, && \text{(B.14b)}\\
&z \neq 0. && && \text{(B.14c)}
\end{aligned}
$$

The path of integration L splits the poles of $\Gamma(b_j - s)$ from the ones of $\Gamma(1 - a_j + s)$. For real argument z, there are three possibilities:

- L going from $-i\infty$ to $+i\infty$,
- L going from $+\infty$ to $+\infty$ for $|z| < 1$ and $q \ge p$,
- L going from $-\infty$ to $-\infty$ for $|z| > 1$ and $q \le p$.

There is a convenient relationship to hypergeometric functions: if we can begin and end the path at $+\infty$, Meijer G-Functions can be expressed in terms of hypergeometric functions

$$
\begin{aligned}
G^{m,n}_{p,q}\left(\left.\begin{matrix}a_1,\dots,a_p\\ b_1,\dots,b_q\end{matrix}\right| z\right) = \sum_{h=1}^{m} & \frac{\prod_{j=1}^{n}\Gamma(1+b_h-a_j)\prod_{j=1,\ j\neq h}^{m}\Gamma(b_j-b_h)}{\prod_{j=m+1}^{q}\Gamma(1+b_h-b_j)\prod_{j=n+1}^{p}\Gamma(a_j-b_h)} z^{b_h} \qquad \text{(B.15)}\\
& \times\ {}_pF_{q-1}\left(\left.\begin{matrix}1+b_h-a_1,\dots,1+b_h-a_p\\ \underbrace{1+b_h-b_1,\dots,1+b_h-b_q}_{\text{without } b_h}\end{matrix}\right| (-1)^{p-m-n}\ z\right).
\end{aligned}
$$

Meijer G-functions are analytic continuation of hypergeometric functions. This allows to consider them in a range where the hypergeometric functions do not converge. In particular for $p = q$, the integral for $z > 1$ can be closed at $-\infty$ and there exist an analogous relationship to hypergeometric functions evaluated at argument z^{-1}. This is not relevant for the work presented in this thesis, but useful when generalizing the used methods.

Meijer G-functions have similar properties as hypergeometric functions. For example, in the case

$$\nu = \sum_{j=1}^{q} b_j - \sum_{j=1}^{p} a_j < -1, \tag{B.16}$$

they converge at unit argument, which corresponds to (B.6) for hypergeometric functions. Furthermore, the contiguous relations for hypergeometric functions (B.11) correspond to recurrence relations

$$\begin{aligned}(a_1 - b_q - 1)\, G_{p,q}^{m,n}\left(\left.\begin{matrix} a_1, \ldots, a_p \\ b_1, \ldots, b_q \end{matrix}\right| z\right) &= G_{p,q}^{m,n}\left(\left.\begin{matrix} a_1, \ldots, a_p \\ b_1, \ldots, b_{q-1}, b_q + 1 \end{matrix}\right| z\right) \\ &\quad - G_{p,q}^{m,n}\left(\left.\begin{matrix} a_1 - 1, \ldots, a_{p-1}, a_p \\ b_1, \ldots, b_q \end{matrix}\right| z\right)\end{aligned} \tag{B.17}$$

for $n < p,\ m < q$.

Useful transformations which transform Meijer G-functions into Meijer G-functions are

$$z^{\rho} \cdot G_{p,q}^{m,n}\left(\left.\begin{matrix} a_1, \ldots, a_p \\ b_1, \ldots, b_q \end{matrix}\right| z\right) = G_{p,q}^{m,n}\left(\left.\begin{matrix} a_1 + \rho, \ldots, a_p + \rho \\ b_1 + \rho, \ldots, b_q + \rho \end{matrix}\right| z\right) \tag{B.18}$$

and for $h \in \mathbb{Z}$

$$z^h \frac{d^h}{dz^h}\, G_{p,q}^{m,n}\left(\left.\begin{matrix} a_1, \ldots, a_p \\ b_1, \ldots, b_q \end{matrix}\right| z\right) = G_{p+1,\,q+1}^{m,\,n+1}\left(\left.\begin{matrix} 0, a_1, \ldots, a_p \\ b_1, \ldots, b_q, h \end{matrix}\right| z\right), \tag{B.19a}$$

$$= (-1)^h\, G_{p+1,\,q+1}^{m+1,\,n}\left(\left.\begin{matrix} a_1, \ldots, a_p, 0 \\ h, b_1, \ldots, b_q \end{matrix}\right| z\right). \tag{B.19b}$$

Own Publications

[P1] J. Erdmenger and N. Miekley, *Non-local observables at finite temperature in AdS/CFT*, *JHEP* **03** (2018) 034, [1709.07016].

Abstract: *Within gauge/gravity duality, we consider the AdS-Schwarzschild metric in arbitrary dimensions. We obtain analytical closed-form results for the two-point function, Wilson loop and entanglement entropy for strip geometries in the finite-temperature field-theory dual. According to the duality, these are given by the area of minimal surfaces of different dimension in the gravity background. Our analytical results involve generalised hypergeometric functions. We show that they reproduce known numerical results to great accuracy. Our results allow to identify new physical behaviour: for instance, we consider the entanglement density, i.e. the difference of entanglement entropies at finite and vanishing temperature divided by the volume of the entangling region. For field theories of dimension seven or higher, we find that the entanglement density displays non-monotonic behaviour as function of* $\ell \cdot T$ *, with* ℓ *the strip width and* T *the temperature. This implies that the area theorem, proven for RG flows in general dimensions, does not apply here. This may signal the emergence of new degrees of freedom for AdS Schwarzschild black holes in eight or more dimensions.*

[P2] J. Erdmenger and N. Miekley, *Subregion complexity in AdS Schwarzschild*, in preparation, to appear in August 2019.

[P3] M. Flory and N. Miekley, *Complexity change under conformal transformations in* AdS_3/CFT_2, *JHEP* **05** (2019) 003, [1806.08376].

Abstract: *Using the volume proposal, we compute the change of complexity of holographic states caused by a small conformal transformation in* AdS_3/CFT_2*. This computation is done perturbatively to second order. We give a general result and discuss some of its properties. As operators generating such conformal transformations can be explicitly constructed in CFT terms, these results allow for a comparison between holographic methods of defining and computing computational complexity and purely field-theoretic proposals. A comparison of our results to one such proposal is given.*

Bibliography

[1] Event Horizon Telescope collaboration, S. Doeleman, "Focus on the first event horizon telescope results." *Astrophys. J.* **875** (2019), https://iopscience.iop.org/journal/2041-8205/page/Focus_on_EHT.

[2] Event Horizon Telescope collaboration, *First M87 Event Horizon Telescope Results. I. The Shadow of the Supermassive Black Hole*, *Astrophys. J.* **875** (2019) L1 [1906.11238].

[3] LIGO Scientific, Virgo collaboration, "Focus on astrophysical implications of the first ligo detection gw150914." 2019, https://iopscience.iop.org/journal/2041-8205/page/Focus_on_LIGO.

[4] LIGO Scientific, Virgo collaboration, *GW151226: Observation of Gravitational Waves from a 22-Solar-Mass Binary Black Hole Coalescence*, *Phys. Rev. Lett.* **116** (2016) 241103 [1606.04855].

[5] P.-A. Moreau, E. Toninelli, T. Gregory, R. S. Aspden, P. A. Morris and M. J. Padgett, *Imaging bell-type nonlocal behavior*, *Science Advances* **5** (2019) .

[6] A. Einstein, B. Podolsky and N. Rosen, *Can quantum mechanical description of physical reality be considered complete?*, *Phys. Rev.* **47** (1935) 777.

[7] J. S. Bell, *On the Einstein-Podolsky-Rosen paradox*, *Physics Physique Fizika* **1** (1964) 195.

[8] J. G. Richens, J. H. Selby and S. W. Al-Safi, *Entanglement is Necessary for Emergent Classicality in All Physical Theories*, *Physical Review Letters* **119** (2017) 080503 [1705.08028].

[9] K. Becker, M. Becker and J. H. Schwarz, *String theory and M-theory: A modern introduction*. Cambridge University Press, 2006.

[10] B. Zwiebach, *A first course in string theory*. Cambridge University Press, 2006.

[11] J. M. Maldacena, *The Large N limit of superconformal field theories and supergravity*, *Int. J. Theor. Phys.* **38** (1999) 1113 [hep-th/9711200].

[12] S. S. Gubser, I. R. Klebanov and A. M. Polyakov, *Gauge theory correlators from noncritical string theory*, *Phys. Lett.* **B428** (1998) 105 [hep-th/9802109].

[13] E. Witten, *Anti-de Sitter space and holography*, *Adv. Theor. Math. Phys.* **2** (1998) 253 [hep-th/9802150].

[14] J. D. Bekenstein, *Black holes and the second law*, *Lett. Nuovo Cim.* **4** (1972) 737.

[15] J. D. Bekenstein, *Black holes and entropy*, *Phys. Rev.* **D7** (1973) 2333.

[16] S. W. Hawking, *Black holes in general relativity*, *Commun. Math. Phys.* **25** (1972) 152.

[17] J. D. Bekenstein, *Generalized second law of thermodynamics in black hole physics*, *Phys. Rev.* **D9** (1974) 3292.

[18] J. D. Bekenstein, *Statistical Black Hole Thermodynamics*, *Phys. Rev.* **D12** (1975) 3077.

[19] J. M. Bardeen, B. Carter and S. W. Hawking, *The Four laws of black hole mechanics*, *Commun. Math. Phys.* **31** (1973) 161.

[20] J. D. Bekenstein, *A Universal Upper Bound on the Entropy to Energy Ratio for Bounded Systems*, *Phys. Rev.* **D23** (1981) 287.

[21] L. Susskind, *The World as a hologram*, *J. Math. Phys.* **36** (1995) 6377 [hep-th/9409089].

[22] G. 't Hooft, *Dimensional reduction in quantum gravity*, *Conf. Proc.* **C930308** (1993) 284 [gr-qc/9310026].

[23] R. Bousso, *The Holographic principle*, *Rev. Mod. Phys.* **74** (2002) 825 [hep-th/0203101].

[24] J. M. Maldacena, *Eternal black holes in anti-de Sitter*, *JHEP* **04** (2003) 021 [hep-th/0106112].

[25] S. Ryu and T. Takayanagi, *Holographic derivation of entanglement entropy from AdS/CFT*, *Phys. Rev. Lett.* **96** (2006) 181602 [hep-th/0603001].

[26] S. Ryu and T. Takayanagi, *Aspects of Holographic Entanglement Entropy*, *JHEP* **08** (2006) 045 [hep-th/0605073].

[27] N. Lashkari, M. B. McDermott and M. Van Raamsdonk, *Gravitational dynamics from entanglement 'thermodynamics'*, *JHEP* **04** (2014) 195 [1308.3716].

[28] T. Faulkner, M. Guica, T. Hartman, R. C. Myers and M. Van Raamsdonk, *Gravitation from Entanglement in Holographic CFTs*, *JHEP* **03** (2014) 051 [1312.7856].

[29] B. Swingle and M. Van Raamsdonk, *Universality of Gravity from Entanglement*, 1405.2933.

[30] M. Van Raamsdonk, *Comments on quantum gravity and entanglement*, 0907.2939.

[31] M. Van Raamsdonk, *Building up spacetime with quantum entanglement*, *Gen. Rel. Grav.* **42** (2010) 2323 [1005.3035].

[32] M. Srednicki, *Entropy and area*, *Phys. Rev. Lett.* **71** (1993) 666 [hep-th/9303048].

[33] M. B. Hastings, *An area law for one-dimensional quantum systems*, *J. Stat. Mech.* **2007** (2007) P08024 [0705.2024].

[34] J. Eisert, M. Cramer and M. B. Plenio, *Area laws for the entanglement entropy - a review*, *Rev. Mod. Phys.* **82** (2010) 277 [0808.3773].

[35] H. Casini and M. Huerta, *On the RG running of the entanglement entropy of a circle*, *Phys. Rev.* **D85** (2012) 125016 [1202.5650].

[36] H. Casini, E. Teste and G. Torroba, *Relative entropy and the RG flow*, *JHEP* **03** (2017) 089 [1611.00016].

[37] A. B. Zamolodchikov, *Irreversibility of the Flux of the Renormalization Group in a 2D Field Theory*, *JETP Lett.* **43** (1986) 730.

[38] L. Susskind, *Butterflies on the Stretched Horizon*, 1311.7379.

[39] D. Stanford and L. Susskind, *Complexity and Shock Wave Geometries*, *Phys. Rev.* **D90** (2014) 126007 [1406.2678].

[40] L. Susskind and Y. Zhao, *Switchbacks and the Bridge to Nowhere*, 1408.2823.

[41] L. Susskind, *Computational Complexity and Black Hole Horizons*, *Fortsch. Phys.* **64** (2016) 44 [1403.5695].

[42] L. Susskind, *Entanglement is not enough*, *Fortsch. Phys.* **64** (2016) 49 [1411.0690].

[43] G. Vidal, *Entanglement Renormalization*, *Phys. Rev. Lett.* **99** (2007) 220405 [cond-mat/0512165].

[44] G. Vidal, *Entanglement Renormalization: an introduction*, *arXiv e-prints* (2009) [0912.1651].

[45] G. Evenbly and G. Vidal, *Tensor Network States and Geometry*, *Journal of Statistical Physics* **145** (2011) 891 [1106.1082].

[46] P. Hayden, S. Nezami, X.-L. Qi, N. Thomas, M. Walter and Z. Yang, *Holographic duality from random tensor networks*, *JHEP* **11** (2016) 009 [1601.01694].

[47] A. R. Brown, D. A. Roberts, L. Susskind, B. Swingle and Y. Zhao, *Holographic Complexity Equals Bulk Action?*, *Phys. Rev. Lett.* **116** (2016) 191301 [1509.07876].

[48] A. R. Brown, D. A. Roberts, L. Susskind, B. Swingle and Y. Zhao, *Complexity, action, and black holes*, *Phys. Rev.* **D93** (2016) 086006 [1512.04993].

[49] M. Flory, *WdW-patches in AdS_3 and complexity change under conformal transformations II*, *JHEP* **05** (2019) 086 [1902.06499].

[50] A. Belin, A. Lewkowycz and G. Sárosi, *Complexity and the bulk volume, a new York time story*, *JHEP* **03** (2019) 044 [1811.03097].

[51] P. Di Francesco, P. Mathieu and D. Senechal, *Conformal Field Theory*, Graduate Texts in Contemporary Physics. Springer-Verlag, New York, 1997, 10.1007/978-1-4612-2256-9.

[52] O. Aharony, S. S. Gubser, J. M. Maldacena, H. Ooguri and Y. Oz, *Large N field theories, string theory and gravity*, *Phys. Rept.* **323** (2000) 183 [hep-th/9905111].

[53] M. Ammon and J. Erdmenger, *Gauge/gravity duality*. Cambridge University Press, Cambridge, 2015.

[54] H. Nastase, *Introduction to the ADS/CFT Correspondence*. Cambridge University Press, 2015.

[55] M. Natsuume, *AdS/CFT Duality User Guide*, *Lect. Notes Phys.* **903** (2015) pp.1 [1409.3575].

[56] J. Dai, R. G. Leigh and J. Polchinski, *New Connections Between String Theories*, *Mod. Phys. Lett.* **A4** (1989) 2073.

[57] J. Polchinski, *Dirichlet Branes and Ramond-Ramond charges*, *Phys. Rev. Lett.* **75** (1995) 4724 [hep-th/9510017].

[58] N. Seiberg and E. Witten, *The D1 / D5 system and singular CFT*, *JHEP* **04** (1999) 017 [hep-th/9903224].

[59] O. Aharony, O. Bergman, D. L. Jafferis and J. Maldacena, *N=6 superconformal Chern-Simons-matter theories, M2-branes and their gravity duals*, *JHEP* **10** (2008) 091 [0806.1218].

[60] N. Seiberg, *Notes on theories with 16 supercharges*, *Nucl. Phys. Proc. Suppl.* **67** (1998) 158 [hep-th/9705117].

[61] V. Balasubramanian, P. Kraus and A. E. Lawrence, *Bulk versus boundary dynamics in anti-de Sitter space-time*, *Phys. Rev.* **D59** (1999) 046003 [hep-th/9805171].

[62] J. D. Brown and M. Henneaux, *Central Charges in the Canonical Realization of Asymptotic Symmetries: An Example from Three-Dimensional Gravity*, *Commun. Math. Phys.* **104** (1986) 207.

[63] P. Kraus, *Lectures on black holes and the AdS(3) / CFT(2) correspondence*, *Lect. Notes Phys.* **755** (2008) 193 [hep-th/0609074].

[64] M. Banados, *Three-dimensional quantum geometry and black holes*, *AIP Conf. Proc.* **484** (1999) 147 [hep-th/9901148].

[65] D. Bruss and G. Leuchs, *Lectures on quantum information*, Physics Textbook. Wiley-VCH, 2007.

[66] M. Wilde, *Quantum Information Theory*. Cambridge University Press, 2017.

[67] E. Schrodinger, *Die gegenwartige Situation in der Quantenmechanik*, *Naturwiss.* **23** (1935) 807.

[68] J. S. Bell, *On the Problem of Hidden Variables in Quantum Mechanics*, *Rev. Mod. Phys.* **38** (1966) 447.

[69] G. Vidal and R. F. Werner, *Computable measure of entanglement*, *Phys. Rev.* **A65** (2002) 032314 [quant-ph/0102117].

[70] A. Peres, *Separability criterion for density matrices*, *Phys. Rev. Lett.* **77** (1996) 1413 [quant-ph/9604005].

[71] P. Calabrese and J. L. Cardy, *Entanglement entropy and quantum field theory*, *J. Stat. Mech.* **0406** (2004) P06002 [hep-th/0405152].

[72] P. Calabrese and J. L. Cardy, *Entanglement entropy and quantum field theory: A Non-technical introduction*, *Int. J. Quant. Inf.* **4** (2006) 429 [quant-ph/0505193].

[73] P. Calabrese and J. Cardy, *Entanglement entropy and conformal field theory*, *J. Phys.* **A42** (2009) 504005 [0905.4013].

[74] V. E. Hubeny, M. Rangamani and T. Takayanagi, *A Covariant holographic entanglement entropy proposal*, *JHEP* **07** (2007) 062 [0705.0016].

[75] M. Rangamani and T. Takayanagi, *Holographic Entanglement Entropy*, *Lect. Notes Phys.* **931** (2017) pp.1 [1609.01287].

[76] H. Casini, M. Huerta and R. C. Myers, *Towards a derivation of holographic entanglement entropy*, *JHEP* **05** (2011) 036 [1102.0440].

[77] A. Lewkowycz and J. Maldacena, *Generalized gravitational entropy*, *JHEP* **08** (2013) 090 [1304.4926].

[78] X. Dong, A. Lewkowycz and M. Rangamani, *Deriving covariant holographic entanglement*, *JHEP* **11** (2016) 028 [1607.07506].

[79] M. Headrick, *General properties of holographic entanglement entropy*, *JHEP* **03** (2014) 085 [1312.6717].

[80] M. Headrick, V. E. Hubeny, A. Lawrence and M. Rangamani, *Causality & holographic entanglement entropy*, *JHEP* **12** (2014) 162 [1408.6300].

[81] T. Hirata and T. Takayanagi, *AdS/CFT and strong subadditivity of entanglement entropy*, *JHEP* **02** (2007) 042 [hep-th/0608213].

[82] M. Headrick and T. Takayanagi, *A Holographic proof of the strong subadditivity of entanglement entropy*, *Phys. Rev.* **D76** (2007) 106013 [0704.3719].

[83] N. Bao, S. Nezami, H. Ooguri, B. Stoica, J. Sully and M. Walter, *The Holographic Entropy Cone*, *JHEP* **09** (2015) 130 [1505.07839].

[84] P. Calabrese, J. Cardy and E. Tonni, *Entanglement negativity in quantum field theory*, *Phys. Rev. Lett.* **109** (2012) 130502 [1206.3092].

[85] P. Calabrese, J. Cardy and E. Tonni, *Entanglement negativity in extended systems: A field theoretical approach*, *J. Stat. Mech.* **1302** (2013) P02008 [1210.5359].

[86] P. Calabrese, J. Cardy and E. Tonni, *Finite temperature entanglement negativity in conformal field theory*, *J. Phys.* **A48** (2015) 015006 [1408.3043].

[87] G. Vidal and R. F. Werner, *Computable measure of entanglement*, *Phys. Rev. A* **65** (2002) 032314 [quant-ph/0102117].

[88] V. Eisler and Z. Zimborás, *Entanglement negativity in the harmonic chain out of equilibrium*, *New Journal of Physics* **16** (2014) 123020 [1406.5474].

[89] P. Chaturvedi, V. Malvimat and G. Sengupta, *Holographic Quantum Entanglement Negativity*, *JHEP* **05** (2018) 172 [1609.06609].

[90] P. Chaturvedi, V. Malvimat and G. Sengupta, *Entanglement negativity, Holography and Black holes*, *Eur. Phys. J.* **C78** (2018) 499 [1602.01147].

[91] M. M. Wolf, F. Verstraete, M. B. Hastings and J. I. Cirac, *Area Laws in Quantum Systems: Mutual Information and Correlations*, *Phys. Rev. Lett.* **100** (2008) 070502 [0704.3906].

[92] B. Chen, L. Chen, P.-x. Hao and J. Long, *On the Mutual Information in Conformal Field Theory*, *JHEP* **06** (2017) 096 [1704.03692].

[93] T. Faulkner, A. Lewkowycz and J. Maldacena, *Quantum corrections to holographic entanglement entropy*, *JHEP* **11** (2013) 074 [1307.2892].

[94] D. Harlow and P. Hayden, *Quantum Computation vs. Firewalls*, *JHEP* **06** (2013) 085 [1301.4504].

[95] M. A. Nielsen, *A geometric approach to quantum circuit lower bounds*, *eprint arXiv:quant-ph/0502070* (2005) [quant-ph/0502070].

[96] M. A. Nielsen, M. R. Dowling, M. Gu and A. C. Doherty, *Quantum Computation as Geometry*, *Science* **311** (2006) 1133 [quant-ph/0603161].

[97] M. R. Dowling and M. A. Nielsen, *The geometry of quantum computation*, *eprint arXiv:quant-ph/0701004* (2007) [quant-ph/0701004].

[98] L. Susskind, *Three Lectures on Complexity and Black Holes*, 2018, 1810.11563.

[99] L. Lehner, R. C. Myers, E. Poisson and R. D. Sorkin, *Gravitational action with null boundaries*, *Phys. Rev.* **D94** (2016) 084046 [1609.00207].

[100] B. Swingle, *Constructing holographic spacetimes using entanglement renormalization*, 1209.3304.

[101] B. Swingle, *Entanglement Renormalization and Holography*, *Phys. Rev.* **D86** (2012) 065007 [0905.1317].

[102] M. Nozaki, S. Ryu and T. Takayanagi, *Holographic Geometry of Entanglement Renormalization in Quantum Field Theories*, *JHEP* **10** (2012) 193 [1208.3469].

[103] G. Evenbly and G. Vidal, *Tensor Network Renormalization Yields the Multiscale Entanglement Renormalization Ansatz*, *Physical Review Letters* **115** (2015) 200401 [1502.05385].

[104] J. Molina-Vilaplana and J. Prior, *Entanglement, Tensor Networks and Black Hole Horizons*, *Gen. Rel. Grav.* **46** (2014) 1823 [1403.5395].

[105] H. Matsueda, M. Ishihara and Y. Hashizume, *Tensor network and a black hole*, *Phys. Rev.* **D87** (2013) 066002 [1208.0206].

[106] J. M. Maldacena, *Wilson loops in large N field theories*, *Phys. Rev. Lett.* **80** (1998) 4859 [hep-th/9803002].

[107] V. Balasubramanian and S. F. Ross, *Holographic particle detection*, *Phys. Rev.* **D61** (2000) 044007 [hep-th/9906226].

[108] T. Banks, M. R. Douglas, G. T. Horowitz and E. J. Martinec, *AdS dynamics from conformal field theory*, hep-th/9808016.

[109] J. Louko, D. Marolf and S. F. Ross, *On geodesic propagators and black hole holography*, *Phys. Rev.* **D62** (2000) 044041 [hep-th/0002111].

[110] Y. Makeenko, *A Brief Introduction to Wilson Loops and Large N*, *Phys. Atom. Nucl.* **73** (2010) 878 [0906.4487].

[111] C. Ewerz, O. Kaczmarek and A. Samberg, *Free Energy of a Heavy Quark-Antiquark Pair in a Thermal Medium from AdS/CFT*, *JHEP* **03** (2018) 088 [1605.07181].

[112] W. Fischler and S. Kundu, *Strongly Coupled Gauge Theories: High and Low Temperature Behavior of Non-local Observables*, *JHEP* **05** (2013) 098 [1212.2643].

[113] D. Birmingham, *Topological black holes in Anti-de Sitter space*, *Class. Quant. Grav.* **16** (1999) 1197 [hep-th/9808032].

[114] E. Witten, *Anti-de Sitter space, thermal phase transition, and confinement in gauge theories*, *Adv. Theor. Math. Phys.* **2** (1998) 505 [hep-th/9803131].

[115] S. de Haro, S. N. Solodukhin and K. Skenderis, *Holographic reconstruction of space-time and renormalization in the AdS / CFT correspondence*, *Commun. Math. Phys.* **217** (2001) 595 [hep-th/0002230].

[116] C. Ecker, D. Grumiller and S. A. Stricker, *Evolution of holographic entanglement entropy in an anisotropic system*, *JHEP* **07** (2015) 146 [1506.02658].

[117] C. Ecker, D. Grumiller, P. Stanzer, S. A. Stricker and W. van der Schee, *Exploring nonlocal observables in shock wave collisions*, *JHEP* **11** (2016) 054 [1609.03676].

[118] V. E. Hubeny, *Extremal surfaces as bulk probes in AdS/CFT*, *JHEP* **07** (2012) 093 [1203.1044].

[119] G. T. Horowitz and R. C. Myers, *The AdS / CFT correspondence and a new positive energy conjecture for general relativity*, *Phys. Rev.* **D59** (1998) 026005 [hep-th/9808079].

[120] J. Casalderrey-Solana, H. Liu, D. Mateos, K. Rajagopal and U. A. Wiedemann, *Gauge/String Duality, Hot QCD and Heavy Ion Collisions*, 1101.0618.

[121] A. Brandhuber, N. Itzhaki, J. Sonnenschein and S. Yankielowicz, *Wilson loops, confinement, and phase transitions in large N gauge theories from supergravity*, *JHEP* **06** (1998) 001 [hep-th/9803263].

[122] J. Sonnenschein, *What does the string / gauge correspondence teach us about Wilson loops?*, in *Supersymmetry in the theories of fields, strings and branes. Proceedings, Advanced School, Santiago de Compostela, Spain, July 26-31, 1999*, pp. 219–269, 1999, hep-th/0003032.

[123] D. Allahbakhshi, M. Alishahiha and A. Naseh, *Entanglement Thermodynamics*, *JHEP* **08** (2013) 102 [1305.2728].

[124] J. Bhattacharya, M. Nozaki, T. Takayanagi and T. Ugajin, *Thermodynamical Property of Entanglement Entropy for Excited States*, *Phys. Rev. Lett.* **110** (2013) 091602 [1212.1164].

[125] N. I. Gushterov, A. O'Bannon and R. Rodgers, *On Holographic Entanglement Density*, *JHEP* **10** (2017) 137 [1708.09376].

[126] S. Minwalla, *Restrictions imposed by superconformal invariance on quantum field theories*, *Adv. Theor. Math. Phys.* **2** (1998) 783 [hep-th/9712074].

[127] S. Shnider, *THE SUPERCONFORMAL ALGEBRA IN HIGHER DIMENSIONS*, *Lett. Math. Phys.* **16** (1988) 377.

[128] W. Nahm, *Supersymmetries and their representations*, *Nuclear Physics B* **135** (1978) 149 .

[129] R. Emparan, D. Grumiller and K. Tanabe, *Large-D gravity and low-D strings*, *Phys. Rev. Lett.* **110** (2013) 251102 [1303.1995].

[130] R. Emparan, R. Suzuki and K. Tanabe, *The large D limit of General Relativity*, *JHEP* **06** (2013) 009 [1302.6382].

[131] M. Alishahiha, *Holographic Complexity*, *Phys. Rev.* **D92** (2015) 126009 [1509.06614].

[132] S. Chapman, H. Marrochio and R. C. Myers, *Complexity of Formation in Holography*, *JHEP* **01** (2017) 062 [1610.08063].

[133] B. Czech, J. L. Karczmarek, F. Nogueira and M. Van Raamsdonk, *The Gravity Dual of a Density Matrix*, *Class. Quant. Grav.* **29** (2012) 155009 [1204.1330].

[134] P. Roy and T. Sarkar, *Note on subregion holographic complexity*, *Phys. Rev.* **D96** (2017) 026022 [1701.05489].

[135] R. Abt, J. Erdmenger, H. Hinrichsen, C. M. Melby-Thompson, R. Meyer, C. Northe et al., *Topological Complexity in AdS_3/CFT_2*, *Fortsch. Phys.* **66** (2018) 1800034 [1710.01327].

[136] O. Ben-Ami and D. Carmi, *On Volumes of Subregions in Holography and Complexity*, *JHEP* **11** (2016) 129 [1609.02514].

[137] G. Evenbly and G. Vidal, *Tensor Network Renormalization*, *Physical Review Letters* **115** (2015) 180405 [1412.0732].

[138] G. Mandal, R. Sinha and N. Sorokhaibam, *The inside outs of AdS_3/CFT_2: exact AdS wormholes with entangled CFT duals*, *JHEP* **01** (2015) 036 [1405.6695].

[139] V. Balasubramanian and P. Kraus, *A Stress tensor for Anti-de Sitter gravity*, *Commun. Math. Phys.* **208** (1999) 413 [hep-th/9902121].

[140] H. Epstein, V. Glaser and A. Jaffe, *Nonpositivity of the energy density in quantized field theories*, *Il Nuovo Cimento* **36** (1965) 1016.

[141] R. Bousso, Z. Fisher, J. Koeller, S. Leichenauer and A. C. Wall, *Proof of the Quantum Null Energy Condition*, *Phys. Rev.* **D93** (2016) 024017 [1509.02542].

[142] C. Ecker, D. Grumiller, W. van der Schee, M. M. Sheikh-Jabbari and P. Stanzer, *Quantum Null Energy Condition and its (non)saturation in 2d CFTs*, *SciPost Phys.* **6** (2019) 036 [1901.04499].

[143] J. Erdmenger, D.-W. Pang and H. Zeller, *Holographic entanglement entropy of semi-local quantum liquids*, *JHEP* **02** (2014) 016 [1311.1217].

[144] M. Freedman and M. Headrick, *Bit threads and holographic entanglement*, *Commun. Math. Phys.* **352** (2017) 407 [1604.00354].

[145] S. X. Cui, P. Hayden, T. He, M. Headrick, B. Stoica and M. Walter, *Bit Threads and Holographic Monogamy*, 1808.05234.

[146] C. A. Agón, J. De Boer and J. F. Pedraza, *Geometric Aspects of Holographic Bit Threads*, *JHEP* **05** (2019) 075 [1811.08879].

[147] R. Jefferson and R. C. Myers, *Circuit complexity in quantum field theory*, *JHEP* **10** (2017) 107 [1707.08570].

[148] R.-Q. Yang, Y.-S. An, C. Niu, C.-Y. Zhang and K.-Y. Kim, *To be unitary-invariant or not?: a simple but non-trivial proposal for the complexity between states in quantum mechanics/field theory*, 1906.02063.

[149] H. A. Camargo, P. Caputa, D. Das, M. P. Heller and R. Jefferson, *Complexity as a novel probe of quantum quenches: universal scalings and purifications*, *Phys. Rev. Lett.* **122** (2019) 081601 [1807.07075].

[150] P. Caputa, N. Kundu, M. Miyaji, T. Takayanagi and K. Watanabe, *Anti-de Sitter Space from Optimization of Path Integrals in Conformal Field Theories*, *Phys. Rev. Lett.* **119** (2017) 071602 [1703.00456].

[151] J. Couch, W. Fischler and P. H. Nguyen, *Noether charge, black hole volume, and complexity*, *JHEP* **03** (2017) 119 [1610.02038].

[152] A. R. Brown and L. Susskind, *Second law of quantum complexity*, *Phys. Rev.* **D97** (2018) 086015 [1701.01107].

[153] Y. Luke, *The Special Functions and Their Approximations*, Mathematics in Science and Engineering. Elsevier Science, 1969.

[154] L. Slater, *Generalized Hypergeometric Functions*. Cambridge University Press, 1966.

[155] I. A. Solomonovich, D. Zwillinger et al., *Table of integrals, series, and products.*, 2014.

Acknowledgments

There are numerous people to whom I am indebted for their help and support.

I would like to express my deepest appreciation to my advisor Johanna Erdmenger. Without her guidance and persistent support this dissertation would not have been possible. The opportunity and her encouragement to grow professionally and personally were invaluable.

Moreover, I am grateful to all my fellow group members in Würzburg as well as former group members in Munich for many interesting discussions and the pleasant time together. In particular, I'd like to extend my gratitude to my collaborator Mario Flory. He created an enjoyable and stimulating working atmosphere in our project. Furthermore, I have greatly benefited from his guidance and persistent help concerning scientific work, postdoc applications and academia in general. I am moreover indebted to Martin Ammon and Andy O'Bannon for various discussions and their support in my postdoc applications.

I am also grateful to the Max Planck Institute for Physics. I would like to thank them for the hospitality during my time in Munich as well as during my numerous visits. Being part of their IMPRS program gave me the opportunity to participate in fruitful interchange among PhD students and to broaden my horizon. I am especially indebted to Dieter Lüst for his continuous interest in my work and academic career as well as supporting me in my postdoc applications.

Finally, I would like to thank my family and friends for their continuous support and encouragement during the years leading to this dissertation.